# ADVANCES IN BIOANALYTICAL METHODS FOR PROBING LIGAND-TARGET INTERACTIONS

EDITED BY: Quezia B. Cass, Gabriella Massolini, Enrica Calleri and Carmen Lucia Cardoso

PUBLISHED IN: Frontiers in Chemistry

frontiers Research Topics

# frontiers



ISSN 1664-8714
ISBN 978-2-88963-818-5
DOI 10.3389/978-2-88963-818-5

## About Frontiers

Frontiers is more than just an open-access publisher of scholarly articles: it is a pioneering approach to the world of academia, radically improving the way scholarly research is managed. The grand vision of Frontiers is a world where all people have an equal opportunity to seek, share and generate knowledge. Frontiers provides immediate and permanent online open access to all its publications, but this alone is not enough to realize our grand goals.

## Frontiers Journal Series

The Frontiers Journal Series is a multi-tier and interdisciplinary set of open-access, online journals, promising a paradigm shift from the current review, selection and dissemination processes in academic publishing. All Frontiers journals are driven by researchers for researchers; therefore, they constitute a service to the scholarly community. At the same time, the Frontiers Journal Series operates on a revolutionary invention, the tiered publishing system, initially addressing specific communities of scholars, and gradually climbing up to broader public understanding, thus serving the interests of the lay society, too.

## Dedication to Quality

Each Frontiers article is a landmark of the highest quality, thanks to genuinely collaborative interactions between authors and review editors, who include some of the world's best academicians. Research must be certified by peers before entering a stream of knowledge that may eventually reach the public - and shape society; therefore, Frontiers only applies the most rigorous and unbiased reviews.
Frontiers revolutionizes research publishing by freely delivering the most outstanding research, evaluated with no bias from both the academic and social point of view. By applying the most advanced information technologies, Frontiers is catapulting scholarly publishing into a new generation.

## What are Frontiers Research Topics?

Frontiers Research Topics are very popular trademarks of the Frontiers Journals Series: they are collections of at least ten articles, all centered on a particular subject. With their unique mix of varied contributions from Original Research to Review Articles, Frontiers Research Topics unify the most influential researchers, the latest key findings and historical advances in a hot research area! Find out more on how to host your own Frontiers Research Topic or contribute to one as an author by contacting the Frontiers Editorial Office: researchtopics@frontiersin.org

# ADVANCES IN BIOANALYTICAL METHODS FOR PROBING LIGAND-TARGET INTERACTIONS

Topic Editors:
**Quezia B. Cass,** Federal University of São Carlos, Brazil
**Gabriella Massolini,** University of Pavia, Italy
**Enrica Calleri,** University of Pavia, Italy
**Carmen Lucia Cardoso,** University of São Paulo, Brazil

**Citation:** Cass, Q. B., Massolini, G., Calleri, E., Cardoso, C. L., eds. (2020). Advances in Bioanalytical Methods for Probing Ligand-Target Interactions. Lausanne: Frontiers Media SA. doi: 10.3389/978-2-88963-818-5

# Table of Contents

frontiers in Chemistry

EDITORIAL
published: 15 May 2020
doi: 10.3389/fchem.2020.00378

# Editorial: Advances in Bioanalytical Methods for Probing Ligand-Target Interactions

*Quezia B. Cass[1]*, Gabriella Massolini[2], Carmen Lucia Cardoso[3] and Enrica Calleri[1]*

[1] Departamento de Química, Universidade Federal de São Carlos, São Carlos, Brazil, [2] Department of Drug Sciences, University of Pavia, Pavia, Italy, [3] Departamento de Química, Faculdade de Filosofia, Ciências e Letras de Ribeirão Preto, Universidade de São Paulo, Ribeirão Preto, Brazil

**Keywords: bioaffinity chromatography, surface plasmon resonance, nuclear magnetic resonance, mass spectrometry-based approaches, ligand-fishing experiments**

## Editorial on the Research Topic

## Advances in Bioanalytical Methods for Probing Ligand-Target Interactions

Protein-ligand interactions are fundamental in all life processes and the comprehension of molecular recognition has an essential role in many scientific areas. Molecular recognition processes involve protein-protein, protein-ligand, or protein-nucleic acid interactions and are mainly driven by weak bonding interactions (hydrogen bonding, electrostatics, van der Waals forces, π-π interactions). The study of drug–target (enzymes, proteins, nucleic acids) interactions is crucial for the discovery and development of new therapeutic molecules as the binding affinity of a ligand may provide important information about *in vivo* efficacy of the compound. In this context, increased attention has been given to the development of ligand-binding assays that target protein interactions using a variety of analytical methods.

Bioaffinity chromatography/electrophoresis (Slon-Usakiewicz et al., 2005; Calleri et al., 2011; Moraes et al., 2016), ligand-fishing experiments (de Moraes et al., 2014; Liu et al., 2017; Zhang et al., 2019), mass spectrometry (MS)-based approaches (Imaduwage et al., 2016), nuclear magnetic resonance (NMR) (Cala et al., 2014; Furukawa et al., 2016), surface plasmon resonance (SPR) (Nedelkov and Nelson, 2003) and other techniques such as quartz crystal microbalance (Naklua et al., 2016), equilibrium dialysis, ultrafiltration (Zhuo et al., 2016), and circular dichroism (Tramarin et al., 2019) have been reported in literature for ligand-target interaction studies.

In this special issue, three reviews and six original research papers provide methodological advances and recent application examples in bioaffinity chromatography, MS based binding assays, SPR, and NMR for ligand-target interactions studies. In the following paragraphs, each of the accepted publications are presented and briefly described.

Regarding chromatography, the topic encompasses two closely related reviews and three application articles. The review from de Moraes et al. covers screening assays in which the binding events are monitored by on-line or off-line liquid chromatography. On-line bioaffinity chromatography, with zonal or frontal elution, in a diverse range of assay systems are presented and their applications for disclosing protein-ligand interactions is discussed. Meanwhile, a diverse range of static, or off-line, assays have been reported that identify ligands in complex mixtures. In the latter cases, the full chemical characterization of the identified ligands is the main attraction of these approaches. Tools for examining the kinetics of biological reactions, such as band-broadening measurements, peak decay analysis, split-peak and peak fitting methods, and ultrafast affinity extraction are beautifully reviewed by Iftekhar et al.. An off-line assay application is reported in the work of Sahm et al. for the TBX2 transcription factor, which plays a key role in oncogenic processes.

OPEN ACCESS

***Edited and reviewed by:***
*Huangxian Ju,*
*Nanjing University, China*

****Correspondence:***
*Quezia B. Cass*
*qcass@ufscar.br*

***Specialty section:***
*This article was submitted to Analytical Chemistry, a section of the journal Frontiers in Chemistry*

***Received:*** *31 March 2020*
***Accepted:*** *09 April 2020*
***Published:*** *15 May 2020*

***Citation:***
*Cass QB, Massolini G, Cardoso CL and Calleri E (2020) Editorial: Advances in Bioanalytical Methods for Probing Ligand-Target Interactions. Front. Chem. 8:378. doi: 10.3389/fchem.2020.00378*

After immobilization to an *N*-terminal resin, the TBX2-DNA-binding domain recombinant protein was used to evaluate the capability of marine chromomycins A5 (CA5) and A6 (CA6) to interact with TBX2. Microscale thermophoresis was used to characterize the interaction observed through the screen modulators static assay. Based on the evidence generated by these assays, it was possible to infer that chromomycins, and particularly CA5, bind to TBX2 and its modulation may explain their cytotoxic properties.

Olsen et al. report on the production of monolithic supports for trypsin immobilization for on-line protein digestion in bottom-up proteomic studies, which can also be tailored for other applications such as on-line drug/target studies. The article by de Lima et al. deals with molecular docking and bioaffinity chromatography as a means to design rational acetylcholinesterase (AChE) inhibitors using stepholidine as a template. In this way it was possible to kinetically characterize the identified inhibitors, and show how the designed alkaloid derivatives interact with AChE.

Mass spectrometry (MS) is recognized as a powerful tool to study the non-covalent interactions between small molecules and proteins (ligand-target interactions) that is a hot topic in medicinal chemistry and life sciences. In this special issue, readers can find an interesting review by Chen et al. where the principles and recent applications of soft ionization mass spectrometry methods (ESI, DESI, and MALDI) and their hyphenated techniques, including hydrogen-deuterium exchange mass spectrometry (HDX-MS), chemical cross-linking mass spectrometry (CX-MS), and ion mobility spectrometry-mass spectrometry (IMS/MS) are described. The Authors underline that the soft ionization MS-based methods can carefully and accurately study protein/enzyme-small molecule interactions, thus providing important information-rich data useful in drug design and development.

In an interesting article Gabriel et al. combined the concepts of MS Binding Assays and affinity selection MS (ASMS). The new, powerful, efficient, and reliable library screening approach has been used for the identification of ligands addressing the GABA transporter subtype 1 (GAT1) responsible of the regulation of GABA levels in the brain. To meet this end a library composed initially of 128, later of 1,280, well-characterized GAT1 inhibitors, drug substances, and pharmacological tool compounds were analyzed. The described approach combines the power of MS Binding Assays and the strength of ASMS, while the weaknesses of both methods are avoided. The capabilities offered by the combination of competitive MS Binding Assays and ASMS can exploited in early drug discovery campaigns.

For the characterization of a binding event and for the affinity screening of libraries of compounds as potential drug candidates, different biophysical techniques can be considered. Among the most informative techniques, surface plasmon resonance (SPR) spectroscopy is a relatively new label-free technique which enables the measurement of real-time ligand-binding affinities and kinetics using small amounts of target immobilized on a sensor-chip.

One of most challenging tasks for SPR methods is the measurement of the binding kinetics and affinities of potential ligands to membrane proteins such as GPCRs. Very few applicative examples have been reported so far. In this special issue an original contribution has been described by Capelli et al.. The article reports the development of an SPR method for the measurement of binding affinities and kinetic parameters of potential ligands for GPR17-an important target for the treatment of demyelinating diseases. The receptor was immobilized from solubilized membrane extracts through a covalently bound anti-6x-His-antibody.

The method was applied to two engineered variants of GPR17, expressed in insect cells and extracted from crude membranes and used for the characterization of the binding of two high affinity ligands, the antagonist Cangrelor and the agonist Asinex 1. The experimentally calculated kinetic parameters and binding constants were in good agreement with those reported in literature.

NMR-based spectroscopic methods can be used to characterize at an atomic level a binding interaction in aqueous media. Kock et al. reported a study where the interaction between a novel ruthenium complex anti-cancer candidate and the biological target DNA is considered. Moreover, the $K_d$ value was estimated and it was in agreement with previously reported studies increasing the potential of the technique for medicinal chemistry programs on new metallodrugs.

The published articles help readers appreciate the usefulness of different analytical tools for studying protein-drug interactions. Researchers working in pharmaceutical industries and academia can greatly benefit from the application of the proposed innovative analytical methods to improve the drug discovery and development processes.

## AUTHOR CONTRIBUTIONS

All authors listed have made a substantial, direct and intellectual contribution to the work, and approved it for publication.

## REFERENCES

Cala, O., Guillière, F., and Krimm, I. (2014). NMR-based analysis of protein-ligand interactions. *Anal. Bioanal. Chem.* 406, 943–956. doi: 10.1007/s00216-013-6931-0

Calleri, E., Temporini, C., and Massolini, G. (2011). Frontal affinity chromatography in characterizing immobilized receptors. *J. Pharm. Biomed. Anal.* 54, 911–925. doi: 10.1016/j.jpba.2010.11.040

de Moraes, M. C., Vanzolini, K. L., Cardoso, C. L., and Cass, Q. B. (2014). New trends in LC protein ligand screening. *J. Pharm. Biomed. Anal.* 87, 155–166. doi: 10.1016/j.jpba.2013.07.021

Furukawa, A., Konuma, T., Yanaka, S., and Sugase, K. (2016). Quantitative analysis of protein-ligand interactions by NMR. *Prog. Nucl. Magn. Reson. Spectrosc.* 96, 47–57. doi: 10.1016/j.pnmrs.2016.02.002

Imaduwage, K. P., Go, E. P., Zhu, Z., and Desaire, H. (2016). HAMS: high-affinity mass spectrometry screening. A high-throughput screening method

for identifying the tightest-binding lead compounds for target proteins with no false positive identifications. *J. Am. Soc. Mass Spectrom.* 27, 1870–1877. doi: 10.1007/s13361-016-1472-3

Liu, D.-M., Chen, J., and Shi, Y.-P. (2017). Screening of enzyme inhibitors from traditional Chinese medicine by magnetic immobilized α-glucosidase coupled with capillary electrophoresis. *Talanta* 164, 548–555. doi: 10.1016/j.talanta.2016.12.028

Moraes, M. C., Cardoso, C., Seidl, C., Moaddel, R., and Cass, Q. (2016). Targeting anti-cancer active compounds: affinity-based chromatographic assays. *Curr. Pharm. Des.* 22, 5976–5987. doi: 10.2174/1381612822666160614080506

Naklua, W., Suedee, R., and Lieberzeit, P. A. (2016). Dopaminergic receptor-ligand binding assays based on molecularly imprinted polymers on quartz crystal microbalance sensors. *Biosens. Bioelectron.* 81, 117–124. doi: 10.1016/j.bios.2016.02.047

Nedelkov, D., and Nelson, R. W. (2003). Surface plasmon resonance mass spectrometry: recent progress and outlooks. *Trends Biotechnol.* 21, 301–305. doi: 10.1016/S0167-7799(03)00141-0

Slon-Usakiewicz, J. J., Ng, W., Dai, J.-R., Pasternak, A., and Redden, P. R. (2005). Frontal affinity chromatography with MS detection (FAC-MS) in drug discovery. *Drug Discov. Today* 10, 409–416. doi: 10.1016/S1359-6446(04)03360-4

Tramarin, A., Tedesco, D., Naldi, M., Baldassarre, M., Bertucci, C., and Bartolini, M. (2019). New insights into the altered binding capacity of pharmaceutical-grade human serum albumin: site-specific binding studies by induced circular dichroism spectroscopy. *J. Pharm. Biomed. Anal.* 162, 171–178. doi: 10.1016/j.jpba.2018.09.022

Zhang, Y., Wang, Q., Liu, R., Zhou, H., Crommen, J., Moaddel, R., et al. (2019). Rapid screening and identification of monoamine oxidase-A inhibitors from Corydalis Rhizome using enzyme-immobilized magnetic beads based method. *J. Chromatogr. A* 1592, 1–8. doi: 10.1016/j.chroma.2019.01.062

Zhuo, R., Liu, H., Liu, N., and Wang, Y. (2016). Ligand fishing: a remarkable strategy for discovering bioactive compounds from complex mixture of natural products. *Molecules* 21, 1516–1532. doi: 10.3390/molecules21111516

**Conflict of Interest:** The authors declare that the research was conducted in the absence of any commercial or financial relationships that could be construed as a potential conflict of interest.

frontiers in Chemistry

ORIGINAL RESEARCH
published: 18 September 2019
doi: 10.3389/fchem.2019.00629

# Synthesis and Inhibition Evaluation of New Benzyltetrahydroprotoberberine Alkaloids Designed as Acetylcholinesterase Inhibitors

*Bruna R. de Lima[1], Juliana M. Lima[2], Jéssica B. Maciel[1], Carolina Q. Valentim[3], Rita de Cássia S. Nunomura[1,4], Emerson S. Lima[3], Hector H. F. Koolen[5], Afonso Duarte L de Souza[1,4], Maria Lúcia B. Pinheiro[1,4], Quezia B. Cass[2]* and Felipe Moura A. da Silva[1]**

[1] Central Analítica-Centro de Apoio Multidisciplinar, Universidade Federal do Amazonas, Manaus, Brazil, [2] Separare, Departamento de Química, Universidade Federal de São Carlos, São Carlos, Brazil, [3] Faculdade de Farmácia, Universidade Federal do Amazonas, Manaus, Brazil, [4] Departamento de Química, Universidade Federal do Amazonas, Manaus, Brazil, [5] Grupo de Pesquisa em Metabolômica e Espectrometria de Massas, Universidade do Estado do Amazonas, Manaus, Brazil

Secondary metabolites from natural products are a potential source of acetylcholinesterase inhibitors (AChEIs), which is a key enzyme in the treatment of many neurodegenerative diseases. Inspired by the reported activities of isoquinoline-derivative alkaloids herein we report the design, one step synthesis and evaluation by capillary enzyme reactor (ICER) of benzyl analogs (**1a**–**1e**) of the tetrahydroprotoberberine alkaloid stepholidine, which is abundant in *Onychopetalum amazonicum*. Docking analysis based on the crystal structure of *Torpedo californica* AChE (*Tc*AChE) indicated that π-π interactions were dominant in all planned derivatives and that the residues from esteratic, anionic and peripheral subsites of the enzyme played key interaction roles. Due to the similarities observed when compared with galantamine in the AChE complex, the results suggest that ligand-target interactions would increase, especially for the *N*-benzyl derivatives. From a series of synthesized compounds, the alkaloids (7*R*,13a*S*)-7-benzylstepholidine (**1a**), (7*S*,13a*S*)-7-benzylstepholidine (**1b**), and (*S*)-10-*O*-benzylstepholidine (**1d**) are reported here for the first time. The on flow bioaffinity chromatography inhibition assay, based on the quantification of choline, revealed the *N*-benzylated compound **1a** and its epimer **1b** to be the most active, with $IC_{50}$ of 40.6 ± 1 and 51.9 ± 1 μM, respectively, and a non-competitive mechanism. The proposed approach, which is based on molecular docking and bioaffinity chromatography, demonstrated the usefulness of stepholidine as a template for the design of rational AChEIs and showed how the target-alkaloid derivatives interact with AChE.

**Keywords: bioaffinity chromatography, molecular docking, on-flow assay, *Onychopetalum amazonicum*, stepholidine derivatives**

OPEN ACCESS

***Edited by:***
*Shusheng Zhang,*
*Linyi University, China*

***Reviewed by:***
*Benjamin L. Oyler,*
*United States Food and Drug Administration, United States*
*Aihua Liu,*
*Qingdao University, China*

****Correspondence:***
*Quezia B. Cass*
*qcass@ufscar.br*
*Felipe Moura A. da Silva*
*felipemas@ufam.edu.br*

***Specialty section:***
*This article was submitted to Analytical Chemistry, a section of the journal Frontiers in Chemistry*

***Received:*** *06 July 2019*
***Accepted:*** *02 September 2019*
***Published:*** *18 September 2019*

***Citation:***
*de Lima BR, Lima JM, Maciel JB, Valentim CQ, Nunomura RdCS, Lima ES, Koolen HHF, de Souza ADL, Pinheiro MLB, Cass QB and da Silva FMA (2019) Synthesis and Inhibition Evaluation of New Benzyltetrahydroprotoberberine Alkaloids Designed as Acetylcholinesterase Inhibitors. Front. Chem. 7:629. doi: 10.3389/fchem.2019.00629*

## INTRODUCTION

The Amazon rainforest is considered the largest natural reservoir of plant diversity and the most diverse ecosystem on the planet (Oliveira and Amaral, 2004). Among this wide biodiversity, numerous species belonging to the Annonaceae family stand out due to their use in traditional medicine, including the treatment of neurodegenerative diseases (Adams et al., 2007), and as promising sources of bioactive natural products, such as *Onychopetalum amazonicum* (Almeida et al., 1976; Silva et al., 2015; Lima et al., 2016, 2019).

Plant natural products (PNPs) have attracted the interest of many researchers around the world due to their chemical diversity and biochemical specificity, which make them favorable as lead structures for drug discovery (Cragg et al., 1997; Harvey, 2008). Notoriously, many of these PNPs (e.g., galantamine and huperzine A) have been used in semisynthetic procedures which are designed by rational modifications in order to increase their biological activity or reduce side effects (Högenauer et al., 2001; Atanasova et al., 2015). Among these promising compounds, alkaloids are highlighted due to their high structural diversity and wide range of biological activities, including Anti-HIV (Kashiwada et al., 2005), anticancer (Lu et al., 2012), and acetylcholinesterase (AChE) inhibition (Tsai and Lee, 2010; Hostalkova et al., 2019).

In regards to AChE, this enzyme has been an attractive target for rational drug design and the discovery of mechanism-based inhibitors for the treatment of central nervous system (CNS) and peripheral diseases, such as myasthenia gravis (Cui et al., 2015), glaucoma (Almasieh et al., 2013), schizophrenia (Patel et al., 2010) and Alzheimer's disease (Murray et al., 2013). Thus, the use of AChE inhibitors (AChEIs) is considered a therapeutically-relevant strategy for these diseases (Houghton et al., 2006; Mukherjee et al., 2007; Anand and Singh, 2013; Mohammad et al., 2017), and justifies the search for new leads. Since the identification of galantamine as a powerful AChEI, the prospection of AChEIs has been boosted in the field of chemistry of natural products (Houghton et al., 2006; Mukherjee et al., 2007; Anand and Singh, 2013; Deka et al., 2017), and, several alkaloid classes, including isoquinolines, indoles, quinolizidines, piperidines, and steroidal alkaloids, have been reported as promising AChEIs ($IC_{50} < 50\,\mu M$) (Murray et al., 2013). Regarding isoquinoline-derived alkaloids, recent studies pointed out berberine and tetrahydroprotoberberine salts as potent AChEIs and therefore, suitable templates to design rational AChE ligands (Tsai and Lee, 2010; Hostalkova et al., 2019).

To meet this end, complementary approaches commonly used in drug discovery are often combined, such as virtual screening and co-crystallization experiments. These allow understanding of how AChE interacts with ligands at the active site, and thus support the design and screening of new AChEIs. As an example, the determination of the crystal structure of *Torpedo californica* AChE (*Tc*AChE) permitted the visualization, at atomic resolution, of the active site of AChE that is unexpectedly located at the bottom of a deep gorge lined largely by aromatic residues (Dvir et al., 2010), suggesting that π-π stacking interactions may be of great relevance to the action of AChEIs, which corroborates the docking results for benzylated compounds and *Tc*AChE (Yamamoto et al., 1994).

Regarding the *in vitro* biological assays, a variety of colorimetric methods based on the Ellman's reagent (Ellman et al., 1961) with either free (Mantoani et al., 2016) or immobilized enzyme (Andrisano et al., 2001; Vilela et al., 2014) have been described in order to identify AChEIs in natural or synthetic libraries. The main drawback of these assays is that they are based on indirect AChE activity measurement and thus prone to false positive and/or negative results. To overcome these problems, an on-flow assay based on the use of AChE immobilized capillary enzyme reactors (AChE-ICERs) has been adopted to directly measure the production of choline (Ch). One of the key advantages of this approach is the use of a mass spectrometer as the detector, which allows differentiation between the ligands from the substrate and reaction products (Vanzolini et al., 2013; Seidl et al., 2019). The usefulness of the AChE-ICERs assay platform has been demonstrated not only as a tool for identifying inhibitors, but also for characterizing inhibition mechanisms (Vanzolini et al., 2013; Sangi et al., 2014; Torres et al., 2016; Seidl et al., 2019).

Herein, we report the design, one-step synthesis, and evaluation by ICER of new benzyl analogs obtained from stepholidine, an isoquinoline-derived neuroprotective alkaloid, which was obtained from the Amazonian plant *O. amazonicum*. The virtual screening associated to the inhibition AChE-ICER assay enabled us to pinpoint the main target-alkaloid interactions.

## MATERIALS AND METHODS

### General Apparatus and Chemicals

Optical rotations were acquired at a Polartronic H-series polarimeter at the sodium D line (589 nm) and 25°C (Schmidt + Haensch, Berlin, Germany). Mass spectrometry data for structural determination were obtained using a triple quadrupole (QqQ) (TSQ Quantum Access, San Jose, CA, USA) and a quadrupole time-of-flight (Q-TOF) (Impact HD, Bruker Daltonics, Bullerica, MA, USA) mass spectrometer, both equipped with an electrospray ion source (ESI), in the positive mode. The biological assay was carried out in a chromatography system that consisted of two LC-20AD pumps, a SIL 20A autosampler, a DGU-20A5 degasser, a CTO-20A column oven and a CBM-20A interface (Shimadzu, Kyoto, Japan). The LC system was coupled to an Esquire 6000 ion trap (IT) mass spectrometer equipped with an ESI source (Bruker Daltonics, Bremen, Germany). The Data Analysis software (Bruker Daltonics, Bremen, Germany) was employed for the data acquisition. One-dimensional (1D) and two-dimensional (2D) nuclear magnetic resonance (NMR) spectroscopy data were acquired using an AVANCE III HD 500 spectrometer (Bruker, Billerica, USA) operating at 11.7 T (500.13 and 125.76 MHz for $^{1}H$ and $^{13}C$, respectively). Chemical shifts ($\delta$) were presented in ppm relative to the tetramethylsilane (TMS) signal at 0.00 ppm as an internal reference and the coupling constants ($J$) were given in Hertz. Deuterated methanol ($CD_3OD$, 99.8%), was obtained from Cambridge

Isotope Laboratories (Tewksbury, MA, USA). Semi-preparative high performance liquid chromatography (HPLC) analysis was performed on a Shimadzu UFLC system (LC-6 AD pump; DGU-20A5 degasser; SPD-20AV UV detector; rheodyne injector; CBM-20A communication module) (Columbia, MD, USA) equipped with a Luna C18(2) column (250 × 10 mm, 5 μm) (Phenomenex–Torrance, CA, USA). Column chromatography (CC) was carried out on silica gel 60 (230–400 mesh; Merck) and KP-C18-HS cartridge (Biotage, VA, USA). All solvents used for chromatography and MS experiments were HPLC grade and were purchased from J. T. Baker (Phillipsburg. NJ, USA), and the water was purified by using a Milli-Q system (Millipore, Bedford, MA, USA). The analytical reagents, ammonium acetate, potassium hydroxide (KOH), dimethylformamide (DMF), benzyl bromide (BnBr), AChE from *Electrophorus electricus* (*eel*AChE) type VI-S, choline iodide (Ch), acetylcholine iodide (ACh), and galanthamine bromide were purchased from Sigma-Aldrich (St. Louis, MO, USA).

## Plant Material

*Onychopetalum amazonicum* R. E. Fr. (Annonaceae) leaves were collected from a specimen previously cataloged during the Flora project (Ribeiro et al., 1999) in March, 2014 in the Adolpho Ducke Forest Reserve (26 km North on the AM-010 highway, in the municipality of Manaus, Amazonas state, Brazil, 2°59′15.9″S, 59°55′35.5″W). The access to genetic heritage was registered at Sistema Nacional de Gestão do Patrimônio Genético e do Conhecimento Tradicional Associado (SisGen) under the code #AE0F182. A voucher (#218341) was deposited in the herbarium of the Instituto Nacional de Pesquisas da Amazônia (INPA). The material was immediately dried at ambient temperature (ca. 20°C) during 20 days.

## Extraction, Synthesis, and Isolation

To obtain a stepholidine-rich fraction (SRF), the dried and powdered leaves of *O. amazonicum* (300 g) were directly subjected to an acid-base extraction (Soares et al., 2015) to give an alkaloid-rich fraction (1.36 g). Then, an aliquot of the alkaloidal fraction (1 g) was subjected to silica gel CC eluted with hexane-ethyl acetate-methanol (30:40:30, v/v), which provided 13 fractions. These fractions were pooled according to MS analysis to provide the SRF (fractions 3–8) (0.44 g), and this sample was submitted to MS, $^1$H NMR analysis, and synthesis procedures.

The compounds **1a−1e** were prepared by following an adapted one-step synthetic method (Karimova et al., 2014). The SRF (0.44 g) was added to a round bottom flask containing KOH (0.56 g) and DMF (10 mL). The resulting mixture was stirred and heated (40°C) for 30 min and then benzyl bromide (1.2 mL) was added. After 24 h, the mixture was partitioned with distilled water (20 mL) and dichloromethane (DCM) (20 mL). The DCM fraction (DCMF) (0.7 g) was dried under a nitrogen gas stream, while the aqueous fraction (AF) (1.4 g) was freeze-dried.

An aliquot (0.50 g) of the AF and DCMF was subjected to C18 CC eluted with gradient systems of water-methanol, affording 4 and 3 fractions, respectively. Fractions coded as AF3 (66.4 mg) and DCMF3 (133.1 mg) were subjected to further purification by semi-preparative HPLC using a C18 column with a constant flow-rate of 3.5 mL/min and UV detection at 235 and 280 nm. Formic acid aqueous solution (1%, v:v) (A) and methanol (B) were used as mobile phases. The gradient elution was as follows: 0–15 min, 20–50% B, 15–27 min, 50–80% B, 27–37 min, 80% B (v:v). AF3 (3 × 20 mg) and DCMF3 (6 × 20 mg) fractions were carried onto the column in water and DMSO (100 μL), respectively. The fractions coded as AF3-1 (19.6 mg–**1b**), AF3-2 (14.8 mg–**1a**), DCMF3-6 (15.3 mg–**1c**), DCMF3-7 (13.5 mg–**1d**), and DCMF3-11 (18.5 mg–**1e**) were submitted to HRMS, 1D and 2D NMR analysis.

**(7*R*,13a*S*)-7-benzylstepholidine (1a)**: yellow powder (14.8 mg); $[\alpha]_D^{25} = -33.88^\circ$ (*c* 0.072, MeOH); $^1$H NMR (500 MHz, CD3OD) $\delta$ 3.27 (m, 1H), 3.42 (m, 1H), 3.72 (m, 1H), 3.80 (m, 1H), 3.84 (s, 3H), 3.93 (s, 3H), 4.01(dd, $J$ = 17.9, 5.6 Hz, 1H), 4.29 (m, 2H), 4.33 (m, 1H), 4.60 (d, $J$ = 15.7 Hz, 1H), 5.26 (dd, $J$ = 12.2, 5.9 Hz, 1H), 6.78 (s, 1H), 6.96 (s, 1H), 7.03 (d, $J$ = 8.3 Hz, 1H), 7.12 (d, $J$ = 8.3 Hz, 1H), 7.27 (m, 2H), 7.49 (m, 2H), 7.54 (m, 1H); $^{13}$C NMR (125.76 MHz, CD3OD) $\delta$ 25.0, 29.9, 52.4, 56.6, 58.3, 58.5, 61.1, 68.9, 112.8, 113.5, 119.4, 121.3, 122.3, 122.8, 123.2, 126.1, 128.3, 130.7, 132.1, 133.8, 145.2, 148.0, 150.1, 150.4; HRMS *m/z* 418.2011 (calcd. for $C_{26}H_{28}NO_4$, 418.2018, $\Delta_{m/z\text{theoretical}} = -1.67$ ppm).

**(7*S*,13a*S*)-7-benzylstepholidine (1b)**: yellow powder (19.6 mg); $[\alpha]_D^{25} = -35.10^\circ$ (*c* 0.082, MeOH); $^1$H NMR (500 MHz, CD3OD) $\delta$ 3.15 (dd, $J$ = 18.1, 10 Hz, 1H), 3.33 (m, 1H), 3.42 (dd, $J$ = 18.1, 10 Hz, 1H), 3.50 (m, 1H), 3.57 (m, 1H), 3.81 (s, 3H), 3.85 (m, 1H), 3.91 (s, 3H), 4.52 (d, $J$ = 15.7 Hz, 1H), 4.66 (m, 2H), 4.71 (d, $J$ = 15.7 Hz, 1H), 4.74 (m, 1H), 6.78 (s, 1H), 6.80 (d, $J$ = 8.3 Hz, 1H), 6.85 (d, $J$ = 8.3 Hz, 1H), 6.96 (s, 1H), 7.50 (m, 2H), 7.54 (m, 2H), 7.57 (m, 1H); $^{13}$C NMR (125.76 MHz, CD3OD) $\delta$ 24.2, 35.3, 51.7, 56.7, 56.9, 60.9, 65.0, 65.5, 113.5, 114.4, 118.9, 120.7, 120.8, 121.8, 125.0, 125.8, 128.4, 130.7, 132.3, 134.4, 145.7, 147.7, 150.2, 150.3; HRMS *m/z* 418.2001 (calcd. for $C_{26}H_{28}NO_4$, 418.2018, $\Delta_{m/z\text{theoretical}} = -4.06$ ppm).

**(*S*)-2-*O*-benzylstepholidine (1c)**: yellow powder (15.3 mg); $[\alpha]_D^{25} = -387.60^\circ$ (*c* 0.26, MeOH); $^1$H NMR (500 MHz, CD3OD) $\delta$ 2.71 (dd, $J$ = 16.1, 11.4 Hz, 1H), 2.80 (m, 1H), 2.87 (m, 1H), 3.12 (ddd, $J$ = 16.1, 11.2, 5.4 Hz, 1H), 3.37 (m, 2H), 3.74 (d, $J$ = 15.6 Hz, 1H), 3.82 (s, 3H), 3.83 (s, 3H), 4.40 (d, $J$ = 15.6 Hz, 1H), 5.09 (s, 2H), 6.75 (s, 1H), 6.76 (d, 8.3 Hz, 1H), 6.80 (d, 8.3 Hz, 1H), 6.90 (s, 1H), 7.29 (m, 1H), 7.37 (m, 2H), 7.44 (m, 2H); $^{13}$C NMR (125.76 MHz, CD3OD) $\delta$ 28.6, 35.7, 52.4, 54.3, 56.5, 60.4, 72.6, 113.3, 113.5, 116.9, 125.4, 126.2, 127.1, 127.6, 128.9, 129.1, 129.4, 138.7, 145.0, 148.2, 149.1, 150.4; HRMS *m/z* 418.2010 (calcd. for $C_{26}H_{28}NO_4$, 418.2018, $\Delta_{m/z\text{theoretical}} = -1.91$ ppm).

**(*S*)-10-*O*-benzylstepholidine (1d)**: yellow powder (13.5 mg); $[\alpha]_D^{25} = -146.02^\circ$ (*c* 0.42, MeOH); $^1$H NMR (500 MHz, CD3OD) $\delta$ 2.74 (m, 1H), 2.79 (m, 2H), 3.10 (m, 1H), 3.34 (m, 1H), 3.38 (dd, $J$ = 16.3, 4.1 Hz, 1H), 3.65 (m, 2H), 3.82 (s, 3H), 4.3 (d, $J$ = 15.6 Hz, 1H), 5.08 (s, 2H), 6.68 (s, 1H), 6.75 (s, 1H), 6.90 (d, $J$ = 8.5 Hz, 1H), 6.97 (d, $J$ = 8.5 Hz, 1H), 7.30 (m, 1H), 7.37 (m, 2H), 7.45 (m, 2H); $^{13}$C NMR (125.76 MHz, CD3OD) $\delta$ 29.0, 36.2, 52.9, 54.7, 56.5, 60.8, 60.9, 72.1, 112.7, 113.3, 115.1, 125.3, 125.9, 128.0, 128.6, 128.8, 129.1, 129.7, 129.8, 138.8, 146.5, 147.0, 148.3, 151.0; HRMS *m/z* 418.2009 (calcd. for $C_{26}H_{28}NO_4$, 418.2018, $\Delta_{m/z\text{theoretical}} = -2.15$ ppm).

**(*S*)-*O*, *O*-dibenzylstepholidine (1e)**: yellow powder (18.5 mg); $[\alpha]_D^{25} = -96.15^{\circ}$ (*c* 0.32, MeOH); $^1$H NMR (500 MHz, CD3OD) $\delta$ 2.71 (m, 1H), 2.65 (m, 2H), 3.08 (m, 1H), 3.21 (m, 1H), 3.25 (m, 1H), 3.52 (m, 2H), 3.82 (s, 3H), 3.86 (s, 3H), 4.21 (d, $J$ = 16.1 Hz, 1H), 5.02 (s, 2H), 5.08 (s, 2H), 6.71 (s, 1H), 6.85 (d, $J$ = 8.2 Hz, 1H), 6.86 (s, 1H), 6.92 (d, $J$ = 8.2 Hz, 1H), 7.30 (m, 2H), 7.36 (m, 4H), 7.44 (m, 4H); $^{13}$C NMR (125.76 MHz, CD3OD) $\delta$ 29.1, 36.3, 52.5, 54.7, 56.5, 60.6, 60.7, 71.9, 113.3, 113.6, 114.7, 125.1, 128.3, 128.6, 128.8, 128.91, 129.0, 130.2, 138.8, 146.8, 148.0, 150.1, 150.7; HRMS *m/z* 508.2473 (calcd. for $C_{33}H_{34}NO_4$, 508.2488, $\Delta_{m/z\text{theoretical}} = -2.95$ ppm).

## Molecular Docking

The docking studies were carried out according to a previously reported approach (Santos et al., 2016). First, the 3D structures of stepholidine and compounds **1a−1e** were generated and checked in relation to the protonated state in pH 7.4, and the tautomers via Marvin Sketch (ChemAxon, 2017). Then, to identify the optimized structures with the lowest energy, the structures were treated by the semi-empirical method PM7 (Stewart, 2013) using MOPAC2016 software (Stewart, 2016). The refined structures were converted into PDBQT files via Autodock tools (Morris et al., 2009). The three-dimensional crystal structure of *Tc*AChE complexed with galantamine was retrieved from the RCSB (Research Collaboratory for Structural Bioinformatics) protein data bank (http://www.rcsb.org) under PDB ID 1QTI (Bartolucci et al., 2001). The receptor preparation was as previously reported (Santos et al., 2016), in which the grid box was centered at the ligand to cover the entire binding site. Finally, a rigid docking process was carried out using Autodock Vina (Trott and Olson, 2010) with Discovery Studio (AccelrysInc, 2016) being used to analyze the binding conformations.

## Biological Evaluation Based on AChE-ICER Assay

AChE from *Electrophorus electricus* (type VI-S) was immobilized in a fused-silica capillary tube (*eel*AChE-ICER) according to a previously reported protocol (Vanzolini et al., 2013). An enzyme solution containing 2 units/mL *eel*AChE was used in the immobilization procedure. The LC-MS system was set up for the *eel*AChE-ICER as previously described (Vanzolini et al., 2013). The mobile phase (15 mM ammonium acetate solution, pH 8.0) was infused by pump 1 at a flow rate of 50 μL/min and pump 2 delivered acetonitrile after the *eel*AChE-ICER at a flow rate of 50 μL/min. IT-MS parameters were: 3,713 V capillary voltage, 500 V end plate voltage, 7.0 mL/min drying gas, 300°C drying temperature and 30 psi nebulizer. In addition, ACh ($[M+H]^+$ *m/z* 146) and Ch ($[M+H]^+$ *m/z* 104), were analyzed by MS operating in the manual $MS^n$ mode under positive ionization (scan 50–550 *m/z*). Enzymatic activity was quantified using a Ch standard external calibration curve prepared in 15 mM ammonium acetate solution, pH 8.0 with the final concentration ranging from 5 to 350 μM. An aliquot (10 μL) of each solution was injected in triplicate into the system using an empty fused silica capillary. The calibration curve was obtained by plotting the Ch $[M+H]^+$ *m/z* 104 area against the injected Ch concentration.

The derivatives compounds **1a−1e**, stepholidine and galantamine were screened with *eel*AChE-ICER. Stock solutions of each compound were prepared in methanol at 1.0 mM. The enzymatic activity of *eel*AChE-ICER was measured in the presence and absence of each compound. Reactions mixtures were prepared by mixing 20 μL of ACh stock solution (350 μM, in 15mM ammonium acetate solution, pH 5.0) with 10 μL of methanol or stock solution of compounds (1.0 mM) and 70 μL ammonium acetate solution (15mM, pH 8.0). Each reaction mixture (10 μL) was injected into the LC-MS system. The percentage of inhibition (%I) was calculated by comparing the product peak area in the presence of tested compound with positive control (absence of inhibitors).

Inhibitory potency ($IC_{50}$) for galantamine and compounds (**1a** and **1b**) was obtained by directly quantifying Ch production in the presence of different concentrations of inhibitors. Stock solutions of galantamine (50–4,000 μM), derivatives **1a** and **1b** (both at 10–5,000 μM) were prepared in methanol. Reactions mixtures were prepared by mixing 20 μL of ACh stock solution (500 μM, in 15 mM ammonium acetate solution, pH 5.0) with 10 μL of stock solution of galantamine, **1a** or **1b**. Final volumes were completed with 70 μL ammonium acetate solution (15mM, pH 8.0) and each reaction mixture (10 μL) was injected into the LC-MS system. The inhibition curve was obtained for each sample by plotting the percentage of inhibition vs. each corresponding inhibitor concentration, and the $IC_{50}$ values were achieved by non-linear regression analysis using GraphPad Prism 5 software.

The mechanism of action and its steady-state inhibition constant ($K_i$) were also determined for derivatives **1a** and **1b**. For this purpose, the *eel*AChE-ICER activity was evaluated under different concentrations of ACh (10 to 150 μM) and at the fixed concentration of derivative **1a** and **1b** (0, 10, 50, and 75 μM). Lineweaver-Burk plots were used to determine the action mechanism for the inhibitors.

$K_i$ values for **1a** and **1b** were determined from the slope of the Lineweaver-Burk plots vs. the respective derivative concentration. A linear replot was obtained, and the division quotient between the linear and angular coefficients provided the Ki values.

# RESULTS AND DISCUSSION

## Molecular Docking of *N*-benzyl and *O*-benzyl Stepholidine Derivatives

The ligand binding pocket of *Tc*AChE is heavily hydrophobic and largely lined by aromatic residues, thus suggesting that an increase in *in vitro* potency could be, theoretically, achievable by the accommodation of compounds with favored π-π stacking interactions in the binding pocket. Therefore, a preliminary docking study was conducted with the tetrahydroprotoberberine alkaloid stepholidine, a neuroprotective natural product, abundant in the Amazonian species *O. amazonicum* (Yang et al., 2007; Hao et al., 2015; Lima et al., 2019) and a series of its *N*-benzyl and *O*-benzyl derivatives. This was achieved by

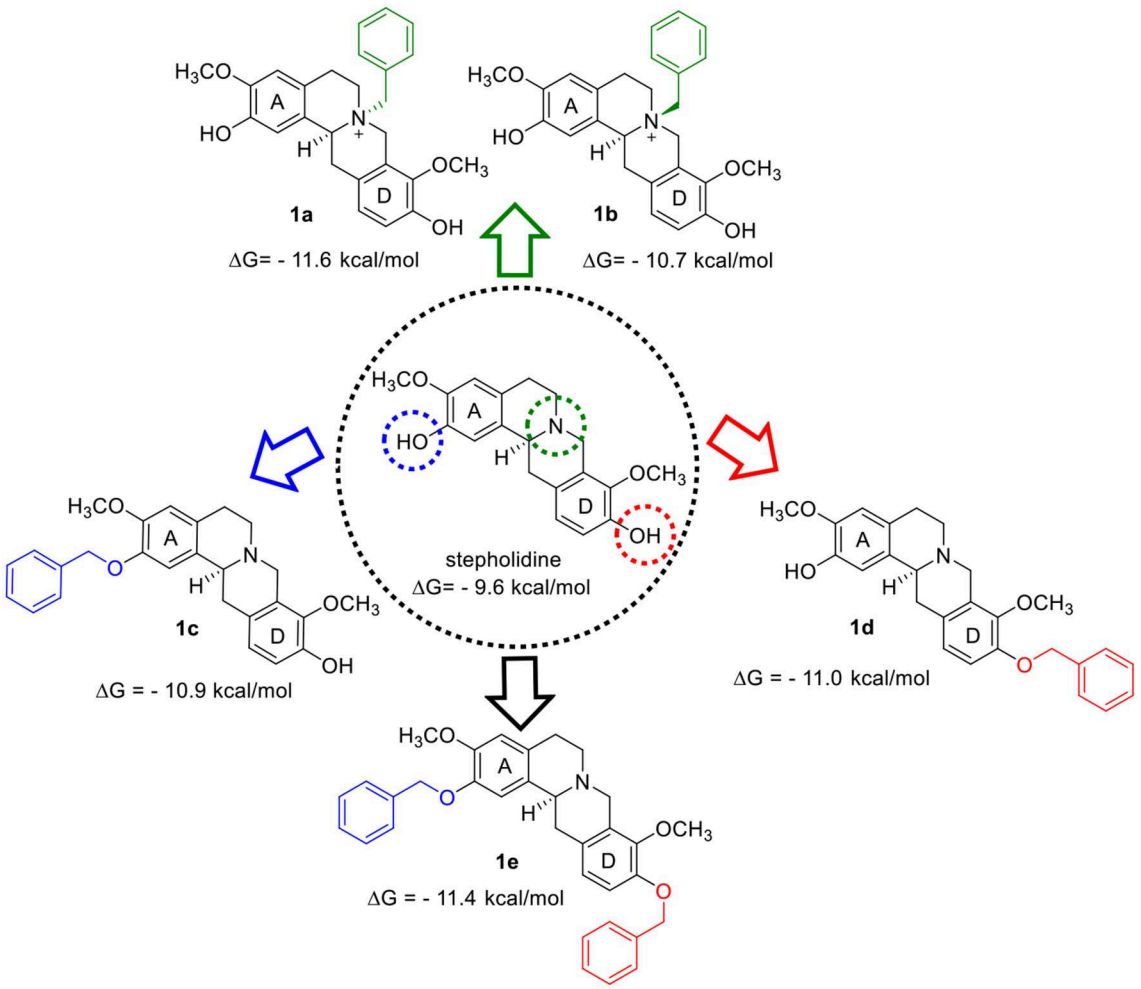


**FIGURE 1 |** Design of the AChEIs from the benzylation of stepholidine.

comparison of their binding energy and main interactions in the crystallographic structure with the galanthamine-*Tc*AChE complex, since this model has already been successfully applied in virtual screening approaches of AChEIs (Rollinger et al., 2004, 2009).

Compounds **1a−1e** (**Figure 1**) presented better scoring function values than stepholidine and galantamine (redocking binding free energy = −9.6 kcal/mol, RMSD < 2), which suggests the establishment of new favorable interactions for the ligands-*Tc*AChE complex. Since the active-site gorge of *Tc*AChE contains two subsites, esteratic and anionic, which correspond to the catalytic machinery (Ser200, Glu327 and His440) and the choline-binding pocket (Trp84 and Phe330), respectively, we therefore focused our interpretation on these interactions, in addition to the interactions in peripheral subsite (Trp279) (Dvir et al., 2010).

Here, the observed interactions for galantamine (**Figure 2A**) were similar to the one described by Bartolucci et al. (2001). The oxygen atom of the *O*-methyl group participated in hydrogen bonding with Ser200 from the esteratic subsite, while its hydroxyl oxygen formed hydrogen bonds with residues Gly118 and Glu199. Also, π-alkyl interactions were observed with Trp84 and Phe330 at the anionic subsite. On the other hand, stepholidine showed π-π stacking interactions of A and D aromatic rings, respectively with the anionic (Trp84 and Phe330) and peripheral subsites (Trp279) (**Figure 2B**).

Compound **1a**, a *N*-benzyl derivative, showed that the oxygen atom of the *O*-methyl group from the D ring established a hydrogen bonding with Ser200 from esteratic subsite (**Figures 3A,B**), similar to galantamine. Besides, the aromatic D ring and the positively charged nitrogen presented π-π stacked and π-cation interactions with Trp84 and Phe330 from the anionic subsite, respectively, which contrasts with the π-alkyl interactions from galantamine. In addition, π-π interaction was observed between the benzyl moiety and the Tyr334, and hydrogen bond interactions between the hydroxyl oxygen from the A aromatic ring with Asn85. On the other hand, compound **1b**, an epimer of **1a**, presented π-π stacked interactions between

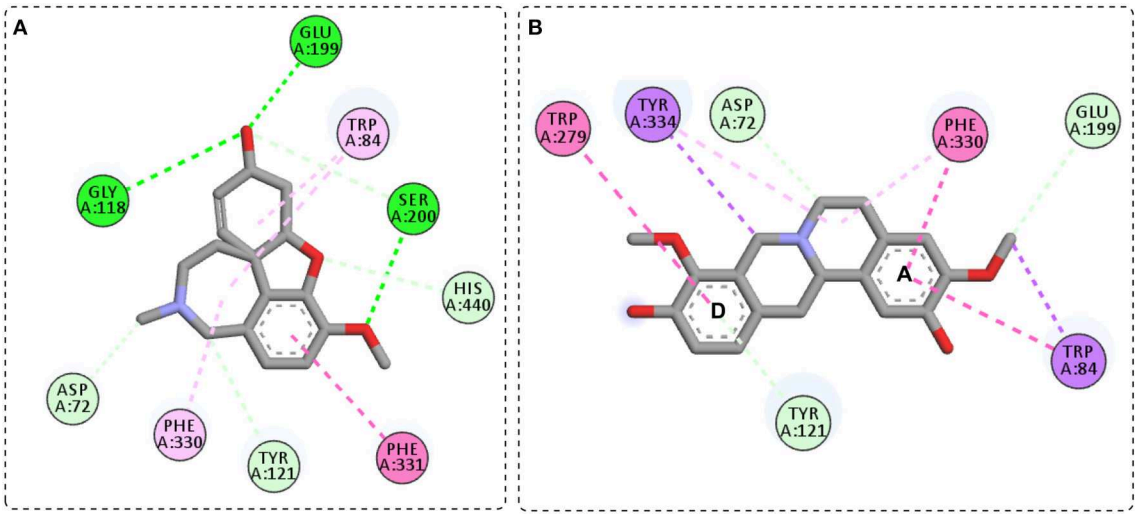


**FIGURE 2 |** General interactions for galantamine-*Tc*AChE **(A)** and stepholidine-*Tc*AChE **(B)** complex.

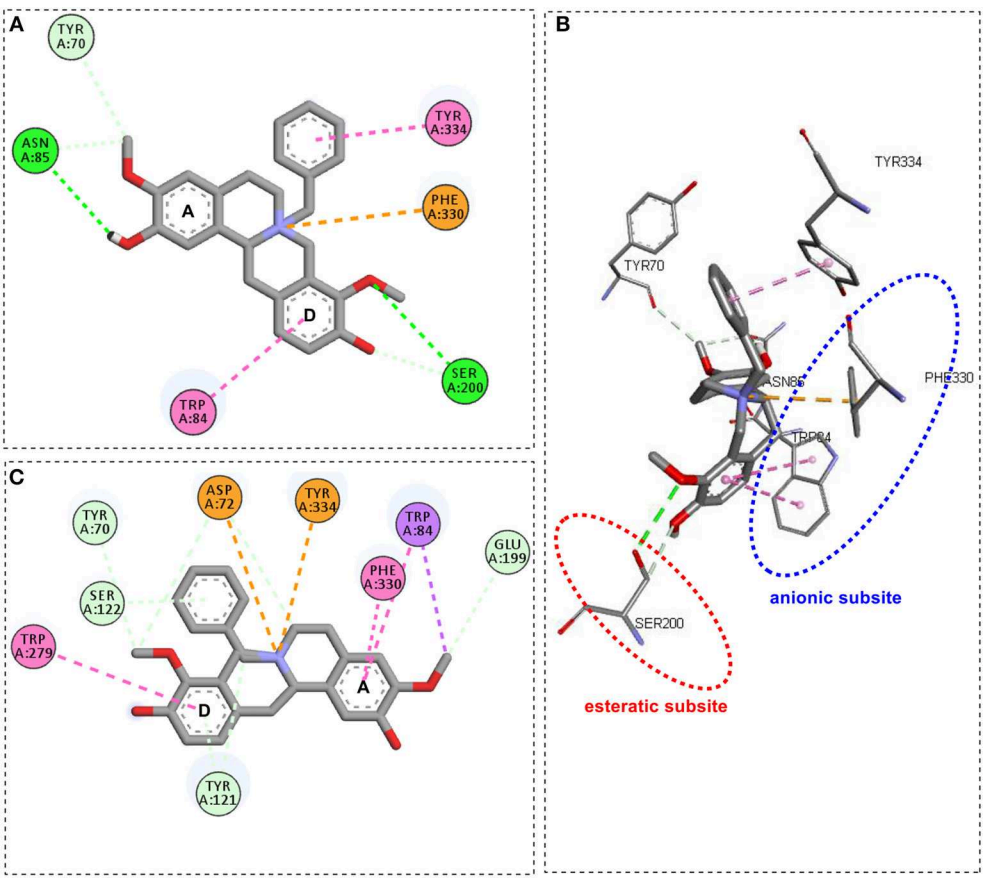


**FIGURE 3 |** General interactions for compound **1a**-*Tc*AChE complex by 2D diagram **(A)** and 3D view **(B)**, and compound **1b**-*Tc*AChE complex by 2D diagram **(C)**.

the A and D aromatic ring and the anionic (Trp84 and Phe330) and peripheral subsites (Trp279) (**Figure 3C**), similarly to stepholidine. Besides this, the positively charged nitrogen presented π-cation and attractive charge interactions with Asp72 and Tyr334, respectively. Surprisingly, no relevant interaction was observed for the benzyl moiety.

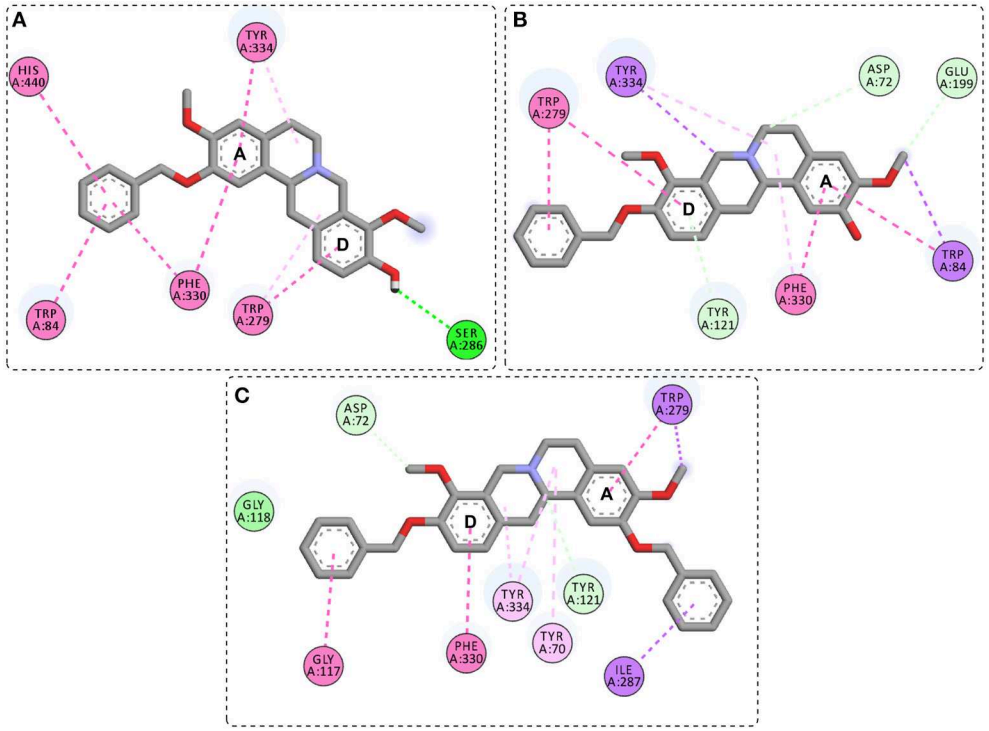


**FIGURE 4 |** General interactions between compound **1c (A)**, **1d (B)**, and **1e (C)**, and the *Tc*AChE enzyme by 2D diagram.

Compound **1c**, an *O*-benzyl derivative, presented several π-π type interactions (**Figure 4A**), highlighting those between benzyl moiety from A ring and Trp84, Phe330 and His440, therefore they comprise part of the catalytic machinery and the choline-binding pocket of *Tc*AChE. The A ring also showed π-π interactions with the residues Phe330 and Tyr334. In addition to the Trp279 interaction in the D ring, also observed in the stepholidine and compound **1b**, a hydrogen bond between the hydroxyl oxygen and Ser286 was observed. Compound **1d**, another *O*-benzyl derivative, displayed similar interactions with stepholidine, except for the π-π stacked between the benzyl moiety from D ring and Trp279 from the peripheral subsite (**Figure 4B**). On the other hand, for compound **1e**, an *O*, *O*-dibenzyl derivative, the interactions of Phe330 and Trp279 with the A and D aromatic rings (**Figure 4C**) were reversed in relation to compounds **1b**, **1d** and stepholidine. Also, for the benzyl moieties, π-sigma and π-π stacked interactions were observed with Ile287 and Gly117, respectively.

Taking into account the docking analysis, it can be perceived that π-π interactions are dominant in compound series **1a−1e** with key interactions with residues from esteratic, anionic and peripheral subsites. It was also construed that the *N*-benzyl derivatives, given their interaction similarities with galantamine in the *Tc*AChE complex, would favor the activity.

Remarkably, the stepholidine *N*-benzyl and *O*-benzyl derivatives showed higher scoring values than either galantamine or stepholidine. Therefore, compounds **1a−1e** were synthesized following reaction steps described at **Scheme 1**, followed by full characterization and, then, submitted to inhibition screening.

## Structural Determination

The MS and $^1$H NMR spectra of SRF (**Supplementary Material**) displayed signals that were consistent with the stepholidine structure, which is in agreement with a recently published study about the *O. amazonicum* alkaloid content (Lima et al., 2019). On the other hand, the stepholidine concentration in the SRF was determined as being >85% based on the integration of the aromatic signals in the $^1$H NMR spectrum. To evaluate the stereochemistry of the 13a position in the stepholidine and of compounds **1a−1e**, stepholidine previously isolated from *O. amazonicum* (Lima, 2005) was subjected to polarimetric analysis, and presented $[\alpha]_D^{25} = -231.69°$ (*c* 0.19, MeOH), this value was in accordance with the 13a*S* configuration (Chen and Yang, 2009).

Compound **1a** was obtained as a yellow amorphous powder. Its molecular formula was determined as $C_{26}H_{28}NO_4$ by HRMS (obs. *m/z* 418.2011; calcd. 418.2018, $\Delta_{m/z\text{theoretical}} = -1.67$ ppm). The MS/MS spectrum of the ion at *m/z* 418 presented two main neutral losses of 92 (*m/z* 326) and 150 Da (*m/z* 268), which are consistent with a tetrahydroprotoberberine alkaloid containing methoxyl and hydroxyl groups at D ring (Lima et al., 2019) and an *N*-benzyl group (Kuck et al., 2011). Ratifying the MS analysis, the $^1$H NMR exhibited signals of an *ortho*-substituted ring at $\delta_H$ 7.12 (d, $J$ = 8.3 Hz, 1H) and 7.03 (d, $J$ = 8.3 Hz, 1H), as well

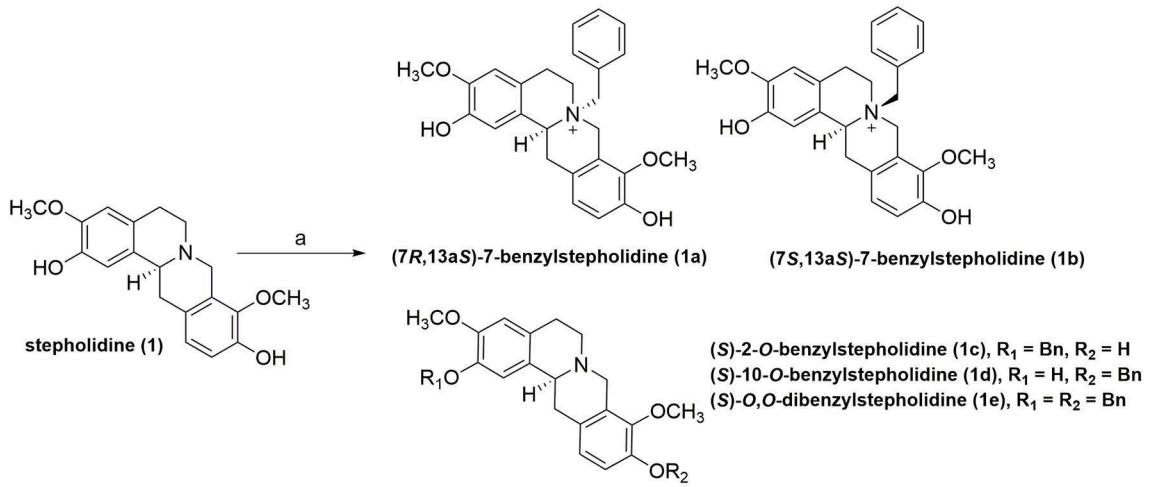


**SCHEME 1 |** One-step synthesis of compounds **1a–1e**[a].

signals of a *para*-substituted ring at $\delta_H$ 6.96 (s) and 6.78 (s), and two methoxyl signals at $\delta_H$ 3.93 (s) and 3.84 (s), all typical signals of the stepholidine structure (Lima et al., 2019), while the benzyl signals were observed at $\delta_H$ 7.54 (m, 1H), 7.49 (m, 2H), 7.27 (m, 2H), and 4.29 (d, $J$ = 4.9 Hz, 2H). The confirmation of the *N*-benzylation was achieved via the heteronuclear multiple bond correlation (HMBC) experiment. In this, $J^3$-couplings for the benzyl methylene protons at $\delta_H$ 4.29 (m, 2H) with the carbons at $\delta_C$ 52.4 and 58.3 confirmed our hypothesis. The stereochemistry of the 13a position was assigned as *S* based on the precursor stereochemistry, and a negative value was also observed in the polarimetric analysis ($[\alpha]_D^{25} = -33.88°$, *c* 0.072, MeOH). Due to the observation of a nuclear Overhauser effect (NOE) between the benzyl methylene protons at $\delta_H$ 4.29 and the methine proton at $\delta_H$ 5.26 (dd, $J$ = 12.2, 5.9 Hz, 1H) in the nuclear Overhauser enhancement spectroscopy (NOESY) spectrum, the stereochemistry of the nitrogen atom was confirmed as *R*. Therefore, compound **1a** was determined as being the previously undescribed tetrahydroprotoberberine alkaloid named (7*R*,13a*S*)-7-benzylstepholidine.

Compound **1b** was obtained as a yellow amorphous powder. Its molecular formula was determined as $C_{26}H_{28}NO_4$ by HRMS (obs. *m/z* 418.2001; calcd. 418.2018, $\Delta_{m/z\text{theoretical}}$ = −4.06 ppm). A comparative analysis of the MS and NMR data for compounds **1a** and **1b** indicated the same structure. Since they were separated via HPLC, it was assumed that **1b** was a diastereomer of **1a**. Similarly, for compound **1a**, the stereochemistry of the 13a position for compound **1b** was assigned as *S* based on the precursor stereochemistry, and a negative value was also observed in the polarimetric analysis ($[\alpha]_D^{25} = -35.10°$, *c* 0.082, MeOH). Due to the observation of a NOE effect between the benzyl methylene proton at $\delta_H$ 4.66 and the methylene proton at $\delta_H$ 3.50 (m, 1H) in the NOESY spectrum, the stereochemistry of the nitrogen atom was confirmed as *S*. Therefore, compound **1b** was determined as being the previously undescribed tetrahydroprotoberberine alkaloid named (7*S*,13a*S*)-7-benzylstepholidine.

Compound **1c** was obtained as a yellow amorphous powder. Its molecular formula was determined as $C_{26}H_{28}NO_4$ by HR-MS (obs. *m/z* 418.2010; calcd. 418.2018, $\Delta_{m/z\text{theoretical}} = -1.91$ ppm). The MS/MS spectrum of the ion at *m/z* 418 presented two main neutral losses of 91 (*m/z* 327) and 150 Da (*m/z* 268), which are consistent with a tetrahydroprotoberberine alkaloid contain methoxyl and hydroxyl groups at D ring (Lima et al., 2019) and an *O*-benzyl group (Kuck et al., 2011). Ratifying the MS analysis, the $^1$H NMR also exhibited typical signals of the stepholidine structure. The aromatic benzyl signals were observed at $\delta_H$ 7.44 (m, 2H), 7.37 (m, 1H), 7.29 (m, 2H), while the methylene signals were observed at $\delta_H$ 5.09 (s, 2H). The confirmation of the *O*-benzylation at A ring was reached via the $J^3$-couplings for the benzyl methylene protons at $\delta_H$ 5.09

**TABLE 1 |** Inhibition percentages of *N*-benzyl and *O*-benzyl stepholidine derivatives against *ee*lAChE.

| Compound | % Inhibition *ee*lAChE-ICER |
|---|---|
| Galantamine | 95.8 ± 1.87 |
| Stepholidine | 40.2 ± 1.65 |
| **1a** | 90.1 ± 2.04 |
| **1b** | 90.5 ± 2.48 |
| **1c** | 35.2 ± 5.02 |
| **1d** | 46.3 ± 5.45 |
| **1e** | 43.6 ± 2.54 |

(s, 2H) with the carbon at $\delta_C$ 148.1 in the HMBC experiment. The stereochemistry of the 13a position was assigned as *S* based on the precursor stereochemistry, a negative value was also observed in the polarimetric analysis ($[\alpha]_D^{25} = -387.60°$, *c* 0.26, MeOH). Therefore, compound **1c** was determined as the previously described tetrahydroprotoberberine alkaloid named (*S*)-2-*O*-benzylstepholidine.

Compound **1d** was obtained as a yellow amorphous powder. Its molecular formula was determined as $C_{26}H_{28}NO_4$ by HRMS (obs. *m/z* 418.2009; calcd. 418.2018, $\Delta_{m/z\text{theoretical}} = -2.15$ ppm). A comparison between the MS and NMR data of compounds **1c** and **1d** indicated that these compounds shared similar skeleton, as the position of the *O*-benzyl group was the main difference between them. The confirmation of the *O*-benzylation at D ring was achieved via the $J^3$-couplings for the benzyl methylene protons at $\delta_H$ 5.08 (s, 2H) with the carbon at $\delta_C$ 150.9 in the HMBC experiment. The stereochemistry of the 13a position was also assigned as *S* based on the precursor stereochemistry, a negative value was also observed in the polarimetric analysis ($[\alpha]_D^{25} = -146.02°$, *c* 0.42, MeOH). Therefore, compound **1d** was determined as being the previously undescribed tetrahydroprotoberberine alkaloid named (*S*)-10-*O*-benzylstepholidine.

Compound **1e** was obtained as a yellow amorphous powder. Its molecular formula was determined as $C_{33}H_{34}NO_4$ by HRMS (obs. *m/z* 508.2473; calcd. 508.2488, $\Delta_{m/z\text{theoretical}} = -2.95$ ppm). A comparison between the MS and NMR data of compounds **1c**, **1d**, and **1e** indicated that **1e** shared similar *O*-benzyl positions with **1c** and **1d**. This was confirmed via the $J^3$-couplings for the benzyl methylene protons at $\delta_H$ 5.08 (s, 2H) and 5.02 (s, 2H) with the carbons at $\delta_C$ 147.9 and 150.6, respectively, in the HMBC experiment. The stereochemistry of the 13a position was also assigned as being *S* based on the precursor stereochemistry, a negative value was also observed in the polarimetric analysis ($[\alpha]_D^{25} = -96.15°$, *c* 0.32, MeOH). Therefore, compound **1e** was determined as the previously described tetrahydroprotoberberine alkaloid named (*S*)-*O*,*O*-dibenzylstepholidine.

## Biological Evaluation Based on AChE-ICER Assay

It is well-accepted that docking studies are carried out using *Tc*AChE due to the availability of its crystal structure and the established knowledge of ligand interactions for this enzyme (Houghton et al., 2006; Mohamed and Rao, 2010; Gupta et al., 2011). In the case of inhibition assays, the use of *eel*AChE is also well-accepted as a substitute for human AChE (Mohamed and Rao, 2010; Gupta et al., 2011; Vanzolini et al., 2013). Moreover, both enzymes have conserved primary sequences in the active residues (Gupta et al., 2011). Thus, stepholidine and its derivatives **1a**–**1e** were screened by the inhibition *eel*AChE-ICER on flow assay. ACh was used as substrate, while galantamine was used as a positive control. The results of inhibition percentages are given in **Table 1**.

The screening assay disclosed compound **1a** and its epimer **1b** as the inhibitors (**Table 1**), with inhibition values close to those obtained for galantamine, while compounds **1c**-**1e** and stepholidine presented values below 50%. Thus, $IC_{50}$ values were

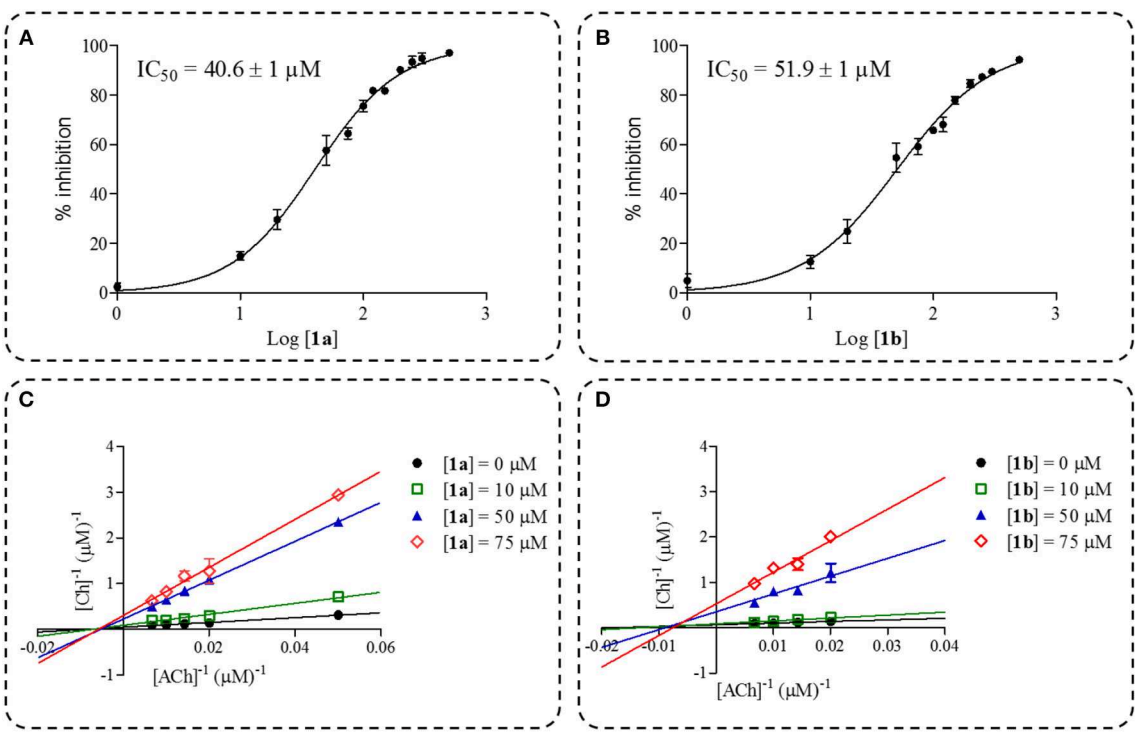


**FIGURE 5 |** Dose-response curve plots of inhibition percentage for compound **1a (A)** and **1b (B)**. Double-reciprocal plots for compound **1a (C)** and **1b (D)**.

determined only for these two compounds, in which the values obtained were of 40.6 ± 1 for **1a** and 51.9 ± 1 μM for **1b** (**Figures 5A,B**). Regarding the increase in activity observed for compounds **1a** and **1b**, this is in accordance with a previous published study (Loizzo et al., 2008) which was carried out with stepholidine ($IC_{50}$ > 100 μM), *N*-methyl stepholidine ($IC_{50}$ = 31.30 μM) and stepharanine ($IC_{50}$ = 14.10 μM), and which showed that stepholidine has significantly less activity than its quaternary derivatives. This suggests that a positive charge at the nitrogen portion can influence AChE inhibitory activity.

In spite of the $IC_{50}$ values of compounds **1a** and **1b** being higher when compared to galantamine under the same experimental conditions ($IC_{50}$ = 17.1 ± 1.1 μM), the mechanism of inhibition and $K_i$ were determined and, both inhibitors **1a** ($K_i$ = 11.6 μM) and **1b** ($K_i$ = 4.7 μM) substantially reduced the rate of the enzymatic reaction, which illustrates a characteristic behavior of non-competitive inhibitors as observed in the double-reciprocal plots (**Figures 5C,D**).

The evaluation of inhibition modality is a relevant assessment in the early stages of drug discovery programs, since the mode of interaction could be affected, however this depends on the physiological contexts to which the enzyme is exposed. As an example, competitive inhibitors bind exclusively to the free enzyme form, while non-competitive or mixed type inhibitors bind with some affinity to both forms e.g., the free enzyme and the enzyme-substrate complex. Thus, the non-competitive inhibition modality can be a significant advantage *in vivo* when the physiological context exposes the enzyme to high substrate concentrations. Although the clinical advantage of non-competitive inhibition has been recognized, there are a very large number of drugs in clinical use today that are competitive enzyme inhibitors, and which can be related to historical approaches for drug discovery that have been focused on active site-directed inhibitors (Copeland, 2016). Here, we presented two benzyl analogs from stepholidine that act via the non-competitive mechanism. The mechanistic differences between compounds **1a**, **1b** and galantamine could be assigned to the π-π interactions with Trp84 and Phe330, which were observed only for these two stepholidine derivatives with higher inhibitory potency. These results highlight the importance of the π-π interaction for the ligands and thus can be used for designing non-competitive AChEIs, which explore the clinical advantages of this inhibition modality.

## CONCLUSION

The proposed approach, which is based on the design of new tetrahydroprotoberberine alkaloids with increased π-π stacking interactions in the ligand binding pocket followed by inhibition analysis through AChE-ICER assay, proved to be a useful strategy for the identification of new AChEIs. Docking analysis results suggest an increase in the inhibition potency for the *N*-benzyl and *O*-benzyl derivatives when compared to the precursor stepholidine, which was corroborated by the biological inhibition data. In addition, the biological results showed that *N*-benzyl stepholidine derivatives are more active than *O*-benzyl derivatives, which suggests that the quaternary nitrogen plays a key role in AChE inhibition. These observations, along with key interactions observed in docking analysis, can be useful in the design of new AChEIs. Overall, the proposed approach demonstrated the usefulness of stepholidine as a suitable template for the design of rational AChEIs and demonstrated how the target-alkaloid derivatives interact with AChE.

## DATA AVAILABILITY

All datasets generated for this study are included in the manuscript/**Supplementary Files.**

## AUTHOR CONTRIBUTIONS

BL and FS were responsible for the molecular docking. BL and JM prepared the stepholidine-rich fraction. BL, CV, and EL were responsible for the synthesis procedure. BL, RN, and AS were responsible for the compounds isolation. BL, HK, FS, and MP were responsible for the characterization of compounds. BL, JL, and QC were responsible for the biological assays. BL, JL, HK, FS, and QC drafted the manuscript and all the other authors contributed to the intellectual content and revision of the manuscript.

## FUNDING

The authors were grateful to Coordenação de Aperfeiçoamento de Pessoal de Nível Superior–Brazil (CAPES) (Finance Code 001; research grant 23038.000726/2013-43), National Council for Scientific and Technological Development (CNPq) FINEP, FAPEAM, São Paulo State Research Foundation-FAPESP (Research grants 2013/01710-1, 2014/50249-8, and 2014/50244-6), Central Analítica (UFAM), and GSK for the financial support.

## SUPPLEMENTARY MATERIAL

The Supplementary Material for this article can be found online at: https://www.frontiersin.org/articles/10.3389/fchem.2019.00629/full#supplementary-material

## REFERENCES

AccelrysInc (2016). *Discovery Studio Visualizer. V 16.1.0.* San Diego, CA: AccelrysInc.

Adams, M., Gmünder, F., and Hamburger, M. (2007). Plants traditionally used in age related brain disorders-a survey of ethnobotanical literature. *J. Ethnopharmacol.* 113, 363–381. doi: 10.1016/j.jep.2007.07.016

Almasieh, M., MacIntyre, J. N., Pouliot, M., Casanova, C., Vaucher, E., Kelly, M. E., et al. (2013). Acetylcholinesterase inhibition promotes retinal vasoprotection and increases ocular blood flow in experimental glaucoma. *Investig. Ophthalmol. Vis. Sci.* 54, 3171–3183. doi: 10.1167/iovs.12-11481

Almeida, M. E. L., Braz-Filho, R., von Bülow, V., Gottlieb, O. R., and Maia, J. G. S. (1976). Onychine, an alkaloid from *Onychopetalum amazonicum*. *Phytochemistry* 15, 1186–1187. doi: 10.1016/0031-9422(76)85134-5

Anand, P., and Singh, B. (2013). A review on cholinesterase inhibitors for Alzheimer's disease. *Arch. Pharmacal. Res.* 36, 375–399. doi: 10.1007/s12272-013-0036-3

Andrisano, V., Bartolini, M., Gotti, R., Cavrini, V., and Felix, G. (2001). Determination of inhibitors' potency ($IC_{50}$) by a direct high-performance liquid chromatographic method on an immobilised acetylcholinesterase column. *J. Chromatogr. B* 753, 375–383. doi: 10.1016/S0378-4347(00)00571-5

Atanasova, M., Stavrakov, G., Philipova, I., Zheleva, D., Yordanov, N., and Doytchinova, I. (2015). Galantamine derivatives with indole moiety: docking, design, synthesis and acetylcholinesterase inhibitory activity. *Bioorg. Med. Chem.* 23, 5382–5389. doi: 10.1016/j.bmc.2015.07.058

Bartolucci, C., Perola, E., Pilger, C., Fels, G., and Lamba, D. (2001). Three-dimensional structure of a complex of galanthamine (Nivalin) with acetylcholinesterase from *Torpedo californica*: Implications for the design of new anti-Alzheimer drugs. *Proteins* 42, 182–191. doi: 10.1002/1097-0134(20010201)42:2<182::AID-PROT50>3.0.CO;2-1

ChemAxon (2017). *MarvinSketch 17.1.2.0*. Budapest: ChemAxon.

Chen, J. J., and Yang, Y. S. (2009). Enantioselective total synthesis of (-)-(*S*)-stepholidine. *J. Org. Chem.* 74, 9225–9228. doi: 10.1021/jo9020826

Copeland, R. A. (2016). The drug-target residence time model: a 10-year retrospective. *Nat. Rev. Drug Discov.* 15, 87–95. doi: 10.1038/nrd.2015.18

Cragg, G. M., Newman, D. J., and Snader, K. M. (1997). Natural products in drug discovery and development. *J. Nat. Prod.* 60, 52–60. doi: 10.1021/np9604893

Cui, L., Wang, Y., Liu, Z., Chen, H., Wang, H., Zhou, X., et al. (2015). Discovering new acetylcholinesterase inhibitors by mining the *Buzhongyiqi* decoction recipe data. *J. Chem. Inform. Model.* 55, 2455–2463. doi: 10.1021/acs.jcim.5b00449

Deka, P., Kumar, A., Nayak, B. K., and Eloziia, N. (2017). Some plants as a source of acetyl cholinesterase inhibitors: a review. *Int. Res. J. Pharm.* 8, 5–13. doi: 10.7897/2230-8407.08565

Dvir, H., Silman, I., Harel, M., Rosenberry, T. L., and Sussman, J. L. (2010). Acetylcholinesterase: from 3D structure to function. *Chem. Biol. Interact.* 187, 10–22. doi: 10.1016/j.cbi.2010.01.042

Ellman, G. L., Courtney, K. D., Andres Jr., V., and Featherstone, R. M. (1961). A new and rapid colorimetric determination of acetylcholinesterase activity. *Biochem. Pharmacol.* 7, 88–95. doi: 10.1016/0006-2952(61)90145-9

Gupta, S., Fallarero, A., Järvinen, P., Karlsson, D., Johnson, M. S., Vuorela, P. M., et al. (2011). Discovery of dual binding site acetylcholinesterase inhibitors identified by pharmacophore modeling and sequential virtual screening techniques. *Bioorgan. Med. Chem. Lett.* 21, 1105–1112. doi: 10.1016/j.bmcl.2010.12.131

Hao, J. R., Sun, N., Lei, L., Li, X. Y., Yao, B., Sun, K., et al. (2015). L-Stepholidine rescues memory deficit and synaptic plasticity in models of Alzheimer's disease via activating dopamine D1 receptor/PKA signaling pathway. *Cell Death Dis.* 6, 1–12 doi: 10.1038/cddis.2015.315

Harvey, A. L. (2008). Natural products in drug discovery. *Drug Discov. Today* 13, 894–901. doi: 10.1016/j.drudis.2008.07.004

Högenauer, K., Baumann, K., Enz, A., and Mulzer, J. (2001). Synthesis and acetylcholinesterase inhibition of 5-desamino huperzine A derivatives. *Bioorg. Med. Chem. Lett.* 11, 2627–2630. doi: 10.1016/S0960-894X(01)00518-2

Hostalkova, A., Marikova, J., Opletal, L., Korabecny, J., Hulcova, D., Kunes, J., et al. (2019). Isoquinoline alkaloids from *Berberis vulgaris* as potential lead compounds for the treatment of Alzheimer's disease. *J. Nat. Prod.* 82, 239–248. doi: 10.1021/acs.jnatprod.8b00592

Houghton, P. J., Ren, Y., and Howes, M. J. (2006). Acetylcholinesterase inhibitors from plants and fungi. *Nat. Prod. Rep.* 23, 181–199. doi: 10.1039/b508966

Karimova, E. R., Spirikhin, L. V., Baltina, L. A., and Abdullin, M. I. (2014). Synthesis and identification of quercetin benzyl ethers. *Russ. J. Gen. Chem.* 84, 1711–1715. doi: 10.1134/S1070363214090126

Kashiwada, Y., Aoshima, A., Ikeshiro, Y., Chen, Y. P., Furukawa, H., Itoigawa, M., et al. (2005). Anti-HIV benzylisoquinoline alkaloids and flavonoids from the leaves of *Nelumbo nucifera*, and structure-activity correlations with related alkaloids. *Bioorg. Med. Chem.* 13, 443–448. doi: 10.1016/j.bmc.2004.10.020

Kuck, D., Grützmacher, H. F., Barth, D., Heitkamp, S., and Letzel, M. C. (2011). The role of ion/neutral complexes in the fragmentation of *N*-benzyl-(alkylpyridinium) ions. *Int. J. Mass Spectr.* 306, 159–166. doi: 10.1016/j.ijms.2010.10.006

Lima, B. R. (2005). *Estudo fitoquímico de Onychopetalum amazonicum R. E. Fr. (Annonaceae)* (Dissertation/Master's thesis), Federal University of Amazonas, Manaus, Brazil.

Lima, B. R., Silva, F. M. A., Soares, E. R., Almeida, R. A., Silva Filho, F. A., Pereira Junior, R. C., et al. (2016). Chemical composition and antimicrobial activity of the essential oils of *Onychopetalum amazonicum* RE Fr. *Nat. Prod. Res.* 30, 2356–2359. doi: 10.1080/14786419.2016.1163691

Lima, B. R., Silva, F. M. A., Soares, E. R., Almeida, R. A., Silva-Filho, F. A., Barison, A., et al. (2019). Integrative approach based on leaf spray mass spectrometry, HPLC-DAD-MS/MS, and NMR for comprehensive characterization of isoquinoline-derived alkaloids in leaves of *Onychopetalum amazonicum* R. E. Fr. *J. Braz. Chem. Soc.* 1–11. doi: 10.21577/0103-5053.20190125

Loizzo, M. R., Tundis, R., Menichini, F., and Menichini, F. (2008). Natural products and their derivatives as cholinesterase inhibitors in the treatment of neurodegenerative disorders: an update. *Curr. Med. Chem.* 15, 1209–1228. doi: 10.2174/092986708784310422

Lu, J. J., Bao, J. L., Chen, X. P., Huang, M., and Wang, Y. T. (2012). Alkaloids isolated from natural herbs as the anticancer agents. *Evid. Based Complement. Altern. Med.* 2012:485042. doi: 10.1155/2012/485042

Mantoani, S., Chierrito, T., Vilela, A., Cardoso, C., Martínez, A., and Carvalho, I. (2016). Novel triazole-quinoline derivatives as selective dual binding site acetylcholinesterase inhibitors. *Molecules* 21:193. doi: 10.3390/molecules21020193

Mohamed, T., and Rao, P. P. N. (2010). Design, synthesis and evaluation of 2,4-disubstituted pyrimidines as cholinesterase inhibitors. *Bioorgan. Med. Chem. Lett.* 20, 3606–3609. doi: 10.1016/j.bmcl.2010.04.108

Mohammad, D., Chan, P., Bradley, J., Lanctôt, K., and Herrmann, N. (2017). Acetylcholinesterase inhibitors for treating dementia symptoms–a safety evaluation. *Expert Opin. Drug Saf.* 16, 1009–1019. doi: 10.1080/14740338.2017.1351540

Morris, G. M., Huey, R., Lindstrom, W., Sanner, M. F., Belew, R. K., Goodsell, D. S., et al. (2009). AutoDock4 and AutoDockTools4: automated docking with selective receptor flexibility. *J. Comput. Chem.* 30, 2785–2791. doi: 10.1002/jcc.21256

Mukherjee, P. K., Kumar, V., Mal, M., and Houghton, P. J. (2007). Acetylcholinesterase inhibitors from plants. *Phytomedicine* 14, 289–300. doi: 10.1016/j.phymed.2007.02.002

Murray, A. P., Faraoni, M. B., Castro, M. J., Alza, N. P., and Cavallaro, V. (2013). Natural AChE inhibitors from plants and their contribution to Alzheimer's disease therapy. *Curr. Neuropharmacol.* 11, 388–413. doi: 10.2174/1570159X11311040004

Oliveira, A. N. D., and Amaral, I. L. D. (2004). Floristic and phytosociology of a slope forest in Central Amazonia, Amazonas, Brazil. *Acta Amazonica* 34, 21–34. doi: 10.1590/S0044-59672004000100004

Patel, S. S., Attard, A., Jacobsen, P., and Shergill, S. (2010). Acetylcholinesterase inhibitors (AChEI's) for the treatment of visual hallucinations in schizophrenia: a review of the literature. *BMC Psychiatry* 10:69. doi: 10.1186/1471-244X-10-69

Ribeiro, J. E. L. S., Hopkins, M. J. G., Vicentini, A., Sothers, C. A., Costa, M. A. S., Brito, J. M., et al. (1999). *Flora da Reserva Ducke: Guia de Identificação das Plantas Vasculares de uma Floresta de Terra Firme na Amazônia Central*. Vol. 1. Manaus: INPA.

Rollinger, J. M., Hornick, A., Langer, T., Stuppner, H., and Prast, H. (2004). Acetylcholinesterase inhibitory activity of scopolin and scopoletin discovered by virtual screening of natural products. *J. Med. Chem.* 47, 6248–6254. doi: 10.1021/jm049655r

Rollinger, J. M., Schuster, D., Danzl, B., Schwaiger, S., Markt, P., Schmidtke, M., et al. (2009). *In silico* target fishing for rationalized ligand discovery exemplified on constituents of *Ruta graveolens*. *Planta Med.* 75, 195–204. doi: 10.1055/s-0028-1088397

Sangi, D. P., Monteiro, J. L., Vanzolini, K. L., Cass, Q. B., Paixão, M. W., and Corrêa, A. G. (2014). Microwave-assisted synthesis of *N*-heterocycles and their evaluation using an acetylcholinesterase immobilized capillary reactor. *J. Braz. Chem. Soc.* 25, 887–889. doi: 10.5935/0103-5053.20140056

Santos, J. O., Pereira, G. R., Brandão, G. C., Borgati, T. F., Arantes, L. M., Paula, R. C., et al. (2016). Synthesis, *in vitro* antimalarial activity and *in silico* studies of hybrid kauranoid 1,2,3-triazoles derived from naturally occurring diterpenes. *J. Braz. Chem. Soc.* 27, 551–565. doi: 10.5935/0103-5053.20150287

Seidl, C., Vilela, A. F. L., Lima, J. M., Leme, G. M., and Cardoso, C. L. (2019). A novel on-flow mass spectrometry-based dual enzyme assay. *Anal. Chim. Acta* 1072, 81–86. doi: 10.1016/j.aca.2019.04.057

Silva, F. M. A., Lima, B. R., Soares, E. R., Almeida, R. A., Silva Filho, F. A., Corrêa, W. R., et al. (2015). Polycarpol in *Unonopsis*, *Bocageopsis* and *Onychopetalum* Amazonian species: chemosystematical implications and antimicrobial evaluation. *Rev. Brasil. Farmacog.* 25, 11–15. doi: 10.1016/j.bjp.2015.01.003

Soares, E. R., Silva, F. M., Almeida, R. A., Lima, B. R., Silva-Filho, F. A., Barison, A., et al. (2015). Direct infusion ESI-IT-MSn alkaloid profile and isolation of tetrahydroharman and other alkaloids from *Bocageopsis pleiosperma* Maas (Annonaceae). *Phytochem. Anal.* 26, 339–345. doi: 10.1002/pca.2568

Stewart, J. J. (2013). Optimization of parameters for semiempirical methods VI: more modifications to the NDDO approximations and re-optimization of parameters. *J. Mol. Model.* 19, 1–32. doi: 10.1007/s00894-012-1667-x

Stewart, J. J. (2016). *Stewart Computational Chemistry*. Colorado Springs, CO. Available online at: http://OpenMOPAC.net

Torres, F. C., Gonçalves, G. A., Vanzolini, K. L., Merlo, A. A., Gauer, B., Holzschuh, M., et al. (2016). Combining the pharmacophore features of coumarins and 1,4-substituted 1,2,3-triazoles to design new acetylcholinesterase inhibitors: fast and easy generation of 4-methylcoumarins/1,2,3-triazoles conjugates via click chemistry. *J. Braz. Chem. Soc.* 27, 1541–1550. doi: 10.5935/0103-5053.20160033

Trott, O., and Olson, A. J. (2010). AutoDockVina: improving the speed and accuracy of docking with a new scoring function, efficient optimization, and multithreading. *J. Comput. Chem.* 31, 455–461. doi: 10.1002/jcc.21334

Tsai, S. F., and Lee, S. S. (2010). Characterization of acetylcholinesterase inhibitory constituents from *Annona glabra* assisted by HPLC microfractionation. *J. Nat. Prod.* 73, 1632–1635. doi: 10.1021/np100247r

Vanzolini, K. L., Vieira, L. C., Corrêa, A. G., Cardoso, C. L., and Cass, Q. B. (2013). Acetylcholinesterase immobilized capillary reactors-tandem mass spectrometry: an on-flow tool for ligand screening. *J. Med. Chem.* 56, 2038–2044. doi: 10.1021/jm301732a

Vilela, A. F. L., Silva, J. I., Vieira, L. C. C., Bernasconi, G. C., Corrêa, A. G., Cass, Q. B., et al. (2014). Immobilized cholinesterases capillary reactors on-flow screening of selective inhibitors. *J. Chromatogr. B* 968, 87–93. doi: 10.1016/j.jchromb.2013.11.037

Yamamoto, Y., Ishihara, Y., and Kuntz, I. D. (1994). Docking analysis of a series of benzylamino acetylcholinesterase inhibitors with a phthalimide, benzoyl, or indanone moiety. *J. Med. Chem.* 37, 3141–3153. doi: 10.1021/jm00045a020

Yang, K., Jin, G., and Wu, J. (2007). The neuropharmacology of (-)-stepholidine and its potential applications. *Curr. Neuropharmacol.* 5, 289–294. doi: 10.2174/13701590778279649

**Conflict of Interest Statement:** The authors declare that the research was conducted in the absence of any commercial or financial relationships that could be construed as a potential conflict of interest.

frontiers in Chemistry

ORIGINAL RESEARCH
published: 04 October 2019
doi: 10.3389/fchem.2019.00665

# A Library Screening Strategy Combining the Concepts of MS Binding Assays and Affinity Selection Mass Spectrometry

*Jürgen Gabriel, Georg Höfner and Klaus T. Wanner**

*Department of Pharmacy, Faculty of Chemistry and Pharmacy, Ludwig Maximilian University München, Munich, Germany*

The primary objective of early drug development is to identify hits and leads for a target of interest. To achieve this aim, rapid, and reliable screening techniques for a huge number of compounds are needed. Mass spectrometry based binding assays (MS Binding Assays) represent a well-established technique for library screening based on competitive binding experiments revealing active sublibraries due to reduced binding of a reporter ligand and following hit identification for active libraries by deconvolution in further competitive binding experiments. In the present study, we combined the concepts of MS Binding Assays and affinity selection mass spectrometry (ASMS) to improve the efficiency of the hit identification step. In that case, only a single competitive binding experiment is performed that is in the first step analyzed for reduced binding of the reporter ligand and—only if a sublibrary is active—additionally for specific binding of individual library components. Subsequently, affinities of identified hits as well as activities of reduced sublibraries (i.e., all sublibrary components without hit) are assessed in additional competitive binding experiments. We exemplified this screening concept for the identification of ligands addressing the most widespread GABA transporter subtype in the brain (GAT1) studying in the beginning a library composed of 128 and further on a library of 1,280 well-characterized GAT1 inhibitors, drug substances, and pharmacological tool compounds. Determination of sublibraries' activities was done by quantification of bound NO711 as reporter ligand and hit identification for the active ones achieved in a further LC-ESI-MS/MS run in the multiple reaction monitoring mode enabling detection of all sublibrary components followed by hit verification and investigation of reduced sublibraries in further competitive binding experiments. In this way, we could demonstrate that all GAT1 inhibitors reducing reporter ligand binding below 50% at a concentration of 1 μM are detected reliably without generation of false positive or false negative hits. As the described strategy is apart from its reliability also highly efficient, it can be assumed to become a valuable tool in early drug research, especially for membrane integrated drug targets that are often posing problems in established screening techniques.

**Keywords: MS Binding Assays, affinity selection mass spectrometry, library screening, hit identification, LC-MS**

OPEN ACCESS

***Edited by:***
*Enrica Calleri,*
*University of Pavia, Italy*

***Reviewed by:***
*Qiuling Zheng,*
*China Pharmaceutical University, China*
*Mohammad Sharif Khan,*
*Dartmouth College, United States*

****Correspondence:***
*Klaus T. Wanner*
*klaus.wanner@cup.uni-muenchen.de*

***Specialty section:***
*This article was submitted to Analytical Chemistry, a section of the journal Frontiers in Chemistry*

***Received:*** *24 July 2019*
***Accepted:*** *18 September 2019*
***Published:*** *04 October 2019*

***Citation:***
*Gabriel J, Höfner G and Wanner KT (2019) A Library Screening Strategy Combining the Concepts of MS Binding Assays and Affinity Selection Mass Spectrometry. Front. Chem. 7:665. doi: 10.3389/fchem.2019.00665*

## INTRODUCTION

The early-phase of drug discovery, where research is focused on exploration of hits and leads for a target of interest, is often a long, inefficient, and therefore expensive venture (Dimasi et al., 2003; Hughes et al., 2011). To keep these expenses as low as possible, efficient, and reliable techniques for the investigation of target-ligand interactions are essential. Despite the availability of a wealth of techniques for this purpose, great efforts are applied to improve data quality and to accelerate this time-consuming step in the drug discovery process. These techniques can be divided in two major categories. The first one is represented by functional assays showing an effect mediated by interaction of a ligand at a target binding site. Functional assays are, depending on the nature of the investigated target (such as e.g., enzymes, receptors, or ion channels), based on diverse read out principles such as cell proliferation, reporter gene expression, or downstream signaling effects as a consequence of ligand binding (Croston, 2002; Trivedi et al., 2010; Babbitt et al., 2015). Although these techniques can provide valuable information about the functional consequence triggered by a test compound at a target, they are also subjected to several limitations such as interferences with the recorded signal which may result in insufficient data quality or sometimes false positive results due to interactions at sites not associated with the addressed target—to mention just a few—and are furthermore, often associated with high efforts for their establishment or implementation. The second category, the so called ligand binding assays directly recording target-ligand binding, provide information about the affinity of a test compound for a target binding site. In comparison with functional assays, binding assays are less prone to interferences and are easier to establish, but have some drawbacks as well. They only reveal affinity but no functional activity and the throughput is often not as high as in functional assays. Ligand binding assays are very popular and particularly helpful in medicinal chemistry projects as they are best suited for the establishment of structure-activity relationships. So far, a vast number of approaches to monitor target-ligand binding with different detection techniques has been established (Fang, 2012). It is distinctly beyond the scope of this introduction to review them, therefore, only some of the most relevant ones should be mentioned here. In terms of affinity assessment, radioligand binding assays still represent the gold standard, due to their high sensitivity, excellent robustness, and simple implementation (Maguire et al., 2012). Especially the first argument is still an important one, as it allows to apply the target at rather low concentrations and does not require high sophisticated target expression or enrichment strategies. Despite these qualities, employment of "hot," i.e., radioisotope labeled ligands is associated with disadvantages such as increased synthetic effort, hazards to human health, restrictions set by authorities, or expensive waste management. In order to overcome these limitations, several alternatives to avoid radioisotope labeled compounds, such as fluorescence, luminescence, surface plasmon resonance, or mass spectrometry (MS) based binding assays were established in the recent year (Geoghegan and Kelly, 2005; Zhu and Cuozzo, 2009; Stahelin, 2013; Höfner and Wanner, 2015; Stoddart et al., 2016). Although all of these alternatives provide specific strengths (and weaknesses) that should not be discussed in detail here, MS may be considered as particularly attractive detection principle as neither ligand nor target has to be modified or labeled for investigation of target-ligand interactions (Geoghegan and Kelly, 2005; Schermann et al., 2005; Höfner and Wanner, 2015). Even in the field of MS based binding assays, a wealth of concepts has been reported covering direct measurement of target-ligand complexes (Hofstadler and Sannes-Lowery, 2006) as well as monitoring bound ligands after their liberation from the target (Annis et al., 2007a; Höfner and Wanner, 2015) or even recording of ligands remaining non-bound (Hofner and Wanner, 2003) in presence of the target. In the context of the present study, we want to focus on two strategies of MS based binding assays, namely MS Binding Assays (Höfner and Wanner, 2015; Massink et al., 2015) and affinity selection mass spectrometry (ASMS) (Van Breemen et al., 1997; Zehender et al., 2004; Annis et al., 2007a; Jonker et al., 2011). MS Binding Assays are closely related to radioligand binding assays and share a lot of common features such as setup of the binding experiment as well as concentrations of ligands and targets. They are based on the use of a non-labeled reporter ligand instead of a ligand labeled with a radioisotope, which can be quantified highly sensitive by means of MS. Accordingly, binding experiments following this strategy can be performed as simple as radioligand binding experiments by incubation of the target with the reporter ligand (together with test compounds if necessary). MS Binding Assays require—just as radioligand binding assays—for termination of the binding experiment separation of the formed target-reporter ligand-complexes from non-bound reporter ligand which is typically achieved by filtration. In MS Binding Assays, subsequently to this separation step, the formerly bound reporter ligand is quantified typically by LC-ESI-MS/MS after its liberation and elution from the target-reporter ligand-complexes remaining on the filter with an organic solvent, whereas in radioligand binding experiments the bound reporter ligand remaining on the filter employed for separation is quantified by liquid scintillation counting (LSC). This strategy has been successfully applied to several membrane integrated drug targets such as neurotransmitter transporters (Zepperitz et al., 2006; Grimm et al., 2015; Ackermann et al., 2019), G protein-coupled receptors (Massink et al., 2015; Neiens et al., 2015; Chen et al., 2017), or ligand gated ion channels (Sichler et al., 2018). Furthermore, as a consequence of the superior selectivity of mass spectrometric detection (in comparison with LSC), MS Binding Assays enable binding experiments for multiple targets with corresponding selective reporter ligands simultaneously in the same binding sample (Schuller et al., 2017; Neiens et al., 2018). As the concept of MS Binding Assays has been established as alternative to radioligand binding assays, it is—in the same way as the latter—primarily suited for affinity determination of single compounds, but it is basically not restricted to this application. With the steadily increasing number of new chemical entities due to utilization of combinatorial chemistry for library synthesis (Aubé et al., 2014), but also to novel purification and exploitation techniques for natural resources (Kingston, 2011), it is more and more common to screen pooled compound libraries instead

of single compounds. Competitive MS Binding Assays have also been demonstrated to be well-suited for this task as shown for the screening of synthesized hydrazone and oxime libraries addressing the GABA transporter 1 (GAT1). In these studies, the libraries were divided in sublibraries of four or eight compounds, which were screened by recording reporter ligand binding remaining in the presence of each sublibrary. In the further course of this work, such individually studied sets will always be referred to as "sublibraries." Subsequently, the most potent sublibraries were subjected to deconvolution experiments, i.e., testing each sublibrary component alone in a single run to identify the corresponding hits (Sindelar et al., 2013; Kern and Wanner, 2019). The strength of this approach is a rather simple setup and an almost complete exclusion of false positive or false negative results due to monitoring of reporter ligand binding instead of directly identifying bound library components. The work required for deconvolution is in the case of focused libraries, where high hit rates are common, acceptable, but can be in the case of big libraries considerable. The other concept of MS based binding assays to be discussed here is gathered under the name ASMS. ASMS approaches primarily differ in their employed technique for the separation of bound and non-bound ligands (e.g., vacuum filtration, ultrafiltration, or size exclusion chromatography). In contrast to MS Binding Assays, ASMS—as already implicated by this term—enables direct identification of target-bound ligands by mass spectrometric detection. A particularly powerful and in the meantime well-established ASMS application is the automated ligand identification system (ALIS) (Annis et al., 2007b) which employs size exclusion chromatography for on-line separation of bound in form of ligand-target complexes from non-bound ligands followed by dissociation of target bound ligands on a reversed phase column and finally, detection (and identification) of the liberated ligands by time of flight MS. ALIS has been successfully employed primarily for soluble proteins, but in some cases also for membrane-bound protein targets and allows—with its outstanding high throughput capacity—to screen thousands of compounds per hour (Whitehurst et al., 2006; Kutilek et al., 2016; Walker et al., 2017). Additionally, Annis et al. applied the ALIS setup for determination of affinity rank-orders and also for affinity determination of ligands (Annis et al., 2007c). Despite these exceptional capabilities, ASMS remains as well-subject to several critical limitations. ASMS approaches are for example often prone to false positive hits which require elaborate hit evaluation experiments. An even more limiting, but at the same time fundamental drawback of this strategy is, however, that ASMS relies on the ability to detect (i.e., to identify) the employed test compounds by MS. This would mean that test compounds providing insufficient signal intensity under the chosen mass spectrometric conditions will be lost, almost fully independent of their affinity to the target. As the chance to identify a binding ligand following the ASMS concept is inherently coupled with the amount of target employed in the binding experiment, this approach is only feasible when considerably high target concentrations can be employed in the binding experiment and therefore, restricted to targets which are easily accessible from native materials or for which powerful expression and purification are available. Having said this, it was the aim of this study to develop an MS based library screening strategy which combines the strengths of competitive MS Binding Assays with those of ASMS, while at the same time overcoming the weaknesses of both concepts. To achieve this goal sublibraries' potencies should be assessed as a function of bound reporter ligand following the concept of competitive MS Binding Assays and in the case of an active sublibrary, the corresponding hit should be identified following the concept of ASMS without performing an additional binding experiment (**Figure 1**). In this way, it can be ascertained that no active ligands due to insufficient mass spectrometric sensitivity or low target concentration is missed due to the use of a reporter ligand in the first step (MS Binding Assays), while at the same time the elaborate deconvolution procedure can be avoided by following the ASMS concept. Thus, the entire library screening strategy presented in this study starts with a binding experiment by incubation of a first sample that contains the target—reporter ligand as well as library components—and defines total binding of reporter ligand and library components, respectively (**Figure 1** "incubation," left part). A second sample contains the same constituents (in the same concentrations) as the first one, but in addition a further ligand in excess to block the addressed target binding site serves as negative control. In this way non-specific binding of reporter ligand and library components, respectively, can be defined (**Figure 1** "incubation," right part). Then for both samples, bound and non-bound ligands (including the reporter ligand) are separated via vacuum filtration (**Figure 1** "separation") and subsequently, the formerly bound ligands (including the reporter ligand) are liberated from the target (**Figure 1** "liberation") and analyzed by LC-ESI-MS. In this way, initially in a first set of LC-MS runs, the sublibraries' activities can be easily assessed by quantification of the reporter ligand, as inhibition of its binding must be due to the presence of active components in sublibraries (**Figure 1** "competitive MS Binding Assay"). For those sublibraries recognized as active, the corresponding hits can then be identified later on directly by mass spectrometric quantification of library components in an additional set of LC-MS runs, without performing another binding experiment (**Figure 1** "affinity selection mass spectrometry"). By comparison of total and non-specific binding for all components of an active sublibrary, exclusively those components are identified as hits exhibiting specific binding, whereas false positive results can be omitted in this way. Finally, the activities of "reduced sublibraries," i.e., sublibraries containing all library components except identified hit compounds, are again characterized in a competitive binding experiment. Thereby, false negative results caused by competitive effects due to the presence of more than one hit in a sublibrary or due to insufficient sensitivity of mass spectrometric quantification of bound library components can be ruled out. To prove the feasibility of this library screening concept, we chose the most widespread GABA transporter subtype in the brain GAT1, for which a competitive MS Binding Assay is already well-established. GAT1 is a membrane transport protein belonging to the solute carrier family SLC6, primarily located in the synaptic region on neurons, where it is primarily responsible for the termination of GABAergic signals (Scimemi,

2014). As several neurological disorders such as neuropathic pain (Gwak and Hulsebosch, 2011), sleep disorders (Gottesmann, 2002), schizophrenia (Lisman et al., 2008), epilepsy (Treiman, 2001), anxiety, or depression (Lydiard, 2003; Kalueff and Nutt, 2007) are associated with a GABAergic dysfunction, GAT1 represents an interesting drug target for several therapeutic indications. Therefore, efficient screening techniques are of great value by facilitating the development of new GAT1 inhibitors.

# MATERIALS AND METHODS

## Chemicals and Reagents

LC-MS grade acetonitrile and methanol as well as tris(hydroxymethyl)-aminomethan (Tris) were purchased from VWR (Darmstadt, Deutschland). Ammonium formate was obtained from Fluka (Sigma Aldrich, Taufkirchen, Germany) in LC-MS ultra-grade purity. Water was purified by lab water purification system (Sartorius, Göttingen, Germany). NO711 and [$^2H_{10}$]NO711 were synthesized in-house and dissolved in DMSO (ACS Reagent Grade, Fisher Scientific UK, Loughborough, UK) to obtain 10 mM stock solutions. The 128 compound library (see below) consisted of well-known GAT1 inhibitors, synthesized in house (DDPM compounds, pre dissolved in 10 mM DMSO stock solution) as well as commercially available drug substances or organic chemicals, received from commercial providers. Chemical structures of DDPM compounds are shown in **Table S1**. All library compounds were dissolved in DMSO to yield 10 mM stock solutions. Compilation of the library: sublibrary A [(4-(4-chloro-phenyl)-piperidine-4-ol, 7-(dipropylamino)-5,6,7,8-tetrahydronaphthalen-1-ol hydrobromide (8-OH DPAT), DDPM2330, DDPM2565, chlorpromazine hydrochloride, doxepin hydrochloride, fenoterol hydrobromide, ketoprofen, meclozine dihydrochloride, metoclopramide hydrochloride, oxazepam, piroxicam, procaine hydrochloride, roxithromycin, sulpiride, telmisartan], sublibrary B [bifonazole, ciprofloxacin hydrochloride, DDPM2188, DDPM3138, glibenclamide, hydromorphone hydrochloride, lisinopril dihydrate, molsidomine, noscapine hydrochloride, pilocarpine nitrate, procainamide hydrochloride, prophyphenazone, reserpine, sulfaguanidine, sulfamethoxazole, triphenylamine], sublibrary C [aciclovir, amitriptyline hydrochloride, atropine sulfate, brucine, cetirizine hydrochloride, clomipramine, DDPM2029, DDPM2077, ethacridine lactate, indometacin, mepivacaine hydrochloride, (2-morpholin-4-ylmethyl-benzoimidazol-1-yl)-acetic acid, papaverine hydrochloride, promethazine hydrochloride, salbutamol sulfate, sertraline hydrochloride], sublibrary D [ambroxol hydrochloride, antazoline hydrochloride, biperidene hydrochloride, clotrimazole, DDPM2187, DDPM2473, diphenhydramine hydrochloride, diltiazem hydrochloride, lidocaine, meloxicam, ofloxacin, physostigmine salicylate, propranolol hydrochloride, ranitidine hydrochloride, sulfisomidine, tianeptine], sublibrary E [(4-(4-(dimethylamino)styryl)-N-methylpyridinium iodide ($ASP^+$), atenolol, benzylpenicillin potassium, chlordiazepoxide hydrochloride, DDPM1349, DDPM1981, drofenine hydrochloride, isoprenaline sulfate dihydrate, meprobamate, morphine hydrochloride, nalidixic acid, phenylbutazone, terfenadine, tetracaine hydrochloride, tolbutamide, verapamil hydrochloride], sublibrary F [(2-(4-methyl-1,4-diazepan-1-yl)benzoic acid, baclofen, chloroquine phosphate, DDPM2009, diazepam, ditolylguanidine, haloperidol, ipratropium bromide, metoprolol tartrate, moxifloxacin hydrochloride, naphazoline hydrochloride, phenobarbital, pimozide, scopolamine hydrobromide, tetracycline hydrochloride, tramadol hydrochloride], sublibrary G [buspirione hydrochloride, clonidine hydrochloride, cimetidine, DDPM3139, imipramine hydrochloride, metipranolol, 8-{3-[bis(4-fluorophenyl)amino]propyl}-3-methyl-1-phenyl-1,3,8-triazaspiro[4.5]decan-4-one maleate (PH014034), quinine hydrochloride, piretanide, ramipril, riboflavin, strychnine nitrate, tiabendazole, trifluoperazine, trimethoprim, xylometazoline hydrochloride], sublibrary H [(3-(2-methyl-1H-imidazol-1-yl)benzoic acid, acetazolamide, captopril, chloramphenicol, chlortalidone, diclofenac sodium, etacrynic acid, furosemide, hydrochlorothiazide, mefenamic acid, methyl orange, naproxen, lauryl maltoside, niclosamide, nitrazepam, phenytoin]. Tocris ScreenPlus library (1280 compounds, 10 mM in DMSO) was purchased from Bio-Techne (Wiesbaden-Nordenstadt, Germany).

## LC-ESI-MS/MS Instrumentation

LC-ESI-MS/MS was performed using a QTRAP5500 triple quadrupole mass spectrometer with a TurboV-ion source (Sciex, Darmstadt, Germany) coupled to an Agilent 1260 HPLC system (G 1322A Degasser, binary pump G1312B, oven G1316A, Agilent, Waldbronn, Germany) and a SIL-20A/HT autosampler (Shimadzu, Duisburg, Germany). Autosampler settings were set as follows: rinsing volume 200 µL (acetonitrile/water 50:50, v/v), needle stroke 52 mm, rinsing speed 35 µL/s, sampling speed 5.0 µl/s, purge time 1.0 min rinse dip time 0 s and rinse mode was set to "before and after aspiration." Data acquisition and analysis was carried out with Analyst 1.6.3 software.

## Chromatography

For LC, a Purospher Star RP18e column (55 × 2 mm, 3 µm, Merck KGaA, Darmstadt, Germany) protected with a C-18 Guard Cartridge column (4 × 2 mm, Phenomenex, Torrance, CA, USA) and two in-line filters (0.5 µm and 0.2 µm, IDEX, Oak Harbor, WA, USA) was used as stationary phase. Column oven temperature was maintained at 25°C. Unless stated otherwise, the samples to be analyzed were dissolved in ammonium formate buffer (10 mM, pH 7.0) and methanol in a ratio of 30:70 (v/v). For recording of the reporter ligand NO711 by LC-MS, an isocratic elution mode with 10 mM ammonium formate buffer at pH 7.0 and acetonitrile at a ratio of 50:50 (v/v) was employed. The injection volume was set to 10 µL at a flow rate of 350 µL/min. For hit identification by LC-MS, a gradient elution at a flow rate of 450 µL/min and 25°C column temperature was performed according to the following conditions: after starting with 10 mM ammonium formate buffer (pH 7.0)/ acetonitrile at a ratio of 60/40 (v/v) the mobile phase was changed to a ratio of 20/80 (v/v) from 0.01 to 0.05 min and held until 3.5 min. Between 3.50 and 3.55 min the ratio was changed back to the starting conditions and held until 9 min. The injection volume was set to 40 µL.

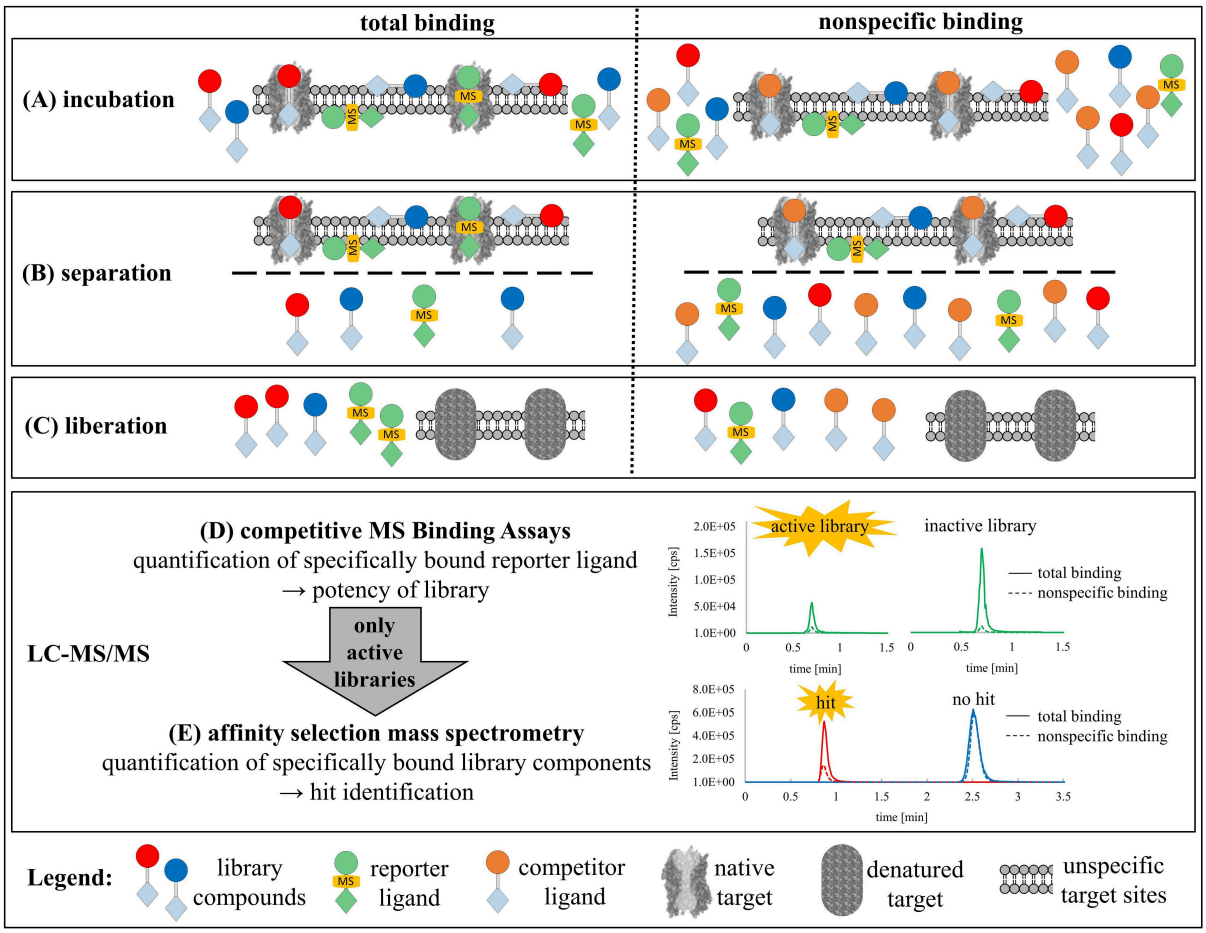


**FIGURE 1 |** Combination of MS Binding Assays and affinity selection mass spectrometry (ASMS) for library screening. **(A)** Incubation of reporter ligand, target, sublibrary to determine the total binding of reporter ligand and library components as well as additionally an excess of competitor ligand for determination of non-specifically bound ligands. **(B)** Separation of bound from non-bound ligands by vacuum filtration. **(C)** Liberation of bound ligands with organic solvent and generation of samples for LC-MS analysis. **(D)** Competitive MS Binding Assay to determine library activity as a function of bound reporter ligand determined by LC-MS. **(E)** ASMS in the case of active sublibraries for the identification of the corresponding hits by means of LC-MS quantification of specifically bound library components as a function of total vs. non-specific binding.

## Compound-Dependent MS Parameters

For quantification of reporter ligand binding, the mass transitions *m/z* 381 →180 and *m/z*391 → 190 for NO711 and [$^2H_{10}$]NO711, respectively, were used as described recently (Zepperitz et al., 2006), applying the following compound-dependent MS parameters: declustering potential 80 V, entrance potential 10 V, collision energy 25 V, and collision cell exit potential 18 V. For hit identification, the compound-dependent MS parameters of precursor ion and the eight most intensive product ions of each library compound were optimized via "Quantitative Optimization." For this purpose, for each sublibrary a solution containing all components in a concentration of 20 nM was prepared in 10 mM ammonium formate buffer at pH 7.0/acetonitrile at a ratio of 20:80 (v/v). These solutions were directly infused into the ESI-source at a flow rate of 7 µL/min via the integrated syringe pump. Detailed instrument settings (see **Table S2**) as well as the compound-dependent MS parameters for every compound obtained thereby are presented in the **Tables S3, S4**. Compounds of sublibrary H were investigated in the negative, all others in the positive ionization mode.

## Source-Dependent MS Parameters

For quantification of the reporter ligand, the following source settings were applied: temperature 650°C, ion-spray voltage 3,000 V, curtain gas ($N_2$) 30 psi, auxiliary gas ($N_2$) 40 psi, nebulizing gas ($N_2$) 50 psi, and collision gas ($N_2$) "high," dwell time 100 ms, mass resolution unit. For hit identification under positive ionization conditions, the settings were as following: source temperature 650°C, ion-spray voltage 2,000 V, curtain gas ($N_2$) 28 psi, auxiliary gas ($N_2$) 40 psi, nebulizing gas ($N_2$) 50 psi and collision gas ($N_2$) "high," dwell time 20 ms (in case of libraries consisting of 64 compounds 5 ms), mass resolution unit. For hit identification under negative ionization conditions the settings were as following: source temperature 650°C, ion-spray voltage −2,500 V, curtain gas ($N_2$) 30 psi, auxiliary gas ($N_2$) 50

psi, nebulizing gas ($N_2$) 60 psi and collision gas ($N_2$) "mid." Dwell time 20 ms, mass resolution unit.

## Evaluation of the Library Components' Mass Transitions by LC-ESI-MS/MS

For each sublibrary, a matrix blank (see generation of matrix) as well as solutions containing all sublibrary components in concentrations of 1 and 10 nM, respectively, in matrix were analyzed with the gradient LC-ESI-MS/MS method employing all the mass transitions with their optimized potentials (obtained as described above) for the corresponding precursor and product ions. Based on the comparison of the MRM chromatograms obtained thereby, the most appropriate mass transitions for quantification of the corresponding compounds were selected (according to the highest signal to noise ratio for 1 nM matrix standards).

## Membrane Preparation

Membranes of HEK293 cells stably expressing mGAT1 were prepared as described previously and stored at −80° C (Zepperitz et al., 2006). Per 96 well-plate, an aliquot of 2 mL was thawed and diluted in 20 mL 0.9% (w/v) sodium chloride solution. After 20 min centrifugation at 20,000 rpm/4°C (Sorvall, rotor SS34, Thermo Fisher, Waltham, US), the pellet was resuspended (Polytron, PT2000, Kinematica AG, Littau, Switzerland) in incubation buffer (50 mM Tris,1 M NaCl, adjusted with citric acid to pH 7.1) resulting in a protein content of ∼100 µg/mL, determined according to Bradford.

## MS Binding Assay

All binding experiments were performed in a polypropylene 96-well plate (1.2 mL well volume, Sarstedt, Nümbrecht, Germany) in analogy to the procedure recently described (Zepperitz et al., 2006). In all cases triplicate samples were prepared in incubation buffer (see above) containing the GAT1 membrane preparation (protein content 20–30 µg/well, yielding a final GAT1 concentration of about 3 nM) and NO711 (final concentration 10 nM) in a total volume of 250 µL. One set of samples additionally contained the sublibraries (each component in a final concentration of 1 µM) for determination of total reporter ligand binding in presence of the sublibraries and total binding of the sublibrary components. Analogously, a second set of samples additionally contained the sublibraries (each component in a final concentration of 1 µM) together with 100 mM GABA for determination of non-specific reporter ligand binding and non-specific binding of the sublibraries' components. Furthermore, a single triplicate without any additions served as a control for total reporter ligand binding in the absence of any other ligand. All samples were incubated for 40 min at 37°C using a plate shaker incubator (Stuart Microtitre SI505, Bibby Scientific Limited, Staffordshire, Great Britain). The incubation was stopped by vacuum filtration using a multi well-plate vacuum manifold (Pall, Dreieich, Germany) in combination with a 96-well glass fiber filter plate (AcroPrep Advance, glass fiber, 1.0 mm, Pall, Dreieich, Germany) pretreated with 200 µL 0.9% (w/v) sodium chloride solution. Aliquots of 200 µL per well were transferred to the filter plate with a 12-channel pipet and subjected to vacuum filtration. Subsequently, the filter plate was washed four times with 150 µL ice-cold 0.9% (w/v) sodium chloride solution and dried at 50°C for 60 min. Afterwards, the filters with the remaining target and target-bound ligands were exposed to 100 µL methanol containing [$^2H_{10}$]NO711 (1.4 nM) as internal standard per well for 15–20 s and then eluted into a deepwell plate by application of vacuum. This step was repeated twice resulting in a total elution volume of 300 µL. Finally, a volume of 130 µL ammonium formate buffer (10 mM, pH 7.0) was added per well. In the end, the resulting samples were equally split into two 96 well-plates and sealed with aluminum foil. The first 96 well-plate was immediately subjected to quantification of reporter ligand by LC-ESI-MS/MS. The second 96 well-plate was stored at −20°C and only examined for target-bound library components by LC-ESI-MS/MS recording the corresponding mass transitions (see Evaluation of the library component's mass transitions by LC-ESI-MS/MS) in the case of active sublibraries.

## Generation of Matrix

Samples of 250 µL in incubation buffer (50 mM Tris, 1 M NaCl, pH 7.1) containing GAT1 membrane preparation (protein content 20–30 µg/well) per well without any ligand were exactly processed according to the procedure of "MS Binding Assay" described above up to the elution step. Elution was done with pure methanol (without internal standard) and the resulting methanolic eluate was stored at −20°C. To prepare the required matrix standards, 130 µL ammonium format buffer (10 mM, pH 7.0), containing internal standard and library components, or in case of blank matrix sample, without both, were added to aliquots of 300 µL methanolic eluate.

## Data Analysis

Based on the calibration function (established for each binding experiment), the concentrations of NO711 resulting from the corresponding binding samples were calculated using Analyst v.1.6.3 (Sciex, Darmstadt, Germany) as described previously (Zepperitz et al., 2006). Remaining bound reporter ligand was calculated as the percentage of the specifically bound reporter ligand in presence of a sublibrary compared to specifically bound reporter ligand in the absence of a sublibrary. All binding experiments were performed in triplicates and results are given as means ± SD. For hit identification, all chromatographic parameters and normalized peak areas (area sublibrary component/area internal standard) of each individual sublibrary component in the corresponding MRM chromatograms of samples representing total and non-specific binding were calculated via Analyst v.1.6.3 (Sciex, Darmstadt, Germany). Consequently, all library components showing significant specific binding as difference of the normalized areas of total and non-specific binding (one site student $t$-test, $n = 3$, CL = 97.5%) were classified as hits.

# RESULTS AND DISCUSSION

## Basic Considerations Before Implementation of the Library Screening Concept

For a methodical combination of the approaches of competitive MS Binding Assays and ASMS for the screening of ligands

addressing GAT1, it is necessary to consider some basic points regarding setup and conditions in the GAT1 binding experiments, LC-MS analytics as well as potencies of the ligands to be identified. First of all, the already established filtration based competitive GAT1 MS Binding Assays, which were already utilized for the screening of hydrazone and oxime compound libraries in our group, should serve as a basis for the development of the new assay (Zepperitz et al., 2006).

If vacuum filtration as separation technique is intended to be employed for the separation of bound ligands from non-bound ligands, it has to be ensured that only minor amounts of the target bound ligand are lost due to dissociation of the target-ligand complex during the necessary washing step.

In the textbooks, it is often stated that this requirement is fulfilled when the affinity of the ligand toward the target expressed as $K_d$-value equals 10 nM or less (Bennett and Yamamura, 1985). However, target-ligand complex dissociation is more a question of the $k_{off}$–rate than of $K_d$. This means that ligands with higher $K_d$-values can also be employed in filtration based binding assays as long as the corresponding $k_{off}$–rate is low enough. NO711, the reporter ligand used in our GAT1 MS Binding Assays, is an example for a compound showing only moderate affinity, characterized by a $K_d$-value of 23.6 nM toward GAT1, but with a comparably low $k_{off}$–rate of about $1.5 \times 10^{-3}$ $s^{-1}$ (Zepperitz et al., 2006). Accordingly, it proved to be excellently suited as reporter ligand for GAT1 in filtration based MS Binding Assays for which purpose it has been extensively applied for more than one decade. Under particularly favorable conditions, such as a low $k_{off}$–rate together with a very short time period for the washing process at low temperature, reporter ligands with $K_d$-values even beyond 100 nM have been used in filtration based binding assays, as for example described for [$^3$H]TCP (Katz et al., 1997), [$^3$H]PCP (Eldefrawi et al., 1982), or [$^3$H]imipramine (Arias et al., 2010) addressing the nACh receptor. Library components binding to the target during a binding experiment, which are to be directly identified by ASMS after filtration, are subject to dissociation during washing in the same way as described above for the reporter ligands. However, in these cases losses of bound ligands can be tolerated to a higher extent, as far as a sufficient amount of the formerly target-bound ligand is left for detection by LC-MS. Therefore, we considered affinities in the high nM range close to 1 μM as the ultimate limit compounds should have to be detectable under the conditions of our filtration based GAT1 MS Binding Assays. Taking into account the situation of a competitive binding experiment applying the reporter ligand NO711 in a concentration of 10 nM and the library components all in a concentration of 1 μM, inhibition of reporter ligand binding due to a single library component down to a level of 50% can be attributed to an affinity (i.e., a $K_i$-value) of about 700 nM for this compound (according to the equation of Cheng-Prusoff, for details see **Table S5**). Following these considerations, we set the concentration for the individual test compounds in the libraries to 1 μM.

Another fundamental parameter in binding assays is the concentration of the target, which is typically kept below 0.1 $K_d$ of the reporter ligand in radioligand as well as in MS Binding Assays to avoid depletion of the reporter ligand (Hulme and Birdsall, 1992). This condition is, however, in clear contrast to the need for target concentrations in affinity selection approaches that should be as high as possible to facilitate hit identification. According to our experiences with quantification of various reporter ligands in MS Binding Assays by means of LC-MS/MS employing triple quadrupole mass spectrometers, we considered it feasible to quantify a vast majority of possible library components down to a concentration level of at least 1 nM in the matrix generated in the binding experiment. Therefore, we expected that a GAT1 concentration of about 0.1 $K_d$ should be high enough to achieve our aims and, hence, decided to employ GAT1 at a concentration of about 3 nM (i.e., 0.125 $K_d$). Accordingly, for a library component reducing NO711 binding to 50% at a concentration of 1 μM, the equilibrium concentration of the corresponding GAT1-ligand complex formed by this compound can be estimated to be about 1.5 nM (for details see **Table S5**) in the binding experiment. It has, however, to be taken into account, that the actual concentration of such a library component in the final sample to be subjected to LC-MS will be distinctly lower than 1.5 nM due to the above mentioned issue of dissociation during the washing step following filtration. It is obvious that library components with higher affinities will lead to higher equilibrium concentrations of target-ligand complexes (maximally approaching the GAT1 concentration of about 3 nM) and that such compounds are in tendency less prone to losses due to dissociation. In contrast to the case with only one active component in the library, the situation changes, when more active library components are present in the binding experiment. For two ligands for example, both with an affinity ($K_i$) of about 700 nM (i.e., an $IC_{50}$ of 1 μM), the equilibrium concentrations for the corresponding target-ligand complexes can be estimated to about 1 nM for both ligands, and it is obvious that target-ligand concentrations will decrease further when even more active components are present. The situation gets particularly unfavorable, when a weak binder and a strong binder are present in same library, for example one with an affinity of about 700 nM (i.e., an $IC_{50}$ of 1 μM) and one with a 100 times higher affinity. In this case, the strong binder will suppress binding of the weak binder, resulting in an equilibrium concentration of the corresponding target-ligand complex of about 30 pM (see **Table S5**). As this concentration will further decrease during washing due to dissociation, the risk to not identify this compound in the affinity selection step is high. According to these considerations and the inherent issue that there might be compounds in the library hardly to quantify by MS, it is clear that under the envisaged screening conditions including detection by MS, false negative results can hardly be avoided in the affinity selection based hit identification step. In combination with the competitive MS Binding Assay, however, such cases can be easily identified, as inhibition of reporter ligand binding unequivocally indicates the presence of hits (as analogously, no inhibition of reporter ligand binding indicates the absence of hits). In the context of a weak binder (with an $IC_{50}$ of 1 μM) that might have been missed in the affinity selection step, due to the presence of strong binder—as mentioned above—an additional subsequently performed competitive binding experiment with

the corresponding sublibrary from which the strong binder identified before as hit (here referred to as "reduced sublibrary") has been removed, will indicate the presence of this binder (reduction of ligand binding below 50%). Therefore, the weak binder initially missed in the first affinity selection step would be detected in the subsequent one.

HPLC coupled mass spectrometric detection is a further essential point in this concept. As we intended to use the already established GAT1 MS Binding Assays with a triple quadrupole mass spectrometer based quantification of the reporter ligand as starting point for this screening approach, it was obvious to employ this type of mass spectrometer also for the affinity selection step. Making use of this instrument type, we tried to benefit from its unsurpassed sensitivity for quantification of known compounds by running it in the multiple reaction monitoring (MRM) mode. To fully exploit the potential of the MRM mode, it is necessary to tune the mass spectrometer in a way that the corresponding mass transitions of all library components can be detected with maximum sensitivity. Although modern triple quadrupole mass spectrometers can provide analyte specific mass transitions together with a set of optimized potentials in automated procedures, the efforts for this step are considerable, when high numbers of compounds have to be investigated. In the presented concept, this additional effort is, however, only necessary, when inhibition of reporter ligand binding indicates the presence of a hit in a sublibrary. Quantification of target-bound reporter ligand and target-bound library components can basically easily be performed in a single LC-MS/MS run. Nevertheless, we decided to separate both steps, as that way the above mentioned efforts to establish MRM based quantification the library components can be minimized. This means that a first LC-MS/MS run is performed for quantification of the reporter ligand NO711 (under already established conditions). In the case of an active sublibrary, the corresponding binding samples are subjected to quantification of all individual library components in a second LC-MS/MS run, the conditions of which have then to be established. In the context of mass spectrometric detection, it should be finally mentioned, that it is surely also possible to use other instrument types such as ion traps, orbitraps, or TOFs, especially for the affinity selection step, but possibly also for quantification of the reporter ligand.

Important points to be considered when planning a screening method are the size of the sublibraries that can be used and the hit rates that are expected. The sizes of sublibraries employed in screening campaigns are often very different, depending on the aim of a screening project. As a size of thousand members and even more is quite common, the issue, how many compounds an individual set should contain is important. Certainly it is in principle possible to quantify at least hundreds of compounds simultaneously in a single LC-MS/MS with triple quadrupole mass spectrometers, sublibraries consisting of so many members are not really convenient to handle, when conditions for an MRM based quantification of the library components have to be established. With respect to the binding experiment, the size of a sublibrary appears—at a first glance—hardly restricted, and obviously expenditure of material (e.g., target, consumables etc.) and time can be saved when big sublibraries are employed. It has to be taken into account, however, that a high number of components will enhance the probability, that weak inhibition of individual binders will sum up to a significant overall inhibition of reporter ligand binding. This means that an inhibition of reporter ligand binding below 50% (i.e., the activity criterion chosen for the assessment of sublibraries) can also be due to numerous weak binders, which would cause severe efforts for their quantification in the affinity selection step. Actually, also the hit rate of library screening will distinctly influence the efficiency of the screening process related with size of the sublibrary, as each "active" sublibrary has to be further investigated in the affinity selection step, according to our concept. As the "activity" criterion applied to the results determining when a library is active or not can be adjusted at will, the described screening strategy provides a high degree of flexibility. Considering the above mentioned arguments, we chose a sublibrary size of 16 components as a compromise, but in order to demonstrate that the concept is not restricted to such a small number only, we exemplarily investigated a sublibrary comprising 64 components.

## Investigation of a Deliberately Compiled Test Library Consisting of 128 Components

### Library Compilation

For implementation of our novel library screening concept, we compiled a library with 128 small molecule compounds (with a molecular weight from 201 to 837 Da) including 116 well-known drug substances or organic chemicals as well as 11 known GAT1 inhibitors and one non-selective low-potent GAT inhibitor with the intention to cover a broad range of structural diversity which is reflected by log $D_{pH7.0}$ values from about −3 to almost 8 (calculated by MarvinSketch software) of the selected compounds. With regard to our aim to identify ligands with an $IC_{50}$-value of about 1 μM or better, we chose—out of the pool of GAT1 inhibitors synthesized in our group—compounds with affinities ranging from p$K_i$-values of 5.94 to 8.13 (data from in-house MS Binding Assays) and differing as far as possible in their structure. Almost all highly potent GAT1 inhibitors known so far share three common structural motifs, namely a heterocyclic amino acid and a lipophilic aryl-moiety both connected via a linker consisting of a hydrocarbon chain with different length, which may contain heteroatoms and multiple bonds. Accordingly, we tried to include test compounds with variations of all three structural motifs in the set of selected GAT1 inhibitors (**Table S1**). This set of 128 compounds was divided in eight sublibraries each consisting of 16 components whereby the following considerations were taken into account. First, the sublibraries were composed in a way that different activity patterns arose. Thus, the sublibraries A-E contained two, sublibrary F one, and sublibraries G and H no GAT1 inhibitor (see experimental section "Chemicals and Reagents"). Secondly, we compiled the sublibraries in a way that A-G could be investigated by using electrospray ionization in the positive and H in the negative ion mode in the MS quantification step, respectively. Thirdly, for the sake of simplicity, we grouped the compounds in a way that mass-encoded sublibraries resulted. That way the selection of appropriate mass transitions for

the individual library components and accordingly, optimized parameters was facilitated.

### Determination of Mass Transitions for the Library Components

As discussed in the basic consideration chapter above, we intended to use the MRM mode of a triple quadrupole mass spectrometer for quantification of total as well as non-specific binding of each component of sublibraries identified as active. Therefore, the compounds' mass transitions as well as the corresponding compound-dependent MS parameters were required for the MS analysis. Basically, only active sublibraries would have to be further investigated according to our described screening concept. In order to estimate the efforts and the efficiency for determination of mass transitions for the individual sublibrary components suited for further LC-MS/MS analysis, however, we decided to study all eight sublibraries of our deliberately compiled library at this step. Furthermore, we wanted to ensure that as much as possible of the selected compounds of the whole library can be detected in the MRM mode and therefore reflecting a broad spectrum of chemical structures during the following development of an "universal" chromatography, finally enabling quantification of the library components by LC-ESI-MS/MS. The desired mass transitions together with the corresponding compound-dependent MS parameters of the test compounds were obtained via the automated tuning mode of the mass spectrometer during infusion of solutions comprising each component of a sublibrary (i.e., 16 components) in a concentration of 20 nM. As preliminary experiments showed that automatic optimization of the intensity of the mass transitions of the eight most intensive fragment ions for each parent ion proved to be a good compromise between the amount of work and the quality of the obtained mass transitions for each library component (see below), all mass transitions (as described in **Table S3**) were determined accordingly.

### Quantification of Library Components by LC-ESI-MS/MS

Based on the mass transitions and compound-dependent MS parameters obtained for the test compounds, an LC-ESI-MS/MS method suited for quantification of each library component should be established. We found the following gradient conditions using the same C18 stationary phase as for the quantification of reporter ligand, appropriate for our purpose: For the start of the chromatography, a solvent mixture with a ratio of 60/40 (v/v, 10 mM ammonium formate, pH 7.0/acetonitrile) had to be used, which after 0.01 min had to be rapidly changed to a solvent ratio of 20/80 thus reducing the aqueous component. This solvent ratio remained unchanged until the run time amounted to 3.5 min. Then, the solvent ratio was rapidly switched back to original conditions (60/40 v/v). This solvent ratio was applied for 5.5 min thus leading to a total runtime of 9.0 min for each sample injection (for more details see **Supplementary Material**).

After optimization of the source-dependent MS parameters for these chromatographic conditions, MRM chromatograms for all sublibraries were recorded based on the mass transitions determined before (see above). For an unambiguous assignment of the peaks in the MRM chromatograms of the sublibraries (showing eight mass transitions per compound) to the corresponding library components, it proved to be helpful to compare for each sublibrary a set of three chromatograms, i.e., a matrix blank as well as two samples containing all the components of a sublibrary at a concentration of 1 and 10 nM, respectively, in the matrix of the binding experiment. Furthermore, we calculated the signal to noise ratios (S/N) for the most promising mass transitions of each compound and selected those providing the highest S/N ratios for final quantification. In this way, we could detect 122 of the 128 compounds based on the mass transitions determined before, presenting a success rate of 95%. A representative MRM chromatogram of sublibrary A is shown in **Figure 2A** and detailed results of all sublibraries are presented in **Table S6**. At this point, it is furthermore worth mentioning that all these compounds could be detected with an S/N ratio distinctly >5, which is the commonly accepted criterion for the lower limit of quantification (LLOQ). The compounds not detectable by MS (in the MRM mode) under these conditions were, triphenylamine, bifonazole, 4-(4-chloro-3-methyl-phenyl)-piperidin-4-ol, phenobarbitone, riboflavin, and clotrimazole. Surely, further efforts could be made for these compounds to find more appropriate mass transitions, but we deliberately decided to rely only on the automated tuning procedure to keep this step as simple as possible. Since [$^2H_{10}$]NO711 at a constant concentration of 1 nM is always present in the samples to be subjected to LC-ESI-MS/MS as internal standard for the quantification of bound reporter ligand NO711, we employed this compound also as internal standard, for quantification of our library components. In this way, the corresponding normalized areas could be calculated for all individual compounds based on their peak areas in relation to the peak area of the internal standard. As all compounds were investigated at the same concentration as the internal standard, i.e., at 1 nM, these normalized areas reflect at the same time the relative response factors (RRF) which are also summarized in **Table S6**. To sum up, it can be stated that the established method for LC-ESI-MS/MS quantification employing a triple quadrupole mass spectrometer is well-suited for quantification of a broad diversity of small molecule compounds down to a concentration of at least 1 nM either using the positive or the negative ionization mode.

### Activity Assessment by Means of Competitive MS Binding Assays

After establishment of an LC-ESI-MS/MS quantification method enabling highly sensitive quantification of the vast majority of library components, the described screening concept should be applied to screening of the 128 compound library for ligands addressing the NO711 binding site of GAT1. According to this concept, the activities of the eight sublibraries (A-H) had to be initially assessed. For this purpose, competitive GAT1 MS Binding Assays were performed completely in analogy to the procedure recently described (Zepperitz et al., 2006), always employing the reporter ligand NO711 at a concentration of 10 nM and mGAT1 at a concentration of about 3 nM. In the

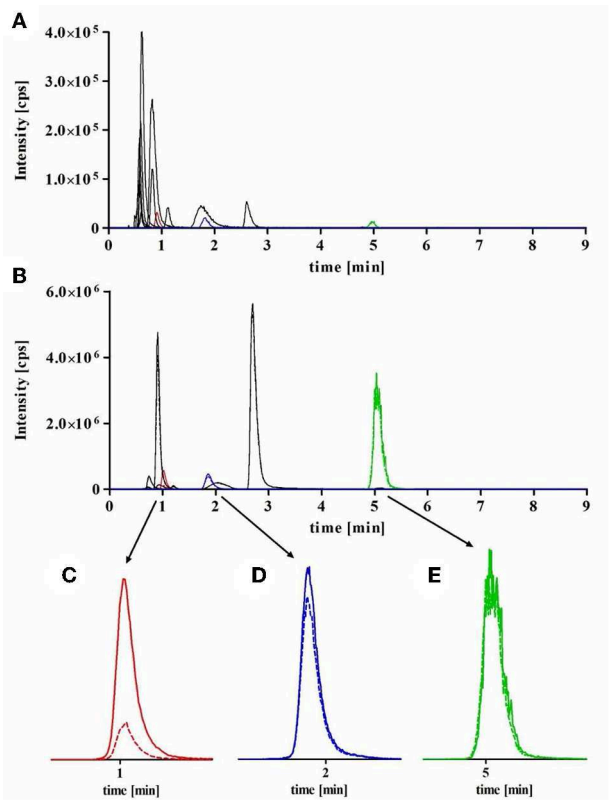


**FIGURE 2 |** Representative MRM chromatograms obtained for sublibrary A during hit identification. For HPLC a Purospher Star RP18e column (55 × 2 mm, 3 μm) in combination with 10 mM ammonium formate buffer (pH 7.0) and acetonitrile (gradient conditions see "materials and methods," injection volume 40 μL) at a flow rate of 450 μL/min and a column temperature of 25°C was used. **(A)** matrix standard containing each library component sample at a concentration of 1 nM, **(B)** total (full line) and non-specific binding (dotted line) samples (same binding samples as used in **Figures 3C,D**) at a concentration of 1 μM for each library component. Nonspecific binding was measured in presence of 100 mM GABA. Enlarged MRM chromatograms of **(C)** GAT1 inhibitors DDPM2565 (*m/z* 403 → 154) and **(D)** DDPM2330 (*m/z* 418 → 191), both showing significant specific binding toward GAT1 and **(E)** meclozine (*m/z* 391 → 201) as a representative compound without specific binding toward GAT1, note that full and dotted lines are in this case so close together that they can hardly be distinguished.

first set of samples of the MS binding experiments in addition to the reporter ligand, the sublibraries were contained with each component in a final concentration of 1 μM for determination of total reporter ligand binding in presence of the sublibraries and noteworthy, also for determination of total binding of the sublibrary components in the subsequent affinity selection step (only necessary in the case of an active sublibrary). Analogously, a second set of samples contained in addition to the sublibraries (with each component in a final concentration of 1 μM) 100 mM GABA for determination of non-specific reporter ligand binding and again, also for determination of non-specific binding of the sublibrary components (so far as necessary). These samples generated in the competitive MS binding experiment were analyzed for remaining reporter ligand binding by means of the isocratic LC-ESI-MS/MS method enabling quantification of NO711. A representative set of chromatograms obtained in this way, is exemplarily shown for sublibrary A in **Figure 3**. From these chromatograms, the percentages of specific NO711 binding remaining in presence of each sublibrary in relation to a control (only containing reporter ligand and target but not any other ligand = 100%) given in **Figure 4A** were determined. As expected, sublibraries A-E, all including two known GAT1 inhibitors, diminished remaining NO711 binding clearly under the 50% limit. Sublibrary F containing only 1 weak GAT1 inhibitor (p$K_i$ of 5.94) was able to reduce reporter binding to 48%, whereas sublibraries G and H—not comprising a known GAT1 inhibitor—diminished NO711 binding only to 86 and 60%, respectively.

## Hit Identification in Active Sublibraries by Means of ASMS

According to the screening concept, already described above in detail, hit identification by mass spectrometric quantification of bound sublibrary components has only to be accomplished for those sublibraries diminishing remaining reporter ligand binding below 50%. In order to investigate and to evaluate the envisaged hit identification procedure as systematically as possible, however, we had decided to evaluate all sublibraries. Accordingly, the samples, representing total and non-specific binding generated in the binding experiments before, were again analyzed by LC-MS (under the established gradient conditions), now recording MRM chromatograms for the individual library components to identify those library members showing a specific binding toward the NO711 binding site of GAT1 (i.e., total binding > non-specific binding). Exemplarily, the MRM chromatograms characterizing total binding (full line) and non-specific binding (dashed line) of the components from sublibrary A obtained in this way are shown in **Figure 2B**. In the corresponding enlarged sections below, specific binding—as difference between total and nonspecific binding—for the GAT1 inhibitors DDPM2565 (**Figure 2C**) and DDPM2330 (**Figure 2D**) is clearly visible. In contrast, compounds not binding at the NO711 binding site of GAT1 show almost the same peak intensities in both chromatograms as exemplified for meclozine (**Figure 2E**).

To compensate for the slight variations in the compounds' peaks intensities in the obtained MRM chromatograms caused by the LC-ESI-MS system, we did not directly compare the peak areas for hit identification but the corresponding normalized peak areas calculated as the quotient of the individual library component area vs. the internal standard [$^2H_{10}$]NO711 area, as shown in **Table 1** exemplarily for sublibrary A (the results for the other sublibraries are compiled in **Table S7**). But even then, i.e., when normalized peak areas are used, total binding higher than non-specific binding may be observed for individual library components which are not due to specific binding at GAT1, but are random results due to inevitable scattering of the data obtained for the triplicate samples, going back to the binding experiments and the LC-MS quantification. Indeed, in sublibrary A we observed distinctly higher normalized areas for total binding as compared to non-specific binding as expected for the GAT1 inhibitors DDPM2565 (p$K_i$ 7.83) and DDPM2330 (p$K_i$

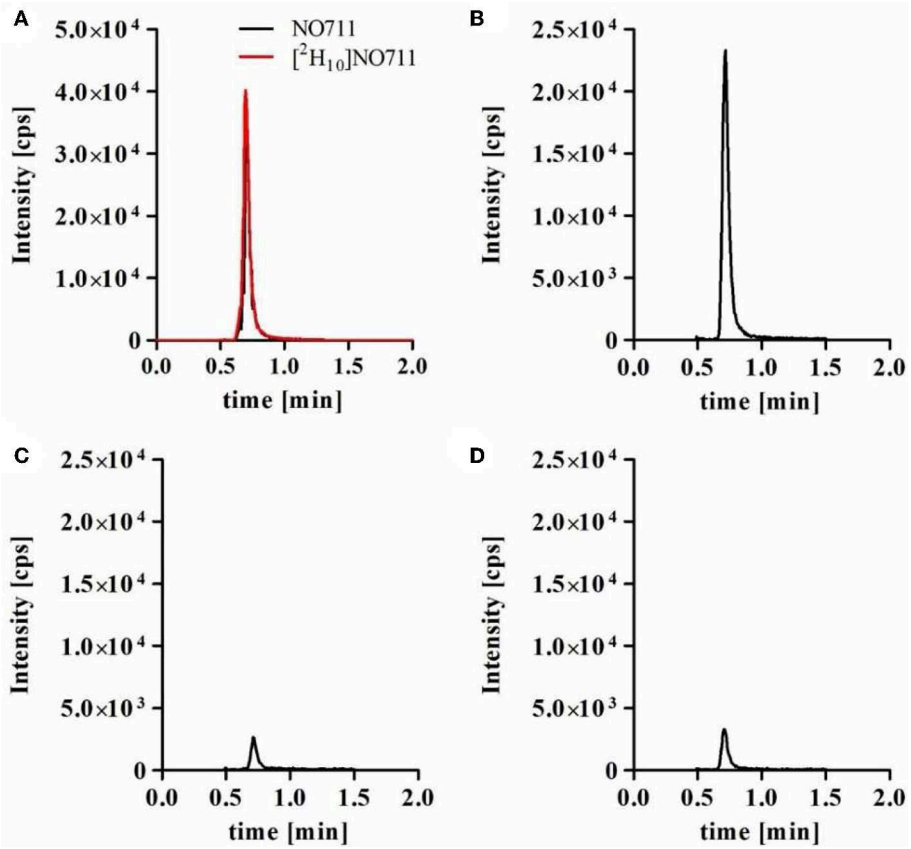


**FIGURE 3 |** Representative MRM chromatograms obtained in competitive MS Binding Assay investigating sublibrary A. For HPLC, a Purospher Star RP18e column (55 × 2 mm, 3 μm) in combination with 10 mM ammonium formate buffer (pH 7.0) and acetonitrile (ratio 50:50, v/v) at a flow rate of 350 μL/min, a column temperature of 25°C and an injection volume of 10 μL. **(A)** calibration standard containing 1 nM NO711 (*m/z* 381 → 180) and 1 nM [$^2H_{10}$]NO711 (*m/z* 391 → 190), **(B)** total binding of NO711. **(C)** Non-specific binding of NO711 was determined in the presence of sublibrary A at a concentration of 1 μM and 100 mM GABA and **(D)** remaining binding of NO711 only in presence of sublibrary A at a concentration of 1 μM. All samples contained [$^2H_{10}$]NO711 (*m/z* 391 → 190) as internal standard at a concentration of 1 nM, but for simplification of the obtained chromatograms the corresponding trace (*m/z* 391 → 190) is only shown in **(A)**. Note that these chromatograms **(C,D)** are based on the same samples as the chromatograms depicted in **Figure 2B**.

7.15), but also slightly higher ones for chlorpromazine, doxepin, oxazepam, and telmisartan, compounds not characterized as GAT1 inhibitors so far (see **Table 1**).

To investigate the probability of potential false positive results due to such random effects, we exemplarily repeated the complete screening procedure two times for sublibrary A. The results obtained in the affinity selection step for hit identification are shown in **Table 1**. For the GAT1 inhibitors DDPM2565 and DDPM2330, the normalized peak areas for total binding were in both repetitions again distinctly higher than those for non-specific binding. For the other compounds with normalized areas for total binding slightly exceeding those for non-specific binding in the first experiment, however, the results were not strictly consistent. Only for telmisartan, the determined total binding was higher in all experiments, whereas for chlorpromazine, doxepin, and oxazepam, this was only the case in one or two experiments. Furthermore, four additional compounds (8-OH DPAT, procaine, metoclopramide, and sulpiride) showing a similar behavior (i.e., higher total binding only in one or two experiments) were found in these repetition experiments (see **Table 1**). Considering these results, we decided to implement a simple statistical criterion to exclude as far as possible false positive results caused by random effects. Therefore, we performed a one-tailed *t*-test to identify those compounds with a total binding significantly exceeding non-specific binding and found that this aim could be fairly well-achieved when the confidence level was set at 97.5%. Applying this criterion to sublibrary A, both GAT1 inhibitors DDPM2565 and DDPM2330 were categorized as hits in all three experiments, whereas telmisartan and sulpiride did only show significant specific binding in one of three experiments. The results for the other seven sublibraries (B-H) obtained in this way are compiled in **Table S7** and can be summarized as following. Affinity selection analyzed by LC-MS as described above led to identification of all known GAT1 inhibitors in sublibraries A-F (DDPM1349, DDPM1981, DDPM2009, DDPM2029, DDPM2077, DDPM2187, DDPM2188, DDPM2330, DDPM2473, DDPM2565, and DDPM3138) as

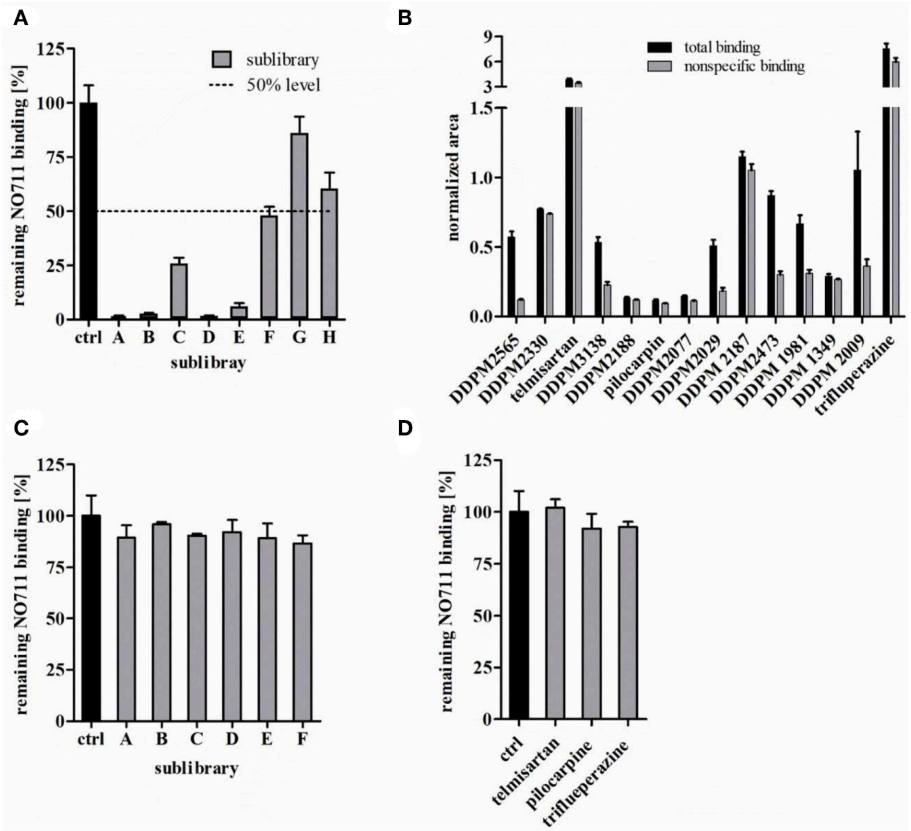


**FIGURE 4 |** Screening of the deliberately compiled 128 compound library. **(A)** Remaining specific NO711 binding in % in presence of the sublibraries A-H (concentration 1 μM each compound) using isocratic LC-ESI-MS/MS. Dashed line indicates the defined limit for further investigation. **(B)** Total and non-specific binding of all identified hits at a concentration each of 1 μM for each sublibraries component. Non-specific binding was determined in the presence of 100 mM GABA. **(C)** Remaining NO711 binding in % in presence of the reduced sublibraries A-F (each sublibrary compound 1 μM) and **(D)** in presence of the putative false positive hits (each compound 1 μM). Reported values represent means ± SD ($n = 3$).

hits. At this point, it is worth mentioning that the GAT1 inhibitor DDPM2077 with a p$K_i$ of 5.94 could be also found as hit, leading to the conclusion, that it is indeed possible to identify ligands up to an affinity of about 1 μM under the chosen screening conditions. In contrast, the non-selective and very weak GAT inhibitor DDPM3139 with a p$K_i$ of 4.18 at GAT1, was not identified as hit. Last but not least, it also worth mentioning, that in sublibraries containing two GAT1 inhibitors always both could be identified. Additionally, to the known GAT1 inhibitors, two further compounds namely, pilocarpine (sublibrary B) and trifluoperazine (sublibrary G) were classified as hits. The obtained normalized areas for total and non-specific binding samples for all classified hits are shown in **Figure 4B**. With respect to trifluperazine, however, it could already be concluded, that the affinity of this compound must be distinctly below the envisaged affinity limit ($K_i$ of about 700 nM), as sublibrary G did not reduce NO711 binding below 50% at a concentration of 1 μM.

In addition to hit identification based on the normalized areas obtained for total vs. non-specific binding as described above, it should be examined, if the recorded data can also give indications regarding affinity of the identified hits. Therefore, the concentrations of the hits specifically bound at the NO711 binding site of GAT1 were calculated from the obtained normalized areas making use of the relative response factor (RRF, see **Table S6**) determined for each library component before as summarized in **Table 2**.

In this context, it is, however, important to point out that such concentrations calculated correspondingly, can only be rough estimates and do by far not have the quality of results determined according to a validated quantification by means of LC-MS. Interestingly, in all libraries with two known GAT1 inhibitors, a higher concentration of specific binding was found for the compound with the higher affinity as compared to the one with the lower affinity. Furthermore, apart from sublibrary A, the total concentrations of bound GAT1 inhibitors in the sublibraries seem to be in the range of about 2–3 nM, which is well in agreement with a GAT1 concentration of about 3 nM in the binding experiment. In contrast, the estimated concentration of 10 nM for the specific binding of DDPM2565 is way too high considering that the target concentration amounts only to ∼3 nM, which as the upper limit for binding is also

**TABLE 1 |** Hit identification for sublibrary A.

| Compound | First experiment | | Second experiment | | Third experiment | |
|---|---|---|---|---|---|---|
| | Total binding (normalized area) | Non-specific binding (normalized area) | Total binding (normalized area) | Non-specific binding (normalized area) | Total binding (normalized area) | Non-specific binding (normalized area) |
| 4-(4-chlorophenyl)-piperidin-4-ol | n.d | n.d | n.d | n.d | n.d | n.d |
| 8-OH DAPT | 0.177 ± 0.006 | 0.193 ± 0.004 | 0.303 ± 0.012 | 0.283 ± 0.042 | 0.176 ± 0.012 | 0.162 ± 0.027 |
| Chlorpromazine | 6.590 ± 0.156 | 6.370 ± 0.198 | 6.173 ± 0.693 | 5.663 ± 0.597 | 6.147 ± 0.314 | 6.280 ± 0.928 |
| DDPM2330 | 0.771 ± 0.003 | 0.738 ± 0.002 | 0.876 ± 0.048 | 0.813 ± 0.031 | 0.490 ± 0.038 | 0.368 ± 0.021 |
| DDPM2565 | 0.571 ± 0.040 | 0.119 ± 0.006 | 0.799 ± 0.063 | 0.335 ± 0.011 | 0.454 ± 0.012 | 0.069 ± 0.017 |
| Doxepin | 0.705 ± 0.025 | 0.666 ± 0.008 | 0.932 ± 0.064 | 0.827 ± 0.096 | 0.433 ± 0.056 | 0.404 ± 0.084 |
| Fenoterol | 0.041 ± 0.008 | 0.041 ± 0.002 | 0.034 ± 0.002 | 0.030 ± 0.004 | 0.021 ± 0.003 | 0.021 ± 0.002 |
| Ketoprofen | 0.004 ± 0.000 | 0.005 ± 0.000 | 0.003 ± 0.000 | 0.003 ± 0.000 | 0.004 ± 0.000 | 0.004 ± 0.001 |
| Meclozine | 4.937 ± 0.861 | 6.095 ± 0.205 | 5.307 ± 0.931 | 5.253 ± 1.007 | 5.188 ± 0.271 | 5.523 ± 0.934 |
| Metoclopramide | 0.370±0.013 | 0.390±0.028 | 0.503±0.027 | 0.457±0.054 | 0.317±0.017 | 0.281±0.042 |
| Oxazepam | 0.132 ± 0.001 | 0.130 ± 0.026 | 0.120 ± 0.020 | 0.111 ± 0.007 | 0.097 ± 0.014 | 0.106 ± 0.024 |
| Piroxicam | 0.054 ± 0.000 | 0.060 ± 0.005 | 0.034 ± 0.001 | 0.034 ± 0.003 | 0.040 ± 0.001 | 0.037 ± 0.004 |
| Procaine | 0.073 ± 0.003 | 0.074 ± 0.006 | 0.092 ± 0.003 | 0.082 ± 0.010 | 0.073 ± 0.005 | 0.063 ± 0.008 |
| Roxithromycin | 0.020 ± 0.003 | 0.021 ± 0.001 | 0.003 ± 0.001 | 0.003 ± 0.001 | 0.012 ± 0.001 | 0.010 ± 0.001 |
| Sulpiride | 0.054 ± 0.002 | 0.056 ± 0.004 | 0.068 ± 0.002 | 0.061 ± 0.009 | 0.055 ± 0.003 | 0.047 ± 0.003 |
| Telmisartan | 3.853 ± 0.130 | 3.405 ± 0.106 | 2.577 ± 0.326 | 2.290 ± 0.340 | 2.257 ± 0.122 | 2.183 ± 0.455 |

*n.d., not determined.*

*Total and nonspecific binding of each sublibrary component at a concentration of 1 μM (three experiments, each performed in triplicates, nonspecific binding determined in presence of 100 mM GABA). Reported values represent means ± SD. Values marked gray represent identified hits based on significantly higher total than nonspecific binding (one-tailed t-test, CL = 97.5%).*

**TABLE 2 |** Estimation of concentrations for specific binding of compounds classified as hits in the deliberately compiled 128 compound library based on RRFs.

| Sublibrary | GAT1 inhibitor | Specific binding (nM) | $pK_i$ |
|---|---|---|---|
| A | DDPM2330 | 0.72 | 7.15 |
| | DDPM2565 | 10.0 | 7.83 |
| | Telmisartan | 1.58 | n.d. |
| B | DDPM3138 | 1.90 | 7.81 |
| | DDPM2188 | 0.38 | 6.42 |
| | Pilocarpine | 0.24 | n.d. |
| C | DDPM2077 | 0.48 | 5.94 |
| | DDPM2029 | 3.18 | 6.32 |
| D | DDPM2187 | 0.22 | 6.50 |
| | DDPM2473 | 3.44 | 8.13 |
| E | DDPM1981 | 2.20 | 7.04 |
| | DDPM1349 | 0.20 | 6.40 |
| F | DDPM2009 | 2.95 | 6.16 |
| G | Trifluoperazine | 1.46 | n.d. |

*n.d., $pK_i$ value unavailable.*

well-confirmed by the binding data found for the other GAT1 inhibitors (DDPM1349, DDPM1981, DDPM2009, DDPM2029, DDPM2077, DDPM2187, DDPM2188, DDPM2330, DDPM2473, and DDPM3138). A closer investigation of this phenomenon revealed strong adherence of DDPM2565 to various surfaces especially when dissolved in aqueous milieu. This results in an overestimated RRF-value and therefore in an overestimated concentration of bound compound.

In summary, it can be concluded, that the results obtained according to our established affinity selection protocol allow a rough categorization of affinity, but definitively not the establishment of a detailed affinity rank order. In this context, it should be kept in mind again, that the concentrations calculated for specific binding do not reflect equilibrium binding concentrations due to the dissociation issue during the washing process.

Finally, we demonstrated, that assessment of library activity and hit identification can also be accomplished simultaneously employing the gradient based LC method. To this end, the mass traces for NO711 together with those of the individual sublibrary components were recorded in MRM chromatograms under gradient conditions. Thereby, in a single set of LC-MS runs remaining reporter ligand binding in the presence of a sublibrary as well as total and non-specific binding of the library components could be quantified. Following this approach, the observed reduction of reporter ligand binding for sublibraries A-H was almost the same as determined before in two separate steps (see **Table S8**).

## Subsequent Investigations—Activity Assessment of Reduced Sublibraries and Hit Verification

Furthermore, Additional experiments should be performed that allow to clarify whether there are further hits besides the ones already identified in sublibraries A-F (characterized as active) during the affinity selection process, which may have been missed due to insufficient sensitivity of LC-MS quantification or due to competitive effects in a sublibrary (i.e., in the presence of high-affinity ligands). This should be assessed by

measuring the activities of the reduced sublibraries delineated form the active sublibraries by omitting the hits identified before in additional competitive binding experiments. The results obtained in this way are shown in **Figure 4C**. In contrast to the original sublibraries A-F, the corresponding reduced sublibraries did hardly reduce reporter ligand binding, indicating that there are no further GAT1 ligands with significant affinity in these sublibraries.

Finally, the activity of compounds classified as hits during the affinity selection process should be verified. As the affinities of the identified GAT1 inhibitors DDPM1349, DDPM1981, DDPM2009, DDPM2029, DDPM2077, DDPM2187, DDPM2188, DDPM2330, DDPM2473, DDPM2565, and DDPM3138 had already been assessed earlier (see **Table 2**), we focused on the compounds additionally classified as hits in the present study, namely telmisartan, pilocarpine, and trifluoperazine (we did not include sulpiride, as this compound was only classified as hit in the exemplarily repeated experiments for sublibrary A). Investigating the three compounds individually in competitive binding experiments showed that none of the compounds could distinctly inhibit NO711 binding as shown in **Figure 4D**, clearly indicating that these compounds do not have significant affinity toward the NO711 binding site of GAT1. In this sense, these compounds represent false positive hits, nevertheless, it cannot be excluded that these compounds might bind to GAT1 at another binding site which is also addressed by GABA. Corresponding investigations have to be done and are not yet finished, at least for trifluoperazine, however, inhibition of GAT1 characterized by a $pIC_{50}$ value of 4.62 could already be found. Summing up the results of these subsequent investigations in the context of the complete screening protocol, it can be concluded, that both false positive as well as false negative hits can be reliably avoided in this way.

## Proof of Concept—Screening of the Tocrisscreen Plus Library for Ligands Addressing GAT1

As a proof of concept of the presented strategy, we applied the developed protocol to screen 1,280 well-characterized pharmacological tool compounds of the Tocris Screen Plus library for ligands addressing the NO711 binding site of GAT1. The entire library was again divided in sublibraries containing 16 compounds, but in this case the sequence set by Tocris was left unchanged or in other words the sublibraries were composed without considering the identity of the library components. This means that the sublibraries were compiled absolutely by random (i.e., without knowledge of molecular weight or biological activity of the individual compounds). Following the established screening protocol, we investigated at first the sublibraries regarding their potency to inhibit reporter ligand binding (again with the individual components at a final concentration of 1 μM). Sublibrary 7, sublibrary 9 as well as sublibrary 38 decreased reporter ligand binding to 12, 8, and 4%, respectively, i.e., distinctly under the defined 50% limit, and were therefore classified as active, whereas the 77 other sublibraries were classified inactive. Surprisingly, for one of these sublibraries, namely sublibrary 14, we determined an unexpectedly high value of 360% of remaining reporter ligand binding (**Figure 5A**). As artifacts due to cross contamination during the process of the binding experiment or cross talk phenomena during LC-ESI-MS/MS analysis could be excluded, we decided to subject sublibrary 14 together with sublibraries 7, 9, and 38 to the hit identification procedure. For the recording of the MRM chromatograms of all components of the active sublibraries the fragmentation (again employing the automated procedure of the mass spectrometer) of the respective constituents had to be determined. To this end, it was necessary to check the identity of the corresponding sublibrary components. Thereby, it turned out that NO711 (referred to as NNC711 in the Tocris library), which is the compound used as reporter ligand in our competitive binding experiment, is a member of sublibrary 14, for which a specific reporter ligand binding of 360% had been found. The observed high reporter ligand binding in this sublibrary is therefore quite simple to explain. It is to be attributed to an enhanced NO711 concentration of 1010 nM in comparison with 10 nM in the control (i.e., in the absence of any GAT ligands), almost completely saturating the GAT1 binding sites and consequently leading to a concentration of bound NO711 close to the total concentration of GAT1 in the binding sample. Additionally, in the other active sublibraries, we also recognized well-known GAT1 inhibitors at this step, namely SKF 89976A (sublibrary 7), CI 966 (sublibrary 9), and tiagabine (sublibrary 38). Despite this knowledge, we followed the established screening protocol to prove, that these GAT1 inhibitors and possibly also other members of the library can be identified as hits.

Initially, we examined again the MRM chromatograms obtained for matrix samples containing the library components of sublibraries 7, 9, 14, and 38 in a concentration of 1 nM, based on the mass transitions generated with the automatic optimization tool of the mass spectrometer. These chromatograms revealed that all compounds except for DuP 697 (sublibrary 9), IEM 1460 (sublibrary 14), and flurizan (sublibrary 38) could be quantified with sufficient sensitivity under these conditions. This means that the rate of quantifiable compounds is again about 95% (detailed results obtained from these MRM chromatograms are shown in the **Table S9**). Next, we recorded MRM chromatograms for the samples representing total and non-specific binding, respectively, of sublibraries 7, 9, 14, and 38 (see **Table S10**). Out of all library components investigated in this way, only SKF 89976A (sublibrary 7), CI 966 (sublibrary 9), NNC711 (sublibrary 14), and tiagabine (sublibrary 38), revealed significantly higher total than non-specific binding (based on the corresponding normalized areas) as shown in **Figure 5B** and could thus be classified as hits. Accordingly, again all "active" ligands could be unveiled by a significant specific binding to the NO711 labeled binding site of GAT1 under the applied conditions and unambiguously identified as hits by our screening concept. The concentrations calculated for specific binding of these GAT1 inhibitors (based on the corresponding RRFs) are shown in **Table 3**. The conclusions to be drawn from these results are again, that the concentrations determined for high-affinity ligands reflecting their specific binding are close to the target

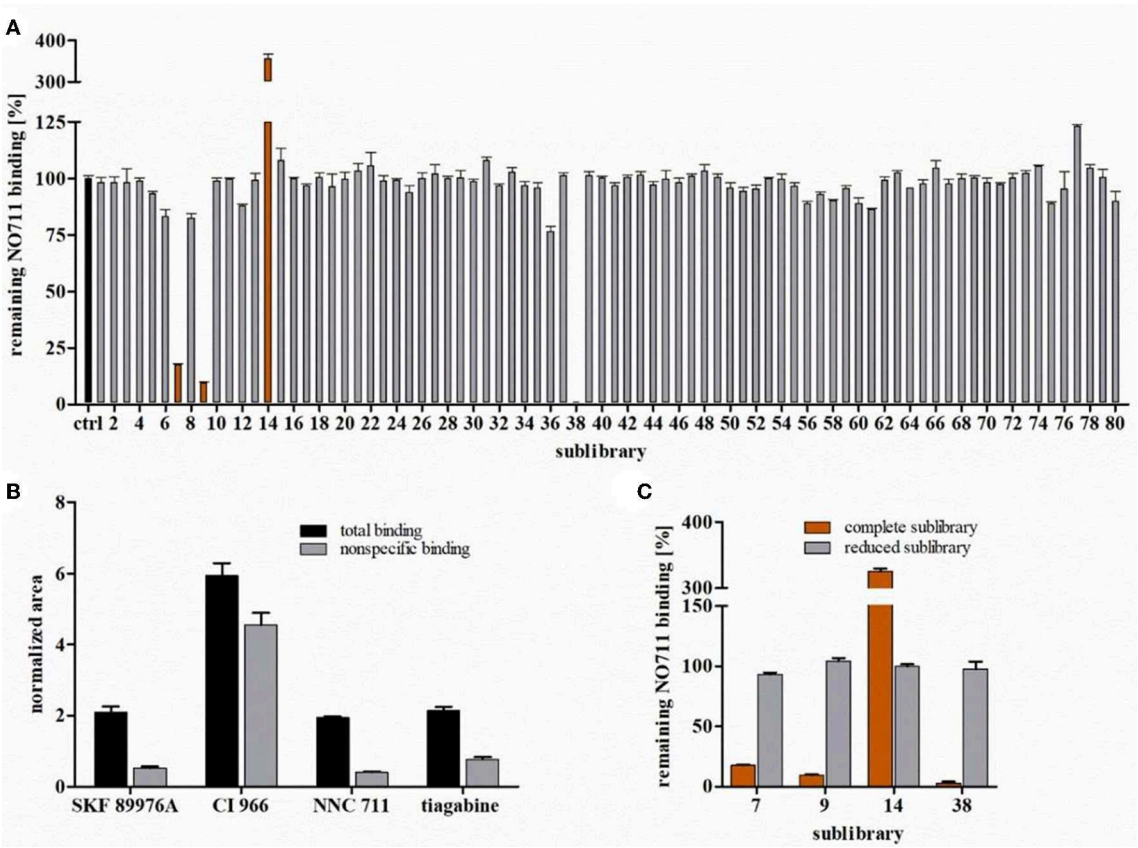


**FIGURE 5 |** Screening of the Tocris Plus Library. **(A)** Remaining NO711 binding % in presence of the sublibraries 1–80. **(B)** Total and non-specific binding of all identified hits at a concentration each of 1 μM for each sublibrary component. Non-specific binding was determined in the presence of 100 mM GABA. **(C)** Remaining NO711 binding % determined in presence of the sublibraries and corresponding reduced sublibraries (without identified hits). Reported values represent means ± SD ($n = 3$).

**TABLE 3 |** Estimation of the concentration of specifically bound GAT1 inhibitors of the Tocris Screen Plus library based on RRFs.

| Sublibrary | GAT1 inhibitor | Specific binding (nM) |
|---|---|---|
| 7 | SKF 89976A | 2.24 |
| 9 | CI 966 | 3.04 |
| 14 | NNC711 (NO711) | 2.93 |
| 38 | Tiagabine | 3.28 |

concentration and furthermore, that the affinities of SKF 89976A, CI 966, and tiagabine can be estimated to be roughly in the same order of magnitude as NO711.

Finally, we removed all identified hits (i.e., SKF 89976A from sublibrary 7, CI 966 from sublibrary 9, NNC711 from sublibrary 14, and tiagabine from sublibrary 38) and studied the resulting "reduced sublibraries" in a further competitive binding experiment for inhibition of reporter ligand binding. The percentages of remaining bound reporter ligand determined for the reduced sublibraries 7 (93%), 9 (104%), 14 (100%), and 38 (97%) are depicted in **Figure 5C** (together with the percentages obtained before for the complete sublibraries). Thereby, it could be demonstrated that these sublibraries do not contain further ligands with significant affinity for the NO711 binding site of GAT1, beyond the above mentioned known GAT1 inhibitors.

As stated in the section "Basic considerations before implementation of the library screening concept," the sublibrary size is flexible and not limited. It can easily be increased to more than 16 constituents, the so far used maximum number. To demonstrate this, the former sublibraries 5-8 were pooled to give a sublibrary comprising 64 compounds. For this 64 compound sublibrary, containing the GAT1 inhibitor SKF 89976A, a reduction of reporter ligand binding down to 3% was determined in the first step. For hit identification, in this case, the mass transitions of 64 components had to be investigated (from which the ones for sublibrary 7 were already known). Again three out of 64 compounds, namely brefeldin A, olvanil, and SDZ 220-581 could not be quantified based on the automatically generated mass transitions in the resulting MRM chromatograms, the success rate for quantifiable compounds down to a concentration of at least 1 nM was again amounting to 95% (**Table S9**). Then in analogy to the procedure described above for the sublibraries containing 16

components, total and non-specific binding were determined for the 64 constituents comprising libraries (for detailed results see **Table S11**). As expected, only SKF 89976A gave a significant specific binding and this could be identified as hit.

The results obtained here demonstrate that our strategy to combine MS Binding Assays and ASMS is indeed successful to overcome the weaknesses of both methods. While screening of the 1,280 compound library by MS Binding Assays alone would require elaborate deconvolution of the four active sublibraries, sole screening on basis of ASMS would come along with great efforts for investigation of 1,280 compounds' mass transitions. In contrast, the combination of both concepts reduces these efforts distinctly, as only 64 of 1,280 compounds have to be characterized for their mass transitions. Additionally, the efforts for deconvolution of four sublibaries can be avoided. Last but not least should be mentioned, that even ligands with weak MS sensitivities, which would stay unidentified in conventional ASMS approaches, can be reliably found.

## CONCLUSION

In the present study, the concepts of competitive MS Binding Assays and ASMS were combined to a new, powerful, efficient, and reliable library screening approach. It starts with a filtration based competitive binding experiment, that is in the first step analyzed for reduced binding of the reporter ligand, and—only if a sublibrary is active—additionally for individual library components showing specific binding (i.e., total binding surpassing non-specific binding). In this way, the strengths of MS Binding Assays and ASMS, i.e., the unambiguous indication of the presence or absence of hits in a library by MS Binding Assays and the efficiency of hit identification by ASMS are merged. Correspondingly, also the weaknesses of both concepts, i.e., the time consuming deconvolution strategies for hit identification in MS Binding Assays and the issue of false negative or false positive results inherently coupled with ASMS, can be avoided. Application of this concept to screening of a small, deliberately compiled library of 128 compounds and a medium-size library of 1,280 compounds for ligands addressing the neuronal GABA transporter GAT1 demonstrated its capability to identify all hits present in the libraries down to an affinity characterized by a p$K_i$ value of about 6.

The concept is based on a high-sensitive LC-ESI-MS method employing a triple quadrupole mass spectrometer (without being restricted to this instrument type) for quantification of a broad variety of small molecule compounds down to the pM concentration level. In this way, binding of 95% of all investigated test compounds could be quantified, distinctly surpassing the success rates for mass spectrometric detection of common ASMS approaches. This highly sensitive quantification enables very low target concentrations (in the low nM range) in the binding experiment, rendering the screening concept particularly attractive for membrane integrated drug targets. Therefore, it does, in contrast to ASMS approaches, not demand high sophisticated expression systems and purification methods for a target of interest. But, to allow reliable hit identification, quantification of library components down to an LLOQ distinctly below the employed target concentration should be possible. With respect to the number of compounds investigated in a single binding experiment (here referred to as "sublibrary"), the concept is very flexible and can be adopted at will depending e.g., on the expected hit rate, the defined activity criterion, or the size of the entire library. In this study, 16 membered sublibraries proved to be very efficient as well as a 64 membered sublibrary investigated exemplarily, but even higher numbers can be envisaged as long as all the compounds can be quantified in a single LC-MS run.

As the presented strategy defines "activity" of compounds in competitive MS Binding Assays, it is ideally suited for the screening of compounds addressing a distinct binding site at a target—that is the one addressed by the reporter ligand. However, the presented concept is not restricted to screening toward ligands occupying this binding site. Inhibition of reporter ligand binding, not due to competitive interactions and furthermore, compounds enhancing reporter ligand binding can be detected as well. It has to be kept in mind only at this point, that non-specific binding of library components has to be defined appropriately to achieve this goal, for example employing a membrane preparation (or another suitable source) lacking the target instead of adding a competitive ligand in high excess, as it was done in this study. Considering the capabilities and the potential provided by the combination of competitive MS Binding Assays and ASMS, the concept described here can be assumed to become a valuable and powerful tool in early drug research.

## DATA AVAILABILITY STATEMENT

All datasets generated for this study are included in the manuscript/**Supplementary Files**.

## AUTHOR CONTRIBUTIONS

JG, GH, and KW wrote or contributed to the writing of the manuscript and participated in research study design. JG carried out laboratory and data analysis.

## DEDICATION

This article is dedicated to Prof. Dr. Dr. h.c. mult. Hildebert Wagner with warmest wishes on the occasion of his 90th birthday.

## SUPPLEMENTARY MATERIAL

The Supplementary Material for this article can be found online at: https://www.frontiersin.org/articles/10.3389/fchem.2019.00665/full#supplementary-material

## REFERENCES


Ackermann, T. M., Bhokare, K., Hofner, G., and Wanner, K. T. (2019). MS Binding Assays for GlyT1 based on Org24598 as nonlabelled reporter ligand. *Neuropharmacology*. doi: 10.1016/j.neuropharm.2019.03.004. [Epub ahead of print].

Annis, A., Chuang, C.-C., and Nazef, N. (2007a). "ALIS: an affinity selection–mass spectrometry system for the discovery and characterization of protein–ligand interactions," in *Mass Spectrometry in Medicinal Chemistry*, eds K. T. Wanner and G. Höfner (Weinheim: Wiley-VCH), 121–156.

Annis, D. A., Nickbarg, E., Yang, X., Ziebell, M. R., and Whitehurst, C. E. (2007b). Affinity selection-mass spectrometry screening techniques for small molecule drug discovery. *Curr. Opin. Chem. Biol.* 11, 518–526. doi: 10.1016/j.cbpa.2007.07.011

Annis, D. A., Shipps, G. W. Jr., Deng, Y., Popovici-Muller, J., Siddiqui, M. A., Curran, P. J., et al. (2007c). Method for quantitative protein-ligand affinity measurements in compound mixtures. *Anal. Chem.* 79, 4538–4542. doi: 10.1021/ac0702701

Arias, H. R., Rosenberg, A., Targowska-Duda, K. M., Feuerbach, D., Jozwiak, K., Moaddel, R., et al. (2010). Tricyclic antidepressants and mecamylamine bind to different sites in the human alpha4beta2 nicotinic receptor ion channel. *Int. J. Biochem. Cell. Biol.* 42, 1007–1018. doi: 10.1016/j.biocel.2010.03.002

Aubé, J., Rogers, S. A., and Santini, C. (2014). "9.01 enabling technologies in high throughput chemistry," in Comprehensive Organic Synthesis II, eds P. Knochel and G. A. Molander (Amsterdam: Elsevier), 1–27.

Babbitt, C. C., Markstein, M., and Gray, J. M. (2015). Recent advances in functional assays of transcriptional enhancers. *Genomics* 106, 137–139. doi: 10.1016/j.ygeno.2015.06.002

Bennett, J. P. J., and Yamamura, H. I. (1985). "Neurotransmitter, hormone, or drug receptor binding methods," in *Neurotransmitter Receptor Binding*, eds H. I. Yamamura, M. J. Kuhar and S. J. Enna (New York, NY: Raven Press), 61–89.

Chen, X., Stout, S., Mueller, U., Boykow, G., Visconti, R., Siliphaivanh, P., et al. (2017). Label-free, LC-MS-based assays to quantitate small-molecule antagonist binding to the mammalian BLT1 receptor. *SLAS Discov*. 22, 1131–1141. doi: 10.1177/2472555217719748.

Croston, G. E. (2002). Functional cell-based uHTS in chemical genomic drug discovery. *Trends Biotechnol.* 20, 110–115. doi: 10.1016/S0167-7799(02)01906-6

Dimasi, J. A., Hansen, R. W., and Grabowski, H. G. (2003). The price of innovation: new estimates of drug development costs. *J. Health Econ.* 22, 151–185. doi: 10.1016/S0167-6296(02)00126-1

Eldefrawi, A. T., Miller, E. R., Murphy, D. L., and Eldefrawi, M. E. (1982). [3H]Phencyclidine interactions with the nicotinic acetylcholine receptor channel and its inhibition by psychotropic, antipsychotic, opiate, antidepressant, antibiotic, antiviral, and antiarrhythmic drugs. *Mol. Pharmacol.* 22, 72–81.

Fang, Y. (2012). Ligand-receptor interaction platforms and their applications for drug discovery. *Expert Opin. Drug Discov.* 7, 969–988. doi: 10.1517/17460441.2012.715631

Geoghegan, K. F., and Kelly, M. A. (2005). Biochemical applications of mass spectrometry in pharmaceutical drug discovery. *Mass Spectrom. Rev.* 24, 347–366. doi: 10.1002/mas.20019

Gottesmann, C. (2002). GABA mechanisms and sleep. *Neuroscience* 111, 231–239. doi: 10.1016/S0306-4522(02)00034-9

Grimm, S. H., Hofner, G., and Wanner, K. T. (2015). MS Binding Assays for the three monoamine transporters using the triple reuptake inhibitor (1R,3S)-Indatraline as native marker. *ChemMedChem* 10, 1027–1039. doi: 10.1002/cmdc.201500084

Gwak, Y. S., and Hulsebosch, C. E. (2011). GABA and central neuropathic pain following spinal cord injury. *Neuropharmacology* 60, 799–808. doi: 10.1016/j.neuropharm.2010.12.030

Hofner, G., and Wanner, K. T. (2003). Competitive binding assays made easy with a native marker and mass spectrometric quantification. *Angew. Chem. Int. Ed. Engl.* 42, 5235–5237. doi: 10.1002/anie.200351806

Höfner, G., and Wanner, K. T. (2015). "MS Binding Assays," in *Analyzing Biomolecular Interactions by Mass Spectrometry*, eds J. Kool and W. M. Niessen (Weinheim: Wiley-VHC), 165–198.

Hofstadler, S. A., and Sannes-Lowery, K. A. (2006). Applications of ESI-MS in drug discovery: interrogation of noncovalent complexes. *Nat. Rev. Drug Discov.* 5, 585–595. doi: 10.1038/nrd2083

Hughes, J. P., Rees, S., Kalindjian, S. B., and Philpott, K. L. (2011). Principles of early drug discovery. *Br. J. Pharmacol.* 162, 1239–1249. doi: 10.1111/j.1476-5381.2010.01127.x

Hulme, E. C., and Birdsall, N. J. M. (1992). "Strategy and tactics in receptor binding studies," in *Receptor-Ligand Interactions. A Practical Approach*, ed E. C. Hulme (Oxford: IRL Press), 63–176.

Jonker, N., Kool, J., Irth, H., and Niessen, W. M. (2011). Recent developments in protein-ligand affinity mass spectrometry. *Anal. Bioanal. Chem.* 399, 2669–2681. doi: 10.1007/s00216-010-4350-z

Kalueff, A. V., and Nutt, D. J. (2007). Role of GABA in anxiety and depression. *Depress. Anxiety* 24, 495–517. doi: 10.1002/da.20262

Katz, E. J., Cortes, V. I., Eldefrawi, M. E., and Eldefrawi, A. T. (1997). Chlorpyrifos, parathion, and their oxons bind to and desensitize a nicotinic acetylcholine receptor: relevance to their toxicities. *Toxicol. Appl. Pharmacol.* 146, 227–236. doi: 10.1006/taap.1997.8201

Kern, F., and Wanner, K. T. (2019). Screening oxime libraries by means of mass spectrometry (MS) binding assays: identification of new highly potent inhibitors to optimized inhibitors gamma-aminobutyric acid transporter 1. *Bioorg. Med. Chem.* 27, 1232–1245. doi: 10.1016/j.bmc.2019.02.015

Kingston, D. G. (2011). Modern natural products drug discovery and its relevance to biodiversity conservation. *J. Nat. Prod.* 74, 496–511. doi: 10.1021/np100550t

Kutilek, V. D., Andrews, C. L., Richards, M. P., Xu, Z., Sun, T., Chen, Y., et al. (2016). Integration of affinity selection-mass spectrometry and functional cell-based assays to rapidly triage druggable target space within the NF-kappaB pathway. *J. Biomol. Screen.* 21, 608–619. doi: 10.1177/1087057116637353

Lisman, J. E., Coyle, J. T., Green, R. W., Javitt, D. C., Benes, F. M., Heckers, S., et al. (2008). Circuit-based framework for understanding neurotransmitter and risk gene interactions in schizophrenia. *Trends Neurosci.* 31, 234–242. doi: 10.1016/j.tins.2008.02.005

Lydiard, R. B. (2003). The role of GABA in anxiety disorders. *J. Clin. Psychiatry* 64(Suppl. 3), 21–27.

Maguire, J. J., Kuc, R. E., and Davenport, A. P. (2012). Radioligand binding assays and their analysis. *Methods Mol. Biol.* 897, 31–77. doi: 10.1007/978-1-61779-909-9_3

Massink, A., Holzheimer, M., Holscher, A., Louvel, J., Guo, D., Spijksma, G., et al. (2015). Mass spectrometry-based ligand binding assays on adenosine A1 and A2A receptors. *Purinergic Signal.* 11, 581–594. doi: 10.1007/s11302-015-9477-0

Neiens, P., De Simone, A., Hofner, G., and Wanner, K. T. (2018). Simultaneous multiple MS Binding Assays for the dopamine, norepinephrine, and serotonin transporters. *ChemMedChem* 13, 453–463. doi: 10.1002/cmdc.201700737

Neiens, P., Hofner, G., and Wanner, K. T. (2015). MS Binding Assays for D1 and D5 dopamine receptors. *ChemMedChem* 10, 1924–1931. doi: 10.1002/cmdc.201500355

Schermann, S. M., Simmons, D. A., and Konermann, L. (2005). Mass spectrometry-based approaches to protein-ligand interactions. *Expert Rev. Proteomics* 2, 475–485. doi: 10.1586/14789450.2.4.475

Schuller, M., Hofner, G., and Wanner, K. T. (2017). Simultaneous multiple MS Binding Assays addressing D1 and D2 dopamine receptors. *ChemMedChem* 12, 1585–1594. doi: 10.1002/cmdc.201700369

Scimemi, A. (2014). Structure, function, and plasticity of GABA transporters. *Front. Cell. Neurosci.* 8:161. doi: 10.3389/fncel.2014.00161

Sichler, S., Hofner, G., Rappengluck, S., Wein, T., Niessen, K. V., Seeger, T., et al. (2018). Development of MS Binding Assays targeting the binding site of MB327 at the nicotinic acetylcholine receptor. *Toxicol. Lett.* 293, 172–183. doi: 10.1016/j.toxlet.2017.11.013

Sindelar, M., Lutz, T. A., Petrera, M., and Wanner, K. T. (2013). Focused pseudostatic hydrazone libraries screened by mass spectrometry binding assay: optimizing affinities toward gamma-aminobutyric acid transporter 1. *J. Med. Chem.* 56, 1323–1340. doi: 10.1021/jm301800j

Stahelin, R. V. (2013). Surface plasmon resonance: a useful technique for cell biologists to characterize biomolecular interactions. *Mol. Biol. Cell.* 24, 883–886. doi: 10.1091/mbc.e12-10-0713

Stoddart, L. A., White, C. W., Nguyen, K., Hill, S. J., and Pfleger, K. D. (2016). Fluorescence- and bioluminescence-based approaches to study GPCR ligand binding. *Br. J. Pharmacol.* 173, 3028–3037. doi: 10.1111/bph.13316

Treiman, D. M. (2001). GABAergic mechanisms in epilepsy. *Epilepsia* 42(Suppl. 3), 8–12. doi: 10.1046/j.1528-1157.2001.042suppl.3008.x

Trivedi, S., Liu, J., Liu, R., and Bostwick, R. (2010). Advances in functional assays for high-throughput screening of ion channels targets. *Expert Opin. Drug Discov.* 5, 995–1006. doi: 10.1517/17460441.2010.513377

Van Breemen, R. B., Huang, C. R., Nikolic, D., Woodbury, C. P., Zhao, Y. Z., and Venton, D. L. (1997). Pulsed ultrafiltration mass spectrometry: a new method for screening combinatorial libraries. *Anal. Chem.* 69, 2159–2164. doi: 10.1021/ac970132j

Walker, S. S., Degen, D., Nickbarg, E., Carr, D., Soriano, A., Mandal, M., et al. (2017). Affinity selection-mass spectrometry identifies a novel antibacterial RNA polymerase inhibitor. *ACS Chem. Biol.* 12, 1346–1352. doi: 10.1021/acschembio.6b01133

Whitehurst, C. E., Nazef, N., Annis, D. A., Hou, Y., Murphy, D. M., Spacciapoli, P., et al. (2006). Discovery and characterization of orthosteric and allosteric muscarinic M2 acetylcholine receptor ligands by affinity selection-mass spectrometry. *J. Biomol. Screen.* 11, 194–207. doi: 10.1177/1087057105284340

Zehender, H., Le Goff, F., Lehmann, N., Filipuzzi, I., and Mayr, L. M. (2004). SpeedScreen: the "Missing Link" between genomics and lead discovery. *J. Biomol. Screen.* 9, 498–505. doi: 10.1177/1087057104267605

Zepperitz, C., Hofner, G., and Wanner, K. T. (2006). MS-binding assays: kinetic, saturation, and competitive experiments based on quantitation of bound marker as exemplified by the GABA transporter mGAT1. *ChemMedChem* 1, 208–217. doi: 10.1002/cmdc.200500038

Zhu, Z., and Cuozzo, J. (2009). Review article: high-throughput affinity-based technologies for small-molecule drug discovery. *J. Biomol. Screen.* 14, 1157–1164. doi: 10.1177/1087057109350114

**Conflict of Interest:** The authors declare that the research was conducted in the absence of any commercial or financial relationships that could be construed as a potential conflict of interest.

frontiers in Chemistry

REVIEW
published: 18 October 2019
doi: 10.3389/fchem.2019.00673

# Kinetic Analysis by Affinity Chromatography

*Sazia Iftekhar, Susan T. Ovbude and David S. Hage**

*Department of Chemistry, University of Nebraska-Lincoln, Lincoln, NE, United States*

Important information on chemical processes in living systems can be obtained by the rates at which these biological interactions occur. This review will discuss several techniques based on traditional and high-performance affinity chromatography that may be used to examine the kinetics of biological reactions. These methods include band-broadening measurements, techniques for peak fitting, split-peak analysis, peak decay studies, and ultrafast affinity extraction. The general principles and theory of each method, as applied to the determination of rate constants, will be discussed. The applications of each approach, along with its advantages and limitations, will also be considered.

**Keywords: affinity chromatography, biological interactions, kinetics, peak profiling, peak decay method, plate height method, split-peak method, ultrafast affinity extraction**

OPEN ACCESS

***Edited by:***
*Gabriella Massolini, University of Pavia, Italy*

***Reviewed by:***
*Nikolaos E. Labrou, Agricultural University of Athens, Greece*
*Wei-Lung Tseng, National Sun Yat-sen University, Taiwan*

****Correspondence:***
*David S. Hage*
*dhage1@unl.edu*

***Specialty section:***
*This article was submitted to Analytical Chemistry, a section of the journal Frontiers in Chemistry*

***Received:*** *09 July 2019*
***Accepted:*** *25 September 2019*
***Published:*** *18 October 2019*

***Citation:***
*Iftekhar S, Ovbude ST and Hage DS (2019) Kinetic Analysis by Affinity Chromatography. Front. Chem. 7:673. doi: 10.3389/fchem.2019.00673*

## INTRODUCTION

The analysis of biological interactions is important in describing and studying the processes that occur in living systems. Many biological interactions are due to non-covalent processes that involve drugs, hormones, proteins, peptides, metal ions, nucleic acids, and lipids (Myszka and Rich, 2000; Schreiber et al., 2009; Vuignier et al., 2010; Williams, 2013; Zheng et al., 2014a, 2015a; Bi et al., 2015). For instance, transport proteins such as $\alpha_1$-acid glycoprotein (AGP) and human serum albumin (HSA) can bind to and carry many drugs within the circulatory system through non-covalent interactions, thereby affecting the absorption, distribution, metabolism, and excretion of these drugs in humans (Zheng et al., 2014a; Bi et al., 2015). Information on the kinetics of a biological interaction can help determine the function of these interactions, as well as the mechanisms through which they occur (Myszka and Rich, 2000; Schreiber et al., 2009; Vuignier et al., 2010; Williams, 2013; Zheng et al., 2014a, 2015b; Bi et al., 2015).

There are a variety of techniques that can be used to study the kinetics of a biological system and to measure the rate constants for this type of process. These methods are currently chosen based on the type of the system that is under investigation, the complexity of the reaction, the rates of the corresponding reactions, and the amounts and concentrations of the reactants and products that are required and available. Approaches that have been used in the past to study reaction rates in biological systems are surface plasmon resonance spectroscopy (SPR), capillary electrophoresis (CE), and stopped-flow analysis (Myszka and Rich, 2000; Krylov, 2007; Williams, 2013; Zheng et al., 2015b). However, each of these methods possesses several disadvantages. For instance, there is the need for a sufficient concentration of the reactant or product and a measurable signal in stopped-flow analysis, the requirement of a special type of surface in SPR, and the need for a measurable difference in mobilities between the products and reactants in CE. There is also the need to consider adsorption of biomolecules to the capillary surface in CE, which can be minimized through capillary treatment with a suitable polymer (Zheng et al., 2015b).

High-performance affinity chromatography (HPAC) is an alternative tool that can be used to determine rate constants in biological systems. HPAC is a form of affinity chromatography which uses a biologically-related binding agent as a stationary phase, which is then placed in a column suitable for high-performance liquid chromatography (HPLC). This binding agent, or affinity ligand, may consist of an immobilized protein, enzyme or antibody; enzyme substrate or inhibitor; antigen; biomimetic dye; and DNA or RNA sequence, among others (Hage, 2006; Schiel and Hage, 2009). HPAC makes use of small and rigid supports such as silica or monoliths which can be used with the immobilized agent to provide rapid and efficient separations. In both HPAC and traditional affinity chromatography, the target analyte undergoes selective and reversible interactions with the binding agent, which allows the target to be captured and retained as it goes through the column (Hage et al., 2012; Bi et al., 2015; Zheng et al., 2015b; Zhang et al., 2018). HPAC and affinity chromatography are often used as separation methods to purify or analyze a given compound or group of related solutes in an applied sample. This has included use of these methods for sample pretreatment, flow-based immunoassays, chiral separations, and multi-dimensional methods (Hage, 2006). However, HPAC and related affinity methods have also been employed to characterize the strength, binding sites, and rates of biological interactions. Examples of systems that have been investigated with such an approach include binding by drugs with serum proteins, antibody-antigen interactions, binding of enzymes with substrates or inhibitors, interactions of immunoglobulin-binding proteins with antibodies, and binding of glycoproteins by lectins (Hage, 2006; Schiel and Hage, 2009; Zhang et al., 2018).

**Figure 1** shows two general formats that have been employed in HPAC and affinity chromatography for determining rate constants. In **Figure 1A**, the target analyte is introduced into an affinity column containing the binding agent in an immobilized form. In this format, the retention and/or elution behavior of the analyte provides information on the dissociation or association rates between the target analyte and binding agent (Schiel and Hage, 2009). The second format is shown in **Figure 1B**. In this approach, the analyte is introduced into the column along with a soluble binding agent. An immobilized binding agent in the column acts as a secondary probe to examine the analyte-binding agent interactions in solution by capturing the target in its free, non-bound state (Bi et al., 2015; Zheng et al., 2015b).

The choice of a method for characterizing the rates of analyte-ligand binding by HPAC and affinity chromatography will depend on several factors. Some important considerations are the overall binding strength and rate of the interaction that is to be observed and the type of information that is required (Schiel and Hage, 2009; Zheng et al., 2014a, 2015b; Bi et al., 2015). Other considerations are the amounts of analyte and binding agent that are available for analysis. For instance, some affinity-based methods rely on application of a target analyte in a continuous manner (i.e., a format known as frontal affinity chromatography

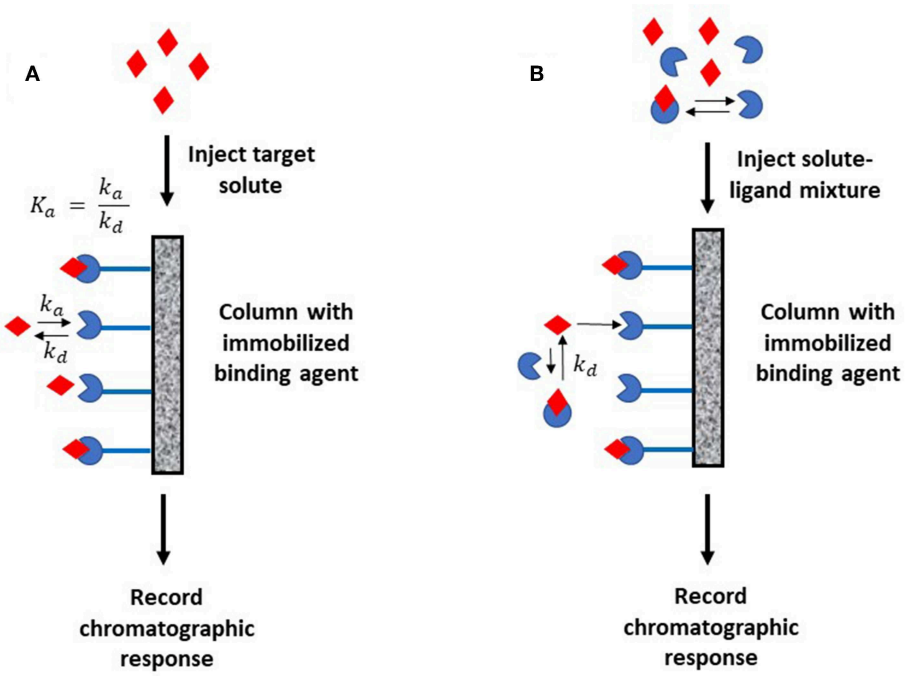


**FIGURE 1 |** Two general formats employed in affinity chromatography and HPAC for examining the kinetics of an analyte interaction with a binding agent. The method in **(A)** is based on the reversible interactions between the analyte and an immobilized binding agent, while **(B)** is based on the utilization of a secondary probe on the column to capture part of the analyte and monitor interactions of this analyte with a binding agent in solution. Terms: $K_a$, association equilibrium constant; $k_a$, association rate constant; $k_d$, dissociation rate constant.

or frontal analysis), while others require injection of only a small quantity of analyte (i.e., an approach known as zonal elution). Methods in which the analyte may approach the amount of binding agent often involve the use of non-linear elution conditions, in which the chromatographic response will depend on the amount of applied analyte. Techniques that need only small amounts of analyte may instead use or require linear elution conditions, in which the observed chromatographic behavior is independent of the amount of analyte (Schiel and Hage, 2009).

Proper selection of the method for immobilizing a binding agent is another important factor to consider in affinity chromatography (Hage and Kim, 2006; Schiel et al., 2006). This is particularly true when the immobilized agent is used directly for binding or kinetic studies. A good coupling method should result in an immobilized agent that is properly oriented and that has high activity, good stability, and easy accessibility to its targets (Hage and Kim, 2006). Many applications of affinity chromatography have used covalent coupling techniques that employ an activated support and amine, hydroxyl, carbonyl or sulfhydryl groups on the binding agent; this approach has been used for a number of proteins and other biological agents (Hage and Kim, 2006; Schiel et al., 2006; Beeram et al., 2018; Liang et al., 2018). Smaller targets can be attached through similar groups to an activated support and by using a spacer arm to avoid steric hindrance effects during binding (Hinze et al., 1985; Wang et al., 2014, 2016). Sometimes adsorption can be used for immobilization. For instance, adsorption has been utilized with membrane-associated receptor proteins that have been placed within immobilized artificial membrane columns (Moaddel et al., 2005). In all of these methods the immobilization technique should be chosen to produce a binding agent that is a good mimic of the same binding agent in its native state. The extent to which this is achieved should be checked and validated by examining interactions of the immobilized agent with model targets that have known binding properties; this should be done prior to further studies with the same binding agent and new or unknown targets (Schiel and Hage, 2009; Bi et al., 2015; Zheng et al., 2015b).

This review will examine several techniques that can be utilized in HPAC or affinity chromatography for studying the kinetics of biologically-relevant systems. A short summary of this topic was provided recently (Bi et al., 2015) and will be expanded upon in this paper, with greater emphasis on the basic principles, theory, and use of HPAC and affinity methods for kinetic studies. The approaches that will be considered are band-broadening measurements, peak decay analysis, the split-peak method, techniques for peak fitting, and ultrafast affinity extraction. Applications of these methods will be discussed, and the advantages and potential limitations of each technique will be considered.

## BAND-BROADENING MEASUREMENTS

An analysis of band-broadening in affinity chromatography is one way kinetic information can be obtained on the interaction of an analyte with a given binding agent (Schiel and Hage, 2009; Bi et al., 2015; Zheng et al., 2015b). This type of method is based on the injection of the target analyte onto both a column containing the binding agent and an inert control column. These injections are typically made under linear elution conditions, with the data from the control column being used to correct for the contributions due to band-broadening processes besides stationary phase mass transfer. The measured peak widths are then used to calculate the plate heights of the system and may also be used to make a van Deemter-type plot in which the total plate height is analyzed as the linear velocity, or flow rate, is varied. This plate height data is then used to provide information on the broadening of peaks that results from stationary phase mass transfer, which is related to the interaction rate between the immobilized binding agent and target. Band-broadening measurements for kinetic studies can be carried out by using two related methods: the plate height method and peak profiling (Schiel and Hage, 2009; Zheng et al., 2014a, 2015b; Bi et al., 2015). Details on each method are provided in the following sections.

### Plate Height Method

The plate height method for kinetic studies makes use of a small quantity of a target that is injected onto an affinity column, as well as onto a control column, at several flow rates. The band-broadening data that are collected from these columns are then used to acquire the total plate height, $H_{total}$, on each column, as well as to estimate and compare the plate height contributions due to individual band-broadening processes on these columns. The resulting information can be combined to find the stationary phase mass transfer plate height contribution, $H_s$, for the affinity column as a function of the mobile phase's linear velocity ($u$) and the target's retention factor ($k$) for the affinity column. This process is illustrated in **Figure 2** (Schiel and Hage, 2009; Bi et al., 2015; Zheng et al., 2015b).

In describing the band-broadening processes that are present in the columns, the term $H_s$ is related to the rate of analyte dissociation from the immobilized binding agent. This relationship is shown in Equation (1) (Schiel and Hage, 2009; Bi et al., 2015; Zheng et al., 2015b).

$$H_s = \frac{2uk}{\left(1+k\right)^2 k_d} \tag{1}$$

In this equation, the dissociation rate constant for the target analyte from the immobilized binding agent is given by the term $k_d$. This equation assumes that the analyte's interactions within the column are occurring with a single set of binding sites and that the injected amount of analyte is small compared to the amount of binding agent that is active and present in the column (i.e., it is assumed the experiment is done under linear elution conditions). When a plot is made of $H_s$ vs. $(uk)/(1+k)^2$ based on Equation (1), a system which follows these assumptions should provide a linear best-fit response with a slope that has a value of $2/k_d$ and an intercept that is equal to zero. **Figure 3** shows an example of a plot for $H_s$ vs. $(uk)/(1 + k)^2$ that was obtained by HPAC when this method was used to examine the dissociation kinetics for D-tryptophan in the presence of immobilized HSA (Yang and Hage, 1997).

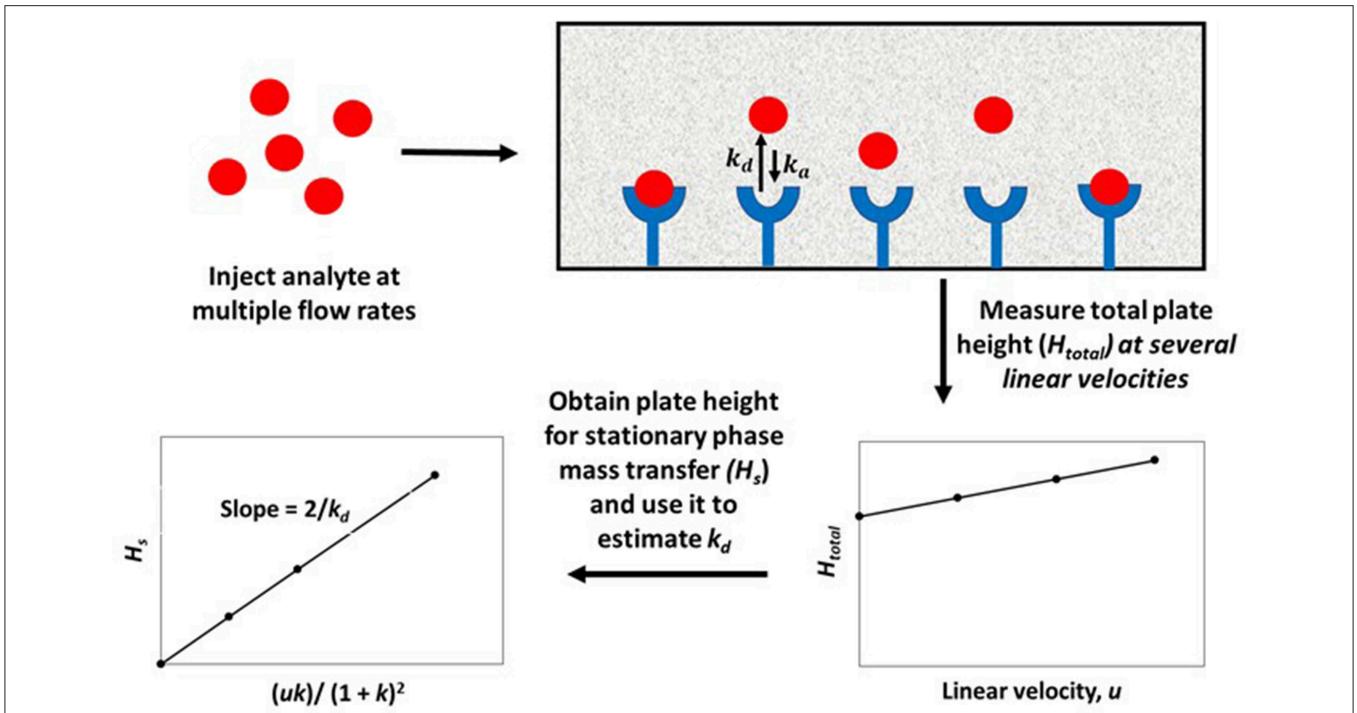


**FIGURE 2 |** General scheme for studying an analyte-binding agent interaction by using the plate height method. Terms: $H_{total}$, total plate height; $H_s$, plate height contribution due to stationary phase mass transfer; $u$, linear velocity of mobile phase; $k$, retention factor of the analyte; $k_d$, dissociation rate constant.

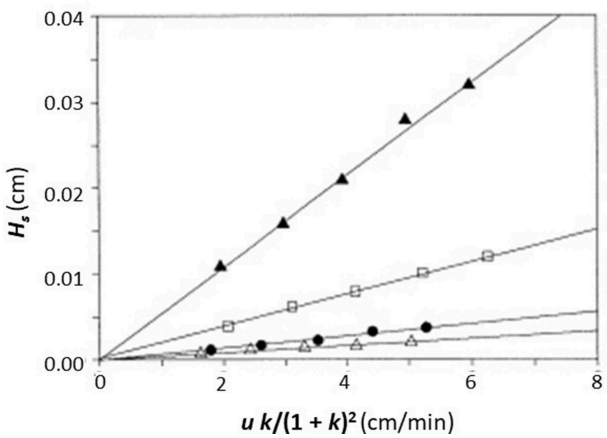


**FIGURE 3 |** Plot of $H_s$ vs. $(uk)/(1+k)^2$, as obtained by the plate height method, to analyze the binding of D-tryptophan with an HPAC column containing immobilized HSA. These data were obtained at 25°C and at mobile phase pH values of 4.0 (Δ), 5.0 (•), 6.0 (□), or 7.0 (▲). Reproduced with permission from Yang and Hage (1997). Copyright 1997 Elsevier.

Once the value of $k_d$ has been obtained, the association rate constant ($k_a$) for an analyte with an immobilized binding agent can also be acquired. This can be found by using the measured value of $k_d$ with a separate known or measured equilibrium constant for the same system. For instance, if the association equilibrium constant ($K_a$) for the particular interaction is determined by an approach such as frontal analysis, $k_a$ can be estimated by using Equation (2) (Schiel and Hage, 2009; Bi et al., 2015; Zheng et al., 2015b).

$$k_a = K_a k_d \tag{2}$$

The plate height technique has been utilized to study the interactions of chiral solutes such as D/L-tryptophan and *R*/*S*-warfarin with HSA, as well as the effect of temperature on the rates of these interactions (see summary in **Tables 1**, **2** of applications for all methods discussed in this review) (Loun and Hage, 1996; Yang and Hage, 1997). Early work with this method used it to examine the interaction rates of various sugars with the lectin concanavalin A (Con A) (Anderson and Walters, 1986). This approach has also been employed to investigate the effects of pH, solvent polarity, and ionic strength with regards to the interaction rates of D- and L-tryptophan with HSA (Yang and Hage, 1997). In addition, this method has been used to assess the employment of monoliths and small affinity columns for studying the interaction kinetics of HSA with *R*-warfarin, L-tryptophan, and carbamazepine (Yoo and Hage, 2009; Yoo et al., 2010).

The plate height method is suitable for studying reactions that have relatively fast association and dissociation rates compared to the time needed for elution from the affinity column. The range of dissociation rate constants that have been determined by this method is $\sim 10^{-2}$-$10^{-1}$ $s^{-1}$ (see summary in **Table 1**) (Loun and Hage, 1996; Schiel and Hage, 2009; Yoo et al., 2010; Bi et al., 2015; Zheng et al., 2015b). Systems which exhibit weak-to-moderate

**TABLE 1 |** General range of rate constants that have been determined by methods using affinity chromatography and HPAC[a].

| Analysis method | Conditions | Range of binding affinities ($K_a$) | Range of measured rate constants |
|---|---|---|---|
| Plate height method | Linear elution conditions; zonal elution format | $10^3$-$10^6$ $M^{-1}$ | $k_d$: $10^{-2}$-10 $s^{-1}$ |
| Peak profiling | Linear elution conditions; zonal elution format | $10^3$-$10^6$ $M^{-1}$ | $k_d$: $10^{-1}$-10 $s^{-1}$ |
| Peak decay method | Non-linear elution conditions; zonal elution format | $10^3$-$10^6$ $M^{-1}$ | $k_d$: $10^{-2}$-10 $s^{-1}$ |
| Split-peak method | Non-linear or linear elution conditions; zonal elution format | $>10^6$ $M^{-1}$ | $k_d$: $10^{-1}$ $s^{-1}$<br>$k_a$: $10^4$-$10^6$ $M^{-1}$ $s^{-1}$ |
| Peak fitting | Non-linear elution conditions; zonal elution or frontal analysis format | $10^3$-$10^6$ $M^{-1}$ | $k_d$: $10^{-1}$-10 $s^{-1}$<br>$k_a$: $10^4$-$10^7$ $M^{-1}$ $s^{-1}$ |
| Ultrafast affinity extraction | Solution-phase interactions; zonal elution format | $10^3$-$10^9$ $M^{-1}$ | $k_d$: $10^{-2}$-10 $s^{-1}$<br>$k_a$: $10^3$-$10^5$ $M^{-1}$ $s^{-1}$ |

[a] *Terms: $K_a$, association equilibrium constant; $k_a$, association rate constant; $k_d$, dissociation rate constant.*

**TABLE 2 |** Applications of affinity chromatography and HPAC in kinetic studies[a].

| Technique | System examined |
|---|---|
| Plate height method | Drug and solute binding with serum proteins (HSA); sugar-lectin interactions (Con A) |
| Peak profiling | Drug, drug metabolite, and solute binding with serum proteins (AGP, HSA); drug binding with cyclodextrins; drug-receptor interactions ($\beta_2$-AR) |
| Peak decay | Drug binding with serum proteins (AGP, HSA); sugar-lectin interactions (Con A); antibody-antigen binding; aptamer-target interactions; interactions of immunoglobulins with protein A or protein G |
| Split-peak method | Antibody-antigen binding; interactions of immunoglobulins with protein A or protein G |
| Peak fitting in zonal elution | Sugar-lectin interactions (Con A); drug/inhibitor-receptor interactions (nAChR, $\beta_2$-AR); drug binding with cyclodextrins; interactions of immunoglobulins with protein A; binding of novobiocin with heat shock protein; lysozyme binding with Cibacron Blue 3GA |
| Peak fitting in frontal analysis | Sugar-lectin interactions (Con A); antibody-antigen binding |
| Ultrafast affinity extraction | Drug and hormone binding with serum proteins (AGP, HSA, SHBG); |

[a] *AGP, $\alpha_1$-acid glycoprotein; $\beta_2$-AR, beta$_2$-adrenoceptor; Con A, concanavalin A; HSA, human serum albumin; nAChR, nicotinic acetylcholine receptor; SHBG, sex-hormone binding globulin.*

binding (i.e., $K_a \leq 10^6$ $M^{-1}$) have been typically studied using this method (Loun and Hage, 1996; Yang and Hage, 1997; Schiel and Hage, 2009; Yoo and Hage, 2009; Yoo et al., 2010; Zheng et al., 2015b). An advantage of this approach is only a small amount of the analyte is needed, as is required to achieve linear elution conditions. A potential limitation of this method is that a detailed analysis of the affinity and control columns, which may include the use of a large number of flow rates and many replicate injections, may be needed to obtain sufficiently precise values for contributions to the plate height by various processes (Schiel and Hage, 2009; Bi et al., 2015; Zheng et al., 2015b).

## Peak Profiling

Peak profiling is a variation of the plate height technique that typically requires work at fewer flow rates and involves more direct calculations of dissociation rate constants (Fitos et al., 2002; Talbert et al., 2002; Schiel et al., 2009; Tong et al., 2011). This technique is based on the measurement of both the retention time and peak variance (i.e., band-broadening) of an analyte on a control column and an affinity column under linear elution conditions. This approach can ideally be carried out at a single flow rate if it is assumed all band-broadening sources besides stationary phase mass transfer are not significant or the same for the analyte in both the affinity column and control column. The apparent dissociation rate constant ($k_{d,app}$) in this situation can be calculated by using the measured parameters along with Equation (3) (Schiel and Hage, 2009).

$$k_{d,app} = \frac{2t_M^2 \ (t_R \ - \ t_M \ )}{\sigma_R^2 t_M^2 - \sigma_M^2 t_R^2} \tag{3}$$

In this equation, the retention or elution times of the analyte on the affinity column and control column are given by $t_R$ and $t_M$, respectively. The terms $\sigma_R^2$ and $\sigma_M^2$ represent the variances of the peaks for the same analyte on the affinity column and control column (Schiel and Hage, 2009).

A modified form of the peak profiling method looks at the difference in total plate heights that are found under linear elution conditions for the analyte on an affinity column ($H_R$) and a control column ($H_M$). A plot of this difference, $H_R$–$H_M$,

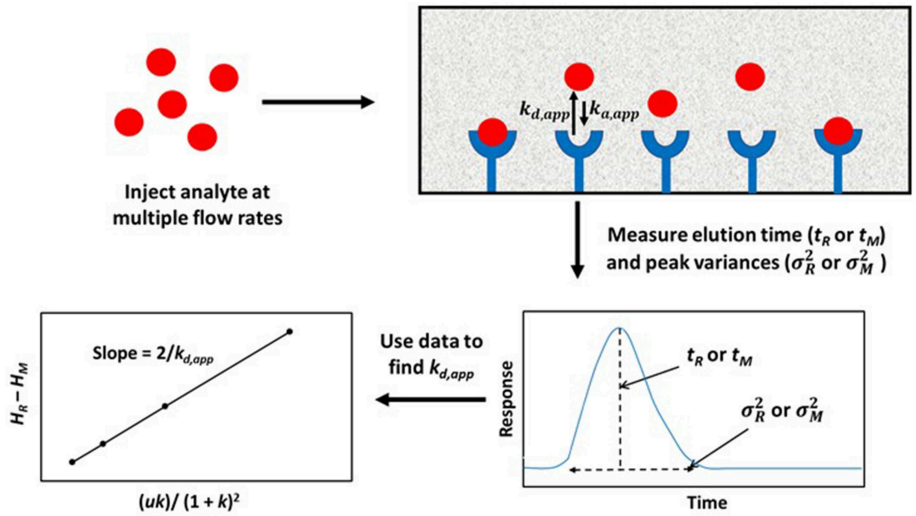


**FIGURE 4 |** General scheme used for studying analyte interactions with a binding agent by using peak profiling. Terms: $t_R$, retention time of the analyte on an affinity column; $t_M$, elution time of a non-retained solute or analyte on a control column; $\sigma_R^2$, peak variance of analyte on the affinity column; $\sigma_M^2$, peak variance of the non-retained solute or analyte on a control column; $H_R$, total plate height obtained for analyte on the affinity column; $H_M$, total plate height obtained for non-retained solute or analyte on a control column; $u$, linear velocity of mobile phase; $k$, retention factor of analyte on the affinity column; $k_{d,app}$, apparent dissociation rate constant; $k_{a,app}$, apparent association rate constant.

is then made vs. the term $(uk)/(1+k)^2$. An example of such a plot is provided in **Figure 4**. Equation (4) can then be employed with the data to obtain $k_{d,app}$ (Schiel and Hage, 2009; Schiel et al., 2009; Bi et al., 2015; Zheng et al., 2015b).

$$H_R - H_M = \frac{2uk}{(1+k)^2 k_{d,app}} = H_s \quad (4)$$

This equation can be used with data that have been obtained for the injection of an analyte at either single or multiple flow rates. This particular expression indicates the behavior that is expected for an analyte at a single type of binding site on the affinity column. If data are acquired at multiple flow rates, a plot of $H_R$–$H_M$ vs. $(uk)/(1+k)^2$ should provide a linear relationship in which the slope is equal to the term $2/k_{d,app}$(Schiel et al., 2009; Tong et al., 2011). **Figure 5** provides an example of a plot that has been obtained by this method (Tong and Hage, 2011).

Peak profiling can also be used to determine dissociation rate constants for systems that have multiple types of binding sites for the analyte within a column. This can be accomplished by using Equation (5) or related expressions.

$$H_R - H_M = \frac{uk}{(1+k)^2}\left[\frac{2\alpha_1}{k_d} + \frac{2\,\alpha_{control}}{k_{d,control}}\right] \quad (5)$$

In this equation, the terms $\alpha_1$ and $\alpha_{control}$ represent the fractions of the total retention factor for the target that are due to interactions with the immobilized binding agent or due to non-specific binding to the support (i.e., as estimated using a control column). The term $k_{d,control}$ is the dissociation rate constant for the retained target as it interacts with the non-specific binding sites (Tong and Hage, 2011; Tong et al., 2011).

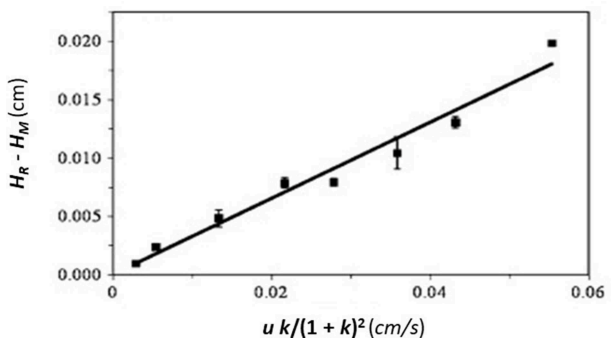


**FIGURE 5 |** Plot of $H_R$–$H_M$ vs. $(uk)/(1+k)^2$, as obtained by peak profiling for the injection of 5-(4-hydroxyphenyl)-5-phenylhydantoin (*p*-HPPH) onto a column containing immobilized HSA. Reproduced with permission from Tong and Hage (2011). Copyright 2011 Elsevier.

An expanded form of Equation (4) can be used in cases where a correction must be made for the change in mass transfer due to the stagnant mobile phase as the degree of analyte is varied. This revised form is given by Equation (6) (Schiel and Hage, 2009; Schiel et al., 2009).

$$H_R - H_M = \frac{uk}{(1+k)^2}\left[\frac{2}{k_d} + \frac{d_p^2\,(2+3k)}{60\,\gamma D}\right] \quad (6)$$

The term $d_p$ in this equation is the particle diameter of the support, $\gamma$ is the tortuosity factor for analyte movement in this support, and $D$ is the analyte's diffusion coefficient in the mobile phase. Based on this expression, a plot of $H_R$-$H_M$ vs. $[uk/(1+$

$k)^2$] can be made for columns that contain supports with various, known particle diameters. A linear plot should be obtained for systems with single-site binding. The slopes of these plots can then be plotted against $d_p^2$ to obtain a new graph in which the true value of $k_d$ is obtained from the intercept (Schiel and Hage, 2009; Schiel et al., 2009).

The peak profiling technique has been used to characterize a number of systems. For instance, this approach has been utilized to study the dissociation kinetics of drugs/solutes such as imipramine, carbamazepine and L-tryptophan with immobilized HSA (Schiel and Hage, 2009; Tong et al., 2011); the interactions of acetaminophen and sertraline with β-cyclodextrin (Li et al., 2013); and the interactions of beta$_2$-adrenoceptor ($\beta_2$-AR) with drugs such as salbutamol, terbutaline, methoxyphenamine, isoprenaline hydrochloride, and ephedrine hydrochloride (Liang et al., 2018). The same general method has been applied to characterizing dissociation rate constants for AGP with the drugs chlorpromazine, disopyramide, imipramine, lidocaine, propranolol, and verapamil based on affinity microcolumns (Beeram et al., 2017). A simultaneous determination of the dissociation rate constants for two chiral phenytoin metabolites with HSA was reported with this method (Tong and Hage, 2011), and a modified peak profiling method based on multianalyte detection has been employed to study interactions of β-cyclodextrin with drugs such as acetaminophen, phenacetin and *S*-flurbiprofen (Wang et al., 2014). Peak profiling has been used in most of these studies with absorbance detection; however, it has also been used with tandem mass spectrometry to characterize the binding kinetics of acetaminophen, trimethoprim, ketoprofen, indapamide, and uracil with β-cyclodextrin (Wang et al., 2016).

The advantages and potential limitations of peak profiling are similar to those already discussed for the plate height method. The dissociation rate constants obtained by this method have been in the range of $10^{-1}$-$10^{1}$ $s^{-1}$, and this approach has generally been used with systems that have weak-to-moderate binding strengths ($K_a \leq 10^6$ $M^{-1}$) (Schiel et al., 2009; Tong and Hage, 2011; Tong et al., 2011; Li et al., 2013; Wang et al., 2014, 2016; Beeram et al., 2017; Liang et al., 2018). Some advantages of this approach over the plate height method are that it can be employed at one or many flow rates and it can use higher flow rates than the plate height method, resulting in higher throughput measurements and faster data collection (Schiel and Hage, 2009; Bi et al., 2015; Zheng et al., 2015b).

## PEAK DECAY METHOD

In peak decay methods, a small plug of a target solute is applied to both a small affinity column and control column, followed by release of the retained analyte under conditions where it does not have an opportunity to rebind. These latter conditions can be achieved by using relatively high flow rates and selective mobile phase conditions to prevent rebinding by the target to the immobilized binding agent and to avoid movement of the analyte back into the stagnant mobile phase. This technique can be performed in two formats: the competitive peak decay method and the non-competitive peak decay method (Schiel and Hage, 2009; Bi et al., 2015; Zheng et al., 2015b).

In the non-competitive method, a significantly large amount of analyte is applied to both a small affinity column and a control column at various flow rates. This causes the target solute to interact and partially saturate the column. Once the analyte is released from the column, any non-bound target in the stagnant mobile phase is washed away, along with target that is non-specifically and weakly-retained by the support. The bound target is then washed from the column at a relatively high flow rate as it dissociates from the immobilized agent. The decay curve or elution profile that is produced is then monitored, as illustrated in **Figure 6** (Chen et al., 2009; Schiel and Hage, 2009; Bi et al., 2015; Zheng et al., 2015b).

The competitive peak decay method has the analyte being introduced into an affinity column and eluted by adding a high concentration of a competing agent. This competing agent binds to the same site of the immobilized agent as the target and prevents re-association of the target as it is released from the column. This produces a scenario in which the target analyte is continuously washed from the affinity column as it is dissociated from the binding agent, creating a decay profile for elution. One disadvantage of this method is that it cannot be used for systems in which both the competing agent and target exhibit a significant response, making it difficult to monitor the target's elution (Schiel and Hage, 2009; Bi et al., 2015; Zheng et al., 2015b).

The elution profile in both of these methods approaches a first-order decay curve when the target analyte is completely prevented from rebinding to the column as it is released from the immobilized binding agent. If dissociation of the analyte is slower than mobile phase mass transfer, the logarithm of the response for the tailing portion of the resulting peak can be plotted against time and used to obtain $k_d$. This can be done by employing Equation (7) (Schiel and Hage, 2009; Bi et al., 2015; Zheng et al., 2015b).

$$\ln\left(\frac{dm_{Ee}}{dt}\right) = \ln\left(m_{Eo}k_d\right) - k_d t \tag{7}$$

In Equation (7), $m_{Ee}$is the moles of target that elute at time $t$ from the column, and $m_{Eo}$is the original moles of target that were present on the column. When plotting $\ln\left(\frac{dm_{Ee}}{dt}\right)$ vs. $t$, $k_d$ can be obtained from the negative slope of the resulting plot (Chen et al., 2009; Schiel and Hage, 2009; Bi et al., 2015; Zheng et al., 2015b). Some plots that have been obtained in the manner by the peak decay method are shown in **Figure 7** (Yoo and Hage, 2011b).

The peak decay method has been used to investigate several types of biological interactions. This method was originally used in a competitive format to study the dissociation rate of the sugar 4-methylumbelliferyl α-D-mannopyranoside from Con A in the presence of the competing agent 4-methylumbelliferyl α-D-galactopyranoside (Moore and Walters, 1987). The non-competitive peak decay method has been utilized to study the interactions of many drugs with serum proteins. This second approach has been used to determine the dissociation rate constants of imipramine, diazepam, tolbutamide, acetohexamide, quinidine, amitriptyline, verapamil, lidocaine, and nortriptyline

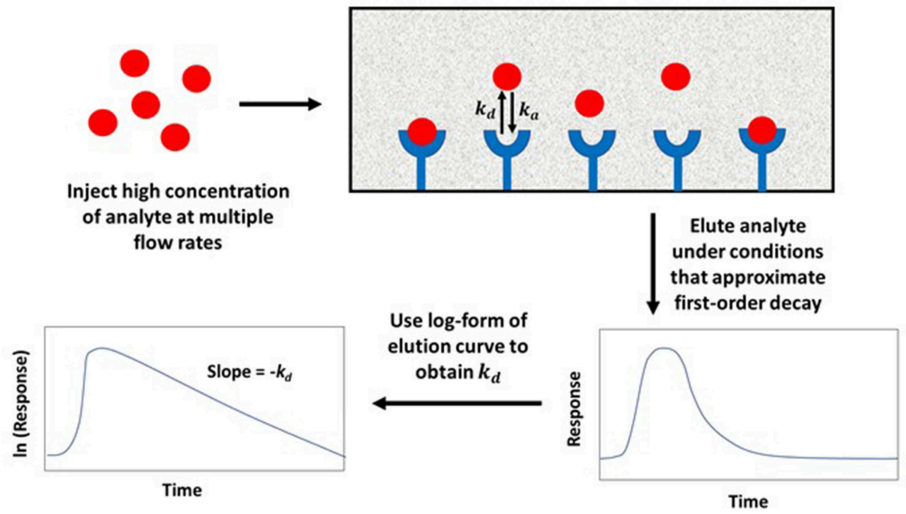


**FIGURE 6 |** General scheme used for studying analyte interactions with an immobilized binding agent by the non-competitive peak decay method. Terms: $k_d$, dissociation rate constant; $k_a$, association rate constant.

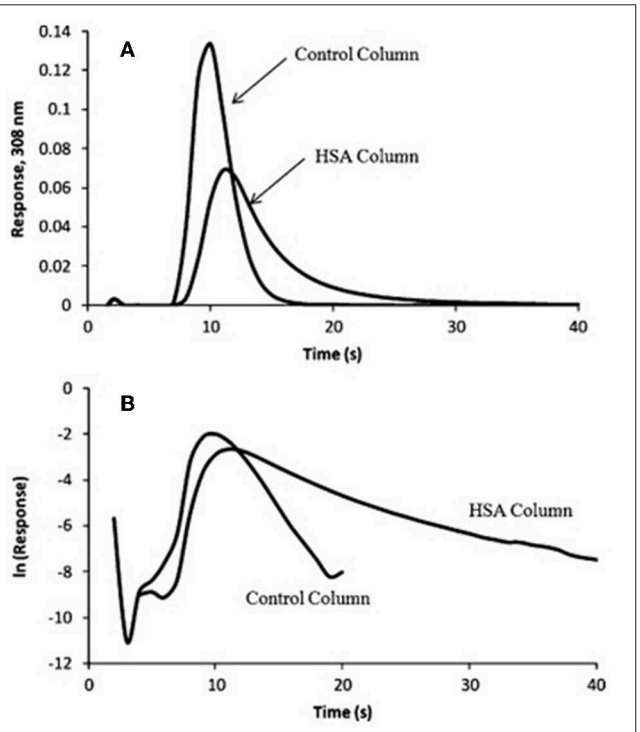


**FIGURE 7 | (A)** Elution profile and **(B)** natural logarithm of the elution profile obtained for the application of a 100 μL sample of 10 μM racemic warfarin onto a control monolith column and an HSA monolith column and by using the peak decay method for data analysis. Reproduced with permission from Yoo and Hage (2011b). Copyright 2011 Elsevier.

with AGP or HSA (Yoo and Hage, 2011a). The binding of *R*-warfarin with monolith columns containing immobilized HSA has also been studied by this method (Yoo and Hage, 2011b). In addition, peak decay analysis has been utilized to determine the dissociation kinetics of immobilized antibodies with 2,4-dichlorophenoxyacetic acid and related herbicides for the selection of elution conditions in immunoaffinity chromatography (Nelson et al., 2010). This approach has further been used to examine the interaction kinetics of immobilized anti-thyroxine antibodies or aptamers with thyroxine, as well as the dissociation of immunoglobulin G (IgG)-class antibodies from protein G columns (Pfaunmiller et al., 2012; Anguizola et al., 2018).

Peak decay analysis has been employed to study many systems exhibiting weak-to-moderate binding interactions ($K_a \leq 10^6$ $M^{-1}$) (Chen et al., 2009; Schiel and Hage, 2009; Nelson et al., 2010; Yoo and Hage, 2011a,b; Bi et al., 2015; Zheng et al., 2015b). However, peak decay is also an effective method for studying the elution conditions that are needed for systems that exhibit much strong binding under their application conditions. Some examples of binding agents that belong to this second category are antibodies, aptamers and protein G (Hage et al., 2012; Pfaunmiller et al., 2012; Anguizola et al., 2018). This set of methods can be applied in cases where the analyte undergoes fast dissociation from the immobilized binding agent, with a $k_d$ in the range of $10^{-2}$-$10^1$ $s^{-1}$ (Chen et al., 2009; Schiel and Hage, 2009; Nelson et al., 2010; Yoo and Hage, 2011a,b; Pfaunmiller et al., 2012; Bi et al., 2015; Zheng et al., 2015b; Anguizola et al., 2018).

Because peak decay analysis is based on linear regression and an elution profile with a logarithmic-based response, data analysis is usually easier to conduct than in band-broadening measurements (Chen et al., 2009; Schiel and Hage, 2009; Yoo and Hage, 2011a,b). This same feature makes peak decay analysis appealing for the study and optimization of elution conditions. If non-specific binding is present in the system, similar studies need to performed using a control column to identify and correct

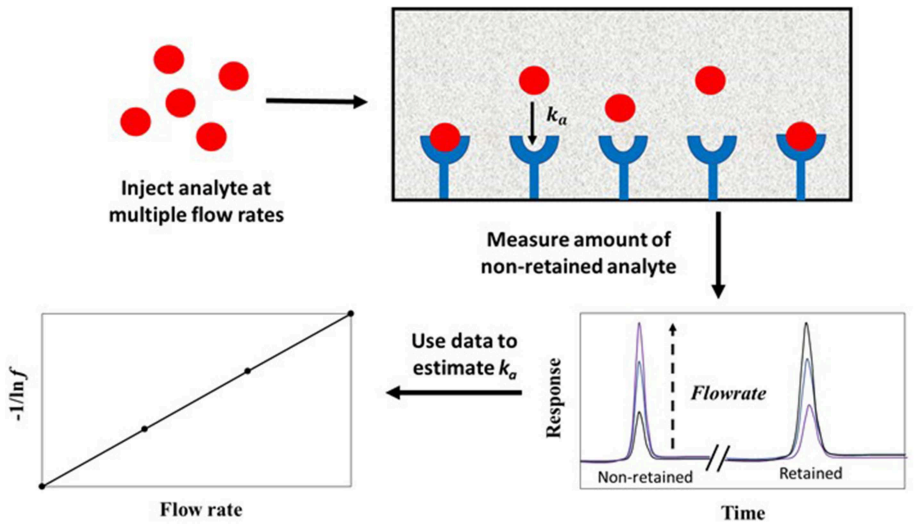


**FIGURE 8 |** General scheme used for studying analyte interactions with an immobilized binding agent by the split-peak method. Terms: $k_a$, association rate constant; $f$, free fraction of the analyte which is non-retained by the column.

for these effects. Another limitation of this method is that the conditions that are needed to make the target re-association negligible, and dissociation the rate determining step, may be difficult to achieve for some systems (Nelson et al., 2010; Yoo and Hage, 2011a,b; Zheng et al., 2015b).

## SPLIT-PEAK METHOD

The split-peak method is an approach for studying solute-ligand interactions in an environment where the solute binds irreversibly to an immobilized binding agent. This approach, which is illustrated in **Figure 8**, is based on the probability (under appropriate application conditions) that a small fraction of an injected analyte may not interact with the stationary phase as the analyte passes through a column. This portion elutes as a non-retained peak; the remainder of the analyte is retained and later elutes from the column. The resulting phenomenon is called the "split-peak effect" (Hage et al., 1986). The split-peak effect increases as the sample residence time in the column decreases or as the injection flow rate increases (Hage et al., 1986; Schiel and Hage, 2009; Bi et al., 2015; Zheng et al., 2015b).

### Methods Using Linear Elution Conditions

The split-peak effect can be employed to obtain the association rate constant ($k_a$) for an injected analyte with an immobilized binding agent under linear elution conditions by using Equation (8) (Hage et al., 1986).

$$-\frac{1}{\ln f} = F\left(\frac{1}{k_1 V_e} + \frac{1}{k_a m_L}\right) \tag{8}$$

The term $f$ is the free fraction of the analyte (which is non-retained by the column), $F$ is the injection flow rate, $m_L$ is the moles of active binding agent, and $V_e$ is the interparticle (or excluded) volume of the mobile phase. The term $k_a$ is the association rate constant for the analyte and immobilized binding agent, and $k_1$ is the forward mass transfer rate constant, which describes the movement of analyte from the flowing mobile phase region to the stagnant mobile phase (Hage et al., 1986).

According to Equation (8), a plot of $-1/\ln f$ against $F$ should result in a linear plot when a small amount of analyte is injected (i.e., linear elution conditions). This equation also indicates that the measured free fraction may be affected by the presence of slow stagnant mobile phase mass transfer, as described by $1/(k_1 V_e)$, or slow adsorption to the immobilized binding agent, as represented by $1/(k_a m_L)$. If the slow step in analyte retention is adsorption, the slope of a plot of $-1/\ln f$ vs. $F$ can provide $k_a$ if the value of $m_L$ is also known (Hage et al., 1986; Schiel and Hage, 2009; Zheng et al., 2015b). This type of plot is shown in **Figure 9** (Hage et al., 1986). If stagnant mobile phase mass transfer is the rate-limiting step, the slope can be used to obtain $k_1$. Intermediate cases, in which both adsorption and stagnant mobile phase mass transfer are important in determining the rate of binding by the analyte, can also occur (Hage et al., 1986; Hage and Walters, 1988). This technique has been employed to study the association kinetics of IgG-class antibodies with HPAC columns that contain protein G, protein A or a mixture of protein G and protein A (Hage et al., 1986; Rollag and Hage, 1998; Anguizola et al., 2018). This approach has also been utilized to optimize the retention and determination of human IgG in clinical samples by means of HPAC and protein A columns (Hage and Walters, 1987).

### Methods Using Non-linear Conditions

The split-peak method can also be used under non-linear conditions. For instance, the slopes for plots obtained according to Equation (8) can be measured at several known amounts of injected analyte and extrapolated to an infinitely small sample concentration (Hage et al., 1986; Hage and Walters, 1988;

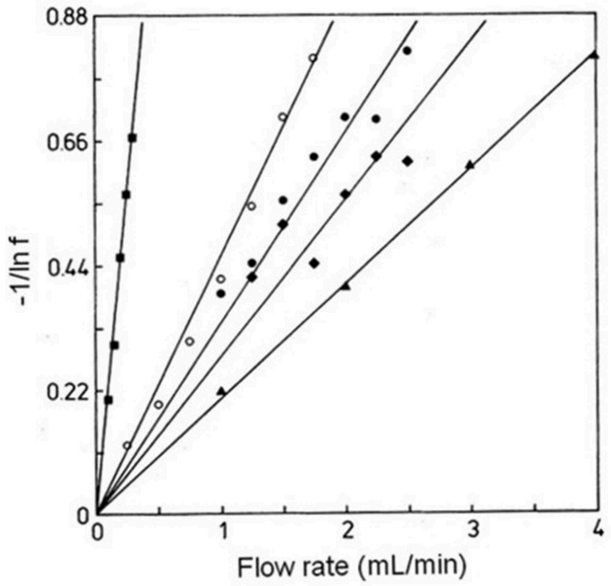


**FIGURE 9 |** Plots of −1/ln *f* vs. *F* for examining interactions of rabbit IgG with immobilized protein A by the split-peak method. These experiments were conducted using various sample sizes, immobilization methods, and support materials, as represented by the plots in (○), (•), (▲), (■), and (♦). Terms: *f*, free fraction of the analyte. Reproduced with permission from Hage et al. (1986). Copyright 1986 American Chemical Society.

Rollag and Hage, 1998). It is further possible to use alternative expressions to Equation (8) that can be used in special cases where the amount of analyte is not negligible. Equation (9) shows one such relationship for a situation in which the rate-limiting step in retention is adsorption of the analyte to the immobilized binding agent (Hage et al., 1993; Vidal-Madjar et al., 1997).

$$f = \frac{S_o}{Load\ A} \ln\left[1 + \left(e^{Load\ A/S_o} - 1\right)\ e^{-1/\ S_o}\right] \qquad (9)$$

In this equation, *Load A* is the relative amount (mol/mol binding agent) of the analyte that is applied to the column. The term *So* is a value equal to $F/k_a m_L$, in which each of the individual parameters are the same as described for Equation (8). This modified split-peak method has been employed in a number of studies to measure the association rate constants of immobilized anti-HSA antibodies with HSA in various assay and injection formats (Hage et al., 1993, 1999; Vidal-Madjar et al., 1997). This expression and approach have also been utilized to determine the association rate constants of herbicides and thyroxine with antibodies in HPAC columns (Nelson et al., 2010; Pfaunmiller et al., 2012).

The split-peak method has been employed with both linear and non-linear conditions to study a variety of systems that exhibit high binding affinities ($K_a > 10^6\ M^{-1}$). Association rate constants determined by this method have typically been in the range of $10^4$-$10^6\ M^{-1}\ s^{-1}$. One advantage of this approach is that it uses peak area measurements, which are often easier to acquire and more precisely analyzed than peak variances (Hage et al., 1986; Vidal-Madjar et al., 1997; Rollag and Hage, 1998; Nelson et al., 2010; Pfaunmiller et al., 2012). One limitation is this method is best suited for biological reactions that have slow dissociation (i.e., $k_d < 10^{-1}\ s^{-1}$) and that allow a good separation between the retained and non-retained fractions of an analyte (Nelson et al., 2010; Pfaunmiller et al., 2012). Furthermore, the column size, flow rate, and other experimental conditions need to be selected in such a way that the split-peak effect is observable (Schiel and Hage, 2009; Zheng et al., 2015b).

## PEAK FITTING

Peak fitting is based on the application of a relatively large amount of a target analyte to an affinity column and fitting the peaks that are observed at known sample concentrations or conditions to a given chromatographic model. The best-fit parameters for the peak are utilized to get the equilibrium and rate constants for the target's interaction with the binding agent (Moaddel and Wainer, 2007; Moaddel et al., 2007). Peak fitting can be performed using either zonal elution or frontal analysis as the format by which the analyte is applied to the column (Schiel and Hage, 2009; Bi et al., 2015; Zheng et al., 2015b).

### Methods Using Zonal Elution

**Figure 10** shows a typical scheme for carrying out peak fitting under zonal elution conditions. The results of such an experiment can be analyzed by employing Equation (10) (Wade et al., 1987; Moaddel and Wainer, 2007; Moaddel et al., 2007).

$$y = \frac{a_o}{a_3}\left[1 - e^{\left(\frac{-a_3}{a_2}\right)}\right]\left[\frac{\left(\sqrt{\frac{a_1}{x}}\right) I_1\left(\frac{2\sqrt{a_1 x}}{a_2}\right) e^{-x-a_1/a_2}}{1 - T\left(\frac{a_1}{a_2},\ \frac{x}{a_2}\right)\left[1 - e^{-a_3/a_2}\right]}\right] \qquad (10)$$

The value of $y$ in this equation is the measured signal at a given reduced retention time $x$. The term $I_1$ is a modified Bessel function, and $T$ is the switching function. The factors $a_o$, $a_1$, $a_2$, and $a_3$ are the parameters obtained by fitting experimental data to Equation (10). These parameters can be used to determine the equilibrium constant and rate constants for the interaction of the analyte with the immobilized agent. For instance, the association equilibrium constant can be found by using the relationship $K_a = a_3/C_o$, and the apparent dissociation rate constant can be obtained by using $k_{d,app} = 1/a_2 t_M$, where $t_M$ is the column void time and $C_o$ is related to the analyte's concentration, the sample volume, and the column's dead volume (Moaddel and Wainer, 2007; Schiel and Hage, 2009).

This method was first employed to characterize the interaction kinetics between *p*-nitrophenyl-α-D-mannopyranoside and immobilized Con A (Wade et al., 1987). This equation has also been utilized to study the binding, rate constants, and quantitative-structure activity relationships for interactions of nicotinic acetylcholine receptor (nAChR) with phencyclidine, 18-methoxycoronaridine, and bupropion plus verapamil (Jozwiak et al., 2002, 2003, 2004, 2007; Moaddel et al., 2005, 2007). Peak fitting has been utilized to measure rate constants for the interactions of novobiocin with heat shock protein

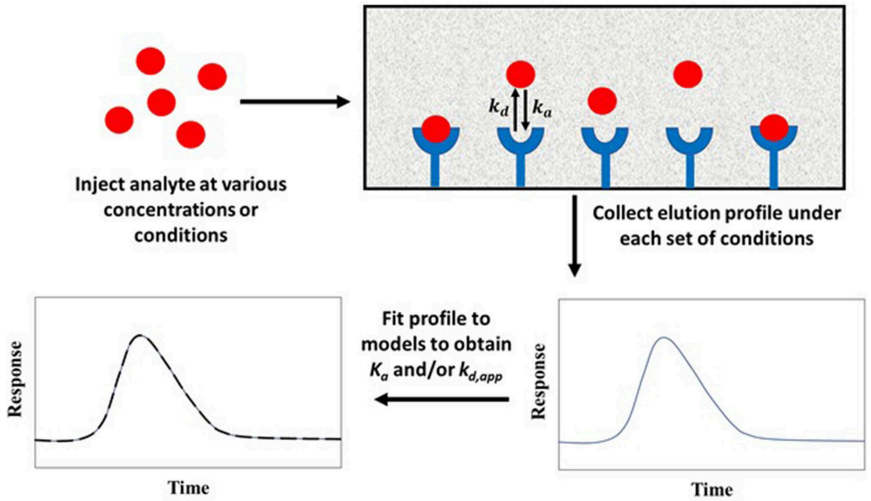


**FIGURE 10 |** General scheme for studying analyte interactions with an immobilized binding agent by peak fitting. Terms: $K_a$, association equilibrium constant; $k_a$, association rate constant; $k_d$, dissociation rate constant; $k_{d,app}$, apparent dissociation rate constant.

90α (Marszałł et al., 2008). This method has also been applied to investigate the rate constants and types of binding sites for drug interactions with $\beta_2$-AR (Li et al., 2015; Liang et al., 2018) and to examine drug binding with β-cyclodextrin with detection based on mass spectrometry (Wang et al., 2016). Similar peak fitting approaches have been described for kinetic studies of IgG with immobilized protein A during elution at pH 3.0 and to determine rate constants for the binding of lysozyme with immobilized Cibacron Blue 3GA at various concentrations of sodium chloride (Lee and Chuang, 1996; Lee and Chen, 2001).

## Methods Using Frontal Analysis

Another way peak fitting can be used for studying biological interactions is with frontal analysis. This combination involves continuously applying an analyte solution to the column. Equation (11) shows one way an association rate constant ($k_a$) can be determined by measuring an apparent association rate constant ($k_{a,app}$) with frontal analysis (Renard et al., 1995).

$$\frac{1}{k_{a,app}} = \frac{q_x\, V_M}{F\, n_{mt}} + \frac{1}{k_a} \tag{11}$$

In this equation, $n_{mt}$ represents the global mass transfer coefficient (i.e., a term dependent on the support size and dimensions of the column), $F$ is the flow rate, $V_M$ is the void volume, and $q_x$ is the loading capacity of the column per unit volume of mobile phase. This equation assumes analyte dissociation from the immobilized agent is not significant during the time of the experiment (Renard et al., 1995; Schiel and Hage, 2009; Zheng et al., 2015b). If this assumption is true, a linear relationship should be produced by a plot of $1/k_{a,app}$ vs. $q_x$. The association rate constant $k_a$ can be determined from the intercept of this plot (Renard et al., 1995). This approach makes it possible to correct for the band-broadening contributions to $k_{a,app}$ due to stagnant mobile phase mass transfer, and has been utilized to find the association rate constant of anti-HSA antibodies with HSA (Renard et al., 1995).

A second way peak fitting can be performed with frontal analysis is by utilizing Equation (12) (Munro et al., 1993, 1994; Schiel and Hage, 2009).

$$k_d = \frac{2\left(V_A - V_A{}^*\right)}{d\sigma_A{}^2/dF} \tag{12}$$

In this equation, $V_A$ and $V_A^*$ are the breakthrough volumes for the retained analyte and a non-retained solute. The term $k_d$ is the dissociation rate constant, $F$ is the flow rate, and $\sigma_A{}^2$ is the variance of the breakthrough curve for the analyte. When a plot of $\sigma_A{}^2$ vs. $F$ is made, the slope $\left(d\frac{\sigma_A{}^2}{dF}\right)$ that is obtained can be used with the other terms in Equation (12) to calculate $k_d$. One advantage of this method is it can be conducted using various sample concentrations to provide a set of values for $\left(d\frac{\sigma_A{}^2}{dF}\right)$ to estimate $k_d$ (Munro et al., 1993, 1994; Schiel and Hage, 2009; Zheng et al., 2015b). This technique has been employed in measuring the dissociation rate constant that describes the interaction of *p*-nitrophenyl-α-D-mannopyranoside with Con A (Munro et al., 1993, 1994).

An advantage of peak fitting is it can be used to study systems exhibiting weak-to-moderate binding under non-linear conditions (Schiel and Hage, 2009; Zheng et al., 2015b). The range of association and dissociation rate constants that have been reported when using this method have spanned from $10^4$-$10^7$ $M^{-1}$ $s^{-1}$ to $10^{-1}$-10 $s^{-1}$, respectively (Moaddel and Wainer, 2007; Moaddel et al., 2007; Schiel and Hage, 2009; Zheng et al., 2015b). One limitation of peak fitting methods is it is necessary to test and verify any assumptions that are made. For instance, it may be necessary to determine whether mobile phase mass

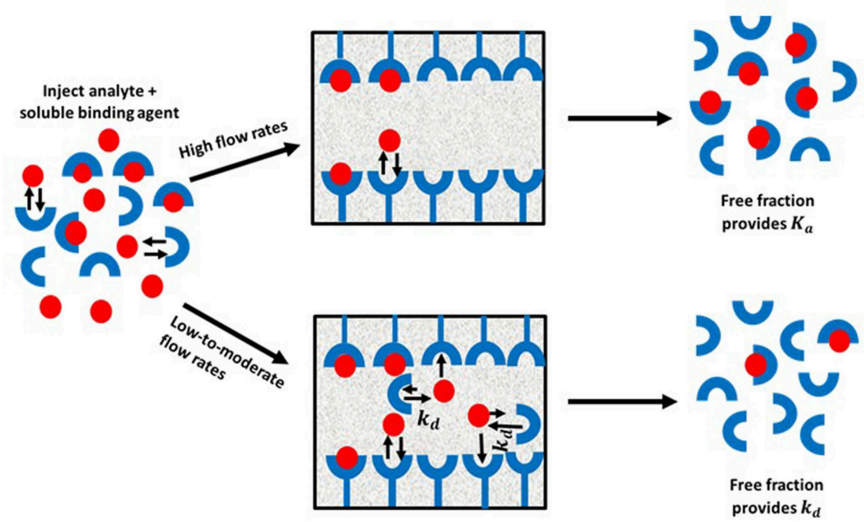


**FIGURE 11 |** General scheme for studying analyte interactions with a soluble binding agent by using ultrafast affinity extraction. Terms: $K_a$, association equilibrium constant; $k_d$, dissociation rate constant.

transfer effects need to be considered (Renard et al., 1995; Schiel and Hage, 2009; Zheng et al., 2015b).

## ULTRAFAST AFFINITY EXTRACTION

Ultrafast affinity extraction is a yet another tool that can be used with affinity chromatography and HPAC for kinetic studies. **Figure 11** illustrates the basic principle of this approach. This method can be used to measure the free or non-bound fraction of an analyte in a mixture of the analyte and a soluble form of the binding agent. This approach was initially developed to measure equilibrium constants for drug-protein binding, as can be obtained from free fractions measured at high flow rates (Mallik et al., 2010; Zheng et al., 2013). However, a modified form of this method has also been reported that can measure both the thermodynamics and kinetics of solute-ligand interactions in solution by using intermediate and high flow rates (Zheng et al., 2014b).

When ultrafast affinity extraction is utilized for kinetic studies, a sample containing a mixture of the analyte and soluble binding agent of interest is injected onto a small HPAC column. If this injection is made at a sufficiently high flow rate, the short residence time of the sample mixture in the column will avoid or minimize release of the analyte from its complex with the soluble binding agent. This causes a separation of the bound and free fractions of the analyte as the analyte's free form is quickly extracted by the immobilized binding agent. These conditions make it possible to obtain the association equilibrium constant ($K_a$) of the analyte with the soluble binding agent through the measured free fraction and the known total concentrations of the analyte and binding agent that were present in the sample. On the other hand, injection at low-to-moderate flow rates will result in longer residence times in the column for the sample and increase the chance of the analyte dissociating from the soluble binding agent. This dissociation will increase the apparent free fraction that is measured for the analyte and will provide information on the interaction kinetics of the analyte with binding agent(s) in the sample (Zheng et al., 2014b, 2015a).

There are two equivalent relationships that can be used to obtain dissociation rate constants when employing ultrafast affinity extraction. These relationships are given in Equations (13) and (14) (Zheng et al., 2014b, 2015a).

$$\ln \frac{1-f_o}{1-f_t} = k_d t \tag{13}$$

$$\ln \frac{1}{1-f_t} = k_d t - ln(1-f_o) \tag{14}$$

The term $f_o$ represents the free or non-bound fraction of A that is present in a mixture of A and the soluble binding agent at equilibrium (i.e., as measured at high flow rates), while $f_t$ is the apparent free fraction for A that is observed in the presence of dissociation of the analyte-binding agent complex in the sample (i.e., as measured at lower flow rates). The term $t$ is the time this dissociation is allowed to occur, as given by the residence time of the sample in the column. If the dissociation process follows pseudo-first order decay, Equations (13) and (14) predict that a linear relation should be obtained when plotting $\ln[(1\text{-}f_o)/(1\text{-}f_t)]$ or $\ln[1/(1\text{-}f_t)]$ against $t$. The slope of these plots can be used to obtain $k_d$ (Zheng et al., 2014b, 2015a). **Figure 12** shows a plot that has been prepared in this manner with Equation (14) and used to determine the value of $k_d$ by means of ultrafast affinity extraction (Zheng et al., 2014b).

Ultrafast affinity extraction has been used as a tool to study the kinetics of many drugs with transport proteins. For instance, this method has been used to examine dissociation rate constants of HSA with warfarin, tolbutamide, acetohexamide, verapamil, gliclazide, chlorpromazine, diazepam, tolbutamide, quinidine,

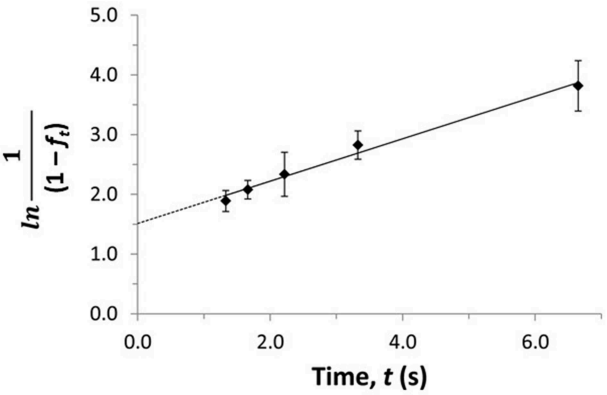


**FIGURE 12 |** Plot of ln[1/(1–$f_t$)] vs. $t$ to estimate the dissociation rate constant for verapamil with soluble HSA by using ultrafast affinity extraction and Equation (14). Terms: $f_t$, apparent free fraction for the analyte measured at a given dissociation time; $t$, dissociation time. Adapted with permission from Zheng et al. (2014b). Copyright 2014 American Chemical Society.

glimepiride, glibenclamide, and glipizide (Zheng et al., 2014b, 2016; Beeram et al., 2018; Yang et al., 2018). Similar work with AGP has been conducted to examine the dissociation rates of verapamil, lidocaine, imipramine, disopyramide, chlorpromazine and propranolol (Beeram et al., 2017, 2018). The same approach has been utilized to determine dissociation rate constants of testosterone with HSA, sex hormone binding globulin (SHBG), and equine serum albumin (ESA) (Zheng et al., 2015a; Czub et al., 2019).

The ultrafast affinity extraction method has been used to study systems that have weak-to-strong affinities ($10^3$-$10^9$ $M^{-1}$). The dissociation rate constants obtained by this technique have been in the general range of $10^{-2}$-10 $s^{-1}$ (Zheng et al., 2014b, 2015a, 2016; Bi et al., 2015; Beeram et al., 2017, 2018; Yang et al., 2018). One advantage of this method is it makes use of moderate-to-high flow rates, which can result in analysis times of only a few minutes. This method also uses only small volumes of the injected sample (i.e., a few μL) and can directly measure the dissociation rate constants for a solute and binding agent in solution. Another advantage is this method uses peak areas instead of peak fitting or band-broadening measurements, which can result in precise estimates of rate constants. One potential limitation of this method is that the column sizes and flow rates that are needed to separate the free and bound forms of the analyte currently need to be optimized for each solute-binding agent system (Zheng et al., 2014b, 2015a; Bi et al., 2015; Beeram et al., 2018). However, previous work has provided a number of guidelines that can be utilized to aid in this process (Beeram et al., 2018).

## CONCLUSIONS

This review discussed various techniques which can be employed in affinity chromatography or HPAC for studying the rates of solute interactions with immobilized or soluble binding agents. These techniques included those based on plate height measurements, peak profiling, peak decay analysis, the split-peak effect, peak fitting, and ultrafast affinity extraction. The association rate constants and dissociation rate constants that have been determined by these methods have spanned from $10^3$-$10^7$ $M^{-1}$ $s^{-1}$ to $10^{-2}$-10 $s^{-1}$, and represent systems with weak-to-strong binding constants ranging from $10^3$ to $10^9$ $M^{-1}$ (Schiel and Hage, 2009; Bi et al., 2015; Zheng et al., 2015b).

These methods have several common advantages. For instance, the affinity column and immobilized binding agent can often be reused for many experiments (i.e., up hundreds of studies), ensuring that good reproducibility and precision are obtained for the kinetic measurements. In addition, many of these methods are "label-free" and can be used with standard HPLC systems, which allows them to be automated and used with a variety of detectors. Detection methods used with HPAC or affinity chromatography in these applications have included absorbance, fluorescence, and mass spectrometry (Schiel and Hage, 2009; Bi et al., 2015; Zheng et al., 2015b). One possible limitation for many of these methods is immobilization of the binding agent is needed; this means that conditions for immobilization should be selected and validated to ensure the solute's interaction with the binding agent is similar to what would be seen in their natural environment (Schiel and Hage, 2009; Bi et al., 2015; Zheng et al., 2015b). One route to overcome this issue is to use the affinity column to indirectly study binding by a target compound with a soluble binding agent, as occurs in ultrafast affinity extraction (Bi et al., 2015; Zheng et al., 2015b).

The applications of these methods have included measurements for the rate constants of drugs as they interact with serum proteins, the binding of antibodies with antigens, the interactions of receptors with inhibitors, and the binding sugars or sugar analogs with lectins. The information that has been obtained on these interactions is of great importance in fields such as clinical chemistry, pharmaceutical science and biomedical research. Based on the current work in this field, and the advantages of using affinity chromatography and HPAC to obtain this information, even more applications are expected as further improvements and advances occur with these methods. Examples of some potential applications include high-throughput screening of drug candidates, use of chromatographic kinetic studies in multi-dimensional systems, and combined use of these methods with other techniques to provide both functional and structural data in areas such as proteomics, glycomics and personalized medicine (Anguizola et al., 2013; Zheng et al., 2013, 2014a; Matsuda et al., 2014).

## AUTHOR CONTRIBUTIONS

SI and DH conducted the literature research that lead to this review and were responsible for proofing and preparing the final copy of this review. SI prepared the initial draft with input from DH and a section from SO on the topic of peak fitting.

## FUNDING

This work was supported, in part, by the National Institutes of Health (NIH) under grants R01 DK069629 and R01 GM044931.

## REFERENCES


Anderson, D. J., and Walters, R. R. (1986). Equilibrium and rate constants of immobilized concanavalin a determined by high-performance affinity chromatography. *J. Chromatogr.* 376, 69–85. doi: 10.1016/S0378-4347(00)80824-5

Anguizola, J., Joseph, K. S., Barnaby, O. S., Matsuda, R., Alvarado, G., Clarke, W., et al. (2013). Development of affinity microcolumns for drug-protein binding studies in personalized medicine: interactions of sulfonylurea drugs with *in vivo* glycated human serum albumin. *Anal. Chem.* 85, 4453–4460. doi: 10.1021/ac303734c

Anguizola, J. A., Pfaunmiller, E. L., Milanuk, M. L., and Hage, D. S. (2018). Peak decay analysis and biointeraction studies of immunoglobulin binding and dissociation on protein G affinity microcolumns. *Methods* 146, 39–45. doi: 10.1016/j.ymeth.2018.03.013

Beeram, S., Bi, C., Zheng, X., and Hage, D. S. (2017). Chromatographic studies of drug interactions with alpha$_1$-acid glycoprotein by ultrafast affinity extraction and peak profiling. *J. Chromatogr. A* 1497, 92–101. doi: 10.1016/j.chroma.2017.03.056

Beeram, S. R., Zheng, X., Suh, K., and Hage, D. S. (2018). Characterization of solution-phase drug-protein interactions by ultrafast affinity extraction. *Methods* 146, 46–57. doi: 10.1016/j.ymeth.2018.02.021

Bi, C., Beeram, S., Li, Z., Zheng, X., and Hage, D. S. (2015). Kinetic analysis of drug-protein interactions by affinity chromatography. *Drug Discov. Today Technol.* 17, 16–21. doi: 10.1016/j.ddtec.2015.09.003

Chen, J., Schiel, J. E., and Hage, D. S. (2009). Non-competitive peak decay analysis of drug-protein dissociation by high-performance affinity chromatography. *J. Sep. Sci.* 32, 1632–1641. doi: 10.1002/jssc.200900074

Czub, M. P., Venkataramany, B. S., Majorek, K. A., Handing, K. B., Porebski, P. J., Beeram, S. R., et al. (2019). Testosterone meets albumin-the molecular mechanism of sex hormone transport by serum albumin. *Chem. Sci.* 10, 1607–1618. doi: 10.1039/C8SC04397C

Fitos, I., Visy, J., and Kardos, J. (2002). Stereoselective kinetics of warfarin binding to human serum albumin: effect of an allosteric interaction. *Chirality* 448, 442–448. doi: 10.1002/chir.10113

Hage, D. S. (ed) (2006). *Handbook of Affinity Chromatography, 2nd Edn.* Boca Raton, FL: CRC Press.

Hage, D. S., Anguizola, J. A., Bi, C., Li, R., Matsuda, R., Papastavros, E., et al. (2012). Pharmaceutical and biomedical applications of affinity chromatography: recent trends and developments. *J. Pharm. Biomed. Anal.* 69, 93–105. doi: 10.1016/j.jpba.2012.01.004

Hage, D. S., and Kim, H. S. (2006). "Immobilization methods for affinity chromatography," in *Handbook of Affinity Chromatography, 2nd Edn*, ed D. S. Hage (Boca Raton, FL: CRC Press), 35–78.

Hage, D. S., Thomas, D. H., and Beck, M. S. (1993). Theory of a sequential addition competitive binding immunoassay based on high-performance immunoaffinity chromatography. *Anal. Chem.* 65, 1622–1630. doi: 10.1021/ac00059a023

Hage, D. S., Thomas, D. H., Chowdhuri, A. R., and Clarke, W. (1999). Development of a theoretical model for chromatographic-based competitive binding immunoassays with simultaneous injection of sample and label. *Anal. Chem.* 71, 2965–2975. doi: 10.1021/ac990070s

Hage, D. S., and Walters, R. R. (1987). Dual-column determination of albumin and immunoglobulin G in serum by high-performance affinity chromatography. *J. Chromatogr.* 386, 37–49. doi: 10.1016/S0021-9673(01)94582-0

Hage, D. S., and Walters, R. R. (1988). Non-linear elution effects in split-peak chromatography. I. Computer simulations for the cases of irreversible diffusion- and adsorption-limited kinetics. *J. Chromatogr.* 436, 111–135. doi: 10.1016/S0021-9673(00)94574-6

Hage, D. S., Walters, R. R., and Hethcote, H. W. (1986). Split-peak affinity chromatographic studies of the immobilization-dependent adsorption kinetics of protein A. *Anal. Chem.* 58, 274–279. doi: 10.1021/ac00293a003

Hinze, W. L., Riehl, T. E., Armstrong, D. W., Demond, W., Alak, A., and Ward, T. (1985). Liquid chromatographic separation of enantiomers using a chiral β-cyclodextrin-bonded stationary phase and conventional aqueous-organic mobile phases. *Anal. Chem.* 57, 237–242. doi: 10.1021/ac00279a055

Jozwiak, K., Haginaka, J., Moaddel, R., and Wainer, I. W. (2002). Displacement and non-linear chromatographic techniques in the investigation of interaction of non-competitive inhibitors with an immobilized α3β4 nicotinic acetylcholine receptor liquid chromatographic stationary phase. *Anal. Chem.* 74, 4618–4624. doi: 10.1021/ac0202029

Jozwiak, K., Hernandez, S. C., Kellar, K. J., and Wainer, I. W. (2003). Enantioselective interactions of dextromethorphan and levomethorphan with the α3β4 -nicotinic acetylcholine receptor: comparison of chromatographic and functional data. *J. Chromatogr. B.* 797, 373–379. doi: 10.1016/S1570-0232(03)00608-1

Jozwiak, K., Ravichandran, S., Collins, J. R., Moaddel, R., and Wainer, I. W. (2007). Interaction of non-competitive inhibitors with the α3β2 nicotinic acetylcholine receptor investigated by affinity chromatography and molecular docking. *J. Med. Chem.* 50, 6279–6283. doi: 10.1021/jm070784s

Jozwiak, K., Ravichandran, S., Collins, J. R., and Wainer, I. W. (2004). Interaction of non-competitive inhibitors with an immobilized α3β2 nicotinic acetylcholine receptor investigated by affinity chromatography, quantitative-structure activity relationship analysis, and molecular docking. *J. Med. Chem.* 47, 4008–4021. doi: 10.1021/jm0400707

Krylov, S. N. (2007). Kinetic CE: foundation for homogeneous kinetic affinity methods. *Electrophoresis* 28, 69–88. doi: 10.1002/elps.200600577

Lee, W. C., and Chen, C. H. (2001). Predicting the elution behavior of proteins in affinity chromatography on non-porous particles. *Biochem. Biophys. Methods* 49, 63–82. doi: 10.1016/S0165-022X(01)00189-0

Lee, W. C., and Chuang, C. Y. (1996). Performance of pH elution in high-performance affinity chromatography of proteins using non-porous silica. *J. Chromatogr. A* 721, 31–39. doi: 10.1016/0021-9673(95)00756-3

Li, H., Ge, J., Guo, T., Yang, S., He, Z., York, P., et al. (2013). Determination of the kinetic rate constant of cyclodextrin supramolecular systems by high performance affinity chromatography. *J. Chromatogr. A* 1305, 139–148. doi: 10.1016/j.chroma.2013.07.010

Li, Q., Wang, J., Yuan, Y., Yang, L., Zhang, Y., Bian, L., et al. (2015). Comparison of zonal elution and non-linear chromatography in determination of the interaction between seven drugs and immobilised $\beta_2$-adrenoceptor. *J. Chromatogr. A* 1401, 75–83. doi: 10.1016/j.chroma.2015.05.012

Liang, Y., Wang, J., Fei, F., Sun, H., Liu, T., Li, Q., et al. (2018). Binding kinetics of five drugs to beta2-adrenoceptor using peak profiling method and non-linear chromatography. *J. Chromatogr. A* 1538, 17–24. doi: 10.1016/j.chroma.2018.01.027

Loun, B., and Hage, D. S. (1996). Chiral separation mechanisms in protein-based HPLC columns. 2. Kinetic studies of (R)- and (S)-warfarin binding to immobilized human serum albumin. *Anal. Chem.* 68, 1218–1225. doi: 10.1021/ac950827p

Mallik, R., Yoo, M. J., Briscoe, C. J., and Hage, D. S. (2010). Analysis of drug-protein binding by ultrafast affinity chromatography using immobilized human serum albumin. *J. Chromatogr. A* 1217, 2796–2803. doi: 10.1016/j.chroma.2010.02.026

Marszałł, M. P., Moaddel, R., Jozwiak, K., Bernier, M., and Wainer, I. W. (2008). Initial synthesis and characterization of an immobilized heat shock protein 90 column for online determination of binding affinities. *Anal. Biochem.* 373, 313–321. doi: 10.1016/j.ab.2007.11.001

Matsuda, R., Bi, C., Anguizola, J., Sobansky, M., Rodriguez, E., Badilla, J. V., et al. (2014). Studies of metabolite-protein interactions: a review. *J. Chromatogr. B* 966, 48–58. doi: 10.1016/j.jchromb.2013.11.043

Moaddel, R., Jozwiak, K., and Wainer, I. W. (2007). Allosteric modifiers of neuronal nicotinic acetylcholine receptors: new methods, new opportunities. *Med. Res. Rev.* 27, 723–753. doi: 10.1002/med.20091

Moaddel, R., Jozwiak, K., Yamaguchi, R., and Wainer, I. W. (2005). Direct chromatographic determination of dissociation rate constants of ligand-receptor complexes: assessment of the interaction of non-competitive inhibitors with an immobilized nicotinic acetylcholine receptor-based liquid chromatography stationary phase. *Anal. Chem.* 77, 14102–14107. doi: 10.1021/ac0504464

Moaddel, R., and Wainer, I. W. (2007). Conformational mobility of immobilized proteins. *J. Pharm. Biomed. Anal.* 43, 399–406. doi: 10.1016/j.jpba.2006.08.021

Moore, R. M., and Walters, R. R. (1987). Peak-decay method for the measurement of dissociation rate constants by high-performance affinity chromatography. *J. Chromatogr.* 384, 91–103. doi: 10.1016/S0021-9673(01)94662-X

Munro, P. D., Winzor, D., and Cann, J. R. (1993). Experimental and theoretical studies of rate constant evaluation by affinity chromatography: determination

of rate constants for the interaction of saccharides with concanavalin A. *J. Chromatogr.* 646, 3–15. doi: 10.1016/S0021-9673(99)87002-2

Munro, P. D., Winzor, D., and Cann, J. R. (1994). Allowance for kinetics of solute partitioning in the determination of rate constants by affinity chromatography. *J. Chromatogr. A* 659, 267–273. doi: 10.1016/0021-9673(94)85068-2

Myszka, D. G., and Rich, R. L. (2000). Implementing surface plasmon resonance biosensors in drug discovery. *Pharm. Sci. Technol. Today* 3, 310–317. doi: 10.1016/S1461-5347(00)00288-1

Nelson, M. A., Moser, A., and Hage, D. S. (2010). Biointeraction analysis by high-performance affinity chromatography: kinetic studies of immobilized antibodies. *Eur PMC* 878, 165–171. doi: 10.1016/j.jchromb.2009.04.004

Pfaunmiller, E., Moser, A. C., and Hage, D. S. (2012). Biointeraction analysis of immobilized antibodies and related agents by high-performance immunoaffinity chromatography. *Methods* 56, 130–135. doi: 10.1016/j.ymeth.2011.08.016

Renard, J., Vidal-Madjar, C., and Lspresle, C. (1995). Determination by chromatographic methods of the adsorption constant of hsa on immobilized polyclonal and monoclonal antibodies. *J. Colloid Interface Sci.* 174, 61–67. doi: 10.1006/jcis.1995.1364

Rollag, J. G., and Hage, D. S. (1998). Non-linear elution effects in split-peak chromatography. II. Role of ligand heterogeneity in solute binding to columns with adsorption-limited kinetics. *J. Chromatogr. A* 795, 185–198. doi: 10.1016/S0021-9673(97)00975-8

Schiel, J. E., and Hage, D. S. (2009). Kinetic studies of biological interactions by affinity chromatography. *J. Sep. Sci.* 32, 1507–1522. doi: 10.1002/jssc.200800685

Schiel, J. E., Mallik, R., Soman, S., Joseph, K. S., and Hage, D. S. (2006). Applications of silica supports in affinity chromatography. *J. Sep. Sci.* 29, 719–737. doi: 10.1002/jssc.200500501

Schiel, J. E., Ohnmacht, C. M., and Hage, D. S. (2009). Measurement of drug-protein dissociation rates by high-performance affinity chromatography and peak profiling. *Anal. Chem.* 81, 4320–4333. doi: 10.1021/ac9000404

Schreiber, G., Haran, G., and Zhou, H. (2009). Fundamental aspects of protein-protein association kinetics. *Chem. Rev.* 109, 839–860. doi: 10.1021/cr800373w

Talbert, A. M., Tranter, G. E., Holmes, E., and Francis, P. L. (2002). Determination of drug-plasma protein binding kinetics and equilibria by chromatographic profiling: exemplification of the method using L-tryptophan and albumin. *Anal. Chem.* 74, 446–452. doi: 10.1021/ac010643c

Tong, Z., and Hage, D. S. (2011). Characterization of interaction kinetics between chiral solutes and human serum albumin by using high-performance affinity chromatography and peak profiling. *J. Chromatogr. A* 1218, 6892–6897. doi: 10.1016/j.chroma.2011.08.026

Tong, Z., Schiel, J. E., Papastavros, E., Ohnmacht, C. M., Smith, Q. R., and Hage, D. S. (2011). Kinetic studies of drug-protein interactions by using peak profiling and high-performance affinity chromatography: examination of multi-site interactions of drugs with human serum albumin columns. *J. Chromatogr. A* 1218, 2065–2071. doi: 10.1016/j.chroma.2010.10.070

Vidal-Madjar, C., Jaulmes, A., Renard, J., Peter, D., and Lafaye, P. (1997). Chromatographic study of the adsorption kinetics of albumin on monoclonal and polyclonal immunoadsorbents. *Chromatographia* 45, 18–24. doi: 10.1007/BF02505531

Vuignier, K., Schappler, J., Veuthey, J. L., Carrupt, P. A., and Martel, S. (2010). Drug–protein binding: a critical review of analytical tools. *Anal. Bioanal. Chem.* 398, 53–66. doi: 10.1007/s00216-010-3737-1

Wade, J. L., Bergold, A. F., and Carr, P. W. (1987). Theoretical description of non-linear chromatography, with applications to physicochemical measurements in affinity chromatography and implications for preparative-scale separations. *Anal. Chem.* 59, 1286–1295. doi: 10.1021/ac00136a008

Wang, C., Ge, J., Zhang, J., Guo, T., Chi, L., He, Z., et al. (2014). Multianalyte determination of the kinetic rate constants of drug–cyclodextrin supermolecules by high performance affinity chromatography. *J. Chromatogr. A* 1359, 287–295. doi: 10.1016/j.chroma.2014.07.012

Wang, C., Wang, X., Xu, X., Liu, B., Xu, X., Sun, L., et al. (2016). Simultaneous high-throughput determination of interaction kinetics for drugs and cyclodextrins by high performance affinity chromatography with mass spectrometry detection. *Anal. Chim. Acta* 909, 75–83. doi: 10.1016/j.aca.2015.12.026

Williams, M. A. (2013). "Protein-ligand interactions: fundamentals," in *Protein-Ligand Interactions, Methods and Applications*, eds M. A. Williams and T. Daviter (New York, NY: Humana Press), 3–34. doi: 10.1007/978-1-62703-398-5_1

Yang, B., Zheng, X., and Hage, D. S. (2018). Binding studies based on ultrafast affinity extraction and single- or two-column systems: interactions of second- and third-generation sulfonylurea drugs with normal or glycated human serum albumin. *J. Chromatogr. B* 1102–1103, 8–16. doi: 10.1016/j.jchromb.2018.10.015

Yang, J., and Hage, D. S. (1997). Effect of mobile phase composition on the binding kinetics of chiral solutes on a protein-based high-performance liquid chromatography column: interactions of D- and L-tryptophan with immobilized human serum albumin. *J. Chromatogr. A* 766, 15–25. doi: 10.1016/S0021-9673(96)01040-0

Yoo, M. J., and Hage, D. S. (2009). Evaluation of silica monoliths in affinity microcolumns for high-throughput analysis of drug–protein interactions. *J. Sep. Sci.* 32, 2776–2785. doi: 10.1002/jssc.200900346

Yoo, M. J., and Hage, D. S. (2011a). High-throughput analysis of drug dissociation from serum proteins using affinity silica monoliths. *J. Sep. Sci.* 34, 2255–2263. doi: 10.1002/jssc.201100280

Yoo, M. J., and Hage, D. S. (2011b). Use of peak decay analysis and affinity microcolumns containing silica monoliths for rapid determination of drug–protein dissociation rates. *J. Chromatogr. A* 1218, 2072–2078. doi: 10.1016/j.chroma.2010.09.070

Yoo, M. J., Schiel, J. E., and Hage, D. S. (2010). Evaluation of affinity microcolumns containing human serum albumin for rapid analysis of drug–protein binding. *J. Chromatogr. B* 878, 1707–1713. doi: 10.1016/j.jchromb.2010.04.028

Zhang, C., Rodriguez, E., Bi, C., Zheng, X., Suresh, D., Suh, K., et al. (2018). High performance affinity chromatography and related separation methods for the analysis of biological and pharmaceutical agents. *Analyst* 143, 374–391. doi: 10.1039/C7AN01469D

Zheng, X., Bi, C., Brooks, M., and Hage, D. S. (2015a). Analysis of hormone–protein binding in solution by ultrafast affinity extraction: interactions of testosterone with human serum albumin and sex hormone binding globulin. *Anal. Chem.* 87, 11187–11194. doi: 10.1021/acs.analchem.5b03007

Zheng, X., Bi, C., Li, Z., Podariu, M., and Hage, D. S. (2015b). Analytical methods for kinetic studies of biological interactions: a review. *J. Pharm. Biomed. Anal.* 113, 163–180. doi: 10.1016/j.jpba.2015.01.042

Zheng, X., Li, Z., Beeram, S., Podariu, M., Matsuda, R., Pfaunmiller, E. L., et al. (2014a). Analysis of biomolecular interactions using affinity microcolumns: a review. *J. Chromatogr. B* 968, 49–63. doi: 10.1016/j.jchromb.2014.01.026

Zheng, X., Li, Z., Podariu, M. I., and Hage, D. S. (2014b). Determination of rate constants and equilibrium constants for solution-phase drug-protein interactions by ultrafast affinity extraction. *Anal. Chem.* 86, 6454–6460. doi: 10.1021/ac501031y

Zheng, X., Podariu, M., Matsuda, R., and Hage, D. S. (2016). Analysis of free drug fractions in human serum by ultrafast affinity extraction and two-dimensional affinity chromatography. *Anal. Bioanal. Chem.* 408, 131–140. doi: 10.1007/s00216-015-9082-7

Zheng, X., Yoo, M. J., and Hage, D. S. (2013). Analysis of free fractions for chiral drugs using ultrafast extraction and multi-dimensional high-performance affinity chromatography. *Analyst* 138, 6262–6265. doi: 10.1039/c3an01315d

**Conflict of Interest:** The authors declare that this manuscript was prepared, and the associated work described in this paper by the authors was conducted, in the absence of any commercial or financial relationships that could be construed as a potential conflict of interest.

frontiers in Chemistry

REVIEW
published: 23 October 2019
doi: 10.3389/fchem.2019.00703

# Advances in MS Based Strategies for Probing Ligand-Target Interactions: Focus on Soft Ionization Mass Spectrometric Techniques

*Guilin Chen*[1,2], *Minxia Fan*[1,2,3], *Ye Liu*[1,2], *Baoqing Sun*[4], *Meixian Liu*[5], *Jianlin Wu*[5], *Na Li*[5] *and Mingquan Guo*[1,2*]

[1] *Key Laboratory of Plant Germplasm Enhancement and Specialty Agriculture, Wuhan Botanical Garden, Chinese Academy of Sciences, Wuhan, China,* [2] *Sino-Africa Joint Research Center, Chinese Academy of Sciences, Wuhan, China,* [3] *Graduate University of Chinese Academy of Sciences, Beijing, China,* [4] *State Key Laboratory of Respiratory Disease, National Clinical Center for Respiratory Diseases, Guangzhou Institute of Respiratory Diseases, First Affiliated Hospital, Guangzhou Medical University, Guangzhou, China,* [5] *State Key Laboratory for Quality Research of Chinese Medicines, Macau University of Science and Technology, Taipa, Macau*

OPEN ACCESS

**Edited by:**
*Enrica Calleri, University of Pavia, Italy*

**Reviewed by:**
*Qiuling Zheng, China Pharmaceutical University, China*
*Chao Lu, Beijing University of Chemical Technology, China*

***Correspondence:**
*Mingquan Guo*
*guomq@wbgcas.cn*

**Specialty section:**
*This article was submitted to Analytical Chemistry, a section of the journal Frontiers in Chemistry*

**Received:** *24 July 2019*
**Accepted:** *08 October 2019*
**Published:** *23 October 2019*

**Citation:**
*Chen G, Fan M, Liu Y, Sun B, Liu M, Wu J, Li N and Guo M (2019) Advances in MS Based Strategies for Probing Ligand-Target Interactions: Focus on Soft Ionization Mass Spectrometric Techniques. Front. Chem. 7:703. doi: 10.3389/fchem.2019.00703*

The non-covalent interactions between small drug molecules and disease-related proteins (ligand-target interactions) mediate various pharmacological processes in the treatment of different diseases. The development of the analytical methods to assess those interactions, including binding sites, binding energies, stoichiometry and association-dissociation constants, could assist in clarifying the mechanisms of action, precise treatment of targeted diseases as well as the targeted drug discovery. For the last decades, mass spectrometry (MS) has been recognized as a powerful tool to study the non-covalent interactions of the ligand-target complexes with the characteristics of high sensitivity, high-resolution, and high-throughput. Soft ionization mass spectrometry, especially the electrospray mass spectrometry (ESI-MS) and matrix assisted laser desorption ionization mass spectrometry (MALDI-MS), could achieve the complete transformation of the target analytes into the gas phase, and subsequent detection of the small drug molecules and disease-related protein complexes, and has exerted great advantages for studying the drug ligands-protein targets interactions, even in case of identifying active components as drug ligands from crude extracts of medicinal plants. Despite of other analytical techniques for this purpose, such as the NMR and X-ray crystallography, this review highlights the principles, research hotspots and recent applications of the soft ionization mass spectrometry and its hyphenated techniques, including hydrogen-deuterium exchange mass spectrometry (HDX-MS), chemical cross-linking mass spectrometry (CX-MS), and ion mobility spectrometry mass spectrometry (IMS-MS), in the study of the non-covalent interactions between small drug molecules and disease-related proteins.

**Keywords: ligand-target interactions, mass spectrometry, soft ionization, drug discovery, ESI-MS, MALDI-MS**

## INTRODUCTION

The life process is closely related to numerous inherent biological macromolecules, such as proteins, peptides, and nucleic acids, which are important components of the biological organisms. These macromolecules, on the one hand, could regulate the body's signal transduction among cells and maintain the normal substantial and energy metabolism to play vital roles in the life activities. On the other hand, a large proportion of small drug molecules take effects by majorly interacting with these disease-related drug targets in the pharmacological process of treatment (Mulabagal and Calderón, 2010; Chen et al., 2018a). Thereof the non-covalent interactions between small drug molecules and biological macromolecules have always been a hot topic in medicinal chemistry and life sciences worldwide. The non-covalent interactions, including the hydrogen bond, Van der Waals forces, electrostatic interactions and hydrophobic effects, between small drug molecules and biological macromolecules are very weak, which are generally $<10$ kJ·mol$^{-1}$ and 1–2 magnitudes smaller than the usual covalent bond with the range of action from 0.3 to 0.5 nm (Zhang and Abliz, 2005). However, these weak intermolecular interactions could exert additive and synergistic effects under certain conditions, and further form some kinds of strong forces with directivity and selectivity. To some extent, the studies of the properties of these forces could strongly help to understand the interactions between molecules and their mutual recognition process in the field of life sciences, medicine, and pharmacy (Ramos and Santana-Marques, 2009; Han et al., 2018). Therefore, the detection and characterization of the non-covalent complexes have become a commonly concerned hot issue.

Currently, the determination methods for studying the non-covalent complexes mainly include spectral methods [UV, IR, fluorescence, circular dichroism (CD), etc.], chromatography, hypervelocity centrifugation, NMR, and X-ray crystal diffraction, which have their own advantages and disadvantages (Mulabagal and Calderón, 2010). The spectral methods could provide the information of the structural changes before and after the formation of complexes, while little or no information on the relative molecular weight ($M_w$) and stoichiometric ratio of complexes (Zhang and Abliz, 2005). The X-ray crystal diffraction method can only be used when suitable crystal is obtained (Wilderman et al., 2010); the NMR method requires a large number of samples, and is inappropriate for those samples with the $M_w > 30$ ku (Marion, 2013).

Mass spectrometry (MS) has been characterized by the high sensitivity, rapidity, and specificity (Ma et al., 2016; Zhu et al., 2018). Recently, the development of soft ionization technologies, especially the electrospray ionization (ESI) and matrix assisted laser desorption ionization (MALDI), has extended the analysis range of MS from small molecules to biological macromolecules (Yao et al., 2013). During the assay, MS could provide a large number of stoichiometric and spectral information with small sample consumption (*p*mol - *f*mol), which makes MS show great advantages in studying the non-covalent complexes. For example, due to its soft ionization conditions, soft ionization MS will not be limited by the solubility and $M_w$ in the study of the interactions between small drug molecules and biological macromolecules (Dettmer et al., 2007). Furthermore, the soft ionization MS can be applied directly to obtain the stoichiometric ratios between drugs and biological macromolecules, calculate the binding strength between the ligand-protein complexes, determine the binding site of drugs, and obtain the reaction kinetics and others (Bolbach, 2005; Hofstadler and Sannes-Lowery, 2006). In addition, unlike the NMR or CD techniques that measure the average properties of biological macromolecules, soft ionization MS coupled with hydrogen/deuterium (H/D) exchange techniques could quantitatively describe the protein folding dynamics (Winston and Fitzgerald, 1997; Ramirez-Sarmiento and Komives, 2018). Finally, MS can be easily combined with various chromatographic techniques, which is very suitable for studying the interactions between various small drug molecules and biological macromolecules in complex systems (Zinn et al., 2012; Guo et al., 2017).

Drug targets commonly refer to the biological macromolecules existing in tissues and cells that exhibit specific interactions with drug molecules and enable drugs to exert their expected biological activities, and more than 95% of which are the proteins, including enzymes, receptor proteins, ion channel proteins, regulatory factors, and nuclear receptors (Evans and Relling, 1999; Gao et al., 2008). Therefore, to accurately explain and describe the ligand-target interactions is not only the key scientific problem for the drug development, but also the most challenging frontier scientific issue in chemical biology, especially in chemical genomics (Sato et al., 2007). In this regard, many new methods and technologies for the detailed interpretation of the ligand-target interactions derived from modern analytical techniques have been brought into being, among which MS and its hyphenated technologies, including but not limited to the cross-linking MS (CX-MS) (Ferraro and Cascio, 2018), hydrogen-deuterium exchange MS (HDX-MS) (Ramirez-Sarmiento and Komives, 2018), ion mobility MS (IM-MS) (Goth and Pagel, 2017), and hydrophilic interaction chromatography MS (HILIC-MS) (Jin et al., 2017), are the most widely used technologies for studying the interactions between small drug molecules and biological macromolecules. To this end, this present manuscript summarized and reviewed the applications of the soft ionization MS, especially the ESI-MS and MALDI-MS, in the study of the interactions between small drug molecules and biological macromolecules.

## SOFT IONIZATION MS TECHNIQUES FOR PROBING THE NON-COVALENT INTERACTIONS

Mass spectrometry, as its name implies, refers to the procedures that after the samples are converted into moving gaseous ions, a variety of charged ions will be separated from each other according to their own specific mass/charge ratio (m/z) and then form their own different motion tracks in a high vacuum mass analyzer with applied electric field or magnetic field, and the final mass spectrogram is generated through data recording

and conversion. The corresponding technology and instrument are called as the mass spectrometer (**Figure 1**), which generally consists of five parts, including the sampling system, ion source, mass analyzer, detector, and data processing system.

In the late 1980s, the soft ionization technologies represented by ESI and MALDI have opened up a new field for the MS, which can be widely applied to analyze the biological macromolecules, synthetic polymers and other thermal unstable, strong polar, and volatile compounds that cannot be detected by the conventional MS. Under certain conditions, non-covalent complexes can be "intactly" transformed from the solution to the gas phase and then directly detected by soft ionization method, which can provide the valuable information of the stoichiometric ratios, the binding types and energies of the ligand-target complexes. In 1991, Ganem and his partners firstly employed the ionspray (similar to ESI) MS to investigate the non-covalent interactions of the complexes formed by the immune protein FKBP and immune drug FK506, and found that the determination conditions strongly affected the ionic strength of the complexes, while the compositions of the complexes were independent of the drug concentration in solution, and the stoichiometric ratio was 1:1 (Ganem et al., 1991). Since then, the ESI-MS and MALDI-MS have been used successfully in the protein and peptide detection and sequencing, DNA sequencing, protein folding, evaluation of the contribution of individual amino acid residues to protein function, *in vitro* drug analysis and new drug research and development (Siuzdak, 1994; Hofstadler and Sannes-Lowery, 2006; Ramos and Santana-Marques, 2009).

# ESI-MS AND ITS APPLICATIONS IN LIGAND-TARGET INTERACTIONS

## Characteristics of the ESI-MS

The ESI process can be generally divided into three stages: droplet formation, droplet atrophy, and gaseous ion formation (**Figure 2**). During the ionization process of ESI, the solute molecules are not attacked by other molecules or particles such as atoms, ions, etc., thus maintaining a "complete" molecular ion into the mass spectrometer. Distinguished from the classical EI source, the ESI produces molecular ions with multiple charges, which broadens the mass range of mass spectrometry detection. Based on the soft ionization characteristics of the ESI source, Loo summed up the 4 "S" characteristics of the ESI-MS: Sensitivity, Speed, Specificity, and could directly give the Stoichiomotry (Loo, 1997).

The soft ionization process of ESI-MS also allows the super-molecular complexes bound with weak non-covalent interactions to be completely detected, which could directly predict the chemical binding quantitative relationships of each component of the complexes, thus providing important structural information for the study of super-molecular systems. In addition, the ESI-MS can measure non-covalent complexes from the solution phase into the gas phase, which is very close to the state of the natural solution and could truly reflect the aggregation state of the test molecules in the solution. Therefore, it plays an important role in the study of the non-covalent complexes of the molecular recognition, and is an ideal analytical tool for studying the interactions between small molecules and biological macromolecules. For example, the interactions of the protein-protein, DNA-protein, DNA-drug, and antibody-antigen complexes have been successfully studied using ESI-MS (Liang et al., 2018).

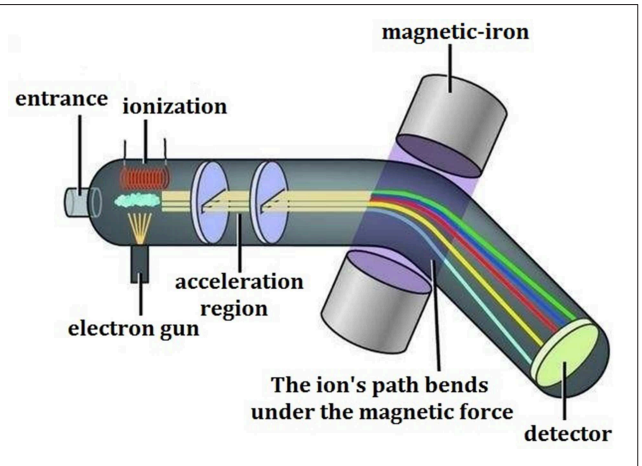


**FIGURE 1 |** The schematic diagram of MS.

## Applications of ESI-MS in the Interactions of Small Drug Molecules With DNA

DNA is the main carrier of genetic information in living organisms. A great number of drugs interact with DNA by interfering with the regulation and expression of disease-related genes, making DNA the target of many drugs in human body (Brodbelt, 2010; Mirzaei et al., 2013; Chan et al., 2017). Therefore, the study of the interactions between drug molecules and DNA not only helps to understand the mechanisms of action of drugs at the molecular level, but also has important theoretical guiding significance for the screening of drugs *in vitro* and the design of the disease-resistant drugs. **Table 1** presents some representative studies and findings in this field.

In this research area, Wan et al. (2000) observed the competitive binding effects of four drugs (distamycin, hoechst 33258, hoechst 33342, and berenil) to one double stranded DNA, and calculated the relative affinity strength of the same pair of stranded DNA according to the abundance ratio of the unbound double stranded DNA and the bound double stranded DNA in ESI-MS. Results suggested that the binding strengths of the four drug molecules to DNA was: hoechst 33342 > hoechst 33258 > distamycin > berenil. In another effort, Carrasco et al. (2002) confirmed the preferential interaction between the antitumor drug ditercalinium and DNA with ESI-MS, and analyzed the ligation reaction in detail by surface plasmon resonance (SPR) spectroscopy, which provided a new idea for the design of drugs that can be designed to be ligated to the human tolemeres. Besides, Dong et al. (2007) studied the interactions between five bis-β-carboline alkaloids and three double-stranded DNA. The results showed that the length of

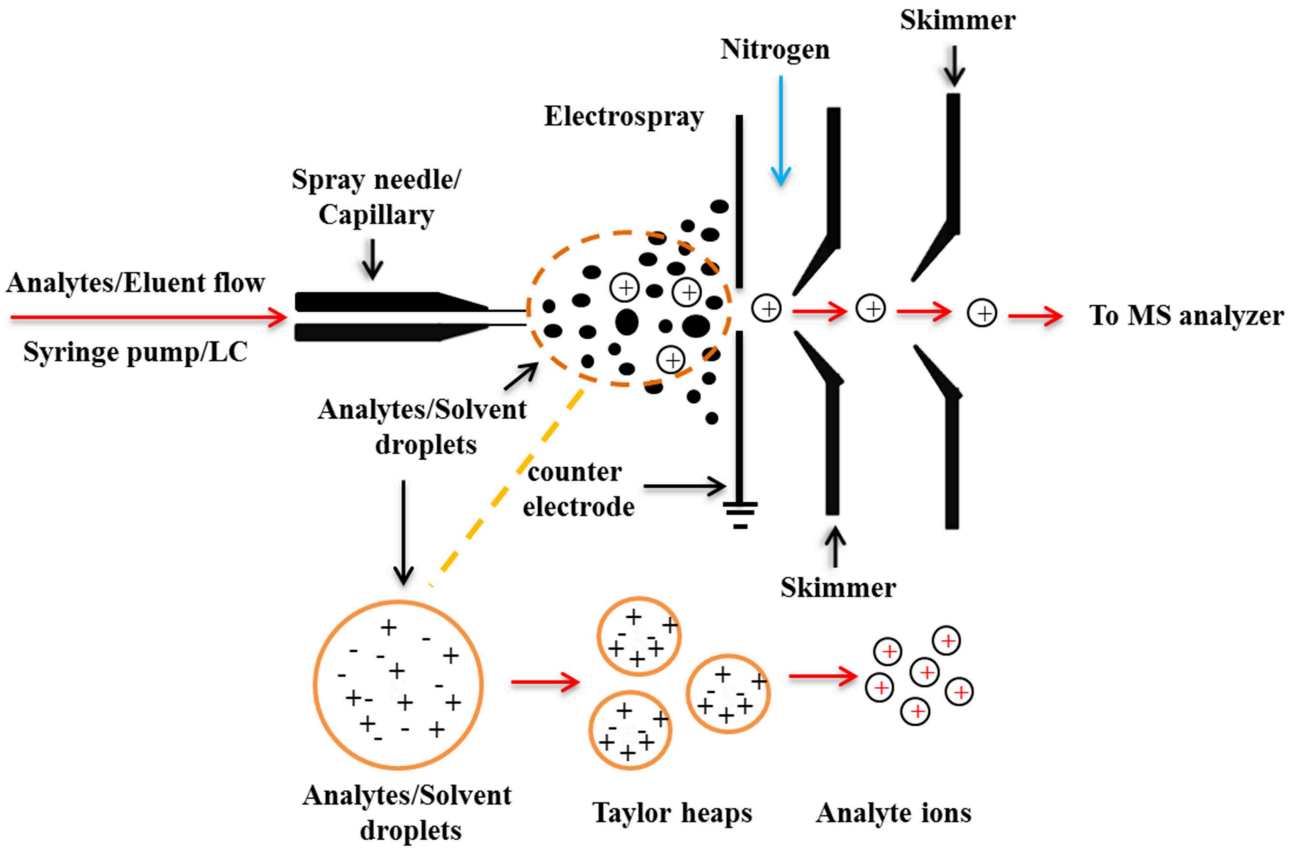


**FIGURE 2 |** The schematic workflow of typical ESI ionization processes.

**TABLE 1 |** Representative studies of ESI-MS technologies for the non-covalent interactions between small drug molecules and DNA.

| Subjects | Ligands | Type of MS | References |
|---|---|---|---|
| Single/double-stranded DNA | EGCG | CSI-MS | Kuzuhara et al., 2006 |
| Hairpin DNA | Chelerythrine, sanguinarine | ESI-TOF MS | Bai et al., 2008 |
| DNA duplexes/triplexes | Mitoxantrone | ESI-FT-ICR MS | Wan et al., 2008 |
| Double-stranded oligodeoxynucleotides | Distamycin, hoechst 33258, hoechst 33342, berenil | ESI-MS | Wan et al., 2000 |
| Three double-stranded oligodeoxynucleotides | Five bis-β-carbolines alkaloids | ESI-FT-ICR MS | Dong et al., 2007 |
| Quadruplex DNA | Ditercalinium | ESI-TOF MS | Carrasco et al., 2002 |
| EthR6-DNA and EthR4-DNA | Ethionamide | NanoESI-Q-TOF MS | Chan et al., 2017 |

the connecting arm in the drug chemical structures could affect the strength of its interaction with DNA, and too short or too long of the connecting arm would weaken the binding ability of alkaloids to DNA. Furthermore, Bai et al. (2008) used ESI-MS to study the interactions between chelerythrine, sanguinarine, and a series of hairpin DNA. The results showed that the two alkaloids exerted strong binding affinities with the hairpin DNA molecules containing a pyrimidine swelled part; and the interaction between sanguinarine and DNA was stronger than that of the chelerythrine, while the sequence selectivity of the latter was higher than that of the former.

In addition, coldspray ionization (CSI) is a novel ionization method based on an improved ESI ion source (Yamaguchi, 2003). With this improved technique, the CSI-MS has shown promising application prospects in the analysis of the self-assembled nano-scale organometallic complexes structures, DNA complexes structures, weak interactions between organic molecules and nucleosides, and the formation of the molecular clusters (Sakamoto et al., 2000; Sakamoto and Yamaguchi, 2003). For instance, Kuzuhara et al. (2006) used CSI-MS to study the interactions between the (-)-epigallocatechin gallate (EGCG) and the single-stranded DNA, single-stranded RNA and double-stranded DNA with the green tea extracts, and the results

showed that the galactyl and catechin groups in EGCG structure contributed to the binding affinities to nucleic acid molecules.

## Applications of ESI-MS in the Interactions of Small Drug Molecules With Proteins

Protein is also one of the main targets for drugs to exert pharmacological effects in human body. On the one hand, drugs can regulate and change the biological functions of receptor proteins by combining with the receptor proteins, such as ion channel and enzymes, which could change the spatial conformation of the receptor proteins or compete with the natural ligand of the receptor proteins, so as to exert their pharmacodynamic effects (Evans and Relling, 1999). On other hand, through the combination with the human serum albumin (HSA), drugs can be delivered to the tissues and organs where they work, which could also effectively control the drug release and prevent the rapid drug metabolism (Iwao et al., 2018; Tzameret et al., 2019). Therefore, the studies on the interactions between small drug molecules and protein targets shown in the following **Table 2**, not only help to understand the mechanisms of pharmacological action of drugs at the molecular level, but also help to fully evaluate the absorption, distribution, metabolism, and excretion of drugs in the body.

Chen et al. (2004, 2008) phosphorylated the flavonoids of myricet, myricetin, and 7-hydroxy flavone, and then compared the interactions between these flavonoids and their related phosphorylated derivatives with proteins by ESI-MS. The results revealed that the binding strength of acylated flavonoids with proteins was stronger than that of flavonoids, and the *in vitro* assays also proved that the former displayed stronger inhibitory activity on tumor cells than the latter. Liu et al. (2008) investigated the effects of tanshinone IIA on the interaction between the anticoagulant drug warfarin and HAS by using ESI-MS. It was found that tanshinone IIA could competitively bind to the HSA with warfarin, which not only resulted in the increase of the free warfarin in the blood, but also accelerated the metabolism of warfarin, and thus this phenomenon was very helpful to elucidate how the tanshinone IIA enhanced the pharmacological effects of warfarin in the body at the molecular level.

β-Lactoglobulin (β-G) exists extensively in the milk of most mammals and is the main component of whey protein. It has good biodegradability and adaptability and can be used as an excellent carrier (Mensi et al., 2013). In this regard, Xu et al. (2018) studied the interactions between flavonoids (morin, quercetin and myricetin) and β-lactoglobulin by high performance liquid chromatography-electrospray-quadrupole-time-of-flight high-resolution mass spectrometry (HPLC-ESI-Q-TOF MS). The binding constants of the β-lactoglobulin interacting with three flavonoids at different volume ratios were determined. The results showed that morin, quercetin and myricetin could form stable complexes with β-lactoglobulin at different volume ratios; the number of the flavonoid molecules bound with a single β-lactoglobulin increased with the decrease of the volume ratio (the proportion of small flavonoid molecules increased); the complexes exhibited strong binding abilities when the binding constant order of magnitude was $10^3$-$10^5$, and the binding ability of the three flavonoid molecules and β-lactoglobulin was of the order: morin> quercetin> myricetin.

Affinity ultrafiltration mass spectrometry (UF-LC/MS) is a high-throughput (HTS) technique for the fast screening and identification of the active components from the complex mixtures, such as the medicinal plant extracts and compounds libraries. Targeted to the key proteins in the process of disease occurrence and development, this technique could effectively fish out the active compounds from the unbound inactive components in the complex mixtures based on the biological affinities between the small molecule compounds and the targeted proteins in the body, and thus has the characteristics of high sensitivity and rapidity (Li et al., 2015; Qin et al., 2015; Chen et al., 2018b).

In this research area, our research group systematically screened out the potential anti-inflammatory components in the lotus plumule, a popular plant material with the same origin of medicine and food, by using the method of UF-LC/MS. For the first time, 12 flavonoids were quickly screened

**TABLE 2 |** Representative studies of ESI-MS technologies for the non-covalent interactions between small drug molecules and proteins.

| Subjects | Ligands | Type of MS | References |
|---|---|---|---|
| hGHbp | Six nonpolar ligands | ESI-Q-TOF MS | Tjernberg et al., 2004 |
| P-glycoprotein | Cyclosporin A and charged/zwitterionic lipids | IM-MS | Marcoux et al., 2013 |
| Chorismate mutase | Adamantyl-1-phosphonate | ESI-TOF MS | Wendt et al., 2003 |
| Ribonuclease A | Cytidine 2'-monophosphate, cytidine triphosphate | NanoESI-Q-TOF MS | Zhang et al., 2003 |
| Norovirus P domain | 41 HBGA oligosaccharides | FT ICR-NanoESI-MS | Han et al., 2013 |
| $\alpha_1$-Acid glycoprotein | Propranolol, pindolol, oxprenolol, alprenolol, carbamazepine, warfarin | CE/FA-ESI-MS | Vuignier et al., 2012 |
| BSA | Warfarin, salicylic acid, diclofenac | CE/FA-ESI-MS | |
| Carbonic anhydrase II (CA II) | Furosemide, acetazolamide, 4-CBSA, DNSA, sulfanilamide, and Sulpiride | MIK-MS | Obi et al., 2018 |
| bCA II | Eighty-five methanolic plant extracts | Online SEC-ESI-FTICR-MS | Vu et al., 2008 |
| HSA | Tanshinon IIA, warfarin | ESI-TOF MS | Liu et al., 2008 |
| β-Lactoglobulin | Morin, quercetin, myricetin | HPLC-ESI-Q-TOF MS | Xu et al., 2018 |
| COX-2 | Flavonoids in lotus plumule | UF-LC/ESI-MS | Chen et al., 2019 |
| COX-2, Top I | *R. davurica* extracts | UF-LC/ESI-MS | Chen et al., 2018b |

out as the potential cyclooxygenase 2 (COX-2, a key enzyme in the inflammatory reaction) inhibitors, in which structure-activity relationship indicated that the flavonoids *C*-glycosides showed comparable binding affinities to COX-2 compared to the flavonoids *O*-glycosides (Chen et al., 2019). In addition, topoisomerase I (Top I) and COX-2 were firstly employed as the dual-target bio-macromolecules to screen for the potential anti-tumor and anti-inflammatory components in the traditional medicinal plant *Rhamnus davurica* (*R. davurica*) with UF-LC/MS (**Figure 3**) (Chen et al., 2018b). As a result, 12 and 11 compounds in *R. davurica* extracts were screened out and identified as the potent Top I and COX-2 inhibitors, in which 10 compounds were indicated to be the common components responsible for the multi-component and multi-target way in *R. davurica*. In this study, UF-LC/MS technique displayed the characteristics of high specificity, rapidity, and simplicity, and the double-target screening of active components could reduce the false negative and false positive results of the selected components with high reliability.

Hydrogen-deuterium exchange mass spectrometry (HDX-MS) refers to the exchange of hydrogen atoms of the sample protein molecules with deuterated solvents ($D_2O$, $CD_3OD$, etc.), and the following detection of the mass shift of the enzymatic peptide by MS to determine the position of the protein sequence where the H/D atoms exchange occurs (Brock, 2012). Generally, hydrogen atoms that are prone to exchange between hydrogen and deuterium are located at the contact interface between protein and solution, and their exchange rate is faster than that of the hydrogen atoms that are located inside the protein structure or involved in hydrogen bond formation. Therefore, the structure and dynamic changes of proteins can be detected according to the different exchange rates of hydrogen and deuterium (Engen, 2009). When a small molecule inhibitor binds to a protein, it affects the hydrogen deuterium exchange rate of the hydrogen atom at the binding site, and thus the interaction region and intensity of the small molecule and the protein can be explored by the change of the hydroquinone exchange rate. As an effective tool for the study of protein structure and interaction kinetics,

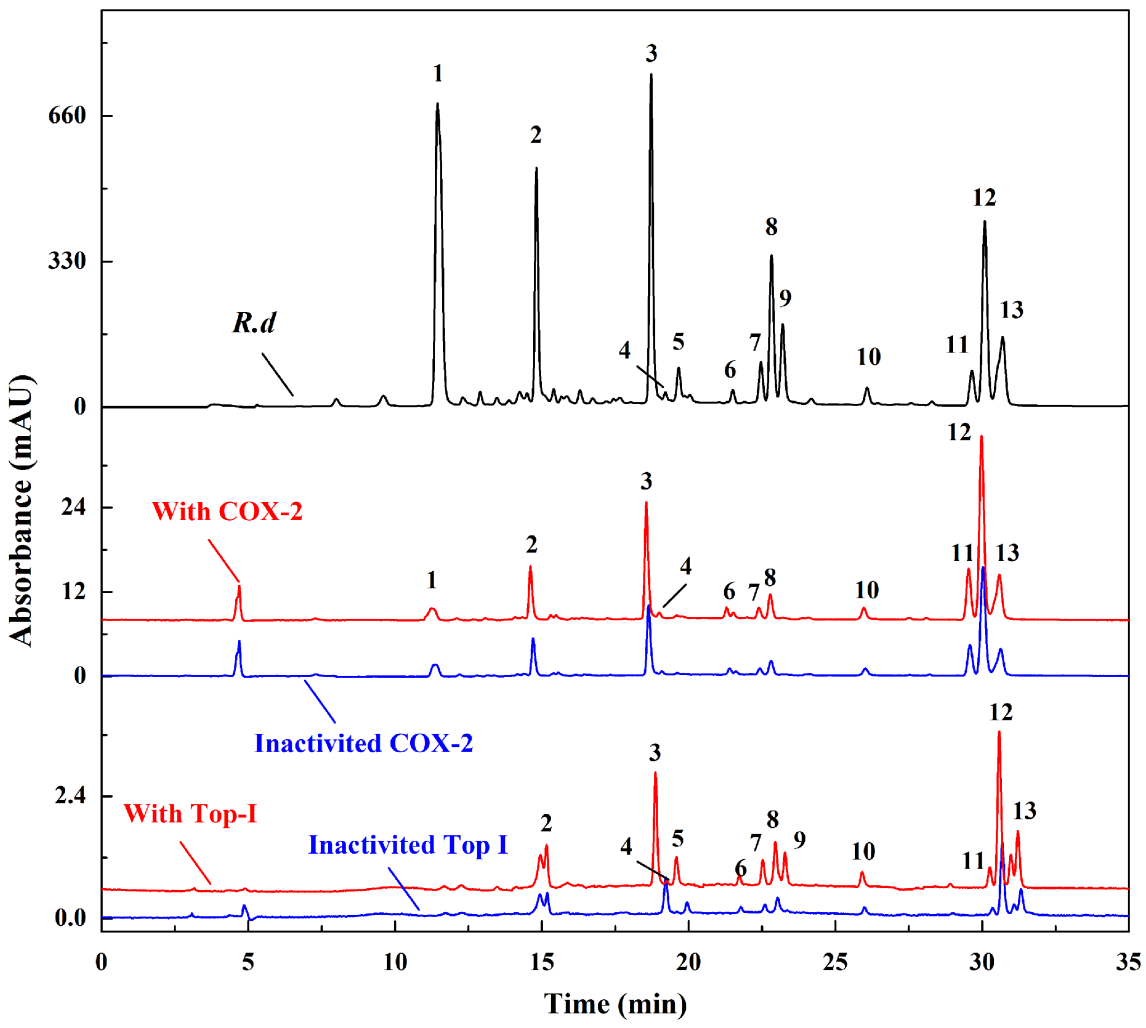


**FIGURE 3 |** The HPLC profiles of the *R. davurica* extracts without ultrafiltration and with activated or inactivated COX-2 and Top I, respectively.

HDX-MS has been successfully used to analyze the interactions and mechanisms of action between proteins and small molecules (such as ATP and its analogs, small nucleic acids, small drug molecules, etc.) (Badireddy et al., 2011; Lorenzen and Pawson, 2014).

Zhang H. M. et al. (2010) used HDX-MS to study the interactions and mechanisms between drugs, imatinib and sunitinib, and the drug-resistant kinase receptor tyrosine kinase (KIT), and found that protein kinase mutant D816H changed KIT into an active form and thus could not bind with inhibitors. However, mutant V560D has two low-energy structures, one is loosely structured and similar to D816H, and the other is relatively compact and similar to wild-type KIT. Affected by these two low-energy structures, the inhibition effect of inhibitors on mutant V560D is between the wild-type and mutant D816H. Furthermore, Zhang J. M. et al. (2010) also succeeded in inspecting the binding positions, interactions and mechanisms of the allosteric inhibitor GNF-2 and tyrosine kinase Bcr-Abl with HDX-MS.

Ion mobility mass spectrometry (IM-MS) is a trace chemical analysis technology developed in the late 1960s and early 1970s by Cohen and Karasek (Armenta et al., 2011). The principle is based on the difference of the migration rate of different gas phase ions in the electric field to separate and characterize the chemical components, especially suitable for the trace detection of some volatile and semi-volatile organic compounds. This technique not only breaks through the limitations of the ion mobility spectrum, but also greatly expands the performance and application range of the mass spectrometer. Moreover, it can obtain the ion mobility and mass-to-charge ratio parameters of the samples and improve the accuracy of traditional mass spectrometry data; and at the same time as the specificity, the collisional cross-section (CCS) of the ions can be calculated, and the structural states of the samples can be obtained, which thus shows a great advantage in the identification of the unknown compounds (Pirok et al., 2017; Vautz et al., 2018).

Recently, a large number of literatures have reported the usages of the IM-MS for the analysis of the protein structures, protein high-throughput analysis, proteomics, protein-protein, and protein-small molecules interactions (Hines et al., 2017; Eyers et al., 2018). For instance, Benigni et al. (2016) established an IM-MS method for the detection of biological macromolecules and their complexes such as proteins, protein-nucleic acid complexes, and protein-protein complexes under denaturing and non-denaturing conditions, and for the first time the 150 kD protein and protein complexes were analyzed through the collision cross sectional area. Besides, Young et al. (2016) conducted the accurate and rapid analysis of the inhibitory effects of the protein aggregates and small molecule inhibition by virtue of the powerful analytical ability of the ESI-IM-MS, and identified two new small molecule inhibitors of Aβ 40 by taking the Aβ 40 amyloid as an example.

In addition, electrospray Fourier transform ion cyclotron resonance mass spectrometry (ESI-FT-ICR MS) can also be used to study the interactions of complex systems with proteins (Poulsen et al., 2006). Vu et al. (2008) investigated the interactions between 85 plant methanol extracts and carbonic anhydrase by ESI-FT-ICR MS, and screened out a specific binding inhibitor 6-(1s-hydroxy-3-methylbutyl)−7-methoxy-2h-chromen-2-one (a hydrolyzed product of coumarin).

## Applications of ESI-MS in the Interactions of Small Drug Molecules With Polypeptides

Peptides are also the targets for drug molecules in the body (**Table 3**). For example, toxic plaques produced by the aggregation of amyloid-β-peptides are one of the causes of Alzheimer's disease (AD), and drugs that show binding affinities to the amyloid-β-peptide segment (29-40) could prevent their aggregation and thus exert therapeutic effects (Skribanek et al., 2001). Bazoti et al. (2006, 2008) studied the interaction between Aβ polypeptide and oleuroprin using ESI-MS, and determined the binding site of oleuropein by enzymatic hydrolysis. The polypeptide side chain of the bacterial cell wall peptidoglycan is the binding site of some antibacterial drugs, which can block the synthesis of bacterial cell wall by binding to the end of the peptide chain, thus achieving the pharmacological effect of inhibiting the growth of bacteria. Lim et al. (1995) compared the relative acting forces of the two antibiotics, vancomycin, and ristocetin, on side chain polypeptides by ESI-MS, and found out that the binding strength of the former was higher than that of the latter. Additionally, some peptides can also be used as the models for proteins to study the interactions between drugs and proteins. For instance, Sarni-Manchado and Cheynier (2002) studied the binding properties of the catechin and their galacyl derivatives to the salivary proline-rich peptides by using ESI-MS, and also investigated the interactions between these components and gelatin proteins.

**TABLE 3 |** Representative studies of ESI-MS technologies for the non-covalent interactions between small drug molecules and polypeptides.

| Subjects | Ligands | Type of MS | References |
|---|---|---|---|
| Insulin | Phosphorylated daidzein derivatives | ESI-MS | Chen et al., 2008 |
| Angiotensin peptide | Gold ion | FT-ICR-ESI-MS | Lee et al., 2012 |
| 18 α-amino acids | 5 Ginsenosides | ESI-QT MS | Qu et al., 2009 |
| Amyloid-β-peptide | Oleuropein | FT-ICR-ESI-MS | Bazoti et al., 2008 |
| Amyloid-β-peptides | Nicotine, melatonin, 5- hydroxy-N-acetyltryptamine, daunomycin, doxorubicin | ESI-MS | Skribanek et al., 2001 |
| Cell wall glycopeptides | Vancomycin, ristocetin | ESI-MS | Lim et al., 1995 |
| Salivary proline-rich peptides | Catechin and its derived compounds | ESI-MS | Sarni-Manchado and Cheynier, 2002 |

## Applications of ESI-MS in the Interactions of Metal Ions With Proteins

Metal ions play an important role in the catalytic activities and structural stability of metalloenzymes and participate in many important biological processes (Carlton and Schug, 2011). *cis*-Platin, the second-generation platinum anticancer drug carboplatin, and the third-generation platinum anticancer drug oxaliplatin have been widely used in the treatment of malignant tumors such as testicular cancer, ovarian cancer, brain cancer, and bladder cancer (Le-Rademacher et al., 2017; Mukherjee et al., 2017). Therefore, to study the interactions between the metal anti-tumor drugs and proteins, and the effects of such interactions on cell intake, transport, metabolism and bioavailability of the drugs, is conducive to the structural design and optimization, the improvement of the anticancer activities and decrement the side effects of metal anticancer drugs, and some representative studies and findings in this field have been shown in the **Table 4**.

The HSA is the most abundant protein in human plasma, which binds to and transports a variety of endogenous metabolites and drugs. Currently, most of the platinum and ruthenium metal anticancer drugs are administered intravenously, and these drugs are widely bound to the HSA after entering the human body (Timerbaev et al., 2006; Hartinger et al., 2008a). These combinations are closely related to the drug activities, drug resistances and side effects, and the study of their interactions is of great significance for the structural design and optimization of this type of anticancer drugs. Hu et al. (2009) investigated the interactions between the HAS and two organometallic anticancer compounds [($\eta^6$-cymene) RuCl (en)] $PF_6$, [($\eta^6$-biphenyl) RuCl (en)] $PF_6$ (en = ethylenediamine) using HPLC-ESI-Q-TOF MS. In order to improve the coverage rate of peptide identification, the protein and protein-ruthenium complexes were denatured, reduced disulfide bonds, and blocked cysteine residues were treated prior to enzymatic hydrolysis of the protein sample to allow HSA trypsin to digest peptides. On this basis, it was found that [($\eta^6$-cymene) Ru (en)]$^{2+}$ could form a coordination bond with the sulfhydryl group of the amino acid residue Cys34, and then induce the sulfhydryl oxidation to produce the sulfinic acid, which has an irreversible effect on the antioxidant function of HAS, while the [($\eta^6$-biphenyl) Ru (en)]$^{2+}$ could not bind to the Cys34 due to the steric hindrance of the organic ligand biphenyl. In addition, the [($\eta^6$-cymene) RuCl (en)] $PF_6$ and [($\eta^6$-biphenyl) RuCl (en)] $PF_6$ could covalently bind to the residues of the His128, His247, His510 histidine, Met298 methionine on the HSA surface in the form of coordination bonds, and the former exhibited higher binding affinities than the latter. Therefore, this finding was of great significance for further optimizing the structure of ruthenium as an organometallic anticancer compound and improving the transport efficiency and bioavailability of drugs in the body.

Ubiquitin is a protein containing 76 amino acid residues and is widely found in the cytoplasm and nucleus. This protein plays a key role in the ubiquitination signaling pathway of cells, which is closely related to the proliferation of tumors and is a potential target of metal anticancer drugs in cancer cells (Hoeller et al., 2006; Williams et al., 2010). Hartinger et al. (2008b) studied the interactions among the *cis*-platin, oxaliplatin, and *tran*-splatin with ubiquitin protein using ESI-FT-MS/MS. After ionizing the platinum drugs-ubiquitin complexes, the protein complexes were directly cleaved by the collision-induced dissociation (CID) method. Analysis of platinum-containing fragments showed that the *cis*-platin and oxaliplatin were both bound to the ubiquitin Met1 residues, while the anti-platinum was bound to the peptide fragment of 19pro-ser-asp-thr-ile-glu24, but the bound amino acid residues could not be further determined. In addition, it was found that the platinum-containing protein fragments could be obtained by the CID and IRMPD (infrared multiphoton dissociation) pyrolysis methods, while could not be detected by the ECD (electron capture dissociation) pyrolysis methods. The reason may be that the platinum-containing fragments produced were neutralized due to the capture of electrons by platinum ions and could not be detected by mass spectrometry.

ESI source has been widely used in the field of protein-ligand non-covalent interactions, and many unstable biological macromolecule complex structures have been characterized. However, it requires the use of electric field and heating in the process of sample ionization. Besides, the removal of the solvent in the solution may cause the difference of the conformation of certain non-covalent protein-ligand complexes between the liquid state and gas phase of the mass spectrometer, and thus it is not suitable for some highly complicated protein-ligand complexes with thermal properties. In order to better maintain

**TABLE 4 |** Representative studies of ESI-MS technologies for the non-covalent interactions between small drug molecules and metal ions.

| Subjects | Ligands | Type of MS | References |
|---|---|---|---|
| Ubiquitin | Platinum | NanoESI-Q-TOF MS | Hartinger et al., 2007 |
| Ubiquitin | *cis*-Platin, *trans*-platin, oxaliplatin | ESI-FT-MS/MS | Hartinger et al., 2008b |
| Ubiquitin | *cis*-Platin | ESI-IM-MS | Williams et al., 2010 |
| Chloroplast protein CP12 | 11 Metal ions | ESI-Qq-TOF MS | Delobel et al., 2005 |
| Three beta-peptides | $Zn^{2+}$ | HPLC-ESI-TOF MS | Wortmann et al., 2005 |
| HSA | Two organometallic ruthenium complexes | HPLC-ESI-Q-TOF MS | Hu et al., 2009 |
| Transferrin, albumin, Ig G | *cis*-Platin | ESI-Q-TOF MS | Esteban-Fernández et al., 2008 |
| Insulin | *cis*-Platin | ESI-IT/TOF MS | Li et al., 2016 |
| Myoglobin | *cis*-Platin, *trans*-platin | ESI-Q-IT MS | Zhao and King, 2010 |

the natural conformation of proteins in solution, researchers have made some improvements to the ESI source, including electrosonic spray ionization (Wiseman et al., 2004) and cold spray mass spectrometry (CSI-MS) (Guo et al., 2009). By increasing the polarizabilities of the molecules by cooling the liquid spray and the solvent removal process, CSI-MS could promote the ionization of molecules and has been successfully applied to the study of supra-molecular systems that are heat unstable and cannot be analyzed by ESI-MS. Hence, the low-flow, ultra-high sensitivity nano-optimized ESI-MS, on the one hand, can achieve maximum sensitivity (up to f mol) with minimum sample consumption; on the other hand, the droplet volume produced by the spray is smaller, which speeds up the process of solvent removal, reduces the temperature and heat required for solvent removal, and facilitates the preservation of weak non-covalent interactions in the system (Yamaguchi, 2003).

## MALDI-MS and Its Applications in Ligand-Target Interactions

### Characteristics of the MALDI-MS

MALDI technology could make the non-volatile and thermal-unstable biological macromolecular compounds to form ions, which are detected at very low concentrations and used to characterize the spatial distributions and contents of the polypeptides and proteins in tissue sections (Mengistu et al., 2005). At this point, this technique could mix the small solid substrates with the analytes to be measured in a ratio of more than 5000:1. When irradiated with a laser, the matrix absorbs the laser energy and transmits it to the molecule to be tested, and which will be vaporized to form an ion. The matrix absorbs most of the laser energy and the fragment ions are reduced (**Figure 4**). Therefore, the main reason for the MALDI's breakthrough in macromolecular ionization is the use of substrates (Talian et al., 2007).

### Applications of MALDI-MS in the Interactions of Small Drug Molecules With Proteins

Compared with ESI-MS, MALDI-MS is used much less in the studies of the interactions between the small drug molecules and the biological macromolecules, mainly because of the strong acidic matrix or organic co-solvents commonly used in sample preparation during MALDI-MS analysis, which is easy to cause the dissociation of non-covalent complexes. At the same time, the ionization process easily produces laser-induced polymers and matrix adducts, which often interferes with the detection of complexes (Bolbach, 2005). Although it is not easy for the MALDI-MS to directly detect complexes of the drugs and biological macromolecules, this analysis has a certain tolerance

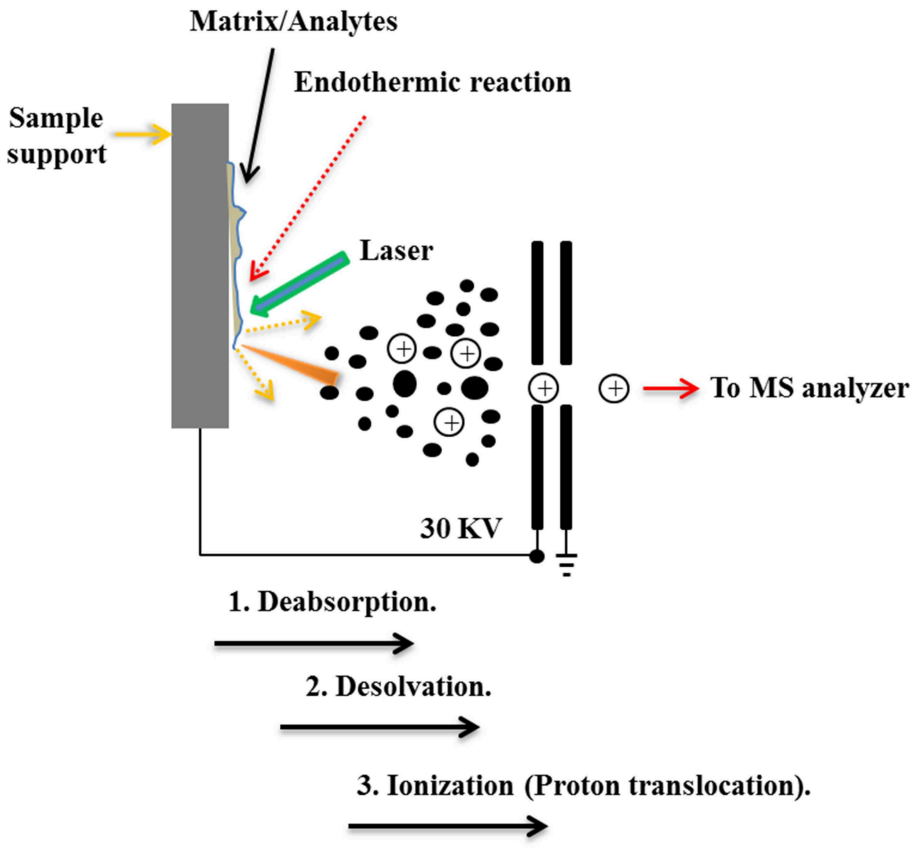


**FIGURE 4 |** The schematic workflow of the typical MALDI ionization processes.

to salt solutions and buffers, which in a sense can better simulate the physiological environment. In addition, the MALDI-MS is fast, sensitive, simple and easy to automate, and thus has been prompted to study the interactions between the small drug molecules and the biological macromolecules with these advantages. Some representative studies and findings in this field have been shown in the following **Table 5**.

Wang et al. (2009) introduced the intensity-attenuated MALDI-MS into the study of the interactions between the small molecules in the traditional Chinese medicine and proteins. To this end, the interactions between the alkaloids, calmodulin, and the melittin were studied by this method, and the relative binding strength of different drugs to targeted proteins was compared through titration and competitive experiments. Chen and Hagerman (2004) employed the MALDI-MS to directly detect the complexes formed by the bovine serum albumin (BSA) and tannin β-1, 2, 3, 4, 6-5-*O*-galacyl-D-glucose (PGG), and found that four PGG molecules could be bound to a single BSA molecule. Moreover, Yanes et al. (2006, 2007) studied the interactions between the ligand molecules and the biological macromolecules by the intensity-attenuated MALDI-MS. The basic principle of this method was to compare the changes of ionic strength of various ligand components (including negative control) in the samples before and after the addition of biological targeted molecules. Compared with the negative control, the ligand molecules were less selective after the addition of biological targeted molecules.

Mass spectrometry imaging (MSI) is a new type of molecular imaging technique that has received great attention in recent years. By scanning samples with ionized probes with different principles and structures, the *in-situ* desorption/ionization of the samples to be measured will be transmitted to the mass spectrum for detection, so as to obtain the mass spectrogram set associated with the spatial position of the samples (McDonnell et al., 2015). And, the tissue distribution image of each m/z is obtained by processing the mass spectrogram set obtained by mass spectrometry imaging software. Besides, the MALDI-MS forms the co-crystallization by mixing the tested components with the substrate capable of absorbing ultraviolet or infrared laser, and the substrate molecules absorb the laser energy and transfers part of it to the substance tested components, so as to achieve soft ionization of the tested components. By combining imaging processing software with mass spectrometry ion scanning technique, the MSI method could obtain the spatial distribution characteristics and content changes of the proteins and small molecules *in vivo*. It has the advantages of high chemical composition coverage and high throughput, and can realize imaging analysis of hundreds of compounds at a time (Spengler, 2015; Hansen and Lee, 2018). The MALDI is most widely used in the analysis of proteins and other macromolecules, but with the continuous development of MALDI technology, especially the rise of MALDI-MSI, it has been increasingly applied in the *in situ* analysis of lipids, small molecule metabolites, and small drug molecules (Bodzon-Kulakowska and Suder, 2016).

With the analysis of MALDI-MSI, McClure et al. (2013) found that after the injection of the antihistamine promethazine (25 mg/kg) in the tail vein, a large amount of Aβ40 peptide signals appeared in the brain tissue of transgenic mice with AD, and the ion signal strength of promethazine was three times that of wild mice, suggesting that Aβ40 peptide is an important biomarker for AD. In another study, Aichler et al. (2013) used MALDI-MSI to observe the protein expression differences in esophageal adenocarcinoma biopsy tissues before and after chemotherapy. The candidate proteins with obvious differences were identified by MS/MS for structure, and the results revealed that the chemo-sensitivity of tumor cells to *cis*-platin was significantly

**TABLE 5 |** Representative studies of MALDI-MS technologies for the non-covalent interactions between small drug molecules and biological macromolecules.

| Subjects | Ligands | Type of MS | References |
|---|---|---|---|
| **DNA** | | | |
| Single-stranded DNA | Au nanoparticles | MALDI-TOF MS | Han et al., 2018 |
| **PROTEINS** | | | |
| Avidin | Polymyxin B, angiotensin II and their biotinylated molecules | MALDI-TOF MS | Jorgensen et al., 2009 |
| BSA | PGG | MALDI-TOF MS | Chen and Hagerman, 2004 |
| Carboxypeptidase A | Three protease inhibitors (PCI, TCI, and LCI) | CL-MALDI-TOF MS | Yanes et al., 2006 |
| **POLYPEPTIDES** | | | |
| Four tripeptides | 2,5-dihyroxybenzoic acid, 3,5-dihyroxybenzoic acid, α-cyano-4-hydroxy-cinnamic acid | MALDI-MS | Ueno-Noto and Marynick, 2009 |
| Angiotensin peptide | Gold ion | MALDI-TOF MS | Lee et al., 2012 |
| Calmodulin | Melittin, substance P | IF-MALDI-MS | Wang et al., 2009 |
| Aβ40 peptide | Promethazine | MALDI-MSI | McClure et al., 2013 |
| **PROTEINS** | | | |
| HAS, Ig G, transferrin, BSA | Au nanoparticles | MALDI-TOF MS | Han et al., 2018 |
| Insulin | *cis*-Platin | MALIDI-TOF/TOF MS | Li et al., 2016 |
| Ubiquitin | Platinum | MALDI-MS | Hartinger et al., 2007 |
| Cytochrome c oxidase | *cis*-Platin | MALDI-MSI | Aichler et al., 2013 |

improved in the case of inhibiting the expression of cytochrome c oxidase. At present, the highest spatial resolution of MALDI-MSI could reach 1.4 μm (Kompauer et al., 2017).

Cross-linked mass spectrometry (CL-MS) is a rapidly evolving mass spectrometry technique for studying protein structures and interactions in recent years (Sinz, 2018). The cross-linking reaction involves covalently linking functional groups in one protein or between two proteins through the chemical crosslinking reagent. After the enzymatic hydrolysis, the peptides undergoing cross-linking reaction are enriched and isolated to determine the two adjacent cross-linking sites in space (Leitner, 2016). Generally, the cross-linking reagent is linked to two functional groups by a spacer arm of a specific length, which can be covalently reacted with the lysine, cysteine or other amino acids of the proteins depending on their properties (Lossl et al., 2016). In addition, the cross-linked peptides after enzymatic hydrolysis could be analyzed by the enzymatic hydrolysis of cross-linked proteins.

Based on the crystal structures of 1252 kinase-ligands, van Linden et al. (2014) obtained 85 amino acids with conserved sequences related to the ligand binding sites, and found that the amino acids such as glycine and lysine were distributed at multiple sites in the conserved region. The analysis of the lysine short-range microenvironment is conducive to the study of the interactions between the protein kinases, especially in the conserved regions, with small molecules. Moreover, the lysine in proteins is generally positively charged under the physiological conditions, and the interactions with adjacent amino acid residues, such as electrostatic interactions and hydrogen bonds, are one of the key factors to regulate protein structures and protein-protein interactions. Small molecule inhibitors often interact with the lysine residues of kinases to better target protein kinases and inhibit their activities, for example, inhibitors MK2206, PIA23, and K268 (Wu et al., 2010), K14 (Milburn et al., 2003) sites of AKT1 kinase, inhibitor imatinib and K271 site of ABL1 kinase (Nagar et al., 2002), inhibitor MP7 and K111 site of PDK1 kinase (Erlanson et al., 2011), and so on. Therefore, the analysis of lysine short-range microenvironment interactions plays an important role in studying the structural and functional regulation mechanisms of protein and protein complexes, and also has shown great potential in studying the interactions between the protein kinases and the small molecule inhibitors.

The main reason for MALDI's breakthrough in macromolecular ionization is the use of matrixes. Black et al. (2006) successfully analyzed polymers and peptides using a pencil lead as the matrix. Langley et al. (2007) also successfully applied this MALDI technique to other compounds. However, matrix effects in MALDI can lead to spatial matching errors (Chughtai and Heeren, 2010), and the sample needs to be introduced into a closed space with high vacuum during MS analysis, which limits the application of MALDI in the analysis of large samples such as whole animals. In 2004, Takáts et al. (2004) pioneered the breakthrough of DESI technique under the normal pressure conditions, which made the development of MS technique a promising step.

## Other Soft Ionization Technologies

### Desorption Electrospray Ionization (DESI) and Its Applications in Ligand-Target Interactions

DESI is a novel mass spectrometry ionization technique that combines the characteristics of ESI and desorption ionization (DI) techniques. Its ionization is achieved by spraying charged droplets generated by ESI onto the samples (**Figure 5**). Generally speaking, the sample is dissolved with appropriate solvent and then dropped onto the surface of insulating materials such as polytetrafluoroethylene (PTFE), polymethyl methacrylate (PMMA), etc., then the solvent is removed, and the sample is deposited on the surface of the carrier. The spray solvent used is first applied with a certain voltage and ejected from the inner casing of the atomizer. The high-speed $N_2$ gas (linear velocity up to 350 m/s) ejected from the outer casing of the atomizer quickly atomizes and accelerates the solvent, causing the charged droplets to hit the sample surface. The sample is sputtered into the gas phase after being hit by high-speed droplets. At the same time, due to the scavenging and drying of $N_2$ gas, the charged droplets containing sample are dissolvated and migrated along the ion transport tube at atmospheric pressure to the capillary at the front end of the mass spectrum, which is then detected by the detector of the mass spectrometer (Takáts et al., 2004; Zhu et al., 2018).

The sample ionization of DESI is carried out under normal pressure and open conditions. Since the sample does not need to be dissolved, the pretreatment is relatively simple, and the accuracy and *in situ* property of the sample are also ensured (Wiseman et al., 2008). At the same time, the DESI mass spectrum is more simplified and has unique advantages in the analysis of small molecules. Thereby, it has been widely used to study the interactions between small drug molecules and biological macromolecules (**Table 6**). In this field, Liu et al. (2013) employed the reactive liquid sample DESI to detect the non-covalent complexes of "ribonuclease A-cytidine nucleotide ligands" and "lysozyme-*N*-acetylglucosamine ligands," and the results indicated that this "reactive" DESI technique could provide integrated information on the binding stiochiometry, selectivity, and kinetics of those two protein-ligand complexes. In another effort, the protein-carbohydrate interactions between lysozyme and L2, L3, and between a single chain variable fragment of Se155-4 and L4, L5, were studied by the liquid sample DESI-MS. It was found that the association constants of these protein-ligand complexes were in good agreement with values detected with the direct ESI-MS and isothermal titration calorimetry assays (Yao et al., 2015).

### Native MS and Its Applications in Ligand-Target Interactions

Traditional protein analysis usually require denaturation of proteins by enzymatic hydrolysis, heating or adding high concentration of deformation agents (such as urea, guanidine hydrochloride, etc.), which will lead to the destruction of three-dimensional structure of proteins. In addition, for some commonly used separation methods, such as reversed-phase HPLC, the pH conditions of the mobile phase and the high concentration of organic compounds that are usually required also cause protein denaturation. When studying the non-covalent

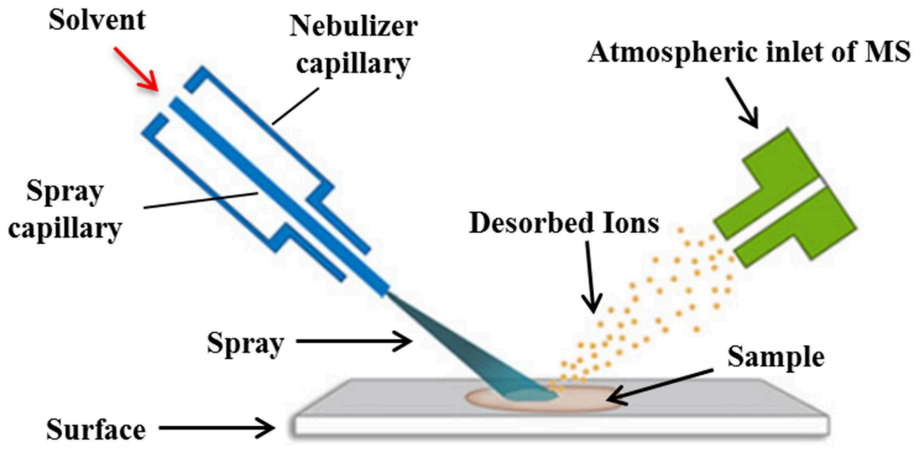


**FIGURE 5 |** The schematic workflow of the typical DESI ionization processes.

**TABLE 6 |** Representative studies of DESI-MS and native MS technologies for the non-covalent interactions between small drug molecules and biological macromolecules.

| Subjects | Ligands | Type of MS | References |
|---|---|---|---|
| Lysozyme | L2, L3 | DESI-MS | Yao et al., 2015 |
| Single chain variable fragment of Se155-4 | L4, L5 | DESI-MS | |
| Ribonuclease A | Cytidine nucleotide ligands | DESI-Q-TOF MS | Liu et al., 2013 |
| Lysozyme | Acetyl chitose ligands | DESI-Q-TOF MS | |
| Lysozyme, trypsin, bovine β-lactoglobulin A, carbonic anhydrase II, concanavalin A, aptamer | Tri-*N*-acetylchitotriose, pefabloc, chlorothiazide, lauric acid, quinine | Native NanoESI-MS | Gavriilidou et al., 2015 |
| Brentuximab vedotin | Brentuximab | Native MS, native IM-MS | Debaene et al., 2014 |
| Adenosine, L-argininamide, cocaine binding aptamers | Sixteen ligands | Native ESI-MS | Gülbakan et al., 2018 |
| Histidine-rich glycoprotein peptide 330 | $Zn^{2+}$ | Native ESI-MS | Martin et al., 2018 |
| Ubiquitin, lysozyme, myoglobin, RNase A | Cytidine 5′- diphosphate disodium salt, N,N',N"-triacetylchitotriose | NDX-MS | Zheng et al., 2018 |
| Chicken egg white lysozyme, bovine pancreas trypsin, bovine β-lactoglobulin A, bCA II | Ammonium acetate, trimethylammonium acetate, triethylammonium acetate | Native ESI-MS | Zhuang et al., 2017 |

protein-ligand complexes, in order to prevent the non-covalent bonds from being destroyed by the above conditions, the native-denatured experimental conditions must be employed, thus producing the native MS technique.

The native MS combines certain soft ionization technique with MS, with the purpose to introduce the protein-ligand complexes into the gas phase environment of the mass spectrometer without destroying the non-covalent interactions, and to be recorded and analyzed completely. So there is no need to use complex protein engineering methods to analyze the protein-target system expressed at the physiological level, thereby completing the interactions of the non-covalent protein-ligand complexes and their structural and dynamic change process. In addition, for a more complex protein sample, the protein charge number will be reduced due to the decreased protons in the system when analyzed under the native-denatured conditions, thus the number of mass spectral peaks is reduced accordingly, and thereby causing the decreases of the overlap between different charge state interference, making it easier to obtain the molecular mass information for each component in the complex protein sample (Debaene et al., 2014). Some representative studies and findings in this field have been shown in the **Table 6**.

In general, ESI-MS is incompatible with non-volatile solution additives. Gavriilidou et al. (2015) studied the effects of ionic strength of ammonium acetate (AmAc) on the dissociation constants of six different non-covalent complexes using the native nano-MS, with a series of dilutions from 10 to 500 mM aqueous solutions, respectively. The results showed that the ionic strength exerted significant effect on the binding affinity of the non-covalent complexes. As the concentration of AmAc increased, the dissociation constant ($K_d$) was affected by more than 50%. This work highlights the regulation of ions on non-covalent interactions and the importance of the selection of AmAc concentrations to quantify the receptor-target binding strengths. Besides, considering the inability of the native MS

to discriminate the specific ligand-protein interactions from the non-specific interactions, Zheng et al. (2018) reported a native-denatured exchange MS (NDX-MS) method to recognize the changes from the native detection of non-covalent ligand-protein complexes to denatured analysis by employing three ligand-protein complexes of NAG3-lysozyme, CDP-ribonuclease and myoglobin. This NDX-MS method, remarkably with the distinguishing $K_d$ dynamic profiles, could particularly recognize the specific ligand-protein interactions, and which could greatly aid to discovery specific protein targets for ligands of interest.

## CONCLUSION AND OUTLOOKS

In recent years, a number of reviews have been published on the applications of the ESI-MS and MALDI-MS in the studies of the non-covalent complexes. It can be seen that the ESI-MS dominates the studies of non-covalent complexes. Although the high sensitivity and relative molecular mass characterization range of the MALDI-MS are generally superior to the ESI-MS for the determination of biological macromolecules, its application in the detection of non-covalent complexes is limited by sample preparation conditions and high action energy. For example, the usage of the strong acidic matrix or organic co-solvents in the ionization process is generally detrimental to the formation of the non-covalent complexes. Moreover, the presence of laser-induced polymerization and matrix adduct formation often interferes with the detection of complexes, which makes MALDI-MS relatively less useful for the studies of the non-covalent complexes.

The non-covalent interactions can be classified as specificity and non-specificity, and the specific non-covalent complexes with biological functions are the focus of attention. The so-called complex peaks on the mass spectrum do not necessarily represent the actual complexes, and sometimes false positives occur. In order for the mass spectrometry data to truly reflect the non-covalent interactions of the system under test, it is necessary to use some experimental methods, such as the usage of the classical biochemical techniques of the enzymatic hydrolysis, chemical modification, etc., to change the sequences or properties of the biopolymers to weaken or destroy the non-covalent bonds, and then to compare the changes in the corresponding signals on the mass spectrum before and after the reaction to infer and verify the structures of the complexes. Secondly, different sample preparation techniques or different buffer systems need to be selected to optimize the test conditions in the experiment. It is also necessary to control the appropriate instrument conditions, especially the parameters of the ion source part, so as to reduce the dissociation of the non-covalent bonds and obtain the structural information of specific non-covalent complexes.

Proteins/enzymes play an important role in the life process, which are closely related to many malignant diseases such as tumors. Therefore, it is urgent to design and develop new small drug molecules targeting those proteins/enzymes. The aforementioned soft ionization MS-based methods could comprehensively, systematically and accurately study the protein/enzyme-small molecule interactions, and provide information such as the action sites (or regions) and the action intensity, so as to provide better help for drug design and disease treatment. With the development of soft ionization technologies, MS-based methods will continue to develop and improve, which will definitely promote the analysis and research of protein/enzyme-ligand interactions, so as to better serve for human health.

## AUTHOR CONTRIBUTIONS

MG, JW, and BS conceived, designed, and supervised the manuscript. GC, MF, YL, ML, and NL collected the literatures, analyzed the data, and wrote the manuscript. All authors reviewed and approved the final manuscript.

## FUNDING

This work was jointly supported by the National Natural Science Foundation of China (Grant No. 81673580 to MG, and Grant No. 81903791 to GC), the Major Project for Special Technology Innovation of Hubei Province (Grant No. 2017AHB054 to MG), the Macao Science and Technology Development Fund (0090/2018/A3), and the Natural Science Foundation of Hubei Province (Grant No. 2019CFB254 to GC). These funders played no roles in the study design, data collection and analysis, and decision to publish.

## REFERENCES

Aichler, M., Elsner, M., Ludyga, N., Feuchtinger, A., Zangen, V., Maier, S. K., et al. (2013). Clinical response to chemotherapy in oesophageal adenocarcinoma patients is linked to defects in mitochondria. *J. Pathol.* 230, 410–419. doi: 10.1002/path.4199

Armenta, S., Alcala, M., and Blanco, M. (2011). A review of recent, unconventional applications of ion mobility spectrometry (IMS). *Anal. Chim. Acta* 703, 114–123. doi: 10.1016/j.aca.2011.07.021

Badireddy, S., Gao, Y. F., Ritchie, M., Akamine, P., Wu, J., Kim, C. W., et al. (2011). Cyclic AMP analog blocks kinase activation by stabilizing inactive conformation: conformational selection highlights a new concept in allosteric inhibitor design. *Mol. Cell. Proteomics* 10, 1–14. doi: 10.1074/mcp.M110.004390

Bai, L. P., Cai, Z. W., Zhao, Z. Z., Nakatani, K., and Jiang, Z. H. (2008). Site-specific binding of chelerythrine and sanguinarine to single pyrimidine bulges in hairpin DNA. *Anal. Bioanal. Chem.* 392, 709–716. doi: 10.1007/s00216-008-2302-7

Bazoti, F. N., Bergquist, J., Markides, K., and Tsarbopoulos, A. (2008). Localization of the noncovalent binding site between amyloid-β-peptide and oleuropein using electrospray ionization FT-ICR mass spectrometry. *J. Am. Soc. Mass Spectrom.* 19, 1078–1085. doi: 10.1016/j.jasms.2008.03.011

Bazoti, F. N., Bergquist, J., Markides, K. E., and Tsarbopoulos, A. (2006). Noncovalent interaction between amyloid-β-peptide (1–40) and oleuropein studied by electrospray ionization mass spectrometry. *J. Am. Soc. Mass Spectrom.* 17, 568–575. doi: 10.1016/j.jasms.2005.11.016

Benigni, P., Marin, R., Molano-Arevalo, J. C., Garabedian, A., Wolff, J. J., Ridgeway, M. E., et al. (2016). Towards the analysis of high molecular weight

proteins and protein complexes using TIMS-MS. *Int. J. Ion. Mobil. Spectrom.* 19, 95–104. doi: 10.1007/s12127-016-0201-8

Black, C., Poile, C., Langley, G. J., and Herniman, J. (2006). The use of pencil lead as a matrix and calibrant for matrix-assisted laser desorption/ionisation. *Rapid Commun. Mass Spectrom.* 20, 1053–1060. doi: 10.1002/rcm.2408

Bodzon-Kulakowska, A., and Suder, P. (2016). Imaging mass spectrometry: instrumentation, applications, and combination with other visualization techniques. *Mass Spectrom. Rev.* 35, 147–169. doi: 10.1002/mas.21468

Bolbach, G. (2005). Matrix-assisted laser desorptionionization analysis of non-covalent complexes fundamentals and application. *Curr. Pharm. Des.* 11, 2535–2557. doi: 10.2174/1381612054546923

Brock, A. (2012). Fragmentation hydrogen exchange mass spectrometry: a review of methodology and applications. *Protein Expr. Purif.* 84, 19–37. doi: 10.1016/j.pep.2012.04.009

Brodbelt, J. S. (2010). Evaluation of DNA/Ligand interactions by electrospray ionization mass spectrometry. *Annu. Rev. Anal. Chem.* 3, 67–87. doi: 10.1146/annurev.anchem.111808.073627

Carlton, J. D. D., and Schug, K. A. (2011). A review on the interrogation of peptide–metal interactions using electrospray ionization-mass spectrometry. *Analy. Chim. Acta* 686, 19–39. doi: 10.1016/j.aca.2010.11.050

Carrasco, C., Rosu, F., Gabelica, V., Houssier, C., Pauw, E. D., Garbay-Jaureguiberry, C., et al. (2002). Tight binding of the antitumor drug ditercalinium to quadruplex DNA. *Chem. Biochem.* 3, 1235–1241. doi: 10.1002/1439-7633(20021202)3:12<1235::AID-CBIC1235>3.0.CO;2-I

Chan, S. H. D., Seetoh, W. G., McConnell, B. N., Matak-Vinković, D., Thomas, S. E., Mendes, V., et al. (2017). Structural insights into the EthR-DNA interaction using native mass spectrometry. *Chem. Comm.* 53, 3527–3530. doi: 10.1039/C7CC00804J

Chen, G. L., Fan, M. X., Wu, J. L., Li, N., and Guo, M. Q. (2019). Antioxidant and anti-inflammatory properties of flavonoids from lotus plumule. *Food Chem.* 277, 706–712. doi: 10.1016/j.foodchem.2018.11.040

Chen, G. L., Huang, B. X., and Guo, M. Q. (2018a). Current advances in screening for bioactive components from medicinal plants by affinity ultrafiltration mass spectrometry. *Phytochem. Anal.* 29, 375–386. doi: 10.1002/pca.2769

Chen, G. L., Wu, J. L., Li, N., and Guo, M. Q. (2018b). Screening for anti-proliferative and anti-inflammatory components from *Rhamnus davurica* Pall. using bio-affinity ultrafiltration with multiple drug targets. *Anal. Bioanal. Chem.* 6, 1–9. doi: 10.1007/s00216-018-0953-6

Chen, X., Shi, X., Qu, L., Yuan, J., and Zhao, Y. (2008). ESI investigation of non-covalent complexes between phosphorylated daidzein derivatives and insulin. *Phosphorus Sulfur* 183, 527–537. doi: 10.1080/10426500701761763

Chen, X. L., Qu, L. B., Zhang, T., Liu, H. X., Yu, F., Yu, Y. Z., et al. (2004). The nature of phosphorylated chrysin-protein interactions involved in noncovalent complex formation by electrospray ionization mass spectroscopy. *Anal. Chem.* 76, 211–217. doi: 10.1021/ac035027q

Chen, Y. M., and Hagerman, A. E. (2004). Characterization of soluble non-covalent complexes between bovine serum albumin and β-1, 2, 3, 4, 6-penta-*O*galloyl-D-glucopyranose by MALDI-TOF MS. *J. Agric. Food Chem.* 52, 4008–4011. doi: 10.1021/jf035536t

Chughtai, K., and Heeren, R. M. (2010). Mass spectrometric imaging for biomedical tissue analysis. *Chem. Rev.* 110, 3237–3277. doi: 10.1021/cr100012c

Debaene, F., Boeuf, A., Wagner-Rousset, E., Colas, O., Ayoub, D., Corvaïa, N., et al. (2014). Innovative native MS methodologies for antibody drug conjugate characterization: High resolution native MS and IM-MS for average DAR and DAR distribution assessment. *Anal. Chem.* 86, 10674–10683. doi: 10.1021/ac502593n

Delobel, A., Graciet, E., Andreescu, S., Gontero, B., Halgand, F., and Laprévote, O. (2005). Mass spectrometric analysis of the interactions between CP12, a chloroplast protein, and metal ions: a possible regulatory role within a PRK/GAPDH/CP12 complex. *Rapid Commun. Mass Spectrom.* 19, 3379–3388. doi: 10.1002/rcm.2192

Dettmer, K., Aronov, P. A., and Hammock, B. D. (2007). Mass spectrometry-based metabolomics. *Mass Spectrom. Rev.* 26, 51–78. doi: 10.1002/mas.20108

Dong, X. C., Xu, Y., Afonso, C., Jiang, W. Q., Laronze, J. Y., Wen, R., et al. (2007). Non-covalent complexes between bis-beta-carbolines and double-stranded DNA: a study by electrospray ionization FT-ICR mass spectrometry (I). *Bioorg. Med. Chem. Lett.* 17, 2549–2553. doi: 10.1016/j.bmcl.2007.02.010

Engen, J. R. (2009). Analysis of protein conformation and dynamics by hydrogen/deuterium exchange MS. *Anal. Chem.* 81, 7870–7875. doi: 10.1021/ac901154s

Erlanson, D. A., Arndt, J. W., Cancilla, M. T., Cao, K., Elling, R. A., English, N., et al. (2011). Discovery of a potent and highly selective PDK1 inhibitor via fragment-based drug discovery. *Bioorg. Med. Chem. Lett.* 21, 3078–3083. doi: 10.1016/j.bmcl.2011.03.032

Esteban-Fernández, D., Montes-Bayón, M., Blanco, G. E., and Gómez Gómez, M. M. (2008). Atomic (HPLC-ICP-MS) and molecular mass spectrometry (ESI-Q-TOF) to study cis-platin interactions with serum proteins. *J. Anal. At. Spectrom.* 23, 378–384. doi: 10.1039/B711922D

Evans, W. E., and Relling, M. V. (1999). Pharmacogenomics translating functional genomics into rational therapeutics. *Science* 286, 487–91. doi: 10.1126/science.286.5439.487

Eyers, C. E., Vonderach, M., Ferries, S., Jeacock, K., and Eyers, P. A. (2018). Understanding protein-drug interactions using ion mobility-mass spectrometry. *Curr. Opin. Chem. Biol.* 42, 167–176. doi: 10.1016/j.cbpa.2017.12.013

Ferraro, N. A., and Cascio, M. (2018). Crosslinking-mass spectrometry (CX-MS) studies of cholesterol interactions with human α1 glycine receptor. *Anal. Chem.* 80, 2508–2516. doi: 10.1021/acs.analchem.7b03639

Ganem, B., Li, Y. T., and Henion, J. D. (1991). Detection of noncovalent receptor-ligand complexes by mass spectrometry. *J. Am. Chem. Soc.* 113, 6295–6296. doi: 10.1021/ja00016a069

Gao, Z. T., Li, H. L., Zhang, H. L., Liu, X. F., Kang, L., Luo, X. M., et al. (2008). PDTD: a web-accessible protein database for drug target identification. *BMC Bioinformatics* 9:104. doi: 10.1186/1471-2105-9-104

Gavriilidou, A. F. M., Gülbakan, B., and Zenobi, R. (2015). Influence of ammonium acetate concentration on receptor-ligand binding affinities measured by native Nano ESI-MS: A systematic study. *Anal. Chem.* 87, 10378–10384. doi: 10.1021/acs.analchem.5b02478

Goth, M., and Pagel, K. (2017). Ion mobility-mass spectrometry as a tool to investigate protein-ligand interactions. *Anal. Bioanal. Chem.* 409, 4305–4310. doi: 10.1007/s00216-017-0384-9

Gülbakan, B., Barylyuk, K., Schneider, P., Pillong, M., Schneider, G., and Zenobi, R. (2018). Native electrospray ionization mass spectrometry reveals multiple facets of aptamer-ligand interactions: from mechanism to binding constants. *J. Am. Chem. Soc.* 140, 7486–7497. doi: 10.1021/jacs.7b13044

Guo, H. B., Peng, H., and Emili, A. (2017). Mass spectrometry methods to study protein-metabolite interactions. *Expert Opin. Drug Discov.* 12, 1271–1280. doi: 10.1080/17460441.2017.1378178

Guo, N., Zhang, R. P., Song, F., He, J. M., Xia, B., and Abliz, Z. (2009). Characterization of acid-induced protein conformational changes and noncovalent complexes in solution by using coldspray ionization mass spectrometry. *J. Am. Soc. Mass Spectrom.* 20, 845–851. doi: 10.1016/j.jasms.2008.12.024

Han, J., Li, Y. F., Zhan, L. P., Xue, J. J., Sun, J., Xiong, C. Q., et al. (2018). A novel mass spectrometry method based on competitive noncovalent interaction for the detection of biomarkers. *Chem. Comm.* 76, 1–4. doi: 10.1039/C8CC06100A

Han, L., Kitov, P. I., Kitova, E. N., Tan, M., Wang, L., Xia, M., et al. (2013). Affinities of recombinant norovirus P dimers for human blood group antigens. *Glycobiology* 23, 276–285. doi: 10.1093/glycob/cws141

Hansen, R. L., and Lee, Y. J. (2018). High-spatial resolution mass spectrometry imaging: toward single cell metabolomics in plant tissues. *Chem. Rec.* 18, 65–77. doi: 10.1002/tcr.201700027

Hartinger, C. G., Ang, W. H., Casini, A., Messori, L.,Keppler, B. K., and Dyson, P. J. (2007). Mass spectrometric analysis of ubiquitin–platinum interactions of leading anticancer drugs: MALDI versus ESI. *J. Anal. At. Spectrom.* 22, 960–967. doi: 10.1039/B703350H

Hartinger, C. G., Jakupec, M. A., Zorbas-Seifried, S., Groessl, M., Egger, A., Berger, W., et al. (2008a). KP1019, a new redox-active anticancer agent-preclinical development and results of a clinical phase I study in tumor patients. *Chem. Biodivers.* 5, 2140–2155. doi: 10.1002/cbdv.200890195

Hartinger, C. G., Tsybin, Y. O., Fuchser, J., and Dyson, P. J. (2008b). Characterization of platinum anticancer drug protein-binding sites using a top-down mass spectrometric approach. *Inorg. Chem.* 47, 17–19. doi: 10.1021/ic702236m

Hines, K. M., Ross, D. H., Davidson, K. L., Bush, M. F., and Xu, L. B. (2017). Large-scale structural characterization of drug and drug-like compounds by high-throughput ion mobility-mass spectrometry. *Anal. Chem.* 89, 9023–9030. doi: 10.1021/acs.analchem.7b01709

Hoeller, D., Hecker, C. M., and Dikic, I. (2006). Ubiquitin and ubiquitin-like proteins in cancer pathogenesis. *Nat. Rev. Cancer* 6, 776–788. doi: 10.1038/nrc1994

Hofstadler, S. A., and Sannes-Lowery, K. A. (2006). Applications of ESI-MS in drug discovery: interrogation of noncovalent complexes. *Nat. Rev. Drug Discov.* 5, 585–595. doi: 10.1038/nrd2083

Hu, W. B., Luo, Q., Ma, X. Y., Wu, K., Liu, J. N., Chen, Y., et al. (2009). Arene control over thiolate to sulfinate oxidation in albumin by organometallic ruthenium anticancer complexes. *Chemistry* 15, 6586–6594. doi: 10.1002/chem.200900699

Iwao, Y., Tomiguchi, I., Domura, A., Mantaira, Y., Minami, A., Suzuki, T., et al. (2018). Inflamed site-specific drug delivery system based on the interaction of human serum albumin nanoparticles with myeloperoxidase in a murine model of experimental colitis. *Eur. J. Pharm. Biopharm.* 125, 141–147. doi: 10.1016/j.ejpb.2018.01.016

Jin, R. Y., Li, L. Q., Feng, J. L., Dai, Z. Y., Huang, Y. W., and Shen, Q. (2017). Zwitterionic hydrophilic interaction solid-phase extraction and multi-dimensional mass spectrometry for shotgun lipidomic study of *Hypophthalmichthys nobilis*. *Food Chem.* 216, 347–354. doi: 10.1016/j.foodchem.2016.08.074

Jorgensen, A. L., Juul-Madsen, H. R., and Stagsted, J. (2009). A novel, simple and sensitive ligand affinity capture method for detecting molecular interactions by MALDI mass spectrometry. *J. Mass Spectrom.* 44, 338–345. doi: 10.1002/jms.1510

Kompauer, M., Heiles, S., and Spengler, B. (2017). Atmospheric pressure MALDI mass spectrometry imaging of tissues and cells at 1.4-μm lateral resolution. *Nat. Methods* 14, 90–96. doi: 10.1038/nmeth.4071

Kuzuhara, T., Sei, Y., Yamaguchi, K., Suganuma, M., and Fujiki, H. (2006). DNA and RNA as new binding targets of green tea catechins. *J. Biol. Chem.* 281, 17446–17456. doi: 10.1074/jbc.M601196200

Langley, G. J., Herniman, J. M., and Townell, M. S. (2007). 2B or not 2B, that is the question: further investigations into the use of pencil as a matrix for matrix-assisted laser desorption/ionisation. *Rapid Commun. Mass Spectrom.* 21, 180–190. doi: 10.1002/rcm.2827

Lee, J., Jayathilaka, L. P., Gupta, S., Huang, J. S., and Lee, B. S. (2012). Gold ion-angiotensin peptide interaction by mass spectrometry. *J. Am. Soc. Mass Spectrom.* 23, 942–951. doi: 10.1007/s13361-011-0328-0

Leitner, A. (2016). Cross-linking and other structural proteomics techniques: how chemistry is enabling mass spectrometry applications in structural biology. *Chem. Sci.* 7, 4792–4803. doi: 10.1039/C5SC04196A

Le-Rademacher, J., Kanwar, R., Seisler, D., Pachman, D. R., Qin, R., Abyzov, A., et al. (2017). Patient-reported (EORTC QLQ-CIPN20) versus physician-reported (CTCAE) quantification of oxaliplatin- and paclitaxel/carboplatin-induced peripheral neuropathy in NCCTG/Alliance clinical trials. *Support. Care Cancer* 25, 3537–3544. doi: 10.1007/s00520-017-3780-y

Li, J., Yue, L., Liu, Y. Q., Yin, X. C., Yin, Q., Pan, Y. J., et al. (2016). Mass spectrometric studies on the interaction of cisplatin and insulin. *Amino Acids* 48, 1033–1043. doi: 10.1007/s00726-015-2159-y

Li, L., Li, B., Zhang, H. R., Zhao, A. Q., Han, B. H., Liu, C. M., et al. (2015). Ultrafiltration LC-ESI-MS$^n$ screening of MMP-2 inhibitors from selected Chinese medicinal herbs *Smilax glabra* Roxb., *Smilax china* L. *and Saposhnikovia divaricata (Turcz.)* Schischk as potential functional food ingredients. *J. Funct. Foods* 15, 389–395. doi: 10.1016/j.jff.2015.03.038

Liang, Z. Q., Luo, Q., Zheng, W., Zhao, Y., and Wang, F. Y. (2018). Progress in identifying target proteins of active ingredients in traditional Chinese medicine by biological mass spectrometry. *Sci. Sin. Vitae* 48, 140–150. doi: 10.1360/N052017-00167

Lim, H. K., Hsieh, Y. L., Ganem, B., and Henion, J. (1995). Recognition of cell-wall peptide ligands by vancomycin group antibiotics studies using ion spray mass spectrometry. *J. Mass Spectrom.* 30, 708–714. doi: 10.1002/jms.1190300509

Liu, J., Wang, X. R., Cai, Z. W., and Lee, F. S. C. (2008). Effect of tanshinone IIA on the noncovalent interaction between warfarin and human serum albumin studied by electrospray ionization mass spectrometry. *J. Am. Soc. Mass Spectrom.* 19, 1568–1575. doi: 10.1016/j.jasms.2008.06.005

Liu, P. Y., Zhang, J., Ferguson, C. N., Chen, H., and Loo, J. A. (2013). Measuring protein-ligand interactions using liquid sample desorption electrospray ionization mass spectrometry. *Anal. Chem.* 85, 11966–11972. doi: 10.1021/ac402906d

Loo, J. A. (1997). Studying noncovalent protein complexes by electrospray ionization mass spectrometry. *Mass Spectrom. Rev.* 16, 1–23. doi: 10.1002/(SICI)1098-2787(1997)16:1<1::AID-MAS1>3.0.CO;2-L

Lorenzen, K., and Pawson, T. (2014). HDX-MS takes centre stage at unravelling kinase dynamics. *Biochem. Soc. Trans.* 42, 145–150. doi: 10.1042/BST20130250

Lossl, P., Van De Waterbeemd, M., and Heck, A. J. (2016). The diverse and expanding role of mass spectrometry in structural and molecular biology. *EMBO J.* 35, 2634–2657. doi: 10.15252/embj.201694818

Ma, H., Chen, G. L., and Guo, M. Q. (2016). Mass spectrometry (ms)-based translational proteomics for biomarker discovery and application in colorectal cancer. *Proteomics Clin. Appl.* 10, 503–515. doi: 10.1002/prca.201500082

Marcoux, J., Wang, S. C., Politis, A., Reading, E., Ma, J., Biggin, P. C., et al. (2013). Mass spectrometry reveals synergistic effects of nucleotides, lipids, and drugs binding to a multidrug resistance efflux pump. *Proc. Natl. Acad. Sci. U.S.A.* 110, 9704–9709. doi: 10.1073/pnas.1303888110

Marion, D. (2013). An introduction to biological NMR spectroscopy. *Mol. Cell. Proteomics* 12, 3006–3025. doi: 10.1074/mcp.O113.030239

Martin, E. M., Kondrat, F. D. L., Stewart, A. J., Scrivens, J. H., Sadler, P. J., and Blindauer, C. A. (2018). Native electrospray mass spectrometry approaches to probe the interaction between zinc and an anti-angiogenic peptide from histidine-rich glycoprotein. *Sci. Rep.* 8:8646. doi: 10.1038/s41598-018-26924-1

McClure, R. A., Chumbley, C. W., Reyzer, M. L., Wilson, K., Caprioli, M. R., Gore, J. C., et al. (2013). Identification of promethazine as an amyloid-binding molecule using a fluorescence high-throughput assay and MALDI imaging mass spectrometry. *Neuroimage Clin.* 2, 620–629. doi: 10.1016/j.nicl.2013.04.015

McDonnell, L. A., Rompp, A., Balluff, B., Heeren, R. M., Albar, J. P., Andren, P. E., et al. (2015). Discussion point: reporting guidelines for mass spectrometry imaging. *Anal. Bioanal. Chem.* 407, 2035–2045. doi: 10.1007/s00216-014-8322-6

Mengistu, T. Z., Desouza, L., and Morin, S. (2005). Functionalized porous silicon surfaces as MALDI-MS substrates for protein identification studies. *Chem. Commun.* 5659–5661. doi: 10.1039/b511457h

Mensi, A., Choiset, Y., Rabesona, H., Haertle, T., Borel, P., and Chobert, J. M. (2013). Interactions of beta-lactoglobulin variants A and B with Vitamin A. Competitive binding of retinoids and carotenoids. *J. Agric. Food Chem.* 61, 4114–4119. doi: 10.1021/jf400711d

Milburn, C. C., Deak, M., Kelly, S. M., Price, N. C., Alessi, D. R., and Van Aalten, D. M. (2003). Binding of phosphatidylinositol 3,4,5-trisphosphate to the pleckstrin homology domain of protein kinase B induces a conformational change. *Biochem. J.* 375, 531–538. doi: 10.1042/bj20031229

Mirzaei, H., Knijnenburg, T. A., Kim, B., Robinson, M., Picotti, P., Carter, G. W., et al. (2013). Systematic measurement of transcription factor-DNA interactions by targeted mass spectrometry identifies candidate gene regulatory proteins. *Proc. Natl. Acad. Sci. U.S.A.* 110, 3645–3650. doi: 10.1073/pnas.1216918110

Mukherjee, S., Hurt, C. N., Gwynne, S., Sebag-Montefiore, D., Radhakrishna, G., Gollins, S., et al. (2017). NEOSCOPE: a randomised phase II study of induction chemotherapy followed by oxaliplatin/capecitabine or carboplatin/paclitaxel based pre-operative chemoradiation for resectable oesophageal adenocarcinoma. *Eur. J. Cancer* 74, 38–46. doi: 10.1016/j.ejca.2016.11.031

Mulabagal, V., and Calderón, A. I. (2010). Development of an ultrafiltration-liquid chromatography/mass spectrometry (UF-LC/MS) based ligand-binding assay and an LC/MS based functional assay for mycobacterium tuberculosis shikimate kinase. *Anal. Chem.* 82, 3616–3621. doi: 10.1021/ac902849g

Nagar, B., Bornmann, W. G., Pellicena, P., Schindler, T., Veach, D. R., and Miller, W. T. (2002). Crystal structures of the kinase domain of c-Abl in complex with the small molecule inhibitors PD173955 and imatinib (STI-571). *Cancer Res.* 62, 4236–4243. doi: 10.2210/pdb1m52/pdb

Obi, N., Fukuda, T., Nakayama, N., Ervin, J., Bando, Y., Nishimura, T., et al. (2018). Development of drug discovery screening system by molecular interaction kinetics-mass spectrometry. *Rapid Commun. Mass Spectrom.* 32, 665–671. doi: 10.1002/rcm.8083

Pirok, B. W. J., Molenaar, S. R. A., Van Outersterp, R. E., and Schoenmakers, P. J. (2017). Applicability of retention modelling in hydrophilic-interaction liquid chromatography for algorithmic optimization programs with gradient-scanning techniques. *J. Chromatogr. A* 1530, 104–111. doi: 10.1016/j.chroma.2017.11.017

Poulsen, S. A., Davis, R. A., and Keys, T. G. (2006). Screening a natural product-based combinatorial library using FTICR mass spectrometry. *Bioorg. Med. Chem.* 14, 510–515. doi: 10.1016/j.bmc.2005.08.030

Qin, S. S., Ren, Y. R., Fu, X., Shen, J., Chen, X., Wang, Q., et al. (2015). Multiple ligand detection and affinity measurement by ultrafiltration and mass spectrometry analysis applied to fragment mixture screening. *Anal. Chim. Acta* 886, 98–106. doi: 10.1016/j.aca.2015.06.017

Qu, C. L., Yang, L. M., Yu, S. C., Wang, S., Bai, Y. P., and Zhang, H. Q. (2009). Investigation of the interactions between ginsenosides and amino acids by mass spectrometry and theoretical chemistry. *Pectrochim. Acta A Mol. Biomol. Spectrosc.* 74, 478–483. doi: 10.1016/j.saa.2009.06.048

Ramirez-Sarmiento, C. A., and Komives, E. A. (2018). Hydrogen-deuterium exchange mass spectrometry reveals folding and allostery in protein-protein interactions. *Methods* 144, 43–52. doi: 10.1016/j.ymeth.2018.04.001

Ramos, C. I. V., and Santana-Marques, M. G. (2009). Electrospray mass spectrometry for the study of the non-covalent interactions of porphyrins and duplex desoxyribonucleotides. *J. Porphyr. Phthalocya.* 13, 518–523. doi: 10.1142/S1088424609000590

Sakamoto, S., Fujita, M., Kim, K., and Yamaguchi, K. (2000). Characterization of self-assembling nano-sized structures by means of coldspray ionization mass spectrometry. *Tetrahedron Lett.* 56, 955–964. doi: 10.1016/S0040-4020(99)01092-3

Sakamoto, S., and Yamaguchi, K. (2003). Hyper-stranded DNA architecture observed by coldspray ionization mass spectrometry. *Angew. Chem. Int. Ed. Engl.* 42, 905–908. doi: 10.1002/anie.200390239

Sarni-Manchado, P., and Cheynier, V. (2002). Study of non-covalent complexation between catechin derivatives and peptides by electrospray ionization mass spectrometry. *J. Mass Spectrom.* 37, 609–616. doi: 10.1002/jms.321

Sato, S. I., Kwon, Y., Kamisuki, S., Srivastava, N., Mao, Q., Kawazoe, Y., et al. (2007). Polyproline-rod approach to isolating rotein targets of bioactive small molecules isolation of a new target of indomethacin. *J. Am. Chem. Soc.* 129, 873–880. doi: 10.1021/ja0655643

Sinz, A. (2018). Cross-linking/mass spectrometry for studying protein structures and protein-protein interactions: where are we now and where should we go from here? *Angew. Chem. Int. Ed. Engl.* 57, 6390–6396. doi: 10.1002/anie.201709559

Siuzdak, G. (1994). The emergence of mass spectrometry in biochemical research. *Proc. Natl. Acad. Sci. U.S.A.* 91, 11290–11297. doi: 10.1073/pnas.91.24.11290

Skribanek, Z., Balaspiri, L., and Mak, M. (2001). Interaction between synthetic amyloid-beta-peptide (1-40) and its aggregation inhibitors studied by electrospray ionization mass spectrometry. *J. Mass Spectrom.* 36, 1226–1229. doi: 10.1002/jms.243

Spengler, B. (2015). Mass spectrometry imaging of biomolecular information. *Anal. Chem.* 87, 64–82. doi: 10.1021/ac504543v

Takáts, Z., Wiseman, J. M., Gologan, B., and Cooks, R. G. (2004). Mass spectrometry sampling under ambient conditions with desorption electrospray ionization. *Science* 306, 471–473. doi: 10.1126/science.1104404

Talian, I., Orinak, A., Preisler, J., Heile, A., Onofrejova, L., Kaniansky, D., et al. (2007). Comparative TOF-SIMS and MALDI TOF-MS analysis on different chromatographic planar substrates. *J. Sep. Sci.* 30, 2570–2582. doi: 10.1002/jssc.200700120

Timerbaev, A. R., Hartinger, C. G., Aleksenko, S. S., and Keppler, B. K. (2006). Interactions of antitumor metallodrugs with serum proteins advances in characterization using modern analytical methodology. *Chem. Rev.* 106, 2224–2248. doi: 10.1021/cr040704h

Tjernberg, A., Carnö, S., Oliv, F., Benkestock, K., Edlund, P. O., Griffiths, W. J., et al. (2004). Determination of dissociation constants for protein-ligand complexes by electrospray ionizationmass spectrometry. *Anal. Chem.* 76, 4325–4332. doi: 10.1021/ac0497914

Tzameret, A., Ketter-Katz, H., Edelshtain, V., Sher, I., Corem-Salkmon, E., Levy, I., et al. (2019). *In vivo* MRI assessment of bioactive magnetic iron oxide/human serum albumin nanoparticle delivery into the posterior segment of the eye in a rat model of retinal degeneration. *J. Nanobiotechnol.* 17:3. doi: 10.1186/s12951-018-0438-y

Ueno-Noto, K., and Marynick, D. S. (2009). A comparative computational study of matrix-peptide interactions in MALDI mass spectrometry: the interaction of four tripeptides with the MALDI matrices 2,5-dihyroxybenzoic acid, α-cyano-4-hydroxy-cinnamic acid and 3,5-dihyroxybenzoic acid. *Mol. Phys.* 107, 777–788. doi: 10.1080/00268970802637828

van Linden, O. P., Kooistra, A. J., Leurs, R., de Esch, I. J., and de Graaf, C. (2014). KLIFS: a knowledge-based structural database to navigate kinase-ligand interaction space. *J. Med. Chem.* 57, 249–277. doi: 10.1021/jm400378w

Vautz, W., Franzke, J., Zampolli, S., Elmi, I., and Liedtke, S. (2018). On the potential of ion mobility spectrometry coupled to GC pre-separation - A tutorial. *Anal. Chim. Acta* 1024, 52–64. doi: 10.1016/j.aca.2018.02.052

Vu, H., Pham, N. B., and Quinn, R. J. (2008). Direct screening of natural product extracts using mass spectrometry. *J. Biomo. Screen.* 13, 265–275. doi: 10.1177/1087057108315739

Vuignier, K., Veuthey, J. L., Carrupt, P. A., and Schappler, J. (2012). Characterization of drug-protein interactions by capillary electrophoresis hyphenated to mass spectrometry. *Electrophoresis* 33, 3306–3315. doi: 10.1002/elps.201200116

Wan, C. H., Guo, X. H., Song, F. R., Liu, Z. Q., and Liu, S. Y. (2008). Interactions of mitoxantrone with duplex and triplex DNA studied by electrospray ionization mass spectrometry. *Rapid Commun. Mass Spectrom.* 22, 4043–4048. doi: 10.1002/rcm.3793

Wan, K. X., Shibue, T., and Gross, M. L. (2000). Non-covalent complexes between DNA-binding drugs and double-stranded oligodeoxynucleotides: a study by ESI ion-trap mass spectrometry. *J. Am. Chem. Soc.* 122, 300–307. doi: 10.1021/ja990684e

Wang, Z. F., Yu, X. M., Cui, M., Liu, Z. Q., Song, F. R., and Liu, S. Y. (2009). Investigation of calmodulin-Peptide interactions using matrix-assisted laser desorption/ionization mass spectrometry. *J. Am. Soc. Mass Spectrom.* 20, 576–583. doi: 10.1016/j.jasms.2008.11.017

Wendt, S., McCombie, G., Daniel, J., Kienhöfer, A., Hilvert, D., and Zenobi, R. (2003). Quantitative evaluation of noncovalent chorismate mutase-inhibitor binding by ESI-MS. *J. Am. Soc. Mass Spectrom.* 14, 1470–1476. doi: 10.1016/j.jasms.2003.08.003

Wilderman, P. R., Shah, M. B., Liu, T., Li, S., Hsu, S., Roberts, A. G., et al. (2010). Plasticity of cytochrome P450 2B4 as investigated by hydrogen-deuterium exchange mass spectrometry and X-ray crystallography. *J. Biol. Chem.* 285, 38602–38611. doi: 10.1074/jbc.M110.180646

Williams, J. P., Phillips, H. I. A., Campuzano, I., and Sadler, P. J. (2010). Shape changes induced by N-terminal platination of ubiquitin by cisplatin. *J. Am. Soc.Mass Spectrom.* 21, 1097–1106. doi: 10.1016/j.jasms.2010.02.012

Winston, R. L., and Fitzgerald, M. C. (1997). Mass spectrometry as a readout of protein structure and function. *Mass Spectrom. Rev.* 16, 165–179. doi: 10.1002/(SICI)1098-2787(1997)16:4<165::AID-MAS1>3.0.CO;2-F

Wiseman, J. M., Ifa, D. R., Venter, A., and Cooks, R. G. (2008). Ambient molecular imaging by desorption electrospray ionization mass spectrometry. *Nat. Protoc.* 3, 517–524. doi: 10.1038/nprot.2008.11

Wiseman, J. M., Takáts, Z., Gologan, B., Davisson, V. J., and Cooks, R. G. (2004). Direct characterization of enzyme-substrate complexes by using electrosonic spray ionization mass spectrometry. *Angew. Chem. Int. Ed. Engl.* 44, 913–916. doi: 10.1002/anie.200461672

Wortmann, A., Rossi, F., Lelais, G., and Zenobi, R. (2005). Determination of zinc to beta-peptide binding constants with electrospray ionization mass spectrometry. *J. Mass Spectrom.* 40, 777–784. doi: 10.1002/jms.852

Wu, W. I., Voegtli, W. C., Sturgis, H. L., Dizon, F. P., Vigers, G. P., and Brandhuber, B. J. (2010). Crystal structure of human AKT1 with an allosteric inhibitor reveals a new mode of kinase inhibition. *PLoS ONE* 23:e12913. doi: 10.1371/journal.pone.0012913

Xu, K. N., Tian, S. Z., Bai, B., Jia, J., Gan, Q. Y., and Chen, Q. (2018). Study on interaction between flavonoids and β-lactoglobulin by elactrospary ionization mass spectrometry. *Chem. Bioengin.* 35, 64–68. doi: 10.3969/j.issn.1672-5245.2018.10.015

Yamaguchi, K. (2003). Cold-spray ionization mass spectrometry: principle and applications. *J. Mass Spectrom.* 38, 473–490. doi: 10.1002/jms.488

Yanes, O., Nazabal, A., Wenzel, R., Zenobi, R., and Aviles, F. X. (2006). Detection of noncovalent complexes in biological samples by intensity fading and high-mass detection MALDI-TOF mass spectrometry. *J. Proteome. Res.* 5, 2711–2719. doi: 10.1021/pr060202f

Yanes, O., Villanueva, J., Querol, E., and Aviles, F. X. (2007). Detection of non-covalent protein interactions by 'intensity fading' MALDI-TOF mass spectrometry: applications to proteases and protease inhibitors. *Nat. Protoc.* 2, 119–130. doi: 10.1038/nprot.2006.487

Yao, C., Na, N., Huang, L., He, D., and Ouyang, J. (2013). High-throughput detection of drugs binding to proteins using desorption electrospray ionization mass spectrometry. *Anal. Chim. Acta* 794, 60–66. doi: 10.1016/j.aca.2013.07.016

Yao, Y. Y., Shams-Ud-Doha, K., Daneshfar, R., Kitova, E. N., and Klassen, J. S. (2015). Quantifying protein-carbohydrate interactions using liquid sample desorption electrospray ionization mass spectrometry. *J. Am. Soc. Mass Spectrom*. 26, 98–106. doi: 10.1007/s13361-014-1008-7

Young, L. M., Saunders, J. C., Mahood, R. A., Revill, C. H., Foster, R. J., Ashcroft, A. E., et al. (2016). ESI-IMS-MS: A method for rapid analysis of protein aggregation and its inhibition by small molecules. *Methods* 95, 62–69. doi: 10.1016/j.ymeth.2015.05.017

Zhang, H. M., Yu, X., Greig, M. J., Gajiwala, K. S., Wu, J. C., Diehl, W., et al. (2010). Drug binding and resistance mechanism of KIT tyrosine kinase revealed by hydrogen/deuterium exchange FTICR mass spectrometry. *Protein Sci.* 19, 703–715. doi: 10.1002/pro.347

Zhang, J. M., Adrián, F. J.,Jahnke, W., Cowan-Jacob, S. W., Li, A. G., Iacob, R. E., et al. (2010). Targeting Bcr–Abl by combining allosteric with ATP-binding-site inhibitors. *Nature* 463, 501–506. doi: 10.1038/nature08675

Zhang, R. P., and Abliz, Z. (2005). Progress in the study of non-covalent intermolecular interactions by mass spectrometry. *J. Instrument. Anal.* 24, 117–122.

Zhang, S., Van Pelt, C. K., and Wilson, D. B. (2003). Quantitative determination of noncovalent binding interactions using automated nanoelectrospray mass spectrometry. *Anal. Chem.* 75, 3010–3018. doi: 10.1021/ac034089d

Zhao, T., and King, F. L. (2010). A mass spectrometric comparison of the interactions of cisplatin and transplatin with myoglobin. *J. Inorg. Biochem.* 104, 186–192. doi: 10.1016/j.jinorgbio.2009.10.019

Zheng, Q. L., Tian, Y., Ruan, X. J., Chen, H., Wu, X. X., Xu, X. W., et al. (2018). Probing specific ligand-protein interactions by native-denatured exchange mass spectrometry. *Anal. Chim. Acta* 1036, 58–65. doi: 10.1016/j.aca.2018.07.072

Zhu, M. Z., Chen, G. L., Wu, J. L., Li, N., Liu, Z. H., and Guo, M. Q. (2018). Recent development in mass spectrometry and its hyphenated techniques for the analysis of medicinal plants. *Phytochem. Anal.* 29, 365–374. doi: 10.1002/pca.2763

Zhuang, X. Y., Gavriilidou, A. F. M., and Zenobi, R. (2017). Influence of alkylammonium acetate buffers on protein–ligand noncovalent interactions. *J. Am. Soc. Mass Spectrom.* 28, 341–346. doi: 10.1007/s13361-016-1526-6

Zinn, N., Hopf, C., Drewes, G., and Bantscheff, M. (2012). Mass spectrometry approaches to monitor protein-drug interactions. *Methods* 57, 430–440. doi: 10.1016/j.ymeth.2012.05.008

**Conflict of Interest:** The authors declare that the research was conducted in the absence of any commercial or financial relationships that could be construed as a potential conflict of interest.

frontiers in Chemistry

ORIGINAL RESEARCH
published: 08 November 2019
doi: 10.3389/fchem.2019.00762

# A Supramolecular Interaction of a Ruthenium Complex With Calf-Thymus DNA: A Ligand Binding Approach by NMR Spectroscopy

*Flávio Vinícius Crizóstomo Kock*[1], *Analu Rocha Costa*[2], *Katia Mara de Oliveira*[2], *Alzir Azevedo Batista*[2], *Antônio Gilberto Ferreira*[1] *and Tiago Venâncio*[1]*

[1] *Laboratory of Nuclear Magnetic Resonance, Department of Chemistry, Federal University of São Carlos, São Carlos, Brazil,*
[2] *Laboratory of Structure and Reactivity of Inorganic Compounds, Department of Chemistry, Federal University of São Carlos, São Carlos, Brazil*

Lawsone itself exhibits interesting biological activities, and its complexation with a metal center can improve the potency. In this context a cytotoxic Ru-complex, [Ru(law)(dppb)(bipy)] (law = lawsone, dppb = 1,4-bis(diphenylphosphino)butane and bipy = 2,2′-bipyridine), named as CBLAU, was prepared as reported. In this work, NMR binding-target studies were performed to bring to light the most accessible interaction sites of this Ru-complex toward Calf-Thymus DNA (CT-DNA, used as a model), in a similar approach used for other metallic complexes with anti-cancer activity, such as cisplatin and carboplatin. Advanced and robust NMR binding-target studies, among them Saturation Transfer Difference (STD)-NMR and longitudinal relaxometry ($T_1$), were explored. The $^{1}H$ and $^{31}P$ -NMR data indicate that the structure of Ru-complex remains preserved in the presence of CT-DNA, and some linewidth broadening is also observed for all the signals, pointing out some interaction. Looking at the binding efficiency, the $T_1$ values are highly influenced by the formation of the CBLAU-DNA adduct, decreasing from 11.4 s (without DNA) to 1.4 s (with DNA), where the difference is bigger for the lawsone protons. Besides, the STD-NMR titration experiments revealed a stronger interaction ($K_D$ = 5.9 mM) for CBLAU-DNA in comparison to non-complexed lawsone-DNA ($K_D$ = 34.0 mM). The epitope map, obtained by STD-NMR, shows that aromatic protons from the complexed lawsone exhibits higher saturation transfer, in comparison to other Ru-ligands (DPPB and bipy), suggesting the supramolecular contact with CT-DNA takes place by the lawsone face of the Ru-complex, possibly by a spatial π-π stacking involving π-bonds on nucleic acids segments of the DNA chain and the naphthoquinone group.

**Keywords: binding interactions, lawsone, ruthenium complex, anti-cancer, CT-DNA, NMR**

OPEN ACCESS

***Edited by:***
*Enrica Calleri,*
*University of Pavia, Italy*

***Reviewed by:***
*Francesco Crea,*
*University of Messina, Italy*
*Qifeng Li,*
*Tianjin University, China*

***Correspondence:**
*Tiago Venâncio*
*venancio@ufscar.br*

***Specialty section:***
*This article was submitted to Analytical Chemistry, a section of the journal Frontiers in Chemistry*

***Received:*** *23 July 2019*
***Accepted:*** *23 October 2019*
***Published:*** *08 November 2019*

***Citation:***
*Kock FVC, Costa AR, de Oliveira KM, Batista AA, Ferreira AG and Venâncio T (2019) A Supramolecular Interaction of a Ruthenium Complex With Calf-Thymus DNA: A Ligand Binding Approach by NMR Spectroscopy. Front. Chem. 7:762. doi: 10.3389/fchem.2019.00762*

## INTRODUCTION

Cancer is among the major public health problems worldwide and is responsible for millions of deaths, only in the United States (Siegel et al., 2019). Many biological macromolecular targets are involved in the complex mechanism of the cancer development, and nucleic acids, such as DNA, are one of these targets. The action of traditional chemotherapeutics based on metallic complexes

(metallodrugs), for example cisplatin and carboplatin, involves their interaction with the DNA. Hence, the search for new metallic complexes with anti-tumor activity is one of the most important research field in bioinorganic chemistry. Regarding this action mechanism, studies aiming to deep the knowledge about the intermolecular interaction between new potential drugs and biological targets are relevant, because it leads the design of new potent and selective anti-cancer candidates.

A strategy used to design new chemotherapeutics candidates and improve its anti-tumoral activity, consists on the complexation of some metallic centers, among them, silver (I) (Ali et al., 2013; Engelbrecht et al., 2018; Hussaini et al., 2019), gold (I)/(III) (Yeo et al., 2018; Dabiri et al., 2019; Hussaini et al., 2019), copper (II) (Khan et al., 2017; Zhang et al., 2018; Chen et al., 2019), and platinum (II) (Hua et al., 2019; Hussaini et al., 2019; Makovec, 2019) with a wide-range of ligands and also with natural molecules that already demonstrate some anti-cancer features, such as quinoline, flavones, and naphthoquinones (Kosmider and Osiecka, 2004; Lu et al., 2016; Oliveira et al., 2017a; Wang et al., 2018; Grandis et al., 2019). In this scenario, ruthenium takes special interests due to the possibility to reach several different metallic-arrangements, supplying distinct reactivities and applications (Oliveira et al., 2017b; Hussaini et al., 2019; Roy et al., 2019).

In this work, the ligand (2-hydroxy-1,4-naphthoquinone), a naphthoquinone with anti-viral, anti-fungal, anti-parasitic, anti-microbial, and anti-cancer biological features well-described in literature (Oliveira et al., 2017a) and the Ru/lawsone complex, [Ru(law)(dppb)(bipy)] (law = lawsone, dppb = 1,4-bis(diphenylphosphino)butane and bipy = 2,2′-bipyridine), named as CBLAU were fully investigated by NMR spectroscopy. The action of this potential metallodrug against tumor cell lines, among them, DU-145 (prostate cancer cells), MCF-7 (breast cancer cells), A549 (lung cancer cells) founds reported in the literature as well as its potential to induce the tumor cells apoptosis (Oliveira et al., 2017a). Considering that for all these cases, DNA is a possible and relevant biological target, similarly that occurs for cisplatin and/or carboplatin that acts binding covalently with pairs of nitrogenous DNA bases (Oliveira et al., 2017a), the intermolecular interaction of this new candidate (CBLAU) toward this biological target, is investigated in this research. In this work the intermolecular binding interactions will be investigated by NMR approaches, aiming to probe the intermolecular contact in the atomic level. These efforts can be reached using NMR techniques able to provide a reliable answer at molecular level (Viegas et al., 2011; Tanoli et al., 2015, 2018; Monaco et al., 2018).

Among several other techniques used for probing binding-targets interaction, among them circular dichroism, viscosimetry, and fluorescence (Oliveira et al., 2017a,b, 2019; Villareal et al., 2017; Gagini et al., 2018; Grandis et al., 2019), NMR-based methods is a unique spectroscopy able to supply in atomic level reliable answers for binding affinities studies in aqueous media (Tanoli et al., 2015, 2018). In addition, this experimental approach requires a very low concentration of protein without isotopic labeling, with any prior knowledge of its structure and/or function and does not have restriction on the protein size (Mayer and Meyer, 1999, 2001; Angulo et al., 2010; Angulo and Nieto, 2011; Viegas et al., 2011; Monaco et al., 2018). Based on the aforementioned features, these NMR experiments are the most routinely used techniques for drug/biological target recognition processes, through the knowledge about the spatial interaction, binding epitope mapping (GEM), and determination of dissociation constants ($K_D$), supplying an unequivocal grasp about the intermolecular interactions, where most of the others analytical methods are unable to provide satisfactory answers (Mayer and Meyer, 1999, 2001; Angulo et al., 2010; Angulo and Nieto, 2011; Viegas et al., 2011; Monaco et al., 2018; Nepravishta et al., 2019).

Therefore, herein, we use NMR binding-target interaction approaches, among them $^{1}$H- and $^{31}$P-NMR, relaxometric experiments, Saturation Transfer Difference (STD)-NMR for scrutiny at atomic level the intermolecular interaction between the potential anti-cancer candidate (CBLAU) toward DNA. To the best of our knowledge few papers devote special attention on a detailed application of NMR spectroscopy to characterize the interaction of metallic complexes with macromolecular targets. As a result, we expect to introduce detailed NMR studies in order to open a new possibility of frontiers researches in bioinorganic chemistry, aiming to rationalize the designing of new metallodrugs based chemotherapeutics, with improved potency and selectivity against cancer, which still remains a challenge.

# EXPERIMENTAL

## Sample Preparation

Calf-thymus DNA (CT-DNA) was purchased from Sigma-Aldrich Ltd (Brazil) and used without previous purification. A 1.078 mM solution of CT-DNA was prepared by dissolving an adequate weight of this macromolecule in a deuterated phosphate buffer. The pH 7.2 phosphate $D_2O$ buffer was prepared by dissolving disodium hydrogen phosphate ($Na_2HPO_4.12H_2O$, 0.1180 g) and sodium dihydrogen phosphate ($NaH_2PO_4.2H_2O$, 0.0217 g) in 10.00 mL $D_2O$ (99.9%, Cambridge Isotopes Laboratories, Inc. with pH 7.2) to make a 0.046 M solution. The (CBLAU)($BF_4^-$) complex was dissolved in a 5:95% v/v of DMSO (99.8% Cambridge Isotopes Laboratories, Inc.) and deuterated buffer respectively. $BF_4^-$ was used as a counter ion together with 5% of DMSO-d6 to increase the solubility of the Ru-complex in aqueous solution. All $^{1}$H NMR and STD-NMR spectra were recorded using a 1:100 (DNA:CBLAU) molar ratio, in a final volume of 500 μL transferred to a 5 mm NMR tube (Norrel, Inc. USA). For the epitope mapping experiment, the final concentration of CBLAU was 5 mM and the concentration for the CT-DNA was 50 μM. On the other hand, for the concentration-dependent STD-NMR experiment, the CBLAU and lawsone concentrations were ranged from 5 to 1 mM. In these experiments, the CT-DNA concentration was fixed in 50 μM. For these studies, 7 independent STD-NMR experiments were acquired for each concentration.

## NMR Spectroscopy

All $^{1}$H-NMR based experiments were recorded on a Bruker Avance III 14.1 T spectrometer equipped with a TCI cryoprobe and the $^{31}$P-NMR experiments were performed on a Bruker

Avance III 9.4 T spectrometer. The proton resonance frequencies for both magnetic fields are 600 and 400 MHz, respectively. Data acquisition and processing were performed with the Bruker software Topspin 3.5 pl. 7 version installed in the spectrometer. All the experiments were done at 298 K.

## One-Dimensional NMR ($^1$H and $^{31}$P Experiments)

The $^1$H-spectra were acquired using a standard Bruker presaturation pulse sequence (zgesgp) pulses length of 9.57 us and 19.14 us for the 90° and 180°, respectively, with a gradient length pulse of 2,000 us. Besides, other experimental conditions were acquisition time of 4.63 s (32 K points), recycle delay of 4 s, spectral window of 20.02 ppm, and accumulation of 128 transients. For the acquisition of $^{31}$P-spectra a standard BRUKER pulse sequence (zgpg30) was used with a pulse length of 25.0 us and 50 us for the 90° and 180°, respectively. In addition, a spectral width of 289.40 ppm, recycle delay of 0.1 s (32 K points) were used and a total of 131,072 transients were co-added.

## Relaxometric Experiments

The relaxometric experiments were acquired using the standard Bruker pulse sequence inversion-recovery (t1ir), spectral window of 15.01 ppm, acquisition time of 1.8 s (32 K points), pulses lengths of 9.35 us and 18.70 us for the 90° and 180°, 16 transients and exponentially ranging the time between the pulses ($\tau$) from 0.001 to 30 s. For the longitudinal relaxation time ($T_1$) constant determination, was used the monoexponential fitting for the experimental obtained data, using for this purpose the software Topspin 3.5 pl.7.

## STD-NMR

These experiments were recorded by using a Bruker standard pulse sequence with water supression (stddiffesgp.3), with a pseudo-2D setup through an intervaled acquisition of an *on*- and *off*-resonance experiment. The water suppression was done under excitation sculpting scheme, properly optimized. Selective irradiation (during saturation time) of CT-DNA was achieved using a train of soft Gaussian-shaped pulses, with attenuation level of 45–55 dB, 50 ms of length and separated by a 2 ms interval. The frequency chosen for an adequate selective irradiation of CT-DNA was 2289.266 Hz (3.8 ppm) for *on*-resonance and 30,000 Hz (50 ppm) for *off*-resonance. The STD build up curve was acquired by ranging the saturation time between 0.5 and 10 s, and recording 14 independent experiments. Finally, the STD amplification factor ($A_{STD}$) was calculated by accounting the signal intensity of the STD difference spectrum relative to the reference (off-resonance) according to Equation (1; Mayer and Meyer, 1999).

$$A_{STD} = \frac{I_0 - I_{STD}}{I_0} \times \frac{[L]}{[P]} \quad (1)$$

For the determination of the relative percentage of $A_{STD}$, the proton signal with biggest integral area received the value of 100% and the other signals were normalized with respect to this signal. For the dissociation constant ($K_D$) estimation, seven STD-NMR concentration-based experiments were performed. The results were plotted using the Equation 2, and the reciprocal of this equation (Lineweaver-Burk plot) was employed for estimation of $K_D$.

$$A_{STD} = \frac{\alpha_{STD}[L]}{K_D + [L]} \quad (2)$$

In this equation, $A_{STD}$ corresponds to STD signal intensity, $\alpha_{STD}$ is the maximum STD intensity assuming infinite concentration, and [L] is the ligand concentration. After getting the $A_{STD}$ and $\alpha_{STD}$ values, the curves $A_{STD}$ vs. concentration were built up, linearized and fitted using a linear fit employing the MS Excel (2007) and plotted using the software Origin, version 8.0.

# RESULTS AND DISCUSSIONS

## Signal Assignment

The $^1$H NMR signal assignment for CBLAU and lawsone are shown in **Figures 1A,B**, respectively. Due to the aromatic character of the ligands, the NMR region above 6.5 ppm at **Figure 1A** exhibits a series of superimposed signals. Despite this spectral feature, the signal discrimination can be done regarding each individual ligand. The set of signals numbered as 1 (black), from 6.8 to 7.4 ppm and at 5.7 ppm, correspond to aromatic hydrogens from lawsone ligand. Moreover, the intense signals assigned by the number 2 (red), from 7.6 to 7.9 ppm are attributed to hydrogens present on DPPB ligand. The signals numbered by 3 (blue), close to 2.0 ppm correspond to aliphatic hydrogens (butyl unit) present on DPPB ligand. To conclude, the set of signals numbered as 4 (pink), above 8.0 ppm and from 7.5 to 7.8 ppm, correspond to hydrogens from Bipy ligand. The presence of some impurities can be observed by the signals assigned with asterisks. These impurities remain even after the laborious process of CBLAU purification. Despite the presence of these residues, they do not interfere in the interaction between CBLAU and CT-DNA, as it will be shown in the following discussions. The **Figure 1B** shows the $^1$H-NMR spectrum for the lawsone ligand. On this spectrum, it is clearly possible to observe 5 signals. The hydrogens 2–5 correspond to the aromatic from 7.5 to 7.8 ppm, as indicated. The signal at 5.7 ppm corresponds to vinylic proton, assigned by the number 1.

On **Figure 2** the $^1$H NMR signal assignment can be better visualized on the chemical structure for CBLAU, highlighting the chemical groups responsible for each signal observed on the NMR spectra previously presented in the **Figure 1A**. The set of these results (**Figures 1**, **2**) will be helpful on the subsequent binding target elucidation studies, providing an atomic comprehension about the contribution of each ligand group present on CBLAU and lawsone responsible by the efficient intermolecular interaction toward the CT-DNA strand.

## Interaction With Calf Thymus DNA

In the first approach (**Figure 3**), the $^1$H-NMR spectra were obtained for the Ru-complex CBLAU in the presence of CT-DNA (red) and without CT-DNA (black) aiming to reach a preliminary picture about the interactions, based on some chemical shift variation and/or linewidth broadening. Interestingly, it is not

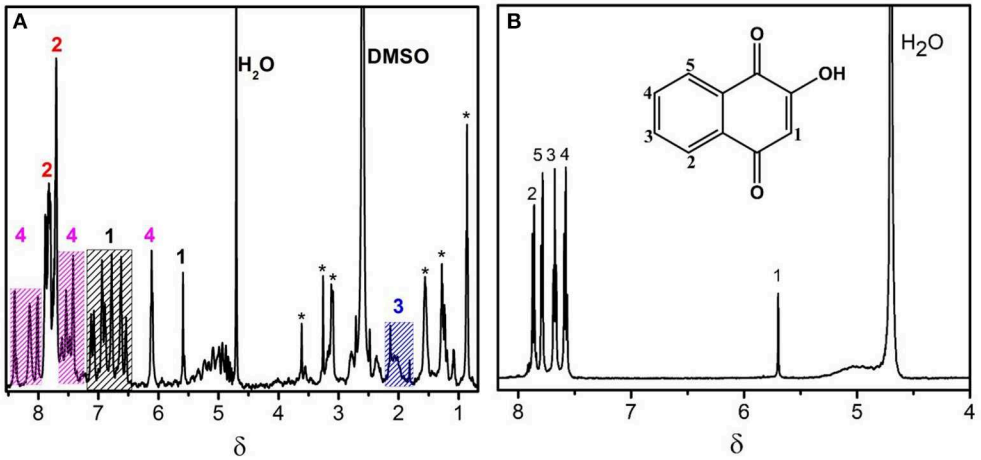


**FIGURE 1 |** $^{1}$H-NMR spectra obtained at 600 MHz (for $^{1}$H nucleus) and at 298 K for the characterization of the Ru-complex CBLAU **(A)** and the free ligand (lawsone) in **(B)**.

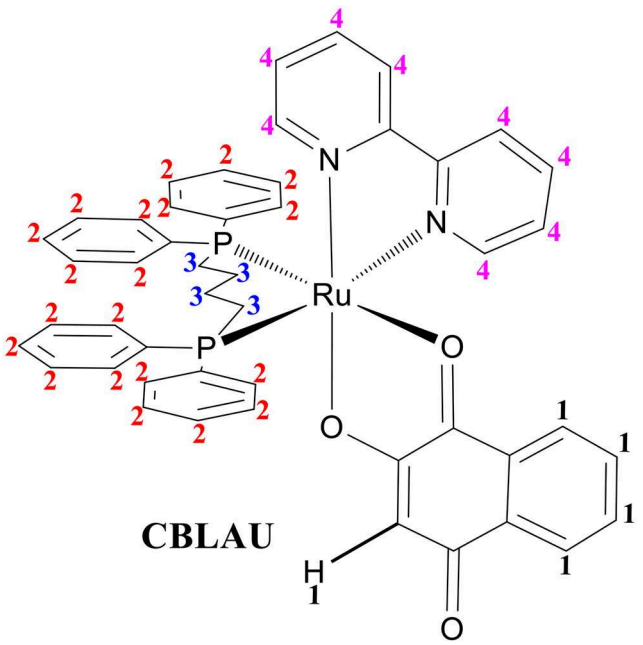


**FIGURE 2 |** Chemical structure for the Ru-complex (CBLAU) addressed in this work: the numbers 1 (black) correspond to the ligand lawsone; the number 2 (red) to aromatic protons of DPPB ligand; the number 3 (blue) to aliphatic hydrogens (butyl unit) between the two DPPB units and the number 4 (pink) to the hydrogens from the Bipy ligand.

observed any significant change in the NMR spectrum profile due to the presence of DNA. Some linewidth broadening is observed on the spectrum without CT-DNA (black) can be attributed to the complex size, its low solubility and the presence of some quadrupolar component present on some active NMR Ru-isotopes (Levitt, 2008; Keller, 2011). In the presence of CT-DNA, any change can be observed.

Regarding these $^{1}$H-NMR results, the intermolecular interaction between CBLAU toward CT-DNA was investigated by $^{31}$P-NMR, aiming to scrutiny the influence of presence of CT-DNA on the DPPB ligand, and the preservation of the Ru-complex. For this purpose, two $^{31}$P-NMR spectra for CBLAU were collected, with and without CT-DNA. The resulting spectra are shown on the **Figure 4**. In the black line it is can be observed the $^{31}$P-NMR signal obtained for the CBLAU at 298 K in DMSO:buffer (5:95 v/v), without CT-DNA. The spectrum in red represents the $^{31}$P-NMR signal obtained for CBLAU in the presence of CT-DNA. By comparing the spectra, it is clearly observed that the presence of the macromolecule is responsible for the increasing of the $^{31}$P linewidth. Besides, the signal intensity is reduced, leading to confirm that the interaction between CBLAU and CT-DNA is highly important and demonstrate that for this case, $^{31}$P-NMR is more sensitive to investigate this binding interaction in comparison to $^{1}$H-NMR.

Therefore, from the analysis of $^{1}$H-NMR spectra it is possible to suggest that the interaction of CBLAU with CT-DNA is weak and possibly takes place through a spatial van-der-Waals intermolecular force. In fact, this type analysis is very preliminary and not conclusive, since the chemical shift variation, as well as the linewidth broadening, can be related to several other effects, such as pH and temperature variation. To circumvent this limitation other robust NMR methods can be better explored, such as NMR-relaxometry and STD-NMR for discriminate at atomic level the binding target intermolecular interactions. These NMR approaches will be explored in the later discussions.

The relaxometric, and particularly the longitudinal relaxation time, is highly useful as a preliminary estimative about the binding-target efficiency, since the longitudinal relaxation times vary according to changes in the molecular mobility. For this purpose, $^{1}$H $T_1$ relaxation times were determined for the Ru-complex CBLAU with and without CT-DNA. The experimental data showed that the average longitudinal relaxation ($T_1$) obtained for CBLAU (11.41 s) is highly influenced, due to the

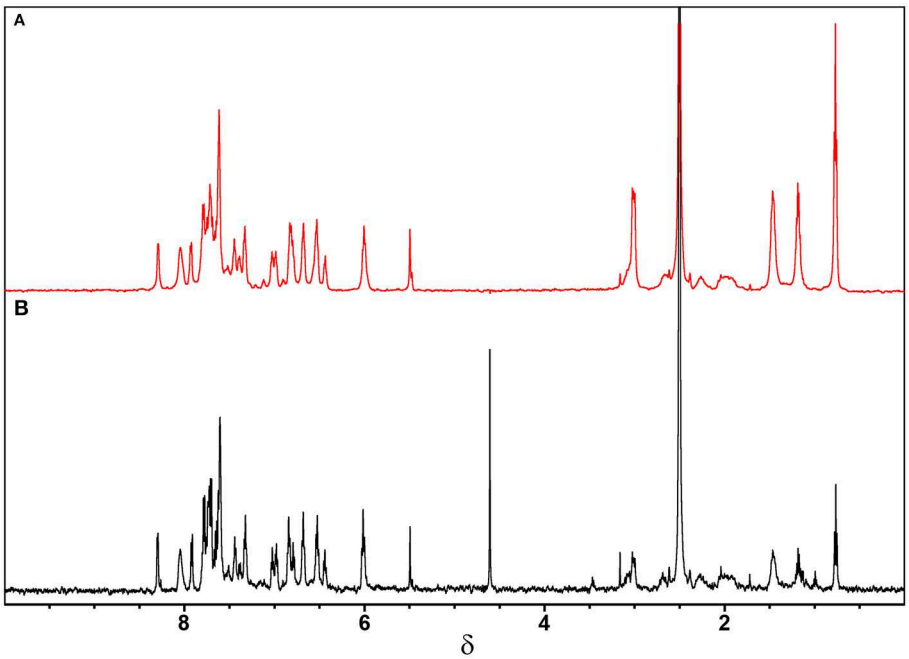


**FIGURE 3 |** $^{1}$H-NMR spectra obtained for CBLAU (5 mM): **(A)** with (red) and **(B)** without (black) CT-DNA (50 μM) at 600 MHz (for $^{1}$H nucleus) and 298 K.

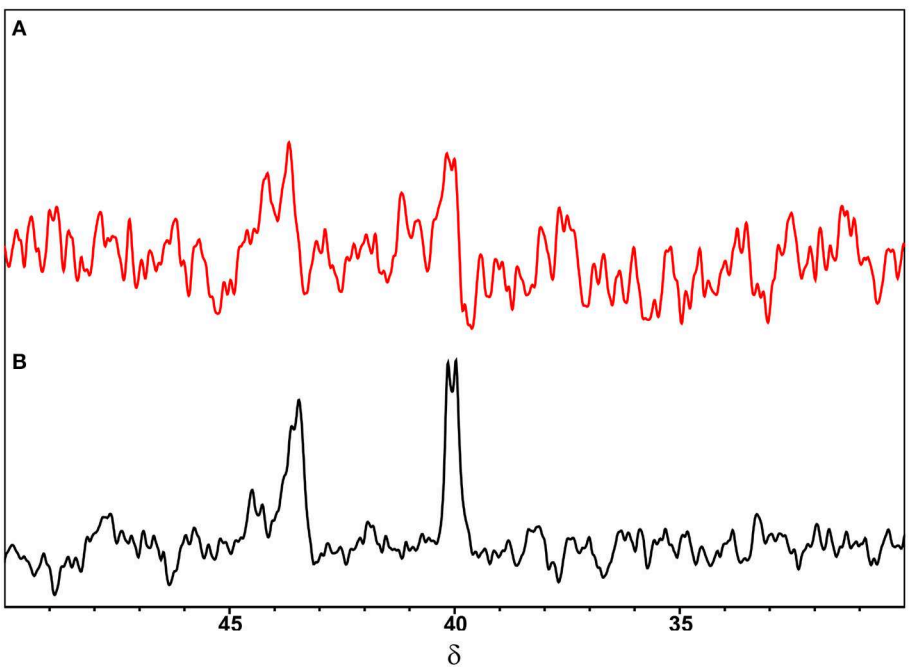


**FIGURE 4 |** $^{31}$P-NMR spectra obtained for CBLAU (5 mM): **(A)** with (red) and **(B)** without (black) CT-DNA (50 μM) at 161.96 MHz (for $^{31}$P nucleus) in DMSO:buffer (5:95 v/v) at 298 K.

final CBLAU/CT-DNA adduct formation (1.40 s) in solution. These variations can be attributed to the reduction on the molecular mobility associated to CBLAU under the presence of CT-DNA, which is an extremely large macromolecule ($8.41 \times 10^{6}$ g.mol$^{-1}$) that increases the viscosity of the solution (Porsch et al., 2009). Therefore, these results point out that CBLAU interacts with CT-DNA. The detailed results are listed on **Table 1**, for all the groups complexed with metallic center. The complexed

**TABLE 1 |** $^1$H $T_1$ relaxation times determined for the Ru-complex CBLAU in solution (5 mM) and in the presence of CT-DNA (50 μM). Results collected at 298 K (600 MHz).

| Group | $T_1$ (s) with CT-DNA | $T_1$ (s) without CT-DNA | $\Delta T_1$ (s) |
|---|---|---|---|
| Lawsone | 1.4 | 11.5 | 10.1 |
| Bipy | 1.1 | 11.4 | 10.3 |
| DPPB | 1.4 | 11.1 | 9.7 |
| Butane branch | 1.8 | 11.6 | 9.8 |

lawsone and bipyridine are mostly affected by the presence of CT-DNA and these findings indicate that these groups exhibit a shorter contact with CT-DNA surface. The formation of the supramolecular adducts, CBLAU/CT-DNA obeys a binding equilibrium, where the lawsone and bipy face of CBLAU seems to be more involved in the intermolecular contact.

Despite these positive results of these relaxometry based binding-target experiments in demonstrating the interaction of CBLAU with CT-DNA, the $T_1$ relaxation times could change due to other effects, such as the viscosity variation. On the other hand, the $T_1$ variation is different for each group complexed to ruthenium, as mentioned. In this scenario, the interaction between CBLAU and CT-DNA was investigated by STD-NMR experiments (**Figure 5**), which is more robust, and depends exclusively on the spatial contact of the molecules involved in the interaction. This experiment allows to estimate not only the most accessible sites of binding contact present but supplies the intensity of these interactions. The epitope map, which describes the spatial proximities between the small molecule (CBLAU and lawsone) and the macromolecular target (CT-DNA), was built up from the acquisition of 14 STD-NMR experiments, ranging the saturation times from 0 to 10 s. Once the data was collected, the STD amplification factor ($A_{STD}$) was calculated using the $STD_{off-resonance}$ (**Figure 5A**) and $STD_{diff}$ (**Figure 5B**) spectra, and performing the ratio of these spectra, in agreement to Equation (1). For the signal with higher $A_{STD}$ value was attributed the percentage of 100% and for the other protons, the $A_{STD}$ values were calculated with relation to this initial consideration. Besides, the signal intensity, as observed in these figures, does not only reflects the relative amount of saturation transferred from CT-DNA to CBLAU *via* cross-relaxation (spin-diffusion), but also reflects the relative proximity of a respective proton from CBLAU to the biological target surface on the final adduct (Mayer and Meyer, 1999, 2001; Angulo et al., 2010; Angulo and Nieto, 2011; Viegas et al., 2011; Monaco et al., 2018). In addition, it is important to stress that, the signal intensities in STD-NMR spectrum strongly depends on the equilibrium established between the species involved in the interaction, with similarities to the enzymatic inhibition equilibrium. Therefore, as in agreement to literature, two factors are important in these terms, one is the concentration of the small molecule and the second is the saturation transfer from the macromolecule to the small molecule (Viegas et al., 2011; Tanoli et al., 2015, 2018; Monaco et al., 2018). In this context, it is expected that longer saturation times improve the saturation transfer in the limit governed by the timescale of the contact between the protons from CBLAU closer to CT-DNA surface. Thus, as the CBLAU concentrations increase, the CT-DNA surface reaches some saturation and, as response, the STD signal intensities should increase (Tanoli et al., 2015, 2018).

Regarding the dependence of the equilibrium with the timescale of the intermolecular contact between CBLAU and CT-DNA several STD experiments were collected by varying the saturation time. Therefore, analyzing the $STD_{off-resonance}$ and $STD_{diff}$ spectra a built-up curve was obtained ranging the saturation time from 0 to 10.0 s for each CBLAU group, as shown in **Figure 6A**, where the exponential growth and the intensity of the curve plateau reflects the proximity of each group to the CT-DNA surface. This analysis allows to reach a map of the proximities between the Ru-complex and the CT-DNA surface, and this is known as epitope map. The results show that the lawsone group is the closest one (100.0%) in comparison to Bipy (58.6%), DPPB (39.7%), and butyl groups (between DPPB units), 14.7%. The epitope map shows that the interaction involves peripheral CBLAU protons, as expected, and an important finding is that the metallic complex structure is preserved, as previously observed by $^1$H-NMR data. But an initial question should be answered regarding the recognized biological activity of lawsone: does the complexation with a metallic center improve its activity? This is an important concerning to justify the Ru-complex preparation. At this point, several STD experiments were conducted for individual lawsone, following the same approach.

For the lawsone, STD experiments showed that the all aromatic protons are close to CT-DNA surface, as expected (**Figure 6B**). The proton 1 (green) refers to a lower (63.9%) $A_{STD}$ value in comparison to the other protons, which $A_{STD}$ values are quite similar: proton 2 (black) (100%), proton 3 (blue) (96.4%), proton 4 (pink) (94.3%), and proton 5 (red) (99.4%), respectively. Therefore, protons numbered from 2 to 5 are closer to CT-DNA and π-π stacking forces seem to govern the contact. Besides, these results reinforce that the presence of ligands containing aromatic groups on the design of anti-cancer candidates favors the contact with the DNA surface.

Interestingly, it is observed on **Figure 6B** that the $A_{STD}$ values for the 2 to 5 protons of the non-Ru complexed lawsone exponentially increased until 10 s of saturation time, but differently to note for the CBLAU protons, the $A_{STD}$ does not reach a stationary plateau, supposed at elevated saturation times conditions. These results indicate that besides these protons are closer to DNA, they are not completely saturated, in despite of the elevated saturation time, which is an additional indicative that the interaction of the non-Ru complexed lawsone with CT-DNA is weaker, in comparison to the Ru-complexed one. In addition, it is also observed for the proton 1 (green) on lawsone, that the $A_{STD}$ values is more randomized in comparison to that one reached for another protons. These observations do not prevent the determination of $A_{STD}$, but demonstrate that the resonances close to solvent signal (4.7 ppm) are more influenced by the solvent suppression scheme used, where the excitation profile associated to the pulse sequence used also reduce the solvent nearby signals.

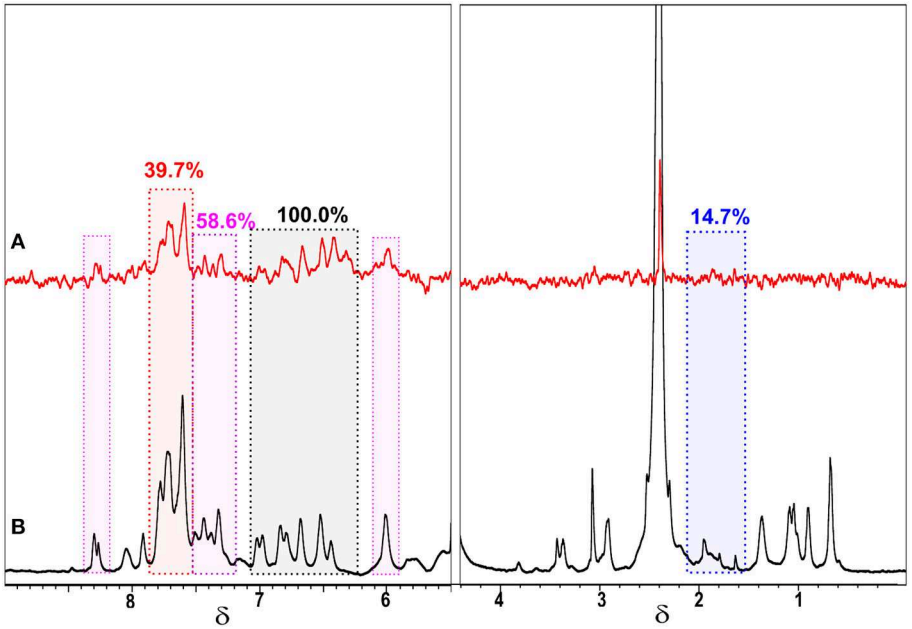


**FIGURE 5 |** Off-resonance STD spectrum **(A)** and STD diff-spectrum **(B)** obtained by applying 10.0 s of saturation time and used for the calculation of $A_{STD}$ and consequent epitope map, highlighting the contribution (proximity) of each group present on CBLAU (5 mM), bipy (58.6%) (pink), butyl protons between the DPPB units (14.7%) (blue), lawsone (100.0%) (black), and DPPB (39.7%) (red) to CT-DNA (50 μM) surface.

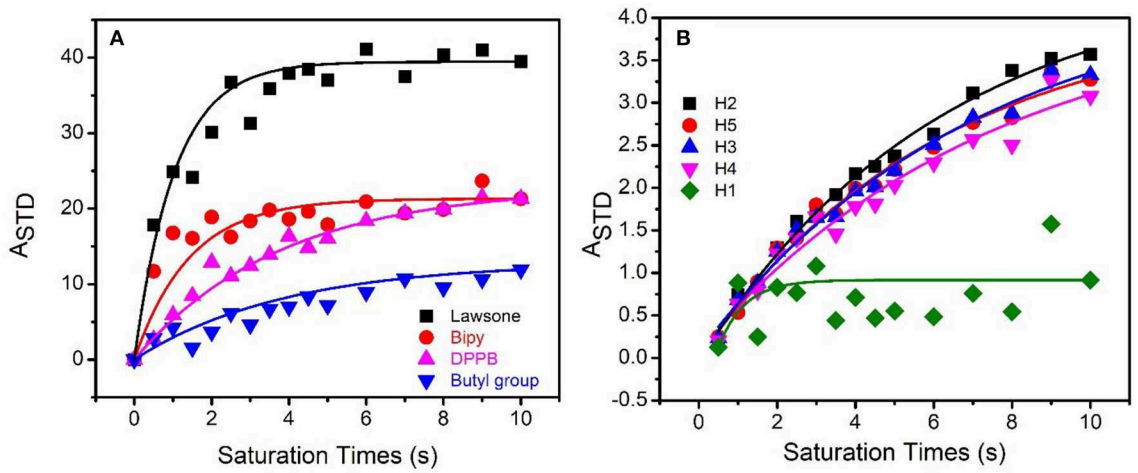


**FIGURE 6 |** Built-up curves of $A_{STD}$ against saturation time at 298 K and 600 MHz ($^1$H nucleus) for CBLAU (5 mM) **(A)** and for the individual lawsone (5 mM) **(B)** in the presence of CT-DNA (50 μM).

Nevertheless, a second question remains unanswered: how strong is the interaction between CBLAU and CT-DNA? To explore the quantitative aspects of the equilibrium established with interaction, the dissociation constants ($K_D$) were estimated for both cases: individual lawsone and Ru-complexed lawsone as in CBLAU. The estimation of $K_D$ was performed by using several STD experiments, now varying the CBLAU concentration, in order to obtain a built-up curve, fitted by using a Lineweaver-Burk approach, as presented in the experimental section. Notably, the Ru-complexed lawsone exhibits an average dissociation constant of 5.9 mM (**Figure 7**), which is much smaller than the average $K_D$ obtained for non-Ru complexed lawsone:CT-DNA supramolecular adduct (34.0 mM) (**Figure S1**). To conclude it is quite clear that when complexed, the lawsone exhibits a stronger interaction with CT-DNA. Therefore, these results put light on the previously reported biological results (Oliveira et al., 2017a; Grandis et al., 2019), demonstrating that the CBLAU

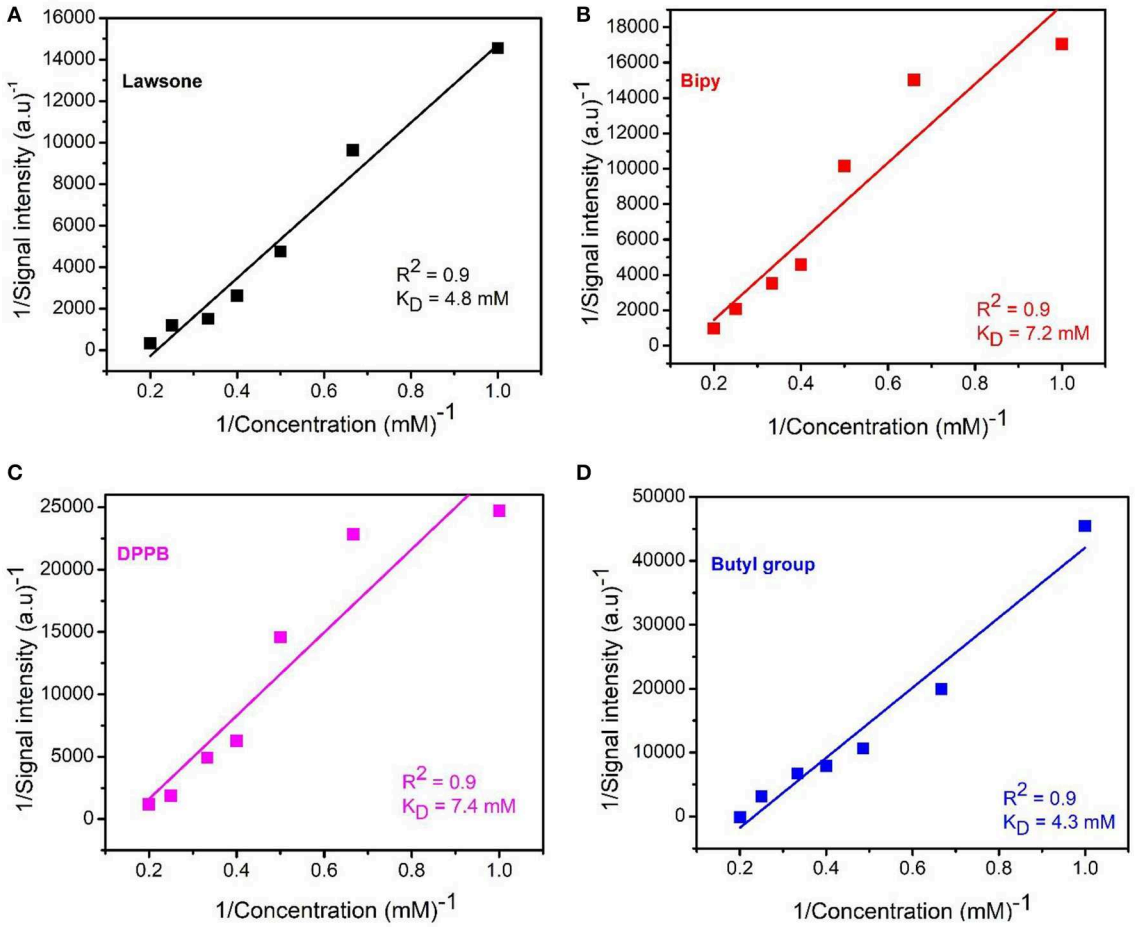


**FIGURE 7 |** Lineweaver-Burk plot for the experimental STD-NMR concentration experiments obtained for CBLAU and used to estimate the dissociation constant ($K_D$) for each group: lawsone (4.8 mM) **(A)**, bipy (7.2 mM) **(B)**, DPPB (7.4 mM) **(C)** and butyl group (4.3 mM) **(D)** and the average $K_D$ value (5.9 mM) for this molecule (CBLAU) in interaction to CT-DNA.

complex interacts toward CT-DNA stronger than for non-Ru complexed lawsone.

## CONCLUSIONS

The interaction between a novel anti-cancer candidate and the biological target DNA was understood at atomic level by NMR-binding approaches. The relaxometric results demonstrated to be an efficient probe to monitor the formation of CBLAU/CT-DNA adduct in solution and the T1 variation is bigger for lawsone and bipyridine groups. Besides, it was also demonstrated that this binding target interaction have a weak nature ($K_D$ = 5.9 mM), experimentally proving the pivotal role assumed by the spatial contact, such as hydrogen bonding, hydrophobic contacts, hydrophilic-hydrophobic interactions and π-π stacking on the final adduct arrangement. The studies involving only the non-complexed lawsone suggests that the binding mode toward DNA occur in a similar way, but the interaction intensity is notably lower ($K_D$ = 34.0 mM) in comparison to the Ru-complexed one. These results also reinforce the search for new metallic complexes with organic molecules with recognized biological activity. The complexation with a metal can improves the interaction of these molecules with macromolecular biological targets. All these results put light on the reasons about the relevant biological features associated to this candidate against tumor cell lines DU-145 (prostate cancer cells), MCF-7 (breast cancer cells), A549 (lung cancer cells) as well as its potential to induce the tumor cells apoptosis. Therefore, we expect that these findings help the researchers working on bioinorganic to design new metallodrugs with improved activity and selectivity.

## DATA AVAILABILITY STATEMENT

The datasets for this study are available on request to the corresponding author.

## AUTHOR CONTRIBUTIONS

FK, AF, and TV designed the experiments. FK and TV generated and analyzed the experimental data. AC, KO, and

AB designed and synthetized the complex CBLAU and provided the non-complexed lawsone. The manuscript was written by FK and TV. TV has supervised and finalized the final version of the manuscript.

## FUNDING

The authors are gratefully acknowledged to the financial support from FAPESP (2018/19342-2, 2018/16040-5, and 2018/09145-5), CNPq (455630/2014-3), and EMBRAPA for the access to the license for the software Origin version 8.0.

## SUPPLEMENTARY MATERIAL

The Supplementary Material for this article can be found online at: https://www.frontiersin.org/articles/10.3389/fchem.2019.00762/full#supplementary-material

## REFERENCES

Ali, K. A., Abd-Elzaher, M. M., and Mahmoud, K. (2013). Synthesis and anticancer properties of Silver(I) complexes containing 2,6-Bis(substituted)pyridine derivatives. *Int. J. Med. Chem*. 2013, 256836–256842. doi: 10.1155/2013/256836

Angulo, J., Enriquez-Navas, P. M., and Nieto, P. M. (2010). Ligand–receptor binding affinities from saturation transfer difference (STD) NMR spectroscopy: the binding isotherm of STD initial growth rates. *Chem. Eur. J*. 16, 7803–7812. doi: 10.1002/chem.200903528

Angulo, J., and Nieto, P. M. (2011). STD-NMR: application to transient interactions between biomolecules-a quantitative approach. *Eur. Biophys. J*. 40, 1357–1369. doi: 10.1007/s00249-011-0749-5

Chen, Z. F., Wu, Y. X., Zhu, Z. Z., and Zhang, Y. M. (2019). DNA cleavage, DNA/HAS binding study, and antiproliferative activity of activity of a phenolate-bridged binuclear copper (II) complex. *Biometals* 32, 227–240. doi: 10.1007/s10534-019-00172-w

Dabiri, Y., Abu el Maaty, M. A., Chan, H. Y., Wolker, J., Ott, I., Wolfl, S., et al. (2019). P53-dependent anti-proliferative and pro-apoptotic effects of a gold (I) N-heterocyclic (NHC) complex in colorectal cancer cells. *Front. Oncol*. 9:438. doi: 10.3389/fonc.2019.00438

Engelbrecht, Z., Meijboom, R., and Cronje, M. J. (2018). The ability of silver (I) thiocyanate 4-methoxyphenyl phosphine to induce apoptotic cell death in esophageal cancer is correlated to mitochondrial perturbations. *Biometals* 31, 189–202. doi: 10.1007/s10534-017-0051-9

Gagini, T., Colina-Vegas, L., Villareal, W., Borba-Santos, L. P., Pereira, C. S., Batista, A. A., et al. (2018). Metal-azole fungistatic drug complexes as anti-Sporothrix spp. agents. *New J. Chem.* 42, 13641–13650. doi: 10.1039/C8NJ01544A

Grandis, R. A., Santos, P. W. S., Oliveira, K. M., Machado, A. R. T., Aissa, A. F., Batista, A. A., et al. (2019). Novel lawsone-containing ruthenium(II) complexes: synthesis, characterization and anticancer activity on 2D and 3D spheroid models of prostate cancer cells. *Biorg. Chem*. 85, 455–468. doi: 10.1016/j.bioorg.2019.02.010

Hua, S. X., Chen, F. H., Wang, X. Y., Wang, Y. J., and Gou, S. H. (2019). Pt(IV) hybrids containing a TDO inhibitor serve as potential anticancer immunomodulators. *J. Inorg. Biochem*. 195, 130–140. doi: 10.1016/j.jinorgbio.2019.02.004

Hussaini, S. Y., Haque, R. A., and Razali, M. R. (2019). Recent progress in silver (I)-, gold (I)/(III)- and palladium (II)-N-heterocyclic carbine complexes: a review towards biological perspectives. *J. Organomet. Chem*. 882, 906–911. doi: 10.1016/j.jorganchem.2019.01.003

Keller, J. (2011). *Understanding NMR Spectroscopy*. Chichester: John Wiley & Sons Ltd.

Khan, S., Malla, A. M., Zafar, A., and Naseem, I. (2017). Synthesis of novel coumarin nucleus-based DPA drug-like molecular entiry: *in vitro* DNA/Cu(II) binding, DNA cleavage and pro-oxidant mechanism for anticancer action. *PLos ONE* 12:e0181783. doi: 10.1371/journal.pone.0181783

Kosmider, B., and Osiecka, R. (2004). Flavonoid compounds: a review of anticancer properties and interactions with cis-diamminedichloroplatinum(II). *Drug Dev. Res*. 63, 200–211. doi: 10.1002/ddr.10421

Levitt, M. (2008). *Spin Dynamics: Basics of Nuclear Magnetic Resonance*. Chichester: John Wiley & Sons Ltd.

Lu, Y. Y., Shen, T., Yanh, H., and Gu, W. G. (2016). Ruthenium complexes induce HepG2 human hepatocellular carcinoma cell apoptosis and inhibit cell migration through regulation of the Nrf2 pathway. *Int. J. Mol. Sci*. 17, 775–785. doi: 10.3390/ijms17050775

Makovec, T. (2019). Cisplatin and beyond: molecular mechanisms of action and drug resistance development in cancer chemotherapy. *Radiol. Oncol.* 53, 148–158. doi: 10.2478/raon-2019-0018

Mayer, M., and Meyer, M. (1999). A Fast and sensitive method to characterize ligand binding by saturation transfer difference NMR spectra. *Angew. Chem*. 111, 1902–1906.

Mayer, M., and Meyer, M. (2001). Group epitope mapping (GEM) by STD NMR to identify segments of a ligand in direct contact with a protein receptor. *J. Am. Chem. Soc*. 123, 6108–6117. doi: 10.1021/ja0100120

Monaco, S., Tailford, L. E., Juge, N., and Angulo, J. (2018). Differential epitope mapping by STD NMR spectroscopy to reveal the nature of protein-ligand contacts. *Angew. Chem. Int. Ed*. 57, 15289–15293. doi: 10.1002/anie.201707682

Nepravishta, R., Monaco, S., Munoz-Garcia, J. C., Khimyak, Y. Z., and Angulo, J. (2019). Spatially resolved STD-NMR applied to the study of solute transport in biphasic systems: application to protein-ligand interactions. *Nat. Prod. Commun*. 14, 1934578–19849789. doi: 10.1177/1934578X19849789

Oliveira, K. M., Correa, R. S., Barbosa, M. I. F., Ellena, J. A., Cominetti, M. R., and Batista, A. A. (2017b). Ruthenium(II)/triphenylphosphine complexes: an effective way to improve the cytotoxicity of lapachol. *Polyhedron* 130, 108–114. doi: 10.1016/j.poly.2017.04.005

Oliveira, K. M., Luna-Dulcey, L., Correa, R. S., Deflon, V. M., Cominetti, M. R., and Batista, A. A. (2017a). Selective Ru(II)/lawsone complexes inhibiting tumor cell growth by apoptosis. *J. Inorg. Biochem*. 176, 66–76. doi: 10.1016/j.jinorgbio.2017.08.019

Oliveira, M. S., Barbosa, M. I. F., Souza, T. B., Moreira, D. R. M., Martins, F. T., Villareal, W., et al. (2019). A novel platinum complex containing a piplartine derivative exhibits enhanced cytotoxicity, causes oxidative stress and triggers apoptotic cell death by ERK/p38 pathway in human acute promyelocytic leukemia HL-60 cells. *Redox Biol*. 20, 182–194. doi: 10.1016/j.redox.2018.10.006

Porsch, B., Laga, R., Horsky, J., Konak, C., and Ulbrich, K. (2009). Molecular weight and polydispersity of Calf-thymus DNA: static light-scattering and size-exclusion chromatography with dual detection. *Biomacromolecules* 10, 3148–3150. doi: 10.1021/bm900768j

Roy, S., Sil, A., and Chakraborty, T. (2019). Potentiating apoptosis and modulation of p53, Bcl2, and Bax by a novel chrysin ruthenium complex for effective chemotherapeutic efficacy against breast cancer. *J. Cell. Physiol.* 234, 4888–4909. doi: 10.1002/jcp.27287

Siegel, R. L., Miller, K. D., and Jemal, A. (2019). Cancer statistics. *CA Cancer J. Clin*. 69, 7–34. doi: 10.3322/caac.21551

Tanoli, N. U., Tanoli, S. A. K., Ferreira, A. G., Gul, S., Ul-Haq, Z. (2015). Evaluation of binding competition and group epitopes of acetylcholinesterase inhibitors by STD NMR, Tr-NOESY, DOSY and molecular docking: an old approach but new findings. *MedChemComm*. 6, 1882–1890. doi: 10.1039/C5MD00231A

Tanoli, N. U., Tanoli, S. A. K., Ferreira, A. G., Mehmood, M., Gul, S., Monteiro, J. L., et al. (2018). Characterization of the interaction between coumarin-derivatives and acethylcholinesterase: examination by NMR and dock simulations. *J. Mol. Model*. 24:207. doi: 10.1007/s00894-018-3751-3

Viegas, A., Manso, J., Nobrega, F. L., and Cabrita, E. J. (2011). Saturation-transfer difference (STD) NMR: a simple and fast method for ligand screening and characterization of protein binding. *J. Chem. Educ*. 88, 990–994. doi: 10.1021/ed101169t

Villareal, W., Colina-Vegas, L., Visbal, G., Corona, O., Correa, R. S., Ellena, J., et al. (2017). Copper(I)-Phosphine polypyridyl complexes: synthesis, characterization, DNA/HSA binding study, and antiproliferative activity. *Inorg. Chem.* 56, 3781–3793. doi: 10.1021/acs.inorgchem.6b02419

Wang, F. Y., Tang, X. M., Wang, X., Huang, K. B., Feng, H. M., Chen, Z. F., et al. (2018). Mitochondria-targeted platinum(II) complexes induce apoptosis-dependent autophagic cell death mediated by ER-stress in A549 cancer cells. *Eur. J. Med. Chem.* 155, 639–650. doi: 10.1016/j.ejmech.2018.06.018

Yeo, C. I., Ooi, K. K., and Tiekink, E. R. T. (2018). Gold-based medicine: a paradigm shift in anti-cancer therapy? *Molecules* 23:E1410. doi: 10.3390/molecules23061410

Zhang, C. T., Li, J., Qian, C. G., Luo, X. P., Wang, K. K., Zhao, P. X., et al. (2018). A multifunctional ternary Cu(II)-carboxylate polymeric nanocomplex for cancer thermochemotherapy. *Int. J. Pharm.* 549, 1–12. doi: 10.1016/j.ijpharm.2018.06.048

**Conflict of Interest:** The authors declare that the research was conducted in the absence of any commercial or financial relationships that could be construed as a potential conflict of interest.

frontiers in Chemistry

REVIEW
published: 15 November 2019
doi: 10.3389/fchem.2019.00752

# Solid-Supported Proteins in the Liquid Chromatography Domain to Probe Ligand-Target Interactions

*Marcela Cristina de Moraes*[1]*, *Carmen Lucia Cardoso*[2] and *Quezia Bezerra Cass*[3]

[1] Laboratório SINCROMA, Instituto de Química, Departamento de Química Orgânica, Universidade Federal Fluminense, Niterói, Brazil, [2] Grupo de Cromatografia de Bioafinidade e Produtos Naturais, Departamento de Química, Faculdade de Filosofia, Ciências e Letras de Ribeirão Preto, Universidade de São Paulo, Ribeirão Preto, Brazil, [3] Separare, Departamento de Química, Universidade Federal de São Carlos, São Carlos, Brazil

Ligand-target interactions play a central role in drug discovery processes because these interactions are crucial in biological systems. Small molecules-proteins interactions can regulate and modulate protein function and activity through conformational changes. Therefore, bioanalytical tools to screen new ligands have focused mainly on probing ligand-target interactions. These interactions have been evaluated by using solid-supported proteins, which provide advantages like increased protein stability and easier protein extraction from the reaction medium, which enables protein reuse. In some specific approaches, precisely in the ligand fishing assay, the bioanalytical method allows the ligands to be directly isolated from complex mixtures, including combinatorial libraries and natural products extracts without prior purification or fractionation steps. Most of these screening assays are based on liquid chromatography separation, and the binding events can be monitored through on-line or off-line methods. In the on-line approaches, solid supports containing the immobilized biological target are used as chromatographic columns most of the time. Several terms have been used to refer to such approaches, such as weak affinity chromatography, high-performance affinity chromatography, on-flow activity assays, and high-performance liquid affinity chromatography. On the other hand, in the off-line approaches, the binding event occurs outside the liquid chromatography system and may encompass affinity and activity-based assays in which the biological target is immobilized on magnetic particles or monolithic silica, among others. After the incubation step, the supernatant or the eluate from the binding assay is analyzed by liquid chromatography coupled to various detectors. Regardless of the selected bioanalytical approach, the use of solid supported proteins has significantly contributed to the development of automated and reliable screening methods that enable ligands to be isolated and characterized in complex matrixes without purification, thereby reducing costs and avoiding time-laborious steps. This review provides a critical overview of recently developed assays.

**Keywords: bioaffinity chromatography, ligand screening, ligand-target interactions, zonal bioaffinity chromatography, frontal bioaffinity chromatography, ligand fishing**

OPEN ACCESS

***Edited by:***
*Cosimino Malitesta, University of Salento, Italy*

***Reviewed by:***
*Carmelo Sgarlata, University of Catania, Italy*
*Xia Guan, Louisiana State University, United States*

***Correspondence:**
*Marcela Cristina de Moraes*
*mcmoraes@id.uff.br*

***Specialty section:***
*This article was submitted to Analytical Chemistry, a section of the journal Frontiers in Chemistry*

***Received:*** *10 September 2019*
***Accepted:*** *21 October 2019*
***Published:*** *15 November 2019*

***Citation:***
*de Moraes MC, Cardoso CL and Cass QB (2019) Solid-Supported Proteins in the Liquid Chromatography Domain to Probe Ligand-Target Interactions. Front. Chem. 7:752. doi: 10.3389/fchem.2019.00752*

## INTRODUCTION

The use of solid-supported proteins to evaluate protein-protein interactions and to purify proteins is a well-founded tool (Muronetz et al., 2001; Perret and Boschetti, 2018). Interactions between proteins and small molecules have also been well-explored (de Moraes et al., 2014a; Zheng et al., 2014; Hage, 2017). More recently, solid-supported proteins have been employed not only to assess these interactions, but mainly as a strategy to isolate small molecules from complex combinatory libraries (Forsberg and Brennan, 2014; Zhuo et al., 2016; Vanzolini et al., 2018a; Wang L. et al., 2018). These applications are based on the principle of specific and reversible affinity interactions with the immobilized target protein and correlate well with zonal and frontal chromatography. For this reason, various chromatographic terms have been used.

Terms such as weak affinity chromatography (WAC) (Meiby et al., 2013; Singh P. et al., 2017; Ohlson and Duong-Thi, 2018; Lecas et al., 2019), high-performance affinity chromatography (HPAC) (Hage, 2017; Li Z. et al., 2017; Beeram et al., 2018; Zhang C. et al., 2018), high-performance liquid affinity chromatography (HPLAC) (Zheng et al., 2014), biointeraction chromatography (Wainer, 2004), affinity monolith chromatography (AMC) (Lecas et al., 2019), and cellular chromatography (CC) (Ciesla et al., 2016; Xu et al., 2019) have been largely and correctly employed, but all of them could be well-settled in the general term bioaffinity chromatography, which has been introduced to differentiate them from the classic affinity chromatography (de Moraes et al., 2016).

Moreover, the diverse ways to use solid-supported proteins have created many protocol possibilities and in some-cases it is misleading to name it as chromatography. The problem clearly is not the adopted name, but confusion arises when one misses a reference for not using the correct acronyms. Another problem is when the procedure is named chromatography just because it uses solid-supported proteins, as in the case of some off-line devices, like bio-SPE (Forsberg and Brennan, 2014; Forsberg et al., 2014), fishing (Wang L. et al., 2018; Xu et al., 2019; Zhang et al., 2019), and "functional chromatography" (Kang et al., 2014; Lau et al., 2015). Off-line assays usually aim to identify protein ligands from a mixture with chemical characterization of the isolated (fished) ligands.

Zonal bioaffinity chromatography has been used in several assays to measure the affinity of a given ligand toward a certain protein, as depicted in numerous comprehensive reviews (Jonker et al., 2011; Hage, 2017; Tao et al., 2018b). One of the nicest applications comes from chiral protein columns for assessing interactions of a given enantiomer with its binding site, as with (S)-lorazepam hemisuccinate separation, which was dramatically affected by the use of (S)-warfarin in the mobile phase. This result was used to demonstrate the allosteric interaction between the binding sites of these chiral drugs. The presence of (S)-warfarin in the mobile phase affected the chiral separation of the lorazepam hemisuccinate racemate (Domenici et al., 1991). Competitive binding experiments can be employed to evaluate whether allosteric interactions are cooperative or anti-cooperative (Wainer, 2004). Furthermore, the use of human serum albumin (HSA) column allows the equilibrium between free and bound solutes to be directly determined and can help to monitor how interaction between different ligands changes the protein binding properties. Zonal elution provides information about ligand binding sites in the protein, and the obtained data might also be applied in studies about structure–retention relationships (QSRRs) (Bertucci et al., 2003; Bertucci and Domenici, 2012). Zonal bioaffinity chromatography has created countless possibilities to study protein-solute interactions by means of linear or non-linear elution data (Jozwiak et al., 2002; Vanzolini et al., 2013b; Zheng et al., 2014; Tao et al., 2018b).

In the realm of immobilized enzymes, kinetic parameters can be measured by on-line assays (De Simone et al., 2019); for example, assays with glyceraldehyde-3-phosphate dehydrogenase (GAPDH) (Cardoso et al., 2006) and purine nucleoside phosphorylase (PNP) (de Moraes et al., 2013). These assays allow not only the activity parameters of the immobilized enzyme to be gathered, but also to screen inhibitors (Vanzolini et al., 2013a; Rodrigues et al., 2016) or substrates (Calleri et al., 2014) and to unveil inhibition mechanisms, even for tight inhibitors (Rodrigues et al., 2015).

Frontal bioaffinity chromatography has been employed in thermodynamic and kinetic analyses and can simultaneously provide information about the amount of immobilized protein, the number of active binding sites, and the equilibrium constants of these sites (Lecas et al., 2019). Additionally, the molecular interaction can be identified and characterized in a concentration-independent manner, and, in a mixture, it can be revealed in the range from millimolar to picomolar dissociation constants (Schriemer, 2008; Calleri et al., 2009; Temporini et al., 2013; Hage, 2017). These are probably the main benefits of frontal elution when it comes to assessing molecular interactions in complex combinatory library as compared to zonal elution (Michel et al., 2013).

The classic approaches to isolating ligand hits selectively and identifying them in natural product libraries are not easy and are usually troublesome (**Figure 1**).

The diverse molecular frameworks that are present in a natural product extract are the major bottleneck regarding ligand identification in this matrix. Therefore, many affinity-based screening platforms have been proposed to overcome the tiresome classic approach. In this context, screening assays carried out in a static fashion (Vanzolini et al., 2018b) have been considered as the most interesting means of identifying or isolating ligand hits from complex natural libraries (Cieśla and Moaddel, 2016; Zhuo et al., 2016; Fu et al., 2019).

A critical overview of the use of solid-supported proteins in the domain of chromatography, to disclose interactions between proteins and small molecules, will be discussed herein. In this respect, we will cover zonal and frontal bioaffinity chromatography as the on-line methods, and we will also discuss the off-line approaches. This review covers articles published after 2014 (de Moraes et al., 2014b).

## ON-LINE APPROACHES

Various solid supports and different immobilization protocols can be used to create bioaffinity stationary phases. Suitable supports include open tubular and packed fused silica capillaries

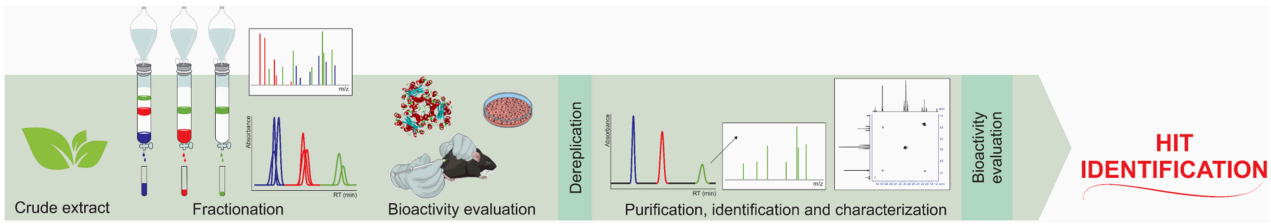


**FIGURE 1 |** Classic bio-guided assay work chart for hit identification in a combinatorial natural product library.

(da Silva et al., 2012; de Moraes et al., 2014a; Wang L. et al., 2018), monolithic supports (Pfaunmiller et al., 2013; Kubota et al., 2017), immobilized artificial membranes (IAM) (Habicht et al., 2015; Yang Y.-X. et al., 2017), silica (Liu G. et al., 2017; Li Z. et al., 2017), and other polymeric and particulate supports. Specificity is the most important characteristic of a solid support: to avoid false positives, the support should not interact with the sample components. Secondary interactions can be examined with a control column, which contains the inactive/denatured target protein or only the solid support that is used to immobilize the target protein. Employing non-ligands as negative controls is another strategy to assess secondary interactions.

In the case of on-line approaches, where the binding event occurs within the liquid chromatography system (i.e., in a chromatographic column), the material that is used as solid support should be mechanically and chemically stable, have rapid mass transfer capacity, and display low backpressure and adequate efficiency. In addition, the solid support should be able to retain the target protein even in the on-flow conditions, while the immobilized target protein should retain the ligand and separate it from the other sample components.

Solid supports can be derivatized with several functional groups, so that countless immobilization procedures can be used to prepare the protein (biological target)-containing stationary phase. One of the most frequently employed methods is to attach primary amines, epoxides, aldehydes, hydroxyls, or carboxylic acids to the solid support structure, which can then form covalent bonds with the different amino acid residues present in the target protein structure (Datta et al., 2013; de Moraes et al., 2013, 2015; Homaei et al., 2013; Mohamad et al., 2015; Li Q. et al., 2017; Tao et al., 2019). Other procedures are based on non-covalent immobilization, like protein adsorption onto the solid support (Ma et al., 2015; Zhan et al., 2016), entrapment (Anguizola et al., 2016; Yang Y.-X. et al., 2017) and biospecific adsorption (Temporini et al., 2013), but they are more susceptible to protein desorption, particularly in on-line systems.

Immobilization can be carried out "*in situ*" (Chen X. et al., 2017; Tao et al., 2018a); that is, all the protein immobilization steps are conducted within the LC-suitable devices (columns, microcolumns, capillaries, disks, etc) or "in batch" (Habicht et al., 2015; Zhan et al., 2016), when the target protein is immobilized on the solid support for later packing. In the former case, the target protein structure can change (including enzyme inactivation) during the column packing process. However, the use of the "in batch" methodology to prepare bioaffinitity columns has spread considerably (see **Table 1** for data about immobilization procedures that are used to prepare solid supports for frontal bioaffinity chromatography (FAC) assays).

Zonal (linear and non-linear) chromatography and frontal affinity chromatography are the elution modes that are most often employed in bioaffinity chromatography assays. This section will discuss the application of zonal and frontal bioaffinity chromatography in on-line systems to probe and to characterize ligand-target protein interactions.

## Frontal Bioaffinity Chromatography

Frontal analysis involves continuous analyte infusion into the chromatographic column, so it generally requires larger sample injection volumes. In this approach, the experiments are carried out under dynamic equilibrium conditions, and the ligands (or the analytes as potential ligands) are continuously infused through the column. As the bioaffinity column stationary phase becomes saturated, the concentration of ligands eluting from the column increases gradually until a plateau is reached. Ligands break through the column at distinct times according to their concentration and affinity for the stationary phase (ideally, for the immobilized protein target). Therefore, the ligands can be ranked, and the binding constants can be precisely determined (Calleri et al., 2009, 2010; de Moraes et al., 2016).

FAC studies can be conducted by directly monitoring the ligand elution profile in an approach known as direct assay, in which the retention pattern is directly associated with ligand concentration and affinity for the immobilized protein target. Displacement studies are considered indirect assays because a known ligand is used as marker, and interaction between an analyte and the immobilized protein target is indirectly evidenced by a displacement of the marker elution profile due to competition by the binding sites, as illustrated in **Figure 2**.

In ranking experiments accomplished by FAC, during which mixtures of compounds are continuously infused into the chromatographic column containing the immobilized protein target, the detector should be able to discriminate the elution profile of each component of the initial mixture, and the use of a selective detector like electrospray ionization mass spectrometry is mandatory due to its ability to distinguish between different co-eluting m/z values (Slon-Usakiewicz et al., 2005; Ng et al., 2007; Calleri et al., 2011).

**TABLE 1 |** Literature studies that have used FAC assays to probe ligand-target interactions.

| Target | Solid support | Immobilization method | Ligands | References |
|---|---|---|---|---|
| Human serum albumin (normal and glycated) | Nucleosil Si-300 silica | Covalent via Schiff base formation (*in situ*) | Chlorpropamide Glimepiride (FAC), warfarin, L-tryptophan, tamoxifen, and digitoxin in zonal elution | Matsuda et al., 2015; Tao et al., 2018a |
| Beta2-adrenoceptor | Silica gel | Covalent (In batch) | Salbutamol and terbutaline for characterization; bioactive compound in Shaoyao-Gancao decoction | Li Z. et al., 2017 |
| Thrombin | IAM | Entrapment (*in situ*) | Ferulic acid, gallic acid, protocatechuiic acid, chlorogenic acid, and sinapic acid | Yang Y.-X. et al., 2017 |
| Angiogenesis inhibitor Kringle 5 | Silica gel | Oriented immobilization by histidine-tagged attachment | L-lysine, epsilon-aminocaproic acid (EACA), 7-aminoheptanoic acid (7-AHA), trans-4-(aminomethyl)cyclohexane carboxylic acid (AMCHA), and benzylamine | Bian et al., 2015 |
| Cell membrane from rat brains containing dopamine receptor | Silica gel | Adsorption onto the solid support (In batch) | Dopamine, olanzapine, quetiapine, bupropion, and domperiodone | Ma et al., 2015 |
| Human Purine Nucleoside Phosphorykase (HsPNP) | Capillary (open tubular and monolithic) | Covalent (*in situ*) | HsPNP inhibitors with different inhibitory potencies | de Moraes et al., 2014a |
| Membranes from cells containing A2A adenosine receptor subtype | IAM and open tubular capillary | Covalent (*in situ*) in the open tubular capillary and biospecific adsorption/entrapment in IAM support (In batch) | 8-substituted-9-ethyladenines (four derivatives) | Temporini et al., 2013 |
| Voltage-dependent anion channel isoform 1 (VDAAC-1) | Macroporous silica gel | Covalent immobilization on silica gel surface using phospholipid monolayer (In batch) | ATP, NADH, and NADPH | Li Q. et al., 2017 |
| Cell membranes containing human α3β4α5 and α3β4 nicotinic receptors | IAM | Entrapment (In batch) | Epibatidine, nicotine, cytisine, nornicotine, and anabasine | Ciesla et al., 2016 |
| Translocator proteins in mitochondrial transmembrane proteins from monkey skeletal muscle and human platelets | IAM | Adsorption/entrapment (In batch) | Dipyridamole and translocator protein ligands (PK11195, photoporphyrin IX, and rotenone) | Singh N. S. et al., 2017 |
| Translocator proteins in mitochondrial transmembrane proteins from U87MG and HEK-293 cells | IAM | Adsorption/entrapment (In batch) | Dipyridamole, PK-11195, mesoporphyrin IX, photoporphyrin IX, and rotenone (translocator protein ligands) | Habicht et al., 2015 |
| β2-adrenoreceptor | Silica gel | Covalent (*in situ*) | Protopine | Liu G. et al., 2017 |
| Cell membranes containing $\alpha_{1A}$ adrenoreceptor from HEK293 cell line | Silica | | Tamsulosin hydrochloride and seven alkaloids | Wei et al., 2017 |
| Human serum albumin (normal and glycated) | Nucleosil Si-300 silica | Covalent via Schiff base formation (*in situ*) | Tolazamide | Tao et al., 2019 |
| High epidermal growth factor from HEW293 cells | Silica | Adsorption (In batch) | Taspine derivatives (TPD7 and HMQ1611) and afatinib | Zhan et al., 2016 |
| TEM-1 beta-lactamase | Silica gel | Covalent (*in situ*) | Beta-lactam antibiotics (cafelexin, penicillin G, and cefoxitin) | Chen X. et al., 2017 |

FAC methods allow ligand-target interactions to be determined in terms of dissociation ($K_d$) or association ($K_a$) constants, where $K_d = 1/K_a$, through the basic FAC equation:

$$(V - V_0) = B_t \times \frac{1}{[L] + K_d} \quad (1)$$

Where $B_t$ is the number of available binding sites, V is the ligand breakthrough volume, $V_0$ is the breakthrough volume in the absence of the binding event, [L] is the ligand concentration, and $K_d$ is the dissociation constant.

A frontal chromatography assay called modified staircase method is an alternative strategy to assess $K_d$ and $B_t$. The washing and equilibrium steps between the individual analysis

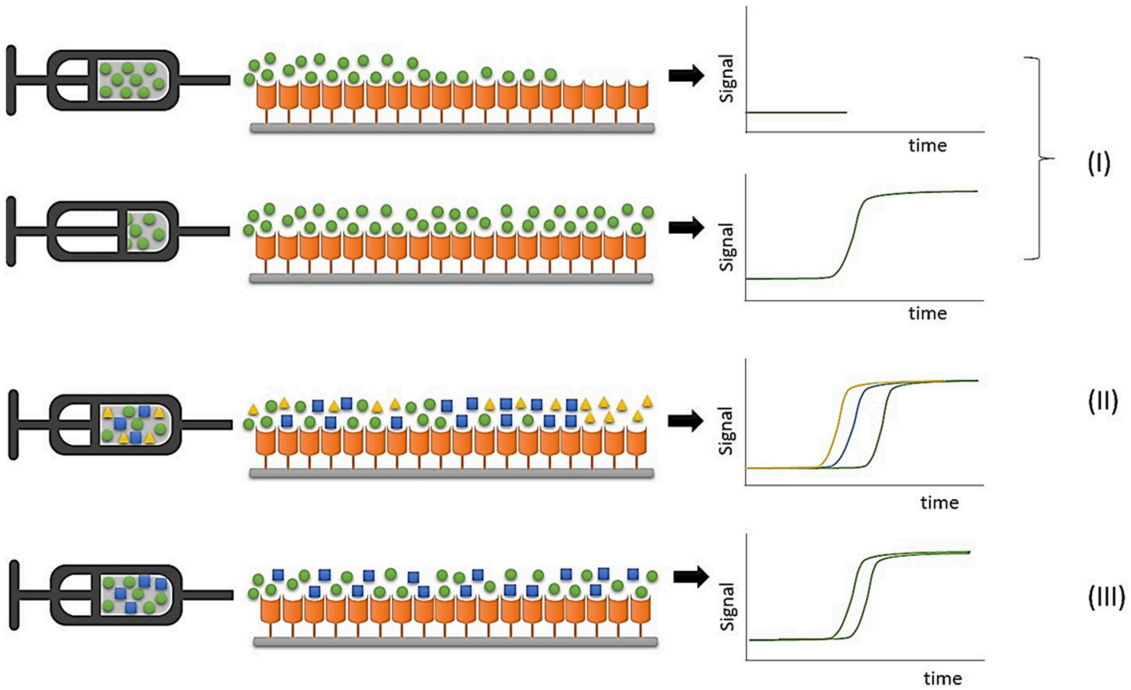


**FIGURE 2 |** Representative illustrations of FAC experiments. (I) Direct assays to determine binding constants with an individual ligand infusion; (II) Ranking assays to classify compounds in mixtures; (III) Displacement experiments to evaluate ligand-protein interaction by monitoring a marker ligand.

of each evaluated concentration in FAC assays is time-consuming, and the modified staircase (or stepwise frontal analysis) (He et al., 2018) constitutes a promising method to determine the binding constants (de Moraes et al., 2016). In this assay, the ligand is sequentially infused until saturation by a series of low-to-high concentrations is achieved, forming a staircase pattern; with simultaneously infusion of a void marker at a fixed concentration. Columns containing human serum albumin (HSA) and alpha-1-acid glycoprotein (AGP) have been employed to determine the equilibrium dissociation constant $K_d$ for warfarin- and digitoxin-HSA and verapamil- and tamsulosin-AGP interactions by direct FAC and stepwise frontal analysis. $K_d$ values obtained through the different approaches correlate well with literature values, evidencing that the modified staircase method can be applied to assess the binding constants (He et al., 2018).

The interaction between three β-lactam antibiotics (penicillin G, penicillin V, and cefalexin) and bovine serum albumin (BSA) has been investigated by FAC–UV (Li et al., 2016), by delivering 200 mg of the target protein through a stainless-steel column (50 × 4.6 mm I.D.) to immobilize the target covalently. When different ligand concentrations are infused during the FAC experiments, the binding constants for the ligand-target protein interaction ($K_a$) and the number of binding sites in the stationary phase can be determined. Displacement experiments were conducted to investigate the binding site of the selected ligands: $K_a$ values of all the three β-lactam antibiotics decrease in the presence of warfarin, an anticoagulant that binds to binding site 1 in subdomain II A, demonstrating that the binding sites of these drugs to BSA are mainly located therein.

FAC–MS has been employed to assess the adsorption data of three drugs (salbutamol, terbutaline, and pseudoephedrine) and the beta-2-adrenoreceptor ($\beta_2$-AR) attached to polystyrene amino microspheres (Li et al., 2018). Adsorption data of the selected drugs obtained by FAC–MS and site-specific studies have helped to investigate the adsorption models for the binding of each ligand through adsorption energy distribution calculations. In addition, FAC–MS competitive assays have been described as an efficient strategy to screen $\beta_2$-AR ligands by displacement experiments.

BSA has also been covalently immobilized on penetrable silica microsphere through an "in batch" methodology (Ma et al., 2016), and the ability of the BSA-containing stationary phase to separate D- and L-tryptophan was assessed in the zonal elution mode, to evidence that the bioaffinity column is enantioselective. Further FAC–UV studies helped to probe the interaction between imatinib mesylate and BSA, allowing the number of active binding sites on the stationary phase and $K_a$ to be determined.

$Alpha_1$-acid glycoprotein (AGP) has been immobilized "*in situ*" by physical entrapment in microcolumns packed with hydrazide-activated porous silica (1 cm × 2.1 mm) and applied in frontal and zonal elution studies to investigate the binding of different ligands. Frontal studies revealed the association equilibrium constant ($K_a$) and the moles of binding sites for the AGP-carbamazepine interaction. FAC experiments with a control microcolumn (without entrapped AGP) pointed to some

non-specific interactions with the support, which has frequently been observed in microparticulate supports (Xuan et al., 2010; Anguizola et al., 2016). Microcolumn heterogeneity can stem from the microparticulate support being incompletely coated with the target protein, to result in specific binding regions (ligand-target protein) and non-specific interaction regions (ligand-solid support) (Muller and Carr, 1984; Tweed et al., 1997).

FAC provides a lot of information about the immobilized target protein and the ligand-target protein interaction recognition. As can be noted in **Table 1**, FAC is a versatile approach that enables various proteins and ligands to be studied by different methods. Some studies have explored all the possibilities of this elution approach to probe ligand-target protein interactions through different assays (ligand characterization by direct assays, ligand ranking, displacement) (Temporini et al., 2013; de Moraes et al., 2014a; Ciesla et al., 2016; Chen X. et al., 2017; Yang Y.-X. et al., 2017), while other studies have used this elution mode to characterize the physicochemical properties of the target protein-containing solid support associated with the zonal elution mode for affinity and displacement studies (Habicht et al., 2015; Ma et al., 2015; Guo et al., 2017; Liu G. et al., 2017; Tao et al., 2018a). The next section discusses the potential of the state-of-the-art zonal elution to probe ligand-target protein interactions.

## Zonal Chromatography

In liquid chromatography, zonal elution encompasses injecting a small amount of analyte through a column and using an online detector to monitor the analyte elution time or volume. This elution mode has great potential to probe ligand-target protein interactions when immobilized target protein-containing stationary phases are employed. Compared to the amount of target protein that is immobilized on the solid support, the amount of injected ligand is negligible (a requisite for linear elution), however, non-linear elution conditions have been also employed to probe ligand-target protein interaction by zonal chromatography (Vanzolini et al., 2013b; Li Q. et al., 2015, 2017; Liang et al., 2018).

Although zonal elution involving on-line detectors has been considered the most common approach, literature papers have also described some off-line assays in which a fraction from the zonal elution experiment is collected and analyzed on an off-line detector, mainly when the experiment is conducted in a low-performance target-containing column (Tao et al., 2018b).

Affinity assays by zonal chromatography can provide information on the ligand-target protein interaction by direct measurements or competition experiments. Direct measurements entail peak retention time monitoring, retention factor determination, or peak profile evaluation. As for competition experiments, a known ligand is added to the mobile phase, and an analyte (second ligand or potential ligand) is injected into the chromatographic system, to monitor the time or volume that is necessary to elute the analyte from the bioaffinity column (Zheng et al., 2014; Tao et al., 2018b). Competition assays are also a useful tool to investigate the binding site of different ligands.

The binding event can be evaluated by injecting a small amount of the ligand into the bioaffinity column and monitoring the elution time (to determine the peak retention time and retention factors) and/or peak profile. When the ligand-target protein interaction occurs through fast association and dissociation kinetics, the ligand retention time should be directly associated with the ligand-target protein interaction strength and the amount of immobilized target protein (Gargano et al., 2014; Zhan et al., 2016; Ohlson et al., 2017). The elution time (or volume) should be monitored along with a void volume marker and, to obtain reliable results, the ligand-target protein interaction specificity should be investigated by using a control column (solid support without the immobilized target protein or with the immobilized inactive target protein). When the elution times of different ligands are compared, they can be ranked according to their affinity for the immobilized target protein. Equations to explore the ligand-target protein binding event are available in recent reports (Zheng et al., 2014; Tao et al., 2018b).

Competition assays are performed by employing a displacer agent in the mobile phase, which shifts the ligand retention as both compounds (the ligand and the displacer agent) compete for the same binding site on the immobilized target protein surface (Gao et al., 2014; Matsuda et al., 2015; Anguizola et al., 2016; Liu G. et al., 2017; Wei et al., 2017; Tao et al., 2018a, 2019).

Information regarding the binding site for the ligand-target protein interaction and the nature of this interaction can be assessed by meticulously examining the experimental conditions in zonal experiments: mobile phase pH, polarity, and ionic force, presence of other ligands (displacing or competing agents), temperature, ligand type, and target protein (Zheng et al., 2014).

Ligand binding to the target protein can be monitored and characterized by the peak profile obtained in the zonal elution assays. In this approach, a small ligand sample is injected into the bioaffinity column and the control column. The eluted peak width is used to gather information regarding the ligand-target protein binding kinetics. This methodology, also known as band-broadening measurement, encompasses the plate height method and the peak profile method (Chen et al., 2009; Yoo and Hage, 2011; Hage, 2017). Other strategies like the peak decay, peak fitting, and split-peak methods can be employed to investigate the ligand-target protein binding event kinetics (Bi et al., 2015; Beeram et al., 2017; Anguizola et al., 2018; Liang et al., 2018), but they are outside the scope of this review.

Zonal elution has also been applied to monitor on-line enzyme activity in ligand screening assays, resulting in reliable and specific assays that allow the biocatalysis product to be directly quantified (da Silva et al., 2012; de Moraes et al., 2013; Calil et al., 2016; Lima et al., 2016; Magalhães et al., 2016; Ferreira Lopes Vilela and Cardoso, 2017; Cornelio et al., 2018; Vilela et al., 2018; Seidl et al., 2019). This approach prevents interferences in inhibitors screening and furnishes reliable data concerning the substrate- and inhibitor-enzyme binding. Recently, the activity of two classes of acetylcholinesterases (AChE) from *Atta sexdens* immobilized on capillary columns was monitored by directly quantifying choline, obtained from the hydrolysis of acetylcholine, which is the AChE natural substrate. The traditional colorimetric assay (Elman method), which employs

acetylthiocoline as substrate, results in inverse AChE-substrate affinities for the two different classes of AChE (Dos Santos et al., 2019). This evidences that direct assays are important to monitor the enzyme activity and to characterize binding affinities.

Some recent papers on zonal bioaffinity chromatography for enzyme activity assays have used different protein targets simultaneously in the chromatography system to yield selectivity and specificity results fast. A simultaneous on-flow enzyme assay that uses two different immobilized enzymes (AChE and butyrylcholinesterase) in parallel in the chromatography system has been recently reported. In this approach, the inhibitory activity of an analyte can be simultaneously evaluated for both enzymes by using two 10-port/two-position switching valves with a single injection in a process that takes <6 min (Seidl et al., 2019).

On-line bioaffinity chromatography studies have been employed to isolate ligands from mixtures by means of different strategies. In 2014, Forsberg and Brennan used covalently linked adenosine deaminase (ADA) columns to isolate and to extract inhibitors from complex mixtures by combining activity- and affinity-based assays (Forsberg and Brennan, 2014). In a first moment, this strategy involved screening different mixtures in an activity-based assay. After that, the identified bioactive mixtures were infused in an ADA-containing monolithic silica capillary column until MS detector saturation was achieved, which is followed by a wash step to remove unbound compounds. The retained ligands were eluted with a harsh wash and identified by MS/MS.

More recently, multidimensional liquid chromatography systems (2D-LC) have been explored to isolate and to extract ligands from complex matrixes through fully automated systems (Han et al., 2013; Jia et al., 2016; Wu et al., 2016; Guo et al., 2017; Wang et al., 2017; Wang X.-Y. et al., 2018). In this context, an immobilized xanthine oxidase microcolumn was used to selectively retain bioactive compounds from *L. macranthoides* extract and to transfer them to an analytical column, where the identified inhibitors are isolated. The 2D LC–MS/MS system enabled nine bioactive compounds from *L. macranthoides* to be rapidly isolated (Peng et al., 2016).

Comprehensive two-dimensional chromatography was applied to investigate bioactive compounds from *Indigo naturalis*, a famous Traditional Chinese Medicine that is used in the treatment of leukemia in China. Columns containing active components and membrane receptors from the K562 cell line were used in the first dimension to retain the bioactive compounds selectively and to transfer them to the second dimension via two trap columns, with an $C_{18}$ analytical column with detection by QqTOF. Three active compounds were characterized, and their anti-leukemia effect was confirmed by cell viability and cell apoptosis assays (Wu et al., 2016).

A 2D-LC–MS screening platform was designed to isolate AChE ligands from *Corydalis yanjusuo* extracts selectively. To this end, monolithic AChE capillaries were used as the bioaffinity columns in the first dimension. To avoid false results caused by non-specific binding, control experiments were run simultaneously with a denatured enzyme column. Eight AChE ligands were isolated from this experiments and their inhibitory activities were confirmed by activity-based assays (Wang L. et al., 2018).

Columns with solid supports containing cell membranes from rat hearts (normal and pathological tissue) have been employed in an on-line chromatography system (comprehensive 2D using a 10-port-dual-position valve) to screen specific therapeutic agents from *Acontium carmichaeli* that can counteract doxorubicin-induced heart failure (Chen et al., 2014).

Advantages of the zonal elution mode for bioaffinity chromatography include versatility in terms of methodology (as seen from the numerous approaches presented and discussed herein), use of a small amount of sample, and possibility of full automation systems even during control experiments conducted in parallel with the binding assays.

## OFF-LINE STATIC APPROACHES

Considered as one of the most efficient and convenient methods to separate potential ligands from complex mixtures, the affinity-based screening assay can be applied to investigate multiple interacting pairs involved in biological systems such as antigen-antibody, receptor-ligand, enzyme-inhibitor/activator, and protein-protein (Hage et al., 2012). These assays employ many macromolecular targets, like receptor, enzyme, transport protein, and cell membrane (Zhuo et al., 2016).

Taking advantage of diverse targeting immobilization methods and several analytical approaches, ligand fishing strategies have emerged as practical and effective procedures to fish out ligands from complex mixtures. Ligand fishing experiments essentially rely on the fact that any compound with affinity for the immobilized target protein is retained (affinity selection) for further analysis, while non-binding compounds remain in the extract/supernatant and can be discarded (Zhuo et al., 2016). Briefly, this approach is carried out by an immobilization procedure, followed by an incubation step, washing to separate binders from non-binders, and binder desorption and characterization (**Figure 3**). Analytical approaches based on LC–MS are generally employed to obtain a chemical profile of the ligands with affinity for the immobilized target protein. These ligands can be structurally characterized either directly, by conducting LC–HRMS of the ligand-containing fraction, or through targeted LC–PDA–HRMS–SPE–NMR analysis of the crude extract (Arai et al., 2009; Wubshet et al., 2015; Cieśla and Moaddel, 2016). The ligand-bound complex is usually separated from the unbound compounds by approaches like ultrafiltration, dialysis, affinity purification, size-exclusion chromatography, magnetic separation, and hollow fiber adsorption, among others (Moaddel et al., 2007; Song et al., 2015; Wang et al., 2015; Zhuo et al., 2016; Hu et al., 2018). The applied method will depend on the support material.

The use of ligand fishing assays has increased in the search for bioactive natural products. Target proteins have been immobilized on various supports, including magnetic beads (de Almeida et al., 2017; Wang Z. et al., 2018; Tang et al., 2019), quantum dots (Hu et al., 2018), hollow fibers (Chen L. et al.,

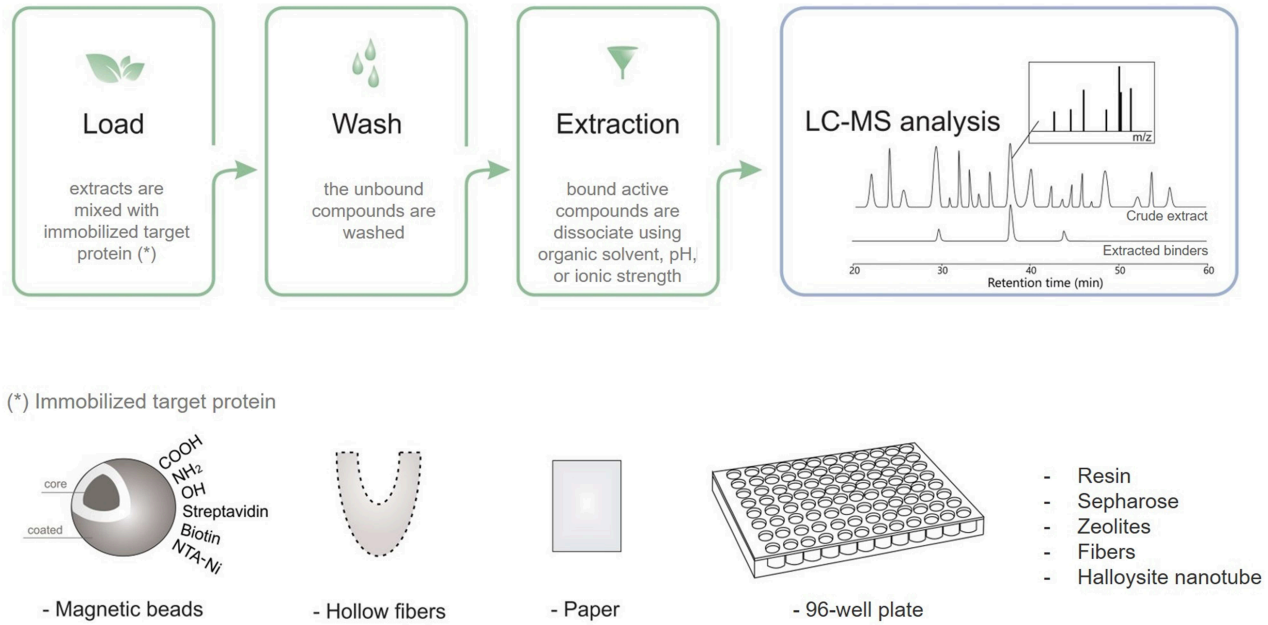


**FIGURE 3 |** Schematic ligand fishing approach applied to screen active compounds from complex mixtures.

2017), nanotubes (Wang et al., 2015), and monolithic silica (Forsberg and Brennan, 2014).

## Magnetic Supports

Magnetic supports or magnetic particles (MPs) are also known as magnetic beads (MBs), micro- and nanosized magnetic beads, paramagnetic beads (PBs), ferrofluids, and magnetic fluids, and they are an excellent support option (Marszałł, 2011). Protein immobilization on MBs offers the following advantages: stable immobilization (protein-protein complexes remain intact on the protein-coated MB surface) and easy magnetic isolation with the use of external magnets (which prevents contact with the analyte solution) (Marszałł et al., 2008; Zhuo et al., 2016). Ligand fishing assays based on magnetic particles are an outstanding tool to identify bioactive constituents in plant extracts (Zhuo et al., 2016; Tang et al., 2017, 2019; Yang X.-X. et al., 2017; Vanzolini et al., 2018b; Wang Z. et al., 2018; Wubshet et al., 2019; Zhang et al., 2019).

One advantage of using MBs is that they allow low-affinity ligands and secondary metabolites of low abundance, but with great affinity for the target protein to be identified. Such ligands and metabolites are normally overlooked when other screening techniques are employed.

Moaddel et al. were the first to apply MBs for ligand fishing (Moaddel et al., 2007). By using human serum albumin (HSA), they showed that a protein-coated MB fishes out known binders from a mixture of binders and non-binders. HAS-coated MBs have affinity selection, as demonstrated in the study involving control beads (blank) without immobilized HSA. The results reported by these authors correlate with data previously reported for bioaffinity chromatography assays. A rate limiting step of ligand fishing experiments is the amount of protein that is required for the successful fishing experiments, typically 50 μg (Cieśla and Moaddel, 2016). Since the publication of this pioneering work, several proteins have been immobilized on MBs and used to disclose ligands from complex mixtures (Cieśla and Moaddel, 2016; Zhuo et al., 2016; Liu et al., 2017a; Yang X.-X. et al., 2017).

de Almeida et al. (2017) extracted angiotensin-converting enzyme (ACE) from bovine lung, purified it, and covalently immobilized it on modified ferrite magnetic beads (ACE-MBs) to fish out not only the reference inhibitor, but also one peptide from a pool of tryptic digested BSA.

A fluorimetric ACE inhibitor assay was developed by immobilizing ACE on anti-FLAG antibody-coated MBs by using a 96-well microplate operation, fluorescence detection, and a two-step screening assay (Tang et al., 2019). On the basis of primary screening, five compounds exhibited inhibition rate >25% [(+)-tetrandrine, fangchinoline, narcissoside, epiberberine, and verbascoside]. Because natural products can affect the fluorescence, the product standard solution was mixed with test compounds and then derivatized for fluorescence detection to evaluate the fluorescence change in the second step. A fluorescence alteration over 25% was considered as interference. Fluorescence intensification can lead to false-negative results, while reduced fluorescence can provide false-positive results. According to the findings, ten compounds, including the five hits from the preliminary screening, decreased the fluorescence by over 25%, but no compound intensified the fluorescence. Epiberberine and fangchinoline displayed better

ACE inhibition activity with $IC_{50}$ values of 52.61 ± 4.12 and 97.48 ± 5.34 μM, respectively.

Membrane-bound α-glucosidase enzyme-coated MBs have successfully fished out four natural α-glucosidase ligands from *E. catharinae* (Wubshet et al., 2015). Designed chitosan-enriched magnetic composites were also used to immobilize α-glucosidase and to disclose enzyme inhibitors from extracts of Traditional Chinese medicines (TCMs) and vegetables (Liu et al., 2017b).

AChE has been successfully immobilized on MBs to screen compounds from plant extracts (Vanzolini et al., 2013b, 2018b). Moreover, *Electrophorus electricus* (*eel*) AChE-coated amino-modified paramagnetic beads have been applied in an affinity-based ligand-fishing assay to discover bioactive peptides from complex protein mixtures from black mamba venoms. Tryptic digestion followed by nano-LC-MS analysis of the material recovered from black mamba venom identified the peptide with the highest AChE-binding affinity as dendrotoxin-I, a pre-synaptic neurotoxin that had not been known to interact with AChE (Vanzolini et al., 2018a).

α-Amylase-coated magnetic nanoparticles have been employed to fish out ligands from *Garcinia xanthochymus* extracts, which led to three biflavonoids being identified as inhibitors (Li et al., 2014).

Deng et al. (2014) established a screening assay based on magnetic $Fe_3O_4$@$SiO_2$-COX-2 ligand fishing combination with LC–DAD–$MS^n$ to screen and to identify COX-2 inhibitors from green tea. The authors fished out eight catechins with COX-2 binding activity, two of which for the first time. For $Fe_3O_4$@$SiO_2$-COX-1, four curcuminoids were isolated as main COX-1 inhibitors (Zhang et al., 2014).

Zhang et al. (2019) used monoamine oxidase-A (MAO-A) immobilized on the MB surface (MAO-A-MBs) to conduct ligand fishing and LC-HRMS to characterize ligands. Seven compounds (tetrahydrocolumbamine, protopine, jatrorrhizine, glaucine, tetrahydropalmatine, palmatine, and dehydrocorydaline) with high binding affinity for MAO-A were identified from the *Corydalis Rhizome* extract ethyl acetate fraction. The immobilized MAO-A activity remained over 80% after storage at 4°C for about seven days.

Glycogen synthase kinase-3β (GSK-3β) was immobilized on MBs and used to screen the inhibitory activities of 15 TCM extracts. Three of these TCMs, *Euonymus fortunei*, *Amygdalus communis*, and *Garcinia xanthochymus*, exhibited high inhibitory activity (inhibition rate > 90%). A new GSK-3β inhibitor, called fukugetin, with an $IC_{50}$ value of 3.18 ± 0.07 μM was discovered in the *G. xanthochymus* extract. The immobilized enzyme was reused 10 times and remained stable at 4°C for 4 days (Li Y. et al., 2015).

de Moraes et al. (2015) immobilized cellular prion protein (PrP) on MB surface and applied it to isolate ligands in a mixture of compounds by employing LC-MS. The anti-prion compound quinacrine, an inhibitor of PrP aggregation, was isolated.

Recent developments in biological systems and overall clinical experience have suggested that, due to homeostatic nature, single-target drugs may not always induce the desired effect on the entire biological system even if they successfully inhibit or activate a specific target (Pang et al., 2012). Thus, the concept and the strategy of developing multi-target or multi-component drugs have recently been proposed (Zimmermann et al., 2007; Wang et al., 2012). Although countless valuable studies have reported the use of approaches based on protein-coated MBs that can identify active compounds from medicinal plant extract fast, most previous research has focused on ligand binding to a single target.

Tao et al. (2013a) developed a multi-target strategy to screen bioactive compounds from a botanical drug by immobilizing multiple targets (maltase, invertase, and lipase) on the MBs through covalent linkage. This approach was applied to screen ligands from the Chinese medicine "Tang-Zhi-Qing," which is used to treat type II diabetes in China. To this end, the authors placed MBs immobilized with different targets (e.g., maltase, invertase, and lipase) into three connecting chambers separately and pumped the unpurified botanical drug into the chambers by means of a peristaltic pump. They found that incubation leads the ligands to bind to the targets, as attested by the LC-MS analysis conducted after the wash and extraction steps. Therefore, this approach successfully fished out seven ligands which bound to the three immobilized target enzymes. Even though paeoniflorin and salvianolic acid B could bind to the enzymes, they showed no maltase, invertase, or lipase inhibitory activity at all. Compared to classic screening methods, the proposed approach can rapidly identify bioactive compounds that specifically bind to different targets, which could enhance the discovery of active compounds.

Imaduwage et al. (2016, 2017) described a detection strategy to fish out strong binders only. In this approach, the inhibitors/binders were incubated with the protein (binding experiment) and, separately, with blocked beads (control experiment). After incubation time the non-binding compounds from both experiments were removed and analyzed by LC-MS. Strong binders were identified by comparing the spectral data of the control and binding experiments. **Table 2** list other applications of MB-bioreactors.

## Other Supports

Over the last decade, many nanomaterials, such as carbon and $TiO_2$ nanotubes, have been used as microextraction medium for selective enrichment with specific compounds (Zhuo et al., 2016).

Hollow fibers have been widely used to pretreat samples (Yang et al., 2015). During hollow fiber adsorption, screening targets are immobilized on the inner wall of a hollow fiber via physical adsorption (Yang X.-X. et al., 2017). Physical adsorption onto hollow fibers is easier and prevents protein structural modification during the chemical binding process (Zhuo et al., 2016).

Wang et al. (2015) were the first to establish lipase-adsorbed halloysite nanotubes (HNTs) for ligand fishing from natural products extracts. They reported that three flavonoids were rapidly isolated and identified as lipase ligands from *Lotus leaf* extract (Tao et al., 2013b). Later, the same research group successfully fished out four neolignan compounds from *Magnoliae cortex* extracts. The target protein adsorbed onto hollow fibers had short activity time, and only a few targets could be adsorbed, so the sensitivity of this method was limited.

**TABLE 2 |** Ligand fishing strategies based on MB-bioreactors on TCM.

| Target | Plant | Method | Active compounds | References |
|---|---|---|---|---|
| α-amylase | Garcinia xanthochymus | Enzyme coated magnetic nanoparticles | GB2a glucoside, GB2a, and fukugetin | Li et al., 2014 |
| Xanthine oxidase | *Radix Salviae Miltiorrhizae* | Affinity selection-based 2D chromatography coupled with LC-MS | Salvianolic acid C and Salvianolic acid A | Fu et al., 2014 |
| Cyclooxygenase-1 (COX-1) | *Turmeric* | Enzyme coated magnetic nanoparticles | Curcumin, demethoxycurcumin, bisdemethoxycurcumin, and 1-(4-hydroxy-3,5-dimethoxyphenyl)-7-(4-hydroxy-3-methoxyphenyl)-(1*E*,6*E*)-1,6-heptadiene-3,5-dione | Zhang et al., 2014 |
| Cyclooxygenase-2 (COX-2) | *Green tea* | Enzyme coated magnetic nanoparticles | (-)-Epigallocatechin-3-(3″-*O*-methyl)-gallate and (-)-epicatechin-3-(3″-*O*-methyl)-gallate | Deng et al., 2014 |
| GSK-3β | *Euonymus fortunei* and *G. xanthochymus* | Magnetic beads | Fukugetin | Li Y. et al., 2015 |
| α-Glucosidase s | *Eugenia catharinae* | Enzyme coated magnetic bead | 5-(2-Oxopentyl)resorcinol 4-*O*-β-D-glucopyranoside, 5-propylresorcinol 4-*O*-β-D-glucopyranoside, 5-pentylresorcinol 4-*O*-[α-D-apiofuranosyl-(1 → 6)]-β-D-glucopyranoside, 5-pentylresorcinol 4-*O*-β-D-glucopyranoside, 4-hydroxy-3-*O*-methyl-5-pentylresorcinol 1-*O*-β-D-glucopyranoside, and 3-*O*-methyl-5 pentylresorcinol 1-*O*-[β-D-glucopyranosyl-(1 → 6)]-β-D-glucopyranoside | Wubshet et al., 2015 |
| Neuronal cells | *Radix Polygalae* | PC12 cell membrane chromatography-LC–(Q)TOF-MS | Onjisaponin B | Wu et al., 2015 |
| Lipase | *Magnoliae cortex* | Lipase-adsorbed nanotube combined with LC–MS analysis | Magnotriol A and magnaldehyde B | Wang et al., 2015 |
| SIRT6 | *Trigonella foenum-graecum* | SIRT6-coated magnetic beads | Orientin and 17 other compounds | Singh et al., 2014 |
| α-glucosidase | *Codonopsis pilosula, Rhizoma coptidis, Forsythia, Radix hedysari, Semen allii tuberosi, Radix isatidis, Rhizoma atractylodis macrocephalae, Glycyrrhiza uralensis Fisch, Folium Mori, Radix Ophiopogonis, Radix Puerariae, Platycodon grandiflorus, Radix Astragali, Radix Notoginseng, Radix et Rhizoma Rhei, Cortex Moutan, Phellodendron amurense, Eucommia ulmoides* | α-glucosidase- coated $Fe_3O_4$/CS/GA/α-Glu nanoparticles coupled to capillary electrophoresis | | Liu et al., 2017a |
| Neuraminidase | | surface of magnetic beads | luteolin-7-O-β-D-glucoside, luteolin, 3,5-di-O-caffeoylquinic acid, and 3,4-di-O-caffeoylquinic acid | Zhao et al., 2018 |

Hollow fiber adsorption has been used to screen ligands of living cells, cell membranes, organelles, and enzymes (Liu et al., 2014; Chen et al., 2016; Zhang Q. et al., 2018). Chen L. et al. (2017) developed a multi-target screening strategy to identify bioactive components in TCMs by using hollow fiber-based ligand fishing (HFLF) followed by identification of the ligands dissociated from the target-ligand complexes by LC–MS. After individual microporous U-bent hollow fibers containing the enzymes α-glucosidase and ACE were prepared, the hollow fibers filled with the enzymes were heat-sealed, and their open end was immersed into the Ganjiang Huangqin Huanglian Renshen Decoction (GHHRD) extract, which include *Rhizoma zingiberis, Rhizoma coptidis, Radix Scutellariae*, and *Radix Ginseng* extracts. This study identified coptisine as the α-glucosidase ligand and baicalin as the ACE ligand. Berberine was found to be a dual inhibitor of α-glucosidase and ACE.

Xu et al. (2019) applied cellulose filter paper (CFP) as carrier of cell membrane (CM) and developed a novel CM-coated CFP. They used this approach to fish active compounds from *Angelica dahurica* extracts. Three potentially active compounds, including bergapten, pabulenol, and imperatorin, were fished out and identified.

Lau et al. (2015) reported the use of resin to immobilize different enzymes (p97, also known as valosin containing protein (VCP) or cdc48), His6-p97, His6-HSC70, HSPA1A13, and malate dehydrogenase (MDH) by affinity method. The authors used these resin-supported enzymes to isolate small molecules from natural products. LC was used to analyze each elution fraction, and unique peaks were subjected to HRMS. As control, the authors used a resin without protein (data not shown) or recombinant *E. coli* FtsZ (which served as a non-specific protein control).

Kang et al. (2014) described the use of a resin-supported target protein p97 to isolate three natural products (rheoemodin, hydroxydehydroherbarin and phomapyrrolidone A) from crude extracts of the fungal strain *Chaetomium globosum*, endolichenic fungus, *Corynespora* sp., and the endophytic fungal strain *Phoma* sp., respectively, each with a different mechanism of action (Kang et al., 2014). Although the authors carried out these studies by a static approach, they called them as "functional chromatography."

Tao et al. (2016) used zeolites and MBs to immobilize AChE. The resulting AChE-zeolites and AChE-MBs were used to extract ligands from *Corydalis yanhusuo* crude extract by LC-HRMS. While zeolite-AChE fished out 14 inhibitors, AChE-MBs helped to isolate 10 inhibitors. A comparison between zeolite and MBs approaches discloses different immobilization methods; that is, adsorption and covalent binding for zeolite and magnetic nanoparticles, respectively. The AChE-zeolite immobilization ratio was three times larger than the AChE-MB immobilization ratio, which means that more AChE could be immobilized on the same amount of zeolite. Although both AChE-zeolite and AChE-MBs could be reused, AChE can be recycled from the zeolites by desorption. As AChE-zeolites only require AChE and zeolite, they are considered environmentally friendly and inexpensive.

The S-transferase-tagged human PPARγLBD (GST-hPPARγLBD) was bacterially produced and directly applied to a 96-well filter plate pre-packed with glutathione sepharose. Due to the strong bioaffinity between GST and glutathione, the GST-hPPARγLBD could selectively attach to glutathione sepharose, to achieve oriented immobilization and rapid purification. The produced 96-affinity column array was used in an LC–HRMS to fish PPARγ ligands from the extracts of *Magnolia officinalis* (Zhu et al., 2017). PPARγ-functionalized affinity chromatography provides excellent selectivity and sensitivity for fishing.

Despite the aforementioned advantages of fishing assays, many challenges remain, including effective ligand desorption from the target and non-specific binding, which can interfere in the identification of real active compounds. Therefore, experimental testing with blank material is always necessary (Zhuo et al., 2016). During immobilization, the target protein can be denatured or have its three-dimensional configuration altered. This culminates in mild binding or even no binding with the active compounds. To maximize protein immobilization and to improve screening sensitivity, immobilization conditions should be optimized for every selected target (Yang X.-X. et al., 2017).

Concerning the drawbacks of the affinity-based method, it requires pure target protein and modulation of each fishing assay step (see **Figure 3**) for each new target and, most of the time, for each natural product library. This is because the extraction step also depends on the ligand interaction mode. Moreover, the greatest challenge is to characterize the structure of the ligands identified in natural terrestrial and marine extracts: only small amounts are obtained, the structure is complex, several spectra are generated, and databases lack more curated information.

## CONCLUSIONS

Zonal and frontal bioaffinity chromatography assays have been successfully employed to identify and to characterize ligands from synthetic combinatorial libraries. In spite of their higher selectivity, due to their lower chromatography efficiency their application for identifying ligands in terrestrial or marine natural product extracts have been hampered. Efforts have been directed toward overcoming, however, these drawbacks and a list of innovative approaches based on bioaffinity retention has been designed. The possibility of hyphenating chromatographic systems to a myriad of mass spectrometers has been well-explored. In these approaches, the complicating factor has been to characterize the structures of the ligands identified on-line. Moreover, it sometimes not easy to adequate the bioaffinity column mobile phase with the one needed for ionization.

To overcome these shortcomings, the use of off-line bioaffinity devices has been expanded in order to isolate ligands for further chemical structure characterization. LC–SPE–NMR has already demonstrated its utility in the structural characterization of isolated ligands by going back to the crude extract chromatograms.

In this context, LC–HRMS is well-suited to high throughput analysis. Nevertheless, the generated databases are not searchable with raw data, and the amount of produced data is too large for manual analysis. As in the case of genomics and proteomics, which use an integrated platform, consolidation of the recently created Global Natural Products Social Molecular Networking (GNPS; http://gnps.ucsd.edu) will surely increase productivity in one of the most difficult steps of the bioaffinity assays.

The ability to determine not only the affinity and the kinetics, but also the structure of a hit compound directly from a complex mixture has accelerated lead identification and encouraged the use of solid-supported protein platforms.

## AUTHOR CONTRIBUTIONS

MM designed the review, wrote the section about the on-line assays, and reviewed the whole manuscript. CC discussed the structure of the manuscript and wrote the section about the off-line assays. QC discussed the structure of the manuscript, wrote the introduction and conclusion sections, and reviewed the whole manuscript.

## FUNDING

We would like to thank the National Council for Scientific and Technological Development (CNPq - Grants 302557/2018-0 and 426649/2016-8), the São Paulo State Research Foundation (FAPESP—Grants 2013/01710-1; 2014/50249-8 and GSK), the Carlos Chagas Filho Foundation for Research Support in the State of Rio de Janeiro (FAPERJ - Grants E-26/010.000978/2019 and E-26/202.909/2019). This study was partially financed by Coordenação de Aperfeiçoamento de Pessoal de Nível Superior—Brazil (CAPES)—Financial Code 001, including the Capes-PrInt Program, project number: 88887.310269/2018-00.

## ACKNOWLEDGMENTS

We would like to thank Dr. Juliana Maria Lima (ID: 0000-0002-3114-5494) for helping us with the **Figures 1** and **3** of this review.

## REFERENCES

Anguizola, J., Bi, C., Koke, M., Jackson, A., and Hage, D. S. (2016). On-column entrapment of alpha1-acid glycoprotein for studies of drug-protein binding by high-performance affinity chromatography. *Anal. Bioanal. Chem.* 408, 5745–5756. doi: 10.1007/s00216-016-9677-7

Anguizola, J. A., Pfaunmiller, E. L., Milanuk, M. L., and Hage, D. S. (2018). Peak decay analysis and biointeraction studies of immunoglobulin binding and dissociation on protein G affinity microcolumns. *Methods* 146, 39–45. doi: 10.1016/j.ymeth.2018.03.013

Arai, M. A., Kobatake, E., Koyano, T., Kowithayakorn, T., Kato, S., and Ishibashi, M. (2009). A method for the rapid discovery of naturally occurring products by proteins immobilized on magnetic beads and reverse affinity chromatography. *Chem. Asian J.* 4, 1802–1808. doi: 10.1002/asia.200900357

Beeram, S., Bi, C., Zheng, X., and Hage, D. S. (2017). Chromatographic studies of drug interactions with alpha1-acid glycoprotein by ultrafast affinity extraction and peak profiling. *J. Chromatogr. A* 1497, 92–101. doi: 10.1016/j.chroma.2017.03.056

Beeram, S. R., Zheng, X., Suh, K., and Hage, D. S. (2018). Characterization of solution-phase drug-protein interactions by ultrafast affinity extraction. *Methods* 146, 46–57. doi: 10.1016/j.ymeth.2018.02.021

Bertucci, C., Bartolini, M., Gotti, R., and Andrisano, V. (2003). Drug affinity to immobilized target bio-polymers by high-performance liquid chromatography and capillary electrophoresis. *J. Chromatogr. B Anal. Technol. Biomed. Life Sci.* 797, 111–129. doi: 10.1016/j.jchromb.2003.08.033

Bertucci, C., and Domenici, E. (2012). Reversible and covalent binding of drugs to human serum albumin: methodological approaches and physiological relevance. *Curr. Med. Chem.* 9, 1463–1481. doi: 10.2174/0929867023369673

Bi, C., Beeram, S., Li, Z., Zheng, X., and Hage, D. S. (2015). Kinetic analysis of drug-protein interactions by affinity chromatography. *Drug Discov. Today. Technol.* 17, 16–21. doi: 10.1016/j.ddtec.2015.09.003

Bian, L., Li, Q., and Ji, X. (2015). Binding of angiogenesis inhibitor kringle 5 to its specific ligands by frontal affinity chromatography. *J. Chromatogr. A* 1401, 42–51. doi: 10.1016/j.chroma.2015.04.058

Calil, F. A., Lima, J. M., de Oliveira, A. H. C., Mariotini-Moura, C., Fietto, J. L. R., and Cardoso, C. L. (2016). Immobilization of NTPDase-1 from *Trypanosoma cruzi* and development of an online label-free assay. *J. Anal. Methods Chem.* 2016, 9846731. doi: 10.1155/2016/9846731

Calleri, E., Ceruti, S., Cristalli, G., Martini, C., Temporini, C., Parravicini, C., et al. (2010). Frontal affinity chromatography–mass spectrometry useful for characterization of new ligands for GPR17 receptor. *J. Med. Chem.* 53, 3489–3501. doi: 10.1021/jm901691y

Calleri, E., Temporini, C., Caccialanza, G., and Massolini, G. (2009). Target-based drug discovery: the emerging success of frontal affinity chromatography coupled to mass spectrometry. *ChemMedChem* 4, 905–916. doi: 10.1002/cmdc.200800436

Calleri, E., Temporini, C., and Massolini, G. (2011). Frontal affinity chromatography in characterizing immobilized receptors. *J. Pharm. Biomed. Anal.* 54, 911–925. doi: 10.1016/j.jpba.2010.11.040

Calleri, E., Ubiali, D., Serra, I., Temporini, C., Cattaneo, G., Speranza, G., et al. (2014). Immobilized purine nucleoside phosphorylase from *Aeromonas hydrophila* as an on-line enzyme reactor for biocatalytic applications. *J. Chromatogr. B Anal. Technol. Biomed. Life Sci.* 968, 79–86. doi: 10.1016/j.jchromb.2013.12.031

Cardoso, C. L., Lima, V. V., Zottis, A., Oliva, G., Andricopulo, A. D., Wainer, I. W., et al. (2006). Development and characterization of an immobilized enzyme reactor (IMER) based on human glyceraldehyde-3-phosphate dehydrogenase for on-line enzymatic studies. *J. Chromatogr. A* 1120, 151–157. doi: 10.1016/j.chroma.2005.10.063

Chen, F. X., Xu, X., and Bai, Y. L. (2016). Research of anti-cancer components in traditional chinese medicine on hollow fibre cell fishing and hollow fibre liquid phase microextraction. *Am. J. Anal. Chem.* 7, 696–711. doi: 10.4236/ajac.2016.710063

Chen, J., Schiel, J. E., and Hage, D. S. (2009). Noncompetitive peak decay analysis of drug-protein dissociation by high-performance affinity chromatography. *J. Sep. Sci.* 32, 1632–1641. doi: 10.1002/jssc.200900074

Chen, L., Wang, X., Liu, Y., and Di, X. (2017). Dual-target screening of bioactive components from traditional Chinese medicines by hollow fiber-based ligand fishing combined with liquid chromatography–mass spectrometry. *J. Pharm. Biomed. Anal.* 143, 269–276. doi: 10.1016/j.jpba.2017.06.001

Chen, X., Cao, Y., Zhang, H., Zhu, Z., Liu, M., Liu, H., et al. (2014). Comparative normal/failing rat myocardium cell membrane chromatographic analysis system for screening specific components that counteract doxorubicin-induced heart failure from *Acontium carmichaeli*. *Anal. Chem.* 86, 4748–4757. doi: 10.1021/ac500287e

Chen, X., Li, Y., Zhang, Y., Yang, J., and Bian, L. (2017). Binding of TEM-1 beta-lactamase to beta-lactam antibiotics by frontal affinity chromatography. *J. Chromatogr. B* 1051, 75–83. doi: 10.1016/j.jchromb.2017.03.013

Cieśla, Ł., and Moaddel, R. (2016). Comparison of analytical techniques for the identification of bioactive compounds from natural products. *Nat. Prod. Rep.* 33, 1131–1145. doi: 10.1039/C6NP00016A

Ciesla, L., Okine, M., Rosenberg, A., Dossou, K. S. S., Toll, L., Wainer, I. W., et al. (2016). Development and characterization of the α3β4α5 nicotinic receptor cellular membrane affinity chromatography column and its application for on line screening of plant extracts. *J. Chromatogr. A* 1431, 138–144. doi: 10.1016/j.chroma.2015.12.065

Cornelio, V. E., de Moraes, M. C., Domingues, V., Fernandes, J. B., da Silva, M. F. D., G. F., Cass, Q. B., et al. (2018). Cathepsin D immobilized capillary reactors for on-flow screening assays. *J. Pharm. Biomed. Anal.* 151, 252–259. doi: 10.1016/j.jpba.2018.01.001

da Silva, J. I., de Moraes, M. C., Vieira, L. C. C., Corrêa, A. G., Cass, Q. B., and Cardoso, C. L. (2012). Acetylcholinesterase capillary enzyme reactor for screening and characterization of selective inhibitors. *J. Pharm. Biomed. Anal.* 73, 44–52. doi: 10.1016/j.jpba.2012.01.026

Datta, S., Christena, L. R., and Rajaram, Y. R. S. (2013). Enzyme immobilization: an overview on techniques and support materials. *3 Biotech* 3, 1–9. doi: 10.1007/s13205-012-0071-7

de Almeida, F. G., Vanzolini, K. L., and Cass, Q. B. (2017). Angiotensin converting enzyme immobilized on magnetic beads as a tool for ligand fishing. *J. Pharm. Biomed. Anal.* 132, 159–164. doi: 10.1016/j.jpba.2016.10.006

de Moraes, M. C., Cardoso, C., Seidl, C., Moaddel, R., and Cass, Q. (2016). Targeting anti-cancer active compounds: affinity-based chromatographic assays. *Curr. Pharm. Des.* 22, 5976–5987. doi: 10.2174/1381612822666160614080506

de Moraes, M. C., Cardoso, C. L., and Cass, Q. B. (2013). Immobilized purine nucleoside phosphorylase from *Schistosoma mansoni* for specific inhibition studies. *Anal. Bioanal. Chem.* 405, 4871–4878. doi: 10.1007/s00216-013-6872-7

de Moraes, M. C., Santos, J. B., dos Anjos, D. M., Rangel, L. P., Vieira, T. C. R. G., Moaddel, R., et al. (2015). Prion protein-coated magnetic beads: synthesis, characterization and development of a new ligands screening method. *J. Chromatogr. A* 1379, 1–8. doi: 10.1016/j.chroma.2014.12.014

de Moraes, M. C., Temporini, C., Calleri, E., Bruni, G., Ducati, R. G., Santos, D. S., et al. (2014a). Evaluation of capillary chromatographic supports for immobilized human purine nucleoside phosphorylase in frontal affinity chromatography studies. *J. Chromatogr. A* 1338, 77–84. doi: 10.1016/j.chroma.2014.02.057

de Moraes, M. C., Vanzolini, K. L., Cardoso, C. L., and Cass, Q. B. (2014b). New trends in LC protein ligand screening. *J. Pharm. Biomed. Anal.* 87, 155–166. doi: 10.1016/j.jpba.2013.07.021

De Simone, A., Naldi, M., Bartolini, M., Davani, L., and Andrisano, V. (2019). Immobilized enzyme reactors: an overview of applications in drug discovery from 2008 to 2018. *Chromatographia* 82, 425–441. doi: 10.1007/s10337-018-3663-5

Deng, X., Shi, S., Li, S., and Yang, T. (2014). Magnetic ligand fishing combination with high-performance liquid chromatography–diode array detector–mass spectrometry to screen and characterize cyclooxygenase-2 inhibitors from green tea. *J. Chromatogr. B* 973, 55–60. doi: 10.1016/j.jchromb.2014.10.010

Domenici, E., Bertucci, C., Salvadori, P., and Wainer, I. W. (1991). Use of a human serum albumin-based high-performance liquid chromatography chiral stationary phase for the investigation of protein binding: detection of the allosteric interaction between warfarin and benzodiazepine binding sites. *J. Pharm. Sci,* 80, 164–166. doi: 10.1002/jps.2600800216

Dos Santos, A. M., Moreira, A. C., Lopes, B. R., Fracola, M. F., de Almeida, F. G., Bueno, O. C., et al. (2019). Acetylcholinesterases from leaf-cutting ant atta sexdens: purification, characterization, and capillary reactors for on-flow assays. *Enzyme Res.* 2019, 1–9. doi: 10.1155/2019/6139863

Ferreira Lopes Vilela, A., and Cardoso, C. L. (2017). An on-flow assay for screening of β-secretase ligands by immobilised capillary reactor-mass spectrometry. *Anal. Methods* 9, 2189–2196. doi: 10.1039/C7AY00284J

Forsberg, E. M., and Brennan, J. D. (2014). Bio-solid-phase extraction/tandem mass spectrometry for identification of bioactive compounds in mixtures. *Anal. Chem.* 86, 8457–8465. doi: 10.1021/ac5022166

Forsberg, E. M., Sicard, C., and Brennan, J. D. (2014). Solid-phase biological assays for drug discovery. *Annu. Rev. Anal. Chem.* 7, 337–359. doi: 10.1146/annurev-anchem-071213-020241

Fu, Y., Luo, J., Qin, J., and Yang, M. (2019). Screening techniques for the identification of bioactive compounds in natural products. *J. Pharm. Biomed. Anal.* 168, 189–200. doi: 10.1016/j.jpba.2019.02.027

Fu, Y., Mo, H.-Y., Gao, W., Hong, J.-Y., Lu, J., Li, P., et al. (2014). Affinity selection-based two-dimensional chromatography coupled with high-performance liquid chromatography-mass spectrometry for discovering xanthine oxidase inhibitors from Radix Salviae Miltiorrhizae. *Anal. Bioanal. Chem.* 406, 4987–4995. doi: 10.1007/s00216-014-7902-9

Gao, X., Li, Q., Zhao, X., Huang, J., Bian, L., Zheng, J., et al. (2014). Investigation on the binding of terazosin hydrochloride and naftopidil to an immobilized α1-adrenoceptor by zonal elution. *Chromatographia* 77, 1235–1239. doi: 10.1007/s10337-014-2716-7

Gargano, A. F. G., Lämmerhofer, M., Lönn, H., Schoenmakers, P. J., and Leek, T. (2014). Mucin-based stationary phases as tool for the characterization of drug–mucus interaction. *J. Chromatogr. A* 1351, 70–81. doi: 10.1016/j.chroma.2014.05.031

Guo, P., Luo, Z., Xu, X., Zhou, Y., Zhang, B., Chang, R., et al. (2017). Development of molecular imprinted column-on line-two dimensional liquid chromatography for selective determination of clenbuterol residues in biological samples. *Food Chem.* 217, 628–636. doi: 10.1016/j.foodchem.2016.09.021

Habicht, K.-L., Singh, N. S., Indig, F. E., Wainer, I. W., Moaddel, R., and Shimmo, R. (2015). The development of mitochondrial membrane affinity chromatography columns for the study of mitochondrial transmembrane proteins. *Anal. Biochem.* 484, 154–161. doi: 10.1016/j.ab.2015.05.018

Hage, D. S. (2017). Analysis of biological interactions by affinity chromatography: clinical and pharmaceutical applications. *Clin. Chem.* 63, 1083–1093. doi: 10.1373/clinchem.2016.262253

Hage, D. S., Anguizola, J. A., Bi, C., Li, R., Matsuda, R., Papastavros, E., et al. (2012). Pharmaceutical and biomedical applications of affinity chromatography: recent trends and developments. *J. Pharm. Biomed. Anal.* 69, 93–105. doi: 10.1016/j.jpba.2012.01.004

Han, S., Zhang, T., Feng, L., Lv, N., and Wang, S. (2013). Screening of target compounds from Fructus Piperis using high α1A adrenoreceptor expression cell membrane chromatography online coupled with high performance liquid chromatography tandem mass spectrometry. *J. Pharm. Biomed. Anal.* 81–82, 133–137. doi: 10.1016/j.jpba.2013.04.001

He, X., Sui, Y., and Wang, S. (2018). Stepwise frontal affinity chromatography model for drug and protein interaction. *Anal. Bioanal. Chem.* 410, 5807–5815. doi: 10.1007/s00216-018-1194-4

Homaei, A. A., Sariri, R., Vianello, F., and Stevanato, R. (2013). Enzyme immobilization: an update. *J. Chem. Biol.* 6, 185–205. doi: 10.1007/s12154-013-0102-9

Hu, Y., Fu, A., Miao, Z., Zhang, X., Wang, T., Kang, A., et al. (2018). Fluorescent ligand fishing combination with *in-situ* imaging and characterizing to screen Hsp 90 inhibitors from *Curcuma longa* L. based on InP/ZnS quantum dots embedded mesoporous nanoparticles. *Talanta* 178, 258–267. doi: 10.1016/j.talanta.2017.09.035

Imaduwage, K. P., Go, E. P., Zhu, Z., and Desaire, H. (2016). HAMS: high-affinity mass spectrometry screening. A high-throughput screening method for identifying the tightest-binding lead compounds for target proteins with no false positive identifications. *J. Am. Soc. Mass Spectrom.* 27, 1870–1877. doi: 10.1007/s13361-016-1472-3

Imaduwage, K. P., Lakbub, J., Go, E. P., and Desaire, H. (2017). Rapid LC-MS based high-throughput screening method, affording no false positives or false negatives, identifies a new inhibitor for carbonic anhydrase. *Sci. Rep.* 7:10324. doi: 10.1038/s41598-017-08602-w

Jia, D., Chen, X., Cao, Y., Wu, X., Ding, X., Zhang, H., et al. (2016). On-line comprehensive two-dimensional HepG2 cell membrane chromatographic analysis system for charactering anti-hepatoma components from rat serum after oral administration of *Radix scutellariae*: a strategy for rapid screening active compounds *in vivo*. *J. Pharm. Biomed. Anal.* 118, 27–33. doi: 10.1016/j.jpba.2015.10.013

Jonker, N., Kool, J., Irth, H., and Niessen, W. M. A. (2011). Recent developments in protein–ligand affinity mass spectrometry. *Anal. Bioanal. Chem.* 399, 2669–2681. doi: 10.1007/s00216-010-4350-z

Jozwiak, K., Haginaka, J., Moaddel, R., and Wainer, I. W. (2002). Displacement and nonlinear chromatographic techniques in the investigation of interaction of noncompetitive inhibitors with an immobilized α3β4 nicotinic acetylcholine receptor liquid chromatographic stationary phase. *Anal. Chem.* 74, 4618–4624. doi: 10.1021/ac0202029

Kang, M. J., Wu, T., Wijeratne, E. M. K., Lau, E. C., Mason, D. J., Mesa, C., et al. (2014). Functional chromatography reveals three natural products that target the same protein with distinct mechanisms of action. *ChemBioChem* 15, 2125–2131. doi: 10.1002/cbic.201402258

Kubota, K., Kubo, T., Tanigawa, T., Naito, T., and Otsuka, K. (2017). New platform for simple and rapid protein-based affinity reactions. *Sci. Rep.* 7:178. doi: 10.1038/s41598-017-00264-y

Lau, E. C., Mason, D. J., Eichhorst, N., Engelder, P., Mesa, C., Kithsiri Wijeratne, E. M., et al. (2015). Functional chromatographic technique for natural product isolation. *Org. Biomol. Chem.* 13, 2255–2259. doi: 10.1039/C4OB02292K

Lecas, L., Randon, J., Berthod, A., Dugas, V., and Demesmay, C. (2019). Monolith weak affinity chromatography for μg-protein-ligand interaction study. *J. Pharm. Biomed. Anal.* 166, 164–173. doi: 10.1016/j.jpba.2019.01.012

Li, Q., Ning, X., An, Y., Stanley, B. J., Liang, Y., Wang, J., et al. (2018). Reliable analysis of the interaction between specific ligands and immobilized beta-2-adrenoceptor by adsorption energy distribution. *Anal. Chem.* 90, 7903–7911. doi: 10.1021/acs.analchem.8b00214

Li, Q., Qiao, P., Chen, X., Wang, J., Bian, L., and Zheng, X. (2017). Affinity chromatographic methodologies based on immobilized voltage dependent anion channel isoform 1 and application in protein-ligand interaction analysis and bioactive compounds screening from traditional medicine. *J. Chromatogr. A* 1495, 31–45. doi: 10.1016/j.chroma.2017.03.023

Li, Q., Wang, J., Zheng, Y. Y., Yang, L., Zhang, Y., Bian, L., et al. (2015). Comparison of zonal elution and nonlinear chromatography in determination of the interaction between seven drugs and immobilised β2-adrenoceptor. *J. Chromatogr. A* 1401, 75–83. doi: 10.1016/j.chroma.2015.05.012

Li, Q., Zhang, T., and Bian, L. (2016). Recognition and binding of β-lactam antibiotics to bovine serum albumin by frontal affinity chromatography in combination with spectroscopy and molecular docking. *J. Chromatogr. B* 1014, 90–101. doi: 10.1016/j.jchromb.2016.02.005

Li, Y., Chen, Y., Xiao, C., Chen, D., Xiao, Y., and Mei, Z. (2014). Rapid screening and identification of α-amylase inhibitors from *Garcinia xanthochymus* using enzyme-immobilized magnetic nanoparticles coupled with HPLC and MS. *J. Chromatogr. B* 960, 166–173. doi: 10.1016/j.jchromb.2014.04.041

Li, Y., Xu, J., Chen, Y., Mei, Z., and Xiao, Y. (2015). Screening of inhibitors of glycogen synthase kinase-3β from traditional Chinese medicines using enzyme-immobilized magnetic beads combined with high-performance liquid chromatography. *J. Chromatogr. A* 1425, 8–16. doi: 10.1016/j.chroma.2015.10.062

Li, Z., Gao, H., Li, J., and Zhang, Y. (2017). Identification of bioactive compounds in Shaoyao-Gancao decoction using β2-adrenoceptor affinity chromatography. *J. Sep. Sci.* 40, 2558–2564. doi: 10.1002/jssc.201700113

Liang, Y., Wang, J., Fei, F., Sun, H., Liu, T., Li, Q., et al. (2018). Binding kinetics of five drugs to beta2-adrenoceptor using peak profiling method and nonlinear chromatography. *J. Chromatogr. A* 1538, 17–24. doi: 10.1016/j.chroma.2018.01.027

Lima, J. M., Salmazo Vieira, P., Cavalcante de Oliveira, A. H., and Cardoso, C. L. (2016). Label-free offline versus online activity methods for nucleoside diphosphate kinase b using high performance liquid chromatography. *Analyst* 141, 4733–4741. doi: 10.1039/C6AN00655H

Liu, D.-M., Chen, J., and Shi, Y.-P. (2017a). Screening of enzyme inhibitors from traditional Chinese medicine by magnetic immobilized α-glucosidase coupled with capillary electrophoresis. *Talanta* 164, 548–555. doi: 10.1016/j.talanta.2016.12.028

Liu, D.-M., Chen, J., and Shi, Y.-P. (2017b). α-Glucosidase immobilization on chitosan-enriched magnetic composites for enzyme inhibitors screening. *Int. J. Biol. Macromol.* 105, 308–316. doi: 10.1016/j.ijbiomac.2017.07.045

Liu, G., Wang, P., Li, C., Wang, J., Sun, Z., Zhao, X., et al. (2017). Confirming therapeutic target of protopine using immobilized β2-adrenoceptor coupled with site-directed molecular docking and the target-drug interaction by frontal analysis and injection amount–dependent method. *J. Mol. Recognit.* 30:e2613. doi: 10.1002/jmr.2613

Liu, X., Hu, S., Chen, X., and Bai, X. (2014). Hollow fiber cell fishing with high-performance liquid chromatography for rapid screening and analysis of an antitumor-active protoberberine alkaloid group from *Coptis chinensis*. *J. Pharm. Biomed. Anal.* 98, 463–475. doi: 10.1016/j.jpba.2014.06.030

Ma, L., Li, J., Zhao, J., Liao, H., Xu, L., and Shi, Z. (2016). Penetrable silica microspheres for immobilization of bovine serum albumin and their application to the study of the interaction between imatinib mesylate and protein by frontal affinity chromatography. *Anal. Bioanal. Chem.* 408, 805–814. doi: 10.1007/s00216-015-9163-7

Ma, W., Zhang, Y., Li, J., Liu, R., Che, D., and He, L. (2015). Analysis of drug interactions with dopamine receptor by frontal analysis and cell membrane chromatography. *Chromatographia* 78, 649–654. doi: 10.1007/s10337-015-2867-1

Magalhães, L., de Oliveira, A. H. C., de Souza Vasconcellos, R., Mariotini-Moura, C., de Cássia Firmino, R., Fietto, J. L. R., et al. (2016). Label-free assay based on immobilized capillary enzyme reactor of *Leishmania infantum* nucleoside triphosphate diphosphohydrolase (LicNTPDase-2-ICER-LC/UV). *J. Chromatogr. B* 1008, 98–107. doi: 10.1016/j.jchromb.2015.11.028

Marszałł, M. P. (2011). Application of magnetic nanoparticles in pharmaceutical sciences. *Pharm. Res.* 28, 480–483. doi: 10.1007/s11095-010-0284-6

Marszałł, M. P., Moaddel, R., Kole, S., Gandhari, M., Bernier, M., and Wainer, I. W. (2008). Ligand and protein fishing with heat shock protein 90 coated magnetic beads. *Anal. Chem.* 80, 7571–7575. doi: 10.1021/ac801153h

Matsuda, R., Li, Z., Zheng, X., and Hage, D. S. (2015). Analysis of multi-site drug–protein interactions by high-performance affinity chromatography: binding by glimepiride to normal or glycated human serum albumin. *J. Chromatogr. A* 1408, 133–144. doi: 10.1016/j.chroma.2015.07.012

Meiby, E., Simmonite, H., le Strat, L., Davis, B., Matassova, N., Moore, J. D., et al. (2013). Fragment screening by weak affinity chromatography: comparison with established techniques for screening against HSP90. *Anal. Chem.* 85, 6756–6766. doi: 10.1021/ac400715t

Michel, T., Halabalaki, M., and Skaltsounis, A.-L. (2013). New concepts, experimental approaches, and dereplication strategies for the discovery of novel phytoestrogens from natural sources. *Planta Med.* 79, 514–532. doi: 10.1055/s-0032-1328300

Moaddel, R., Marszałł, M. P., Bighi, F., Yang, Q., Duan, X., and Wainer, I. W. (2007). Automated ligand fishing using human serum albumin-coated magnetic beads. *Anal. Chem.* 79, 5414–5417. doi: 10.1021/ac070268+

Mohamad, N. R., Marzuki, N. H. C., Buang, N. A., Huyop, F., and Wahab, R. A. (2015). An overview of technologies for immobilization of enzymes and surface analysis techniques for immobilized enzymes. *Biotechnol. Biotechnol. Equip.* 29, 205–220. doi: 10.1080/13102818.2015.1008192

Muller, A. J., and Carr, P. W. (1984). Chromatographic study of the thermodynamic and kinetic characteristics of silica-bound concanavalin A. *J. Chromatogr. A* 284, 33–51. doi: 10.1016/S0021-9673(01)87800-6

Muronetz, V. I., Sholukh, M., and Korpela, T. (2001). Use of protein–protein interactions in affinity chromatography. *J. Biochem. Biophys. Methods* 49, 29–47. doi: 10.1016/S0165-022X(01)00187-7

Ng, E. S. M., Chan, N. W. C., Lewis, D. F., Hindsgaul, O., and Schriemer, D. C. (2007). Frontal affinity chromatography—mass spectrometry. *Nat. Protoc.* 2:1907. doi: 10.1038/nprot.2007.262

Ohlson, S., and Duong-Thi, M.-D. (2018). Fragment screening for drug leads by weak affinity chromatography (WAC-MS). *Methods* 146, 26–38. doi: 10.1016/j.ymeth.2018.01.011

Ohlson, S., Kaur, J., Raida, M., Niss, U., Bengala, T., Drum, C. L., et al. (2017). Direct analysis – no sample preparation – of bioavailable cortisol in human plasma by weak affinity chromatography (WAC). *J. Chromatogr. B* 1061–1062, 438–444. doi: 10.1016/j.jchromb.2017.07.035

Pang, M.-H., Kim, Y., Jung, K. W., Cho, S., and Lee, D. H. (2012). A series of case studies: practical methodology for identifying antinociceptive multi-target drugs. *Drug Discov. Today* 17, 425–434. doi: 10.1016/j.drudis.2012.01.003

Peng, M. J., Shi, S. Y., Chen, L., Zhang, S. H., and Cai, X. C. (2016). Online coupling solid-phase ligand-fishing with high-performance liquid chromatography–diode array detector–tandem mass spectrometry for rapid screening and

identification of xanthine oxidase inhibitors in natural products. *Anal. Bioanal. Chem.* 408, 6693–6701. doi: 10.1007/s00216-016-9784-5

Perret, G., and Boschetti, E. (2018). Aptamer affinity ligands in protein chromatography. *Biochimie* 145, 98–112. doi: 10.1016/j.biochi.2017.10.008

Pfaunmiller, E. L., Paulemond, M. L., Dupper, C. M., and Hage, D. S. (2013). Affinity monolith chromatography: a review of principles and recent analytical applications. *Anal. Bioanal. Chem.* 405, 2133–2145. doi: 10.1007/s00216-012-6568-4

Rodrigues, M. V. N., Barbosa, A. F., da Silva, J. F., dos Santos, D. A., Vanzolini, K. L., de Moraes, M. C., et al. (2016). 9-Benzoyl 9-deazaguanines as potent xanthine oxidase inhibitors. *Bioorg. Med. Chem.* 24, 226–231. doi: 10.1016/j.bmc.2015.12.006

Rodrigues, M. V. N., Santos, D. S., Cass, Q. B., Batista, A. A., Corrêa, R. S., and Vanzolini, K. L. (2015). Characterization and screening of tight binding inhibitors of xanthine oxidase: an on-flow assay. *RSC Adv.* 5, 37533–37538. doi: 10.1039/C5RA01741F

Schriemer, D. C. (2008). Peer reviewed: biosensor alternative: frontal affinity chromatography. *Anal. Chem.* 76, 440A−448A. doi: 10.1021/ac041684m

Seidl, C., Vilela, A. F. L., Lima, J. M., Leme, G. M., and Cardoso, C. L. (2019). A novel on-flow mass spectrometry-based dual enzyme assay. *Anal. Chim. Acta* 1072, 81–86. doi: 10.1016/j.aca.2019.04.057

Singh, N., Ravichandran, S., Spelman, K., Fugmann, S. D. D., and Moaddel, R. (2014). The identification of a novel SIRT6 modulator from *Trigonella foenum-graecum* using ligand fishing with protein coated magnetic beads. *J. Chrom. B* 968, 105–111. doi: 10.1016/j.jchromb.2014.03.016

Singh, N. S., Habicht, K.-L., Moaddel, R., and Shimmo, R. (2017). Development and characterization of mitochondrial membrane affinity chromatography columns derived from skeletal muscle and platelets for the study of mitochondrial transmembrane proteins. *J. Chromatogr. B* 1055–1056, 144–148. doi: 10.1016/j.jchromb.2017.04.022

Singh, P., Madhaiyan, K., Duong-Thi, M.-D., Dymock, B. W., and Ohlson, S. (2017). Analysis of protein target interactions of synthetic mixtures by affinity-LC/MS. *SLAS Discov. Adv. Life Sci. Rand. D* 22, 440–446. doi: 10.1177/2472555216687964

Slon-Usakiewicz, J. J., Ng, W., Dai, J.-R., Pasternak, A., and Redden, P. R. (2005). Frontal affinity chromatography with MS detection (FAC-MS) in drug discovery. *Drug Discov. Today* 10, 409–416. doi: 10.1016/S1359-6446(04)03360-4

Song, H.-P., Chen, J., Hong, J.-Y., Hao, H., Qi, L.-W., Lu, J., et al. (2015). A strategy for screening of high-quality enzyme inhibitors from herbal medicines based on ultrafiltration LC-MS and *in silico* molecular docking. *Chem. Commun.* 51, 1494–1497. doi: 10.1039/C4CC08728C

Tang, C., Mao, R., Liu, F., Yu, Y., Xu, L., and Zhang, Y. (2017). Ligand fishing with cellular membrane-coated magnetic beads: a new method for the screening of potentially active compounds from natural products. *Chromatographia* 80, 1517–1525. doi: 10.1007/s10337-017-3370-7

Tang, W., Jia, B., Zhou, J., Liu, J., Wang, J., Ma, D., et al. (2019). A method using angiotensin converting enzyme immobilized on magnetic beads for inhibitor screening. *J. Pharm. Biomed. Anal.* 164, 223–230. doi: 10.1016/j.jpba.2018.09.054

Tao, P., Li, Z., Matsuda, R., and Hage, D. S. (2018a). Chromatographic studies of chlorpropamide interactions with normal and glycated human serum albumin based on affinity microcolumns. *J. Chromatogr. B* 1097–1098, 64–73. doi: 10.1016/j.jchromb.2018.09.001

Tao, P., Li, Z., Woolfork, A. G., and Hage, D. S. (2019). Characterization of tolazamide binding with glycated and normal human serum albumin by using high-performance affinity chromatography. *J. Pharm. Biomed. Anal.* 166, 273–280. doi: 10.1016/j.jpba.2019.01.025

Tao, P., Poddar, S., Sun, Z., Hage, D. S., and Chen, J. (2018b). Analysis of solute-protein interactions and solute-solute competition by zonal elution affinity chromatography. *Methods* 146, 3–11. doi: 10.1016/j.ymeth.2018.01.020

Tao, Y., Chen, Z., Zhang, Y., Wang, Y., and Cheng, Y. (2013a). Immobilized magnetic beads based multi-target affinity selection coupled with high performance liquid chromatography–mass spectrometry for screening anti-diabetic compounds from a Chinese medicine "Tang-Zhi-Qing." *J. Pharm. Biomed. Anal.* 78–79, 190–201. doi: 10.1016/j.jpba.2013.02.024

Tao, Y., Jiang, Y., Li, W., and Cai, B. (2016). Zeolite based solid-phase extraction coupled with UPLC-Q-TOF-MS for rapid analysis of acetylcholinesterase binders from crude extract of: *Corydalis yanhusuo*. *RSC Adv.* 6, 98476–98486. doi: 10.1039/C6RA24585D

Tao, Y., Zhang, Y., Wang, Y., and Cheng, Y. (2013b). Hollow fiber based affinity selection combined with high performance liquid chromatography–mass spectroscopy for rapid screening lipase inhibitors from lotus leaf. *Anal. Chim. Acta* 785, 75–81. doi: 10.1016/j.aca.2013.04.058

Temporini, C., Massolini, G., Marucci, G., Lambertucci, C., Buccioni, M., Volpini, R., et al. (2013). Development of new chromatographic tools based on A2A adenosine receptor subtype for ligand characterization and screening by FAC-MS. *Anal. Bioanal. Chem.* 405, 837–845. doi: 10.1007/s00216-012-6353-4

Tweed, S. A., Loun, B., and Hage, D. S. (1997). Effects of ligand heterogeneity in the characterization of affinity columns by frontal analysis. *Anal. Chem.* 69, 4790–4798. doi: 10.1021/ac970565m

Vanzolini, K. L., Ainsworth, S., Bruyneel, B., Herzig, V., Seraus, M. G. L., Somsen, G. W., et al. (2018a). Rapid ligand fishing for identification of acetylcholinesterase-binding peptides in snake venom reveals new properties of dendrotoxins. *Toxicon* 152, 1–8. doi: 10.1016/j.toxicon.2018.06.080

Vanzolini, K. L., da F Sprenger, R., Leme, G. M., de S Moraes, V. R., Vilela, A. F. L., Cardoso, C. L., et al. (2018b). Acetylcholinesterase affinity-based screening assay on *Lippia gracilis* Schauer extracts. *J. Pharm. Biomed. Anal.* 153, 232–237. doi: 10.1016/j.jpba.2018.02.035

Vanzolini, K. L., Vieira, L. C. C., Correîa, A. G., Cardoso, C. L., and Cass, Q. B. (2013a). Acetylcholinesterase immobilized capillary reactors-tandem mass spectrometry: an on-flow tool for ligand screening. *J. Med. Chem.* 56, 2038–2044. doi: 10.1021/jm301732a

Vanzolini, K. L., Zhengjin, J., Zhang, X., Vieira, L. C. C., Corrêa, A. G., Cardoso, C. L., et al. (2013b). Acetylcholinesterase immobilized capillary reactors coupled to protein coated magnetic beads: A new tool for plant extract ligand screening. *Talanta* 116, 647–652. doi: 10.1016/j.talanta.2013.07.046

Vilela, A. F. L., Seidl, C., Lima, J. M., and Cardoso, C. L. (2018). An improved immobilized enzyme reactor-mass spectrometry-based label free assay for butyrylcholinesterase ligand screening. *Anal. Biochem.* 549, 53–57. doi: 10.1016/j.ab.2018.03.012

Wainer, I. W. (2004). Finding time for allosteric interactions. *Nat. Biotechnol.* 22, 1376–1377. doi: 10.1038/nbt1104-1376

Wang, H., Zhao, X., Wang, S., Tao, S., Ai, N., and Wang, Y. (2015). Fabrication of enzyme-immobilized halloysite nanotubes for affinity enrichment of lipase inhibitors from complex mixtures. *J. Chromatogr. A* 1392, 20–27. doi: 10.1016/j.chroma.2015.03.002

Wang, L., Zhao, Y., Zhang, Y., Zhang, T., Kool, J., Somsen, G. W., et al. (2018). Online screening of acetylcholinesterase inhibitors in natural products using monolith-based immobilized capillary enzyme reactors combined with liquid chromatography-mass spectrometry. *J. Chromatogr. A* 1563, 135–143. doi: 10.1016/j.chroma.2018.05.069

Wang, Q., Xu, J., Li, X., Zhang, D., Han, Y., and Zhang, X. (2017). Comprehensive two-dimensional PC-3 prostate cancer cell membrane chromatography for screening anti-tumor components from Radix *Sophorae flavescentis*. *J. Sep. Sci.* 40, 2688–2693. doi: 10.1002/jssc.201700208

Wang, X.-Y., Ding, X., Yuan, Y.-F., Zheng, L.-Y., Cao, Y., Zhu, Z.-Y., et al. (2018). Comprehensive two-dimensional APTES-decorated MCF7-cell membrane chromatographic system for characterizing potential anti-breast-cancer components from Yuanhu–Baizhi herbal medicine pair. *J. Food Drug Anal.* 26, 823–833. doi: 10.1016/j.jfda.2017.11.010

Wang, Y., Fan, X., Qu, H., Gao, X., and Cheng, Y. (2012). Strategies and techniques for multi-component drug design from medicinal herbs and traditional Chinese medicine. *Curr. Top. Med. Chem.* 12, 1356–1362. doi: 10.2174/156802612801319034

Wang, Z., Li, X., Chen, M., Liu, F., Han, C., Kong, L., et al. (2018). A strategy for screening of α-glucosidase inhibitors from *Morus alba* root bark based on the ligand fishing combined with high-performance liquid chromatography mass spectrometer and molecular docking. *Talanta* 180, 337–345. doi: 10.1016/j.talanta.2017.12.065

Wei, F., Wang, S., Lv, N., Bu, Y., and Xie, X. (2017). Characterization the affinity of α1A adrenoreceptor by cell membrane chromatography with frontal analysis and stoichiometric displacement model. *J. Chromatogr. B* 1040, 273–281. doi: 10.1016/j.jchromb.2016.11.002

Wu, A.-G., Kam-Wai Wong, V., Zeng, W., Liu, L., and Yuen-Kwan Law, B. (2015). Identification of novel autophagic Radix Polygalae fraction by cell membrane chromatography and UHPLC-(Q)TOF-MS for degradation of neurodegenerative disease proteins. *Sci. Rep.* 5:17199. doi: 10.1038/srep17199

Wu, X., Chen, X., Jia, D., Cao, Y., Gao, S., Guo, Z., et al. (2016). Characterization of anti-leukemia components from *Indigo naturalis* using comprehensive two-dimensional K562/cell membrane chromatography and *in silico* target identification. *Sci. Rep.* 6:25491. doi: 10.1038/srep25491

Wubshet, S. G., Brighente, I. M. C., Moaddel, R., and Staerk, D. (2015). Magnetic ligand fishing as a targeting tool for HPLC-HRMS-SPE-NMR: α-glucosidase inhibitory ligands and alkylresorcinol glycosides from *Eugenia catharinae*. *J. Nat. Prod.* 78, 2657–2665. doi: 10.1021/acs.jnatprod.5b00603

Wubshet, S. G., Liu, B., Kongstad, K. T., Böcker, U., Petersen, M. J., Li, T., et al. (2019). Combined magnetic ligand fishing and high-resolution inhibition profiling for identification of α-glucosidase inhibitory ligands: a new screening approach based on complementary inhibition and affinity profiles. *Talanta* 200, 279–287. doi: 10.1016/j.talanta.2019.03.047

Xu, L., Tang, C., Li, X., Li, X., Yang, H., Mao, R., et al. (2019). Ligand fishing with cellular membrane-coated cellulose filter paper: a new method for screening of potential active compounds from natural products. *Anal. Bioanal. Chem.* 411, 1989–2000. doi: 10.1007/s00216-019-01662-z

Xuan, H., Joseph, K. S., Wa, C., and Hage, D. S. (2010). Biointeraction analysis of carbamazepine binding to alpha1-acid glycoprotein by high-performance affinity chromatography. *J. Sep. Sci.* 33, 2294–2301. doi: 10.1002/jssc.201000214

Yang, X.-X., Gu, W., Liang, L., Yan, H.-L., Wang, Y.-F., Bi, Q., et al. (2017). Screening for the bioactive constituents of traditional Chinese medicines—progress and challenges. *RSC Adv.* 7, 3089–3100. doi: 10.1039/C6RA25765H

Yang, Y., Chen, J., and Shi, Y.-P. (2015). Recent developments in modifying polypropylene hollow fibers for sample preparation. *TrAC Trends Anal. Chem.* 64, 109–117. doi: 10.1016/j.trac.2014.08.016

Yang, Y.-X., Li, S.-Y., Zhang, Q., Chen, H., Xia, Z.-N., and Yang, F.-Q. (2017). Characterization of phenolic acids binding to thrombin using frontal affinity chromatography and molecular docking. *Anal. Methods* 9, 5174–5180. doi: 10.1039/C7AY01433C

Yoo, M. J., and Hage, D. S. (2011). High-throughput analysis of drug dissociation from serum proteins using affinity silica monoliths. *J. Sep. Sci.* 34, 2255–2263. doi: 10.1002/jssc.201100280

Zhan, Y., Li, J., Ma, W., Zhang, D., and Luo, W. (2016). Characterization of interactions between taspine derivate TPD7 and EGF receptor by cell membrane chromatography with zonal elution and frontal analysis. *Chromatographia* 79, 1585–1592. doi: 10.1007/s10337-016-3189-7

Zhang, C., Rodriguez, E., Bi, C., Zheng, X., Suresh, D., Suh, K., et al. (2018). High performance affinity chromatography and related separation methods for the analysis of biological and pharmaceutical agents. *Analyst* 143, 374–391. doi: 10.1039/C7AN01469D

Zhang, Q., Tan, C.-N., Wang, Y., Liu, W.-J., Yang, F.-Q., Chen, H., et al. (2018). Adsorbed hollow fiber-based biological fingerprinting for the discovery of platelet aggregation inhibitors from Danshen-Honghua decoction. *J. Sep. Sci.* 41, 2651–2660. doi: 10.1002/jssc.201701434

Zhang, Y., Shi, S., Chen, X., and Peng, M. (2014). Functionalized magnetic nanoparticles coupled with mass spectrometry for screening and identification of cyclooxygenase-1 inhibitors from natural products. *J. Chromatogr. B* 960, 126–132. doi: 10.1016/j.jchromb.2014.04.032

Zhang, Y., Wang, Q., Liu, R., Zhou, H., Crommen, J., Moaddel, R., et al. (2019). Rapid screening and identification of monoamine oxidase-A inhibitors from Corydalis Rhizome using enzyme-immobilized magnetic beads based method. *J. Chromatogr. A* 1592, 1–8. doi: 10.1016/j.chroma.2019.01.062

Zhao, Y.-M., Wang, L.-H., Luo, S.-F., Wang, Q.-Q., Moaddel, R., Zhang, T.-T., et al. (2018). Magnetic beads-based neuraminidase enzyme microreactor as a drug discovery tool for screening inhibitors from compound libraries and fishing ligands from natural products. *J. Chromatogr. A* 1568, 123–130. doi: 10.1016/j.chroma.2018.07.031

Zheng, X., Li, Z., Beeram, S., Podariu, M., Matsuda, R., Pfaunmiller, E. L., et al. (2014). Analysis of biomolecular interactions using affinity microcolumns: A review. *J. Chromatogr. B* 968, 49–63. doi: 10.1016/j.jchromb.2014.01.026

Zhu, J., Yi, X., Liu, W., Xu, Y., Chen, S., and Wu, Y. (2017). Immobilized fusion protein affinity chromatography combined with HPLC–ESI-Q-TOF-MS/MS for rapid screening of PPARγ ligands from natural products. *Talanta* 165, 508–515. doi: 10.1016/j.talanta.2016.12.089

Zhuo, R., Liu, H., Liu, N., and Wang, Y. (2016). Ligand fishing: a remarkable strategy for discovering bioactive compounds from complex mixture of natural products. *Molecules* 21:1516. doi: 10.3390/molecules21111516

Zimmermann, G. R., Lehár, J., and Keith, C. T. (2007). Multi-target therapeutics: when the whole is greater than the sum of the parts. *Drug Discov. Today* 12, 34–42. doi: 10.1016/j.drudis.2006.11.008

**Conflict of Interest:** The authors declare that the research was conducted in the absence of any commercial or financial relationships that could be construed as a potential conflict of interest.

frontiers in Chemistry

ORIGINAL RESEARCH
published: 03 December 2019
doi: 10.3389/fchem.2019.00835

# Investigating Monoliths (Vinyl Azlactone-co-Ethylene Dimethacrylate) as a Support for Enzymes and Drugs, for Proteomics and Drug-Target Studies

*Christine Olsen*[1], *Frøydis Sved Skottvoll*[1], *Ole Kristian Brandtzaeg*[1], *Christian Schnaars*[2], *Pål Rongved*[2], *Elsa Lundanes*[1] *and Steven Ray Wilson*[1]*

[1] Department of Chemistry, University of Oslo, Oslo, Norway, [2] Department of Pharmaceutical Chemistry, University of Oslo, Oslo, Norway

Prior to mass spectrometry, on-line sample preparation can be beneficial to reduce manual steps, increase speed, and enable analysis of limited sample amounts. For example, bottom-up proteomics sample preparation and analysis can be accelerated by digesting proteins to peptides in an on-line enzyme reactor. We here focus on low-backpressure 100 μm inner diameter (ID) × 160 mm, 180 μm ID × 110 mm or 250 μm ID × 140 mm vinyl azlactone-co-ethylene dimethacrylate [poly(VDM-co-EDMA)] monoliths as supports for immobilizing of additional molecules (i.e., proteases or drugs), as the monolith was expected to have few unspecific interactions. For on-line protein digestion, monolith supports immobilized with trypsin enzyme were found to be suited, featuring the expected characteristics of the material, i.e., low backpressure and low carry-over. Serving as a functionalized sample loop, the monolith units were very simple to connect on-line with liquid chromatography. However, for on-line target deconvolution, the monolithic support immobilized with a Wnt pathway inhibitor was associated with numerous secondary interactions when exploring the possibility of selectively trapping target proteins by drug-target interactions. Our initial observations suggest that (poly(VDM-co-EDMA)) monoliths are promising for e.g., on-line bottom-up proteomics, but not a "fit-for-all" material. We also discuss issues related to the repeatability of monolith-preparations.

**Keywords: monolithic support, immobilized enzyme reactor, target deconvolution, drug-target interaction, immobilized drug reactor**

OPEN ACCESS

***Edited by:***
*Carmen Lucia Cardoso, University of São Paulo, Brazil*

***Reviewed by:***
*Frantisek Svec, Lawrence Berkeley National Laboratory, United States*
*Jorge Cesar Masini, University of São Paulo, Brazil*

***Correspondence:**
*Steven Ray Wilson*
*s.r.h.wilson@kjemi.uio.no*

***Specialty section:***
*This article was submitted to Analytical Chemistry, a section of the journal Frontiers in Chemistry*

***Received:*** *05 September 2019*
***Accepted:*** *18 November 2019*
***Published:*** *03 December 2019*

***Citation:***
*Olsen C, Skottvoll FS, Brandtzaeg OK, Schnaars C, Rongved P, Lundanes E and Wilson SR (2019) Investigating Monoliths (Vinyl Azlactone-co-Ethylene Dimethacrylate) as a Support for Enzymes and Drugs, for Proteomics and Drug-Target Studies. Front. Chem. 7:835. doi: 10.3389/fchem.2019.00835*

## INTRODUCTION

With the recent advances in liquid chromatography (LC) and mass spectrometry (MS), sample preparation is the most time-consuming part of the method and is often the largest contributor to false analysis results. Sample preparation may be separated into two main categories: off-line procedures and on-line procedures. In on-line sample preparation techniques, the samples are prepared and measured in the same workflow in a closed system, often offering improved performance as both loss of sample and possibility of contamination is reduced. In

an automated on-line method the contribution from human error is reduced, increasing the repeatability/reproducibility of the method (Kataoka, 2003; Nováková and Vlčková, 2009; Pan et al., 2014).

A specific on-line sample preparation step that can be beneficial to have up-stream in an LC-MS analysis system, is the digestion of proteins to peptides for bottom-up proteomics. This can be achieved by immobilizing enzymes on suitable supports compatible with a capillary- or nanoLC-MS set-up, e.g., particle packed (Moore et al., 2016), porous layer open tubular (PLOT) (Brandtzaeg et al., 2017) and monolithic capillaries (Geiser et al., 2008).

The particle packed variant can be associated with high backpressure due to the small particle dimensions (1.5 to 5 μm), dense packing and narrow pores (10 to 30 nm/100 to 300 Å). The high pressure force the liquid to flow around the particles instead of into the pores, reducing the surface of active sites (e.g., the immobilized enzyme) available to interact with the proteins (Xie et al., 1999). In addition, high backpressure can require complex solutions for introducing samples to the enzyme reactor. Also, packed columns often contain filters, or frits, in the ends of the capillary for keeping the particles in place, which increases dead-volumes in the connections that can be especially evident when operating miniaturized systems.

The PLOT and the capillary monolithic formats do not need frits as the porous structure is covalently attached to the wall as a thin layer or a rigid porous structure that fills the entire cavity, respectively (Eeltink et al., 2017). With the same length and ID, monolithic columns offer a larger available surface area than PLOT columns and at a much lower backpressure compared to particle packed columns (Platonova and Tennikova, 2005; Geiser et al., 2008). Another format of PLOT capillaries that can provide an increased number of active sites by increasing the surface area are multichannel columns (i.e., a single piece of capillary with several channels). We have successfully applied multichannel columns for enzyme digestion in an on-line LC-MS system for detection of ricin (Brandtzaeg et al., 2017). However, multichannel PLOT formats can (today) be quite expensive to produce, due to their custom housings, and are less accessible compared to traditional capillaries.

Monoliths can be silica-based or organic polymer-based, where organic polymer monoliths are typically regarded as more suited for macromolecules (Masini and Svec, 2017). Organic polymer monoliths will be the focus of this study as they may have the highest potential for immobilization of ligands due to their characteristics of low backpressure, stability in most solvents and in a wide pH range, accessibility of the active sites due to their pore sizes and structure, and the possibilities of tailoring the functionality of the polymer (Svec, 2006; Krenkova and Svec, 2009; Vlakh and Tennikova, 2013; Safdar et al., 2014; Meller et al., 2017; Naldi et al., 2018). The monolithic format used in this study is also quite inexpensive as no custom parts and reagents are used. The organic monolith immobilized enzyme reactor (IMER) should also be very straightforward to couple on-line with separation systems, e.g., as a functionalized injection loop. To our knowledge, this approach has not been employed for monolith reactors, and is applied in this paper.

There exists a wide variety of organic polymer monoliths which characteristics depend on the monomers used for polymerization (Svec, 2010). The selected vinyl azlactone-co-ethylene dimethacrylate = (poly(VDM-co-EDMA)) monolith is a polymer formed by a relatively polar and a reactive monomer, EDMA and VDM, respectively, and the resulting rather hydrophilic surface will prevent contribution of non-specific hydrophobic interactions with proteins and peptides. The following ring-opening reaction between VDM and a functional group (e.g., amino, hydroxyl, and thiol) will allow for post-modification of the monolithic surface for attachment of ligands, e.g., enzymes and drugs (Coleman et al., 1990; Platonova and Tennikova, 2005). The hydrophilic surface and the post-modification of poly(VDM-co-EDMA) monoliths offer a potential versatile on-line support for different protein sample preparation methods depending on the nature of the immobilized ligands. Thus, in addition to investigating the poly(VDM-co-EDMA) monolith as a support for immobilization of a protease (i.e., trypsin), an IMER, the monolith was also immobilized with a modified Wnt-inhibitor drug, called here a *capti remedium ad monolitus* (CRAM) reactor ("monolith trapped drug"), as a possible tool for target deconvolution in drug discovery. The CRAM reactor would be used to trap the drug target through drug-target interactions, and subsequently elute purified target eluate for identification. The Wnt-inhibitor anti-cancer drug (LDW639) targeting tankyrase 1 and 2 (TNKS1/2) in the Wnt/β-catenin signaling pathway was selected as the model system for the CRAM reactor (Zhan et al., 2017). The inhibition of TNKS1/2 (Solberg et al., 2018) and an inactive Wnt/β-catenin signaling pathway (Mook et al., 2017; Nusse and Clevers, 2017) are attractive for treatment of several types of cancer.

## EXPERIMENTAL SECTION

The overview of chemicals used in the following experiments are presented in **Supplementary Material Sections 1**, **3**, **4**. The poly(VDM-co-EDMA) monoliths were prepared in polyimide-coated fused silica tubing with an 180 ± 6 or 250 ± 6 μm ID, both with an outer diameter (OD) of 360 ± 6 μm, from Polymicro Technologies now a part of Molex (Lisle, IL, USA). The monolithic polymer support for immobilization of enzymes and drugs was formed *in-situ* by free-radical addition polymerization of EDMA and VDM utilizing α-α'-azoisobutyronitrile (AIBN) as initiator. In brief, the fused silica capillaries were filled with 1 M NaOH using an previously described in-house pressurized filling system and sealed in both ends by septa (Berg et al., 2017). After 22 h, the capillaries were washed with water and ACN before being dried with $N_2$(g). The NaOH treated capillaries were filled with a silanization solution [0.5% 2,2-diphenyl-1-picrylhydrazyl (DPPH), 66.08% *N*, *N*-dimethylformamide (DMF) and 32.32% 3-(trimethoxysilyl)propyl methacrylate (ɣ-MAPS), (w/w/w)], which was sonicated for 5 min before filling. The filled capillaries were sealed by septa and placed in an oven (Shimadzu, Kyoto, Japan) at 110°C for 6 h. Subsequently, the capillaries were flushed with acetonitrile (ACN) and dried with $N_2$(g). The silanization procedure was based on Hustoft et al.

(2013). Finally, the capillaries were filled with a polymerization mixture [1% AIBN, 23% VDM, 16% EDMA, 34% 1-propanol and 26% 1,4-butanediol, (w/w/w/w/w)], sealed and placed in an oven at 70°C for 24 h. Subsequently, the capillaries were washed with acetone and dried with $N_2$(g). The polymerization procedure was based on Geiser et al. (2008). The chemicals used for production of the poly(VDM-co-EDMA) monoliths were analyzed by proton nuclear magnetic resonance ($^1$H-NMR), further details are given in **Supplementary Material Section 6**.

For characterization of the morphology of the monoliths, a micrograph of the cross-section was captured with a Quanta 200 FEG-E scanning electron microscope (SEM) from FEI Company (Hillsboro, OR, USA) now a part of Thermo Fisher Scientific. From the dry poly(VDM-co-EDMA) monolith, 1 cm was cut off and glued in an upright position on a sample holder with carbon tape. The sample holder was placed in the sample chamber before the chamber was pumped to low vacuum. A large field detector operating at 15.0 kV, 12 mm distance for the sample and with a 4.0 spot size was used to capture the micrographs.

For immobilizing trypsin to VDM on the monolithic support, a solution consisting of 0.25 mg/mL trypsin and 2.25 mg/mL benzamidine in 50 mM phosphate buffer (pH 7.2) was flushed through the monoliths for 3.5 h. The resulting immobilized enzyme reactors (IMERs) were filled with 50 mM ammonium acetate buffer (pH 8.75), sealed with septa and stored at 4°C.

The modified LDW639 Wnt-inhibitor drug was synthesized in-house from methyl-4-oxotetrahydro-2H-thiopyran-3-carboxylate (**I**, beta-keto ester, 95%) and 4-boc-aminomethylbenzamidine (**II**, boc-benzamidine, 97%), and modified by the addition of a linker (**V**, 2,2-dimethyl-4-oxo-3,8,11-trioxa-5-azatridecan-13-oic acid, 97%) all purchased from Fluorochem (Hadfield, United Kingdom). The finalized product (**VII**), structure shown in **Figure 1,** was examined for Wnt-signaling activity using a SuperTOPFlash-luciferase assay (STF-Luc) at the Unit of Cell Signaling, Oslo University Hospital. The synthesis, characterization and determination of Wnt-activity of modified LDW639 (**VII**) is described in **Supplementary Material Section 3**, **Figures S4–S9**.

The CRAM reactor was prepared by immobilizing the modified LDW639 Wnt-inhibitor drug on the poly(VDM-co-EDMA) monolith by flushing a solution of 5 mg/mL drug in 50 mM phosphate buffer (pH 7.2) through the capillary for 3 h (∼0.5 mL). Additionally, a reference monolith was made by flushing 1 M monoethanolamine (MEA) through a monolith in the same manner. Both the CRAM reactor and the MEA monolith were filled with 50 mM phosphate buffer, sealed with septa and stored at 4°C.

For evaluation of the protein digestion potential of the immobilized enzyme reactors, solutions of 500 μg/mL reduced [by dithiothreitiol (DDT)] and alkylated [by iodoacetamide (IAM)] myoglobin dissolved in 50 mM ammonium acetate were used. The in-solution digested myoglobin solutions were prepared by adding 10 μg trypsin per 500 μg myoglobin, and incubation at 37°C for 45 min. The solutions were stored at −20°C.

To investigate the possibility of trapping the protein target of the immobilized Wnt-inhibitor, human embryonic kidney 293 (HEK293) cells were received, after cell cultivation, from the unit of Cell Signaling, Oslo University Hospital. The cell line HEK293 were purchased from American Type Culture Collection (ATCC, Manassas, VA, USA), and maintained according to the ATCC guidelines. For cell lysis with a non-denaturing buffer (4.0 mL glycerol, 4 mL 10x protease inhibitor, 700 mg sodium chloride, 28 mg imidazole, 3 mg DTT and 1.2 mL 1 M tris buffer (pH 8.0), diluted with water to 40 mL), a procedure based on Voronkov et al. (2013) was used. In brief, the cell samples (∼1 million cells) were added 200 μL of the buffer and vortexed by pipetting up and down a minimum of 10 times. The samples were ultrasonicated at 40 kHz for 30 s before 15 min incubation on ice, and the ultrasonication step was repeated once before another 15 min of incubation on ice. After incubation, the samples were centrifuged for 15 min at 14,000 relative centrifugal force (rcf), and the supernatant was pipetted into new tubes and stored at −20°C.

For evaluation of protein digestion by the IMERs, an on-line IMER-LC-UV system utilizing an Agilent 1,100 series pump (Agilent technologies, Santa Clara, CA, USA) (LC pump in **Figure 1A**) connected to a two-position 6-port valve from Vici Valco (Houston, TX, USA) was used. The mobile phase reservoir A contained 0.1% trifluoroacetic acid (TFA)/ACN (95/5, v/v) while B contained 0.1% TFA in ACN. A 180 μm ID × 110 mm IMER was directly attached to two ports of the external valve as shown in **Figure 1A**. The porosity of the IMER was estimated to be 74% (by elution of a non-retained compound on a 250 μm ID × 141 mm poly(VDM-co-EDMA) compared to that on an empty 250 μm ID × 141 mm fused silica capillary), the volume of the reactor was 2 μL. A total of 10 μL of myoglobin solution was applied by syringe on to the 2 μL IMER injection loop, and was trapped in the loop for 5 min at room temperature. After digestion, the treated solution was transferred in 1 min to an in-house packed 0.3 × 100 mm BetaMax Neutral C18 (5 μm particle diameter) steel capillary analytical column for separation at a flow rate of 2 μLmin$^{-1}$. A gradient was run at a flow rate of 10 μLmin$^{-1}$ for 25 min bypassing the IMER (started after 1 min); at 0% B for 0–1.5 min, linearly increased to 55% B for from 1.5 to 17 min, kept at 55% B at 17–23 min, quickly increased to 90% B for 1 min and then reversed to 0% B for 1 min. Detection was performed at 210 nm by a WellChrome K-2600 UV-detector (Knauer, Berlin, Germany), equipped with a 65 nL (100 μm ID/375 μm OD) flow cell. A Perkin Elmer Nelson 900 series analog-to-digital interface (Waltham, MA, USA) and a computer with a TotalChrom software were used for obtaining the chromatograms.

An EASY nLC pump from Proxeon now a part of Thermo Fisher (nanopump in **Figure 1B**) with mobile phase reservoirs A and B both containing 100% HPLC-grade water was used for evaluation of trapping of TNKS1/2 on CRAM reactors and MEA monoliths. Injection was manually performed with a glass syringe using an external two-position 6-port valve from Vici Valco with an attached 20 μL polyetheretherketone (PEEK) sample loop from Proxeon. A 250 μm ID × 140 mm CRAM reactor was attached to the external port as shown in **Figure 1B**, and the pump was used at 1 μLmin$^{-1}$ flow rate. From an estimate of 74% porosity the volume of the CRAM reactor was 5.1 μL. The CRAM reactor was first rinsed for 30 min with HPLC water, while the loop was manually loaded with 20 μL of cell lysate sample. For the next 30 min the sample was transported from

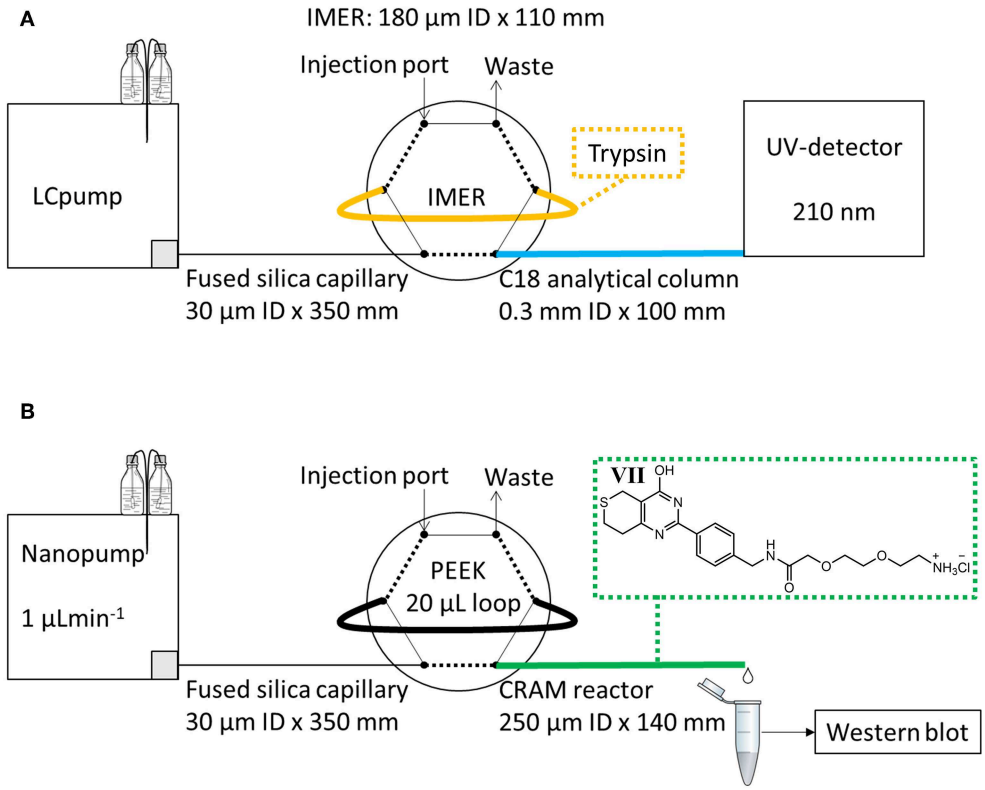


**FIGURE 1 |** Experimental set-up for evaluation of **(A)** IMERs with trypsin and **(B)** CRAM reactors with modified LDW639 (**VII**).

the loop onto the CRAM reactor, and the eluate was collected in a tube marked "Flush 1." During the last minute of collection, the valve was switched to load position and another 20 µL of sample was loaded onto the loop. For another 30 min the second portion of sample was transferred onto the CRAM reactor, and the eluate was collected in a tube marked "Flush 2." For the subsequent 30 min, HPLC water was flushed through the loop and the CRAM reactor, and collected in a tube marked "Wash 1." A second wash eluate was collected, while bypassing the loop, in a tube marked "Wash 2." For elution of bound TNKS1/2 on the CRAM reactor, 20 µL of 2% formic acid in HPLC-grade water was applied on the loop, flushed through the reactor for 30 min (total volume 30 µL) and collected in a tube marked "EluateF," which was added 5 µL of 1 M NaOH prior to and 5 µL following sample collection to immediately neutralize the sample. A second elution was performed in the same manner with 2% sodium dodecyl sulfate (SDS, denaturing agent) in 60 mM tris buffer (w/v) and collected in a tube marked "EluateS." All of the collected eluates were analyzed by western blot for TNKS1/2 using actin as loading control. Western blot procedure is explained in detail in **Supplementary Materials Section 4**.

## RESULTS AND DISCUSSION

In this project, an poly(VDM-co-EDMA) monolith was assessed as a support for immobilized ligands to enable on-line sample preparations in bottom-up proteomics and target deconvolution in drug discovery using trypsin and modified LDW639, respectively.

### IMERs: Trypsin Immobilized on Poly(VDM-co-EDMA) Monoliths for Digestion of Myoglobin

First, we wanted to investigate if the poly(VDM-co-EDMA) monolith was suitable as a support for immobilized trypsin to enable fast on-line digestion of proteins to peptides. An evaluation of 9 replicates of 100 µm ID × 160 mm and 9 replicates of 180 µm ID × 110 mm poly(VDM-co-EDMA) monoliths were successfully prepared with a homogeneous, uniform morphology, shown in **Supplementary Materials Section 5**, **Figures S11**, **S12**, respectively. Important for practical use, the monoliths allowed easy manual injection using a loop on a 6-port valve due to low pressure (**Figure 1**). The poly(VDM-co-EDMA) monoliths show an average backpressure of 30 bar/m at a flow rate of 1 µL/min of 100% ACN with a permeability of $5.0 \times 10^{-14}$ $m^2$, calculated as described in Meller et al. (2016), based on backpressure measurements (n = 17). The permeability of the poly(VDM-co-EDMA) monolith is in same range as other organic monoliths (Vlakh et al., 2013; Volokitina et al., 2017), commercial particle packed columns (Song et al., 2014), and

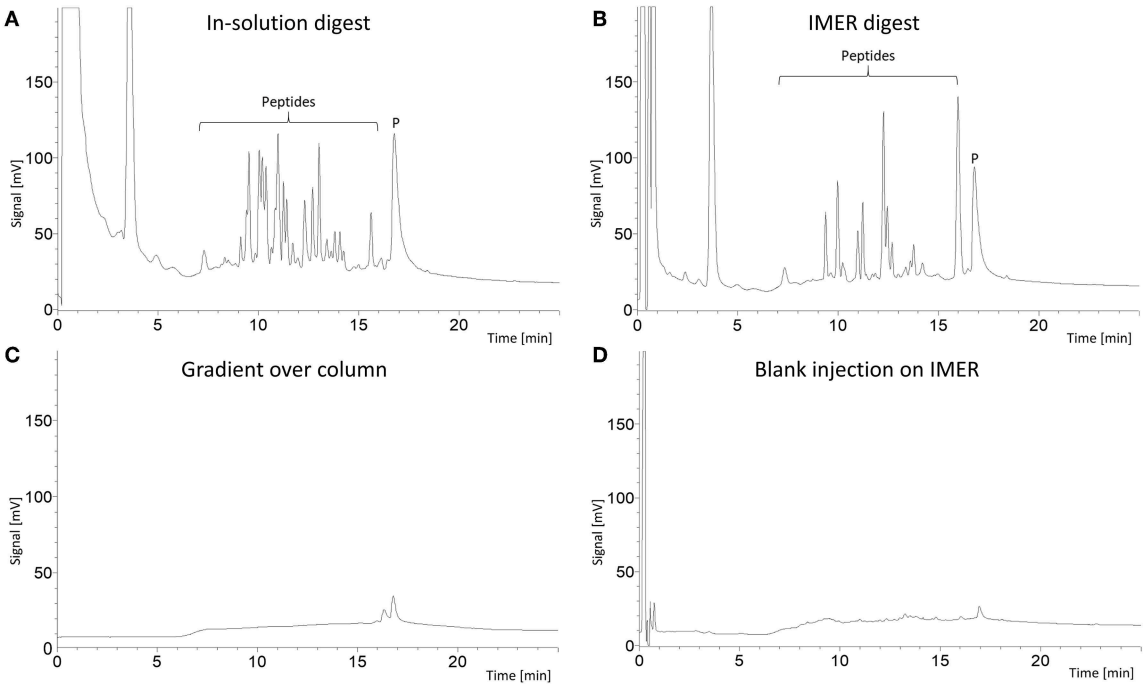


**FIGURE 2 |** LC-UV chromatograms (210 nm) of: **(A)** 1.4 μL 500 μg/mL myoglobin (reduced and alkylated by DTT and IAM) in-solution digest (trypsin:protein, 1:50) injected into a 180 μm × 110 mm poly(VDM-co-EDMA) monolithic support. **(B)** 1.4 μL 500 μg/mL myoglobin (reduced and alkylated by DTT and IAM) injected into a 180 μm × 110 mm poly(VDM-co-EDMA) trypsin IMER for 5 min on-line digestion. **(C)** blank gradient run excluding the IMER and **(D)** injection of 1.4 μL 50 mM ammonium acetate on the 180 μm × 110 mm poly(VDM-co-EDMA) trypsin IMER which had been washed with 5 μL 30% ACN in 50 mM ammonium acetate following the myoglobin injection. The intact protein peak (P) occurs at 17 min, while the peptide peaks are concentrated from 7 to 16 min. The analytical column was a 0.3 × 100 mm BetaMax Neutral C18 (5 μm particle diameter) in a steel housing. Mobile phase A consisted of ACN/0.1% TFA (5/95, v/v), while mobile phase B consisted of 0.1% TFA in ACN. The gradient was performed with %B: at 0% for 0–1.5 min, linearly increased to 55% for from 1.5 to 17 min, kept at 55% at 17–23 min, quickly increased to 90% for 1 min and then reversed to 0% for 1 min.

silica based monoliths (Motokawa et al., 2002; Zhang et al., 2013). The performance of the produced trypsin IMERs was evaluated by comparing the peptide fingerprint region of an on-line IMER digestion (5 min, **Figure 2B**) to that of myoglobin digested in-solution (**Figure 2A**). The peptide region confirmed that the IMERs had trypsin activity leading to digestion of myoglobin. To be able to compare the IMER digest with the in-solution digest, the in-solution digestion was injected on a monolithic support with no immobilized enzyme and analysis was run in the same manner as the IMER digestion. Possible carry-over of proteins and peptides was checked bypassing the IMER. The analytical column was responsible for the contribution of carry-over of protein as shown in **Figure 2C**. A blank run of 50 mM ammonium acetate following digestion of myoglobin on the IMER was executed after a simple washing step (5 μL of 30% ACN in 50 mM ammonium acetate). The simple washing step eliminated any significant carry-over from the IMER shown in **Figure 2D**. All 9 replicates of 100 μm ID IMERs and 9 replicates of 180 μm ID IMERs were successful in digesting myoglobin, as shown in **Supplementary Materials Section 2**, **Figures S1**, **S2**, respectively. On-line IMER-LC-MS was demonstrated with one reactor (**Supplementary Materials Section 2**, **Figure S3**); proteins spanning 10–70 kDa in mixture were readily identified with sequence coverages ranging from 26 to 69%. These values are comparable to that obtained with open tubular variants which included both trypsin and Lys C enzymes (Hustoft et al., 2014). However, we were unable to identify larger proteins e.g., fibrinogen alpha and transferrin, suggesting a protein size limitation regarding the current set-up.

Thus, the poly(VDM-co-EDMA) based trypsin IMERs allow easy manual injection due to low backpressure (no need for a separate loading pump, or e.g., having to time when digested fraction would enter the LC-system) and a simple washing step eliminates possible carry-over after successful digestion of myoglobin in 5 min. The trypsin poly(VDM-co-EDMA) IMERs can be used up-stream LC-MS in bottom-up proteomic studies to reduce time consumption on sample preparation and loss of sample.

## CRAM Reactors: LDW639 Immobilized Poly(VDM-co-EDMA) Monoliths for Selective Trapping and Elution of Target TNKS1/2

In drug discovery, development and optimization of new (and old) drugs depends on target identification (Terstappen et al., 2007), and a multitude of chemical proteomics methods exists (Kubota et al., 2019). However, target purification up-stream LC-MS would reduce loss of target and contaminations, give

higher throughput and possible enable identification of low abundant targets.

An evaluation of poly(VDM-co-EDMA) monoliths immobilized with modified LDW639 drug for trapping and purification of target tankyrase 1/2 was executed. The modified LDW639 drug was successfully synthesized and found to inhibit Wnt-signaling in STF-Luc assay (**Supplementary Materials Section 3**, **Figure S9**). Both the 250 μm ID poly(VDM-co-EDMA) monolith immobilized with modified Wnt-pathway inhibitor (CRAM reactor) and the reference 250 μm ID poly(VDM-co-EDMA) monolith immobilized with monoethanolamine (MEA monolith) were successfully prepared; see below for discussion on the use of larger IDs than with the IMERs. A comparison between the CRAM reactor and the MEA monolith was carried out to assess whether or not immobilization of LDW639 offered trapping potential of the drug target TNKS1/2 in a different manner than the MEA monolith. Residues of the reactive VDM monomer in the CRAM reactor can give formation of covalent bonds between proteins and VDM (Coleman et al., 1990). Possible reaction between proteins and VDM was addressed by making the MEA monolith (described in Experimental), where all of the azlactone functionalities has been quenched by MEA, making the MEA monolith a suitable reference for no reaction between proteins and VDM.

The eluates collected from the CRAM reactor and the MEA monolith after applying HEK293 cell lysate were analyzed by western blot for target TNKS1/2 using actin as loading control, because actin is commonly expressed in all eukaryotic cell types. TNKS1/2 was not found in any eluates collected during flushing, washing or eluting from the CRAM reactor or the MEA monolith (**Figure 3**). TNKS1/2 was however present in a detectable amount in an equivalent aliquot of cell lysate as used for the CRAM reactor and the MEA monolith. TNKS1/2 was also detected in a positive TNKS1/2 control (cell lysate of HEK293 cells treated with Wnt-inhibitor 007-LK). The loading control actin was detectable in all controls and in the following eluates: Flush1, Flush2, Wash1 and Wash2, collected from both the CRAM reactor and the MEA monolith. Hence, TNKS1/2 was present in the cell lysate that was applied on the CRAM reactor and the MEA monolith, but TNKS1/2 was not eluted off in a western blot detectable amount during flushing with cell lysate, washing with water or eluting with acid or SDS. Thus, TNKS1/2 is retained, likely due to secondary interactions, on the poly(VDM-co-EDMA) based reactors which negates the selective affinity between drug and target in this format. The conditions attempted for elution of TNKS1/2 was changes in pH (2% formic acid, 1M and 3M NaOH), different ranges of salt (50 mM to 1 M ammonium acetate at pH 7.2), different percentages of ACN (10% to 50%) and denaturing agent (2% SDS). The induced changes in pH and salt concentration, and elution solutions consisting of ACN and SDS are common eluting methods for purification by affinity (Cuatrecasas et al., 1968; Shimizu et al., 2000). None of the selected elution solutions were successful at eluting TNKS1/2 in

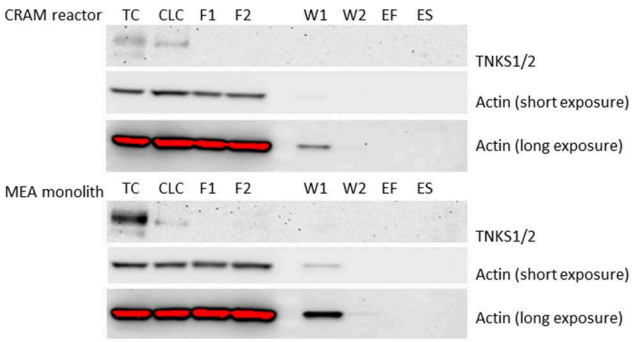


**FIGURE 3 |** Western blot of: (TC–Tankyrase Control) lane of 21 μg of protein from 007-LK control and (CLC–Cell lysate control) lane of 36.3 μg of protein from cell lysate of HEK293. Samples collected from the CRAM reactor (Upper) and MEA monolith (Lower) in the following lanes: (F1) Flush of 36.3 μg protein from cell lysate of HEK293, (F2) Flush of 36.3 μg protein from cell lysate of HEK293, (W1) Wash 1 with water, (W2) Wash 2 with water, (ES) eluted with 2% formic acid and (ES) eluted with 2% SDS. The exposure time was 7,200 s for TNKS1/2, and for actin 10 s (short exposure) and 180 s (long exposure). The raw files from western blot are given in **Supplementary material section 4**, **Figure S10**.

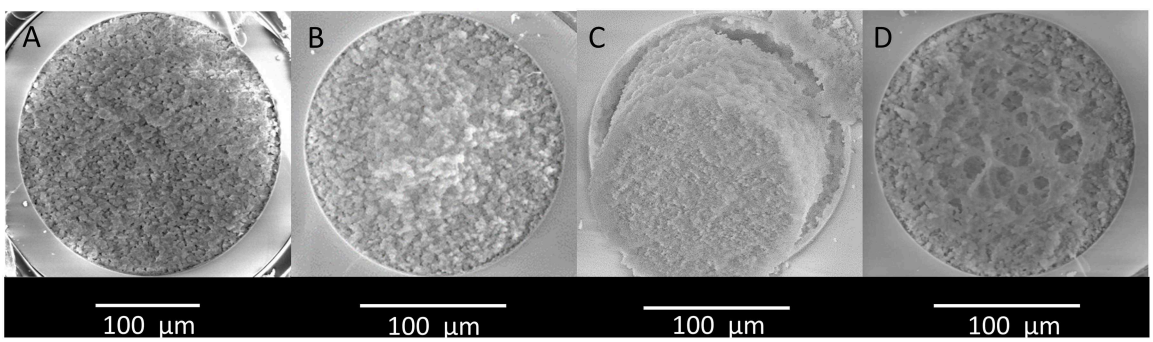


**FIGURE 4 |** Micrographs of the cross-section of **(A)** a 250 μm ID and **(B)** a 180 μm ID poly(VDM-co-EDMA) monolith. **(C)** A 180 μm ID monolith not attached to the wall, and **(D)** a 180 μm ID monolith with large pores. The micrographs were captured by a large field detector (LFD) at 15.0 kV working at a distance of minimum 12 mm from the sample in low vacuum with a spot size of 4.0.

western blot detectable amount (only results for FA and SDS are shown).

The CRAM reactor used in this study shows that common elution conditions in affinity purification is not sufficient for eluting trapped target proteins from immobilized drugs. However, elution with 2% FA was sufficient for elution of peptides from poly(VDM-co-EDMA) monoliths with immobilized antibodies (Levernæs et al., 2018). The MEA monolith, with quenched azlactone functionalities, did not elute the target proteins, TNKS1/2, indicating that proteins are retained on the poly(VDM-co-EDMA) monolith by other interactions besides reaction with VDM. The unspecific interactions between proteins and the poly(VDM-co-EDMA) based CRAM reactors and MEA monoliths may indicated that an even more hydrophilic surface on the organic polymer is needed for intact protein assessments.

### Robustness of Recipe for Poly(VDM-co-EDMA) Monoliths Prepared in Capillaries

For immobilization of modified LDW639, monolithic supports with the highest possible amounts of active sites were desired. Thus, in addition to preparing the poly(VDM-co-EDMA) monolith in 180 μm ID capillaries, the monolith was also prepared in 250 μm ID capillaries. At this stage of the project, the uniform morphology was only successful in 250 μm ID capillaries (**Figure 4A** and **Supplementary Materials Section 5**, **Figure S14**). In contrast to the earlier production of monoliths for IMERs, the 180 μm ID capillaries later on displayed large pores disrupting the monolithic structure and was not correctly attached to the wall of the fused silica capillary (**Figure 4** and **Supplementary Materials Section 5**, **Figure S13**). Because of this, the liquid chemicals used in production of the monoliths: DMF, γ-MAPS, EDMA, VDM, 1-propanol and 1,4-butanediol were replaced, and $^{1}$H-NMR spectra of the new and old chemicals were compared (**Figures S15–S20** in **Supplementary Materials Section 6**). Virtually identical NMR spectra were obtained for the old and the new chemicals, indicating that no detectable degradation or contamination of the chemicals could explain why the poly(VDM-co-EDMA) monolith could not be produced in 180 μm ID capillaries anymore. However, monoliths prepared in 250 μm ID capillaries with new and old chemicals were not significantly different at a 95% confidence level based on backpressure measurements at 6 different flow rates.

Hence, we could not trace repeatability issues to the chemicals employed, suggesting that other conditions/factors e.g., subtle variations in humidity and temperature may play more substantial roles for the morphology of the monoliths (for example, the porogenic mixture consisting of 1-propanol and 1,4-butanediol is highly sensitive to presence of water). One of the reviewers suggested that including a protonation step of the silanols, using HCl after treatment of NaOH, may give a better activation of the silica surface before silanization by γ-MAPS and consequently a more consistent attachment of the monolith. Concerning the polymerization, the solution of the monomer EDMA consisted of 90–110 ppm of monomethyl ether hydroquinone (MeHQ, polymerization inhibitor). The MeQH has been suggested to be removed prior to polymerization to increase reproducible morphology of the monoliths.

The poly(VDM-co-EDMA) monolith has a good mechanical strength suitable for attachment as a loop on a 6-port valve and is easily prepared in fused silica capillaries with various IDs. The reactive VDM monomer also allows for tailoring toward specific applications by post-modification with ligands after formation of the organic polymer.

## CONCLUSION

The poly(VDM-co-EDMA) monoliths shows potential as trypsin-based IMERs with low backpressure and fast digestion of protein standards, and was very simple to incorporate in an on-line system as a functionalized loop with little carry-over. A next step will be to investigate their potential in on-line systems to be used in e.g., the field of "organ-on-a-chip" mass spectrometry-based proteomics. We have undertaken initial steps toward on-line drug/target studies using monolithic supports. Based on the same type of poly(VDM-co-EDMA) monolith, the CRAM reactor revealed that selective trapping and subsequent purified elution of high molecular weight protein targets (>110 kDa) in complex cell lysate was not straightforward, highlighting some limitations of this otherwise promising material and format. Nonetheless, due to the advantages that on-line drug/target studies can have, we are encouraged to explore alternative monoliths due to the format's versatility and ease of coupling with analytical instrumentation.

## DATA AVAILABILITY STATEMENT

Datasets generated for this study are included in the article/**Supplementary Material**, with the exception of backpressure measurements. Requests to access the backpressure measurements data should be directed to the corresponding author.

## AUTHOR CONTRIBUTIONS

CO, FS, and OB contributed to monolith work. CO performed LC-UV and LC-MS experiments. CO and FS performed biochemical experiments. CO, PR, and CS performed drug synthesis. SW, EL, and PR were supervisors. All authors contributed to planning experiments and writing the manuscript.

## FUNDING

This work was partially supported by the Research Council of Norway through its Center of Excellence scheme, project number 262613.

## SUPPLEMENTARY MATERIAL

The Supplementary Material for this article can be found online at: https://www.frontiersin.org/articles/10.3389/fchem.2019.00835/full#supplementary-material

## REFERENCES

Berg, H. S., Seterdal, K. E., Smetop, T., Rozenvalds, R., Brandtzaeg, O. K., Vehus, T., et al. (2017). Self-packed core shell nano liquid chromatography columns and silica-based monolithic trap columns for targeted proteomics. *J. Chromatogr. A* 1498, 111–119. doi: 10.1016/j.chroma.2017.03.043

Brandtzaeg, O. K., Røen, B. T., Enger, S., Lundanes, E., and Wilson, S. R. (2017). Multichannel open tubular enzyme reactor online coupled with mass spectrometry for detecting ricin. *Analyt. Chem.* 89, 8667–8673. doi: 10.1021/acs.analchem.7b02590

Coleman, P. L., Walker, M. M., Milbrath, D. S., Stauffer, D. M., Rasmussen, J. K., Krepski, L., et al. (1990). Immobilization of Protein A at high density on azlactone-functional polymeric beads and their use in affinity chromatography. *J. Chromatogr. A* 512, 345–363. doi: 10.1016/S0021-9673(01)89501-7

Cuatrecasas, P., Wilchek, M., and Anfinsen, C. B. (1968). Selective enzyme purification by affinity chromatography. *Proc. Natl. Acad. Sci. U.S.A.* 61, 636–643. doi: 10.1073/pnas.61.2.636

Eeltink, S., Wouters, S., Dores-Sousa, J. L., and Svec, F. (2017). Advances in organic polymer-based monolithic column technology for high-resolution liquid chromatography-mass spectrometry profiling of antibodies, intact proteins, oligonucleotides, and peptides. *J. Chromatogr. A*, 1498, 8–21. doi: 10.1016/j.chroma.2017.01.002

Geiser, L., Eeltink, S., Svec, F., and Fréchet, J. M. (2008). In-line system containing porous polymer monoliths for protein digestion with immobilized pepsin, peptide preconcentration and nano-liquid chromatography separation coupled to electrospray ionization mass spectroscopy. *J. Chromatogr. A*, 1188, 88–96. doi: 10.1016/j.chroma.2008.02.075

Hustoft, H. K., Brandtzaeg, O. K., Rogeberg, M., Misaghian, D., Torsetnes, S. B., Greibrokk, T., et al. (2013). Integrated enzyme reactor and high resolving chromatography in "sub-chip" dimensions for sensitive protein mass spectrometry. *Sci. Rep.* 3:3511. doi: 10.1038/srep03511

Hustoft, H. K., Vehus, T., Brandtzaeg, O. K., Krauss, S., Greibrokk, T., Wilson, S. R., et al. (2014). Open tubular lab-on-column/mass spectrometry for targeted proteomics of nanogram sample amounts. *PloS ONE* 9:*e*106881. doi: 10.1371/journal.pone.0106881

Kataoka, H. (2003). New trends in sample preparation for clinical and pharmaceutical analysis. *TrAC Trends Analyt. Chem.* 22, 232–244. doi: 10.1016/S0165-9936(03)00402-3

Krenkova, J., and Svec, F. (2009). Less common applications of monoliths: IV. Recent developments in immobilized enzyme reactors for proteomics and biotechnology. *J. Separat. Sci.* 32, 706–718. doi: 10.1002/jssc.200800641

Kubota, K., Funabashi, M., and Ogura, Y. (2019). Target deconvolution from phenotype-based drug discovery by using chemical proteomics approaches. *Biochim. Biophys. Acta Proteins Proteom.* 1867, 22–27. doi: 10.1016/j.bbapap.2018.08.002

Levernæs, M. C. S., Brandtzaeg, O. K., Amundsen, S. F., Reubsaet, L., Lundanes, E., Halvorsen, T. G., et al. (2018). Selective fishing for peptides with antibody-immobilized acrylate monoliths, coupled online with NanoLC-MS. *Analyt. Chem.* 90, 13860–13866. doi: 10.1021/acs.analchem.8b00935

Masini, J. C., and Svec, F. (2017). Porous monoliths for on-line sample preparation: a review. *Analyt. Chim. Acta* 964, 24–44. doi: 10.1016/j.aca.2017.02.002

Meller, K., Pomastowski, P., Grzywinski, D., Szumski, M., and Buszewski, B. (2016). Preparation and evaluation of dual-enzyme microreactor with co-immobilized trypsin and chymotrypsin. *J. Chromatogr. A* 1440, 45–54. doi: 10.1016/j.chroma.2016.02.070

Meller, K., Szumski, M., and Buszewski, B. (2017), Microfluidic reactors with immobilized enzymes—Characterization, dividing, perspectives. *Sensors Actuat B Chem.* 244, 84–106. doi: 10.1016/j.snb.2016.12.021

Mook, R. A., Ren, X. R., Wang, J., Piao, H., Barak, L. S., Lyerly, H. K., et al. (2017). Benzimidazole inhibitors from the Niclosamide chemotype inhibit Wnt/β-catenin signaling with selectivity over effects on ATP homeostasis. *Bioorgan. Med. Chem.* 25, 1804–1816. doi: 10.1016/j.bmc.2017.01.046

Moore, S., Hess, S., and Jorgenson, J. (2016). Characterization of an immobilized enzyme reactor for on-line protein digestion. *J. Chromatogr. A* 1476, 1–8. doi: 10.1016/j.chroma.2016.11.021

Motokawa, M., Kobayashi, H., Ishizuka, N., Minakuchi, H., Nakanishi, K., Jinnai, H., et al. (2002). Monolithic silica columns with various skeleton sizes and through-pore sizes for capillary liquid chromatography. *J. Chromatogr. A* 961, 53–63. doi: 10.1016/S0021-9673(02)00133-4

Naldi, M., Tramarin, A., and Bartolini, M. (2018). Immobilized enzyme-based analytical tools in the -omics era: recent advances. *J. Pharmaceut. Biomed. Analy.* 160, 222–237. doi: 10.1016/j.jpba.2018.07.051

Nováková, L., and Vlčková, H. (2009). A review of current trends and advances in modern bio-analytical methods: chromatography and sample preparation. *Analyt. Chim. Acta* 656, 8–35. doi: 10.1016/j.aca.2009.10.004

Nusse, R., and Clevers, H. (2017). Wnt/β-catenin signaling, disease, and emerging therapeutic modalities. *Cell* 169, 985–999. doi: 10.1016/j.cell.2017.05.016

Pan, J., Zhang, C., Zhang, Z., and Li, G. (2014). Review of online coupling of sample preparation techniques with liquid chromatography. *Analyt. Chim. Acta* 815, 1–15. doi: 10.1016/j.aca.2014.01.017

Platonova, G. A., and Tennikova, T. B. (2005). Affinity processes realized on high-flow-through methacrylate-based macroporous monoliths. *J. Chromatogr. A* 1065, 19–28. doi: 10.1016/j.chroma.2004.12.008

Safdar, M., Sproß, J., and Jänis, J. (2014). Microscale immobilized enzyme reactors in proteomics: latest developments. *J. Chromatogr. A*, 1324, 1–10. doi: 10.1016/j.chroma.2013.11.045

Shimizu, N., Sugimoto, K., Tang, J., Nishi, T., Sato, I., Hiramoto, M., et al. (2000). High-performance affinity beads for identifying drug receptors. *Nat. Biotechnol.* 18, 877–881. doi: 10.1038/78496

Solberg, N. T., Waaler, J., Lund, K., Mygland, L., Olsen, P. A., and Krauss, S. (2018). TANKYRASE inhibition enhances the antiproliferative effect of PI3K and EGFR inhibition, mutually affecting β-CATENIN and AKT signaling in colorectal cancer. *Mol. Cancer Res.* 16, 543–553. doi: 10.1158/1541-7786.MCR-17-0362

Song, H., Adams, E., Desmet, G., and Cabooter, D. (2014). Evaluation and comparison of the kinetic performance of ultra-high performance liquid chromatography and high-performance liquid chromatography columns in hydrophilic interaction and reversed-phase liquid chromatography conditions. *J. Chromatogr. A* 1369, 83–91. doi: 10.1016/j.chroma.2014.10.002

Svec, F. (2006), Less common applications of monoliths: I. Microscale protein mapping with proteolytic enzymes immobilized on monolithic supports. *Electrophoresis* 27, 947–961. doi: 10.1002/elps.200500661

Svec, F. (2010), Porous polymer monoliths: amazingly wide variety of techniques enabling their preparation. *J. Chromatogr. A* 1217, 902–924. doi: 10.1016/j.chroma.2009.09.073

Terstappen, G. C., Schlüpen, C., Raggiaschi, R., and Gaviraghi, G. (2007). Target deconvolution strategies in drug discovery. *Nat. Rev. Drug Discov.* 6, 891–903. doi: 10.1038/nrd2410

Vlakh, E. G., Maksimova, E. F., and Tennikova, T. B. (2013). Monolithic polymeric sorbents for high-performance chromatography of synthetic polymers. *Polymer Sci. Series B* 55, 55–62. doi: 10.1134/S1560090413020061

Vlakh, E. G., and Tennikova, T. B. (2013). Flow-through immobilized enzyme reactors based on monoliths: II. Kinetics study and application. *J. Separat. Sci.* 36, 1149–1167. doi: 10.1002/jssc.201201090

Volokitina, M. V., Nikitina, A. V., Tennikova, T. B., and Korzhikova-Vlakh, E. G. (2017). Immobilized enzyme reactors based on monoliths: effect of pore size and enzyme loading on biocatalytic process. *Electrophoresis* 38, 2931–2939. doi: 10.1002/elps.201700210

Voronkov, A., Holsworth, D. D., Waaler, J., Wilson, S. R., Ekblad, B., Perdreau-Dahl, H., et al. (2013). Structural basis and SAR for G007-LK, a lead stage 1, 2, 4-triazole based specific tankyrase 1/2 inhibitor. *J. Med. Chem.* 56, 3012–3023. doi: 10.1021/jm4000566

Xie, S., Svec, F., and Fréchet, J. M. (1999). Design of reactive porous polymer supports for high throughput bioreactors: poly (2-vinyl-4, 4-dimethylazlactone-co-acrylamide-co-ethylene dimethacrylate) monoliths. *Biotechnol. Bioeng.* 62, 30–35.

Zhan, T., Rindtorff, N., and Boutros, M. (2017). Wnt signaling in cancer. *Oncogene* 36, 1461–1473. doi: 10.1038/onc.2016.304

Zhang, Z., Wang, F., Ou, J., Lin, H., Dong, J., and Zou, H. (2013). Preparation of a butyl–silica hybrid monolithic column with a "one-pot" process for bioseparation by capillary liquid chromatography. *Analyt. Bioanalyt. Chem.* 405, 2265–2271. doi: 10.1007/s00216-012-6589-z

**Conflict of Interest:** The authors declare that the research was conducted in the absence of any commercial or financial relationships that could be construed as a potential conflict of interest.

frontiers in Chemistry

ORIGINAL RESEARCH
published: 10 January 2020
doi: 10.3389/fchem.2019.00910

# Surface Plasmon Resonance as a Tool for Ligand Binding Investigation of Engineered GPR17 Receptor, a G Protein Coupled Receptor Involved in Myelination

*Davide Capelli[1†], Chiara Parravicini[2†], Giorgio Pochetti[1], Roberta Montanari[1], Caterina Temporini[3], Marco Rabuffetti[4], Maria Letizia Trincavelli[5], Simona Daniele[5], Marta Fumagalli[2], Simona Saporiti[2], Elisabetta Bonfanti[2], Maria P. Abbracchio[2], Ivano Eberini[6], Stefania Ceruti[2], Enrica Calleri[3]* and Stefano Capaldi[7]**

[1] Istituto di Cristallografia, Consiglio Nazionale delle Ricerche, Rome, Italy, [2] Department of Pharmacological and Biomolecular Sciences, Università degli Studi di Milano, Milan, Italy, [3] Department of Drug Sciences, University of Pavia, Pavia, Italy, [4] Department of Food, Environmental and Nutritional Sciences, Università degli Studi di Milano, Milan, Italy, [5] Department of Pharmacy, University of Pisa, Pisa, Italy, [6] Department of Pharmacological and Biomolecular Sciences, Data Science Research Center, Università degli Studi di Milano, Milan, Italy, [7] Department of Biotechnology, University of Verona, Verona, Italy

The aim of this study was to investigate the potential of surface plasmon resonance (SPR) spectroscopy for the measurement of real-time ligand-binding affinities and kinetic parameters for GPR17, a G protein-coupled receptor (GPCR) of major interest in medicinal chemistry as potential target in demyelinating diseases. The receptor was directly captured, in a single-step, from solubilized membrane extracts on the sensor chip through a covalently bound anti-6x-His-antibody and retained its ligand binding activity for over 24 h. Furthermore, our experimental setup made possible, after a mild regeneration step, to remove the bound receptor without damaging the antibody, and thus to reuse many times the same chip. Two engineered variants of GPR17, designed for crystallographic studies, were expressed in insect cells, extracted from crude membranes and analyzed for their binding with two high affinity ligands: the antagonist Cangrelor and the agonist Asinex 1. The calculated kinetic parameters and binding constants of ligands were in good agreement with those reported from activity assays and highlighted a possible functional role of the N-terminal residues of the receptor in ligand recognition and binding. Validation of SPR results was obtained by docking and molecular dynamics of GPR17-ligands interactions and by functional *in vitro* studies. The latter allowed us to confirm that Asinex 1 behaves as GPR17 receptor agonist, inhibits forskolin-stimulated adenylyl cyclase pathway and promotes oligodendrocyte precursor cell maturation and myelinating ability.

**Keywords: GPR17, G-protein coupled receptors, SPR, ligand binding, Cangrelor, Asinex 1**

OPEN ACCESS

***Edited by:***
*Nicole J. Jaffrezic-Renault, Université Claude Bernard Lyon 1, France*

***Reviewed by:***
*Carole Chaix, Centre National de la Recherche Scientifique (CNRS), France*
*Juan Manuel Lázaro-Martínez, University of Buenos Aires, Argentina*

***Correspondence:**
*Enrica Calleri*
*enrica.calleri@unipv.it*
*Stefano Capaldi*
*stefano.capaldi@univr.it*

*[†] These authors have contributed equally to this work*

***Specialty section:***
*This article was submitted to Analytical Chemistry, a section of the journal Frontiers in Chemistry*

***Received:*** *17 October 2019*
***Accepted:*** *16 December 2019*
***Published:*** *10 January 2020*

***Citation:***
*Capelli D, Parravicini C, Pochetti G, Montanari R, Temporini C, Rabuffetti M, Trincavelli ML, Daniele S, Fumagalli M, Saporiti S, Bonfanti E, Abbracchio MP, Eberini I, Ceruti S, Calleri E and Capaldi S (2020) Surface Plasmon Resonance as a Tool for Ligand Binding Investigation of Engineered GPR17 Receptor, a G Protein Coupled Receptor Involved in Myelination. Front. Chem. 7:910. doi: 10.3389/fchem.2019.00910*

## INTRODUCTION

The molecular targets for about 50–60% of currently validated drugs are membrane proteins, such as G-protein coupled receptors (GPCRs); this class of proteins still features the main target in drug discovery programs (Hauser et al., 2017; Ribeiro-Oliveira et al., 2019). To this purpose, a range of chemical, biochemical and biophysical techniques are available for the characterization of ligand binding and for screening libraries of compounds searching for potential drug candidates. One of such techniques is surface plasmon resonance (SPR) spectroscopy, a label-free technique which enables measurement of real-time ligand-binding affinities and kinetics using relatively small amounts of membrane protein in a native or native-like environment (Olaru et al., 2015).

The typical SPR experimental protocol involves the direct binding of ligands on an immobilized target, which is usually a pure protein. Measuring the binding kinetics and affinities of ligands to intact membrane proteins by SPR is a challenging task, largely because of the inherent difficulties in capturing membrane proteins on chip surfaces while retaining their native conformation (Maynard et al., 2009; Patching, 2014) either in the original membrane environment or in membrane-mimicking structures, such as for example, lipid bilayer disks (Lundquist et al., 2010). An alternative method consists in capturing the detergent-solubilized receptor, engineered with a tag (such as multiple histidine residues or a short peptide sequence), with an appropriate antibody which has been previously covalently immobilized onto a chip through covalent bonding (Rich et al., 2011).

A gap still holds between the consolidated SPR technology and the request for innovative and robust immobilization methods for GPCRs. Indeed, in face of their importance as pharmacological targets, the intrinsic instability of GPCRs when extracted from the lipid milieu in the unligated form, makes them very challenging objects for SPR techniques, with only few examples of successful processing reported so far (i.e., neurotensin receptor type 1, chemokine receptor type 5 (CXCR5), β1 adrenergic receptor and purified adenosine 2A receptor) (Congreve et al., 2011; Adamson and Watts, 2014; Aristotelous et al., 2015; Bocquet et al., 2015; Chu et al., 2015).

Among the GPCR receptors, GPR17 holds a place of special interest in medicinal chemistry, being a key regulator of oligodendrocyte precursor cells (OPC) maturation (Fumagalli et al., 2016; Alavi et al., 2019). From a structural point of view, several binding sites have been described, which are the target of different classes of highly heterogeneous ligands (i.e., uracil nucleotides, cysteinyl leukotrienes, chemokines, and oxysterols) (Ciana et al., 2006; Eberini et al., 2011; Sensi et al., 2014; Parravicini et al., 2016). From a functional point of view, GPR17 is one of the most interesting targets for neurodegenerative disorders, since it crucially modulates the maturation of oligodendrocytes, the cells responsible for the production of myelin that, in turn, ensheates neuronal endings, thus allowing nerve impulse transmission. Myelin preservation and reconstruction accelerate neuronal repair and neurological recovery, and indeed represents a highly innovative approach to diseases, such as multiple sclerosis, Alzheimer's and cerebral ischemia (Fumagalli et al., 2015; Bonfanti et al., 2017; Seyedsadr and Ineichen, 2017). Therefore, new, more selective and pharmacokinetically suitable molecules are presently needed to translate promising preclinical data into patients care.

[$^{35}$S]GTPγS binding-assay is an analytical method that has been used to investigate the activity of potential new GPR17 ligands with high accuracy and selectivity. The assay uses a GTP analog ([$^{35}$S]GTPγS) which cannot be hydrolyzed by the GTPasic activity of the Gα subunit. Thus, GPCR activation or inhibition can be quantified by measuring the amount of radiolabelled GTP bound to the receptor-G protein complex (Harrison and Traynor, 2003). However, this standard functional assay does not provide any information on the direct molecular interaction between the ligand and the receptor.

In a previous work, frontal affinity chromatography-mass spectrometry (FAC-MS) was used to directly measure the direct binding of ligands to GPR17. In this assay, a liquid stationary phase containing membrane preparations from GPR17-expressing cells was coupled to an electrospray mass spectrometer as detector. Through the continuous infusion into the column of a solution of nucleotide analog it was possible to screen a high number of molecules in a single analysis, and to calculate the interaction between the receptor and different potential ligands (Calleri et al., 2010). Although this assay proved to be a powerful tool for the rapid screening of many compounds and for the assessment of low-to-medium affinity ligands, the approach is less effective in the characterization of the binding in the low nanomolar range.

Here, we report an SPR-based protocol that allowed us to efficiently immobilize two engineered variants of GPR17 on a sensor chip and to detect and measure the direct binding of two high affinity ligands. The calculated kinetic parameters and binding constants are in good agreement with those previously reported by activity assays and highlight a possible role of the N-terminal residues of receptor in ligand recognition.

## MATERIALS AND METHODS

### Reagents and Instrumentation

Surface Plasmon Resonance (SPR) experiments with the ligands were performed at 25°C using a Pioneer AE optical biosensor (Molecular Devices-ForteBio) equipped with a PCH sensor chip (linear polycarboxylate hydrogel), and equilibrated with running buffer 20 mM Hepes, pH 7.5, 0.15 M NaCl, 0.03% Dodecyl Maltoside (DDM) and Cholesteryl Hemisuccinate (CHS) solution (DDM/CHS ratio 5:1) (with 1% DMSO, in the experiment with the agonist compound).

The GPR17 antagonist Cangrelor in its purified enantiomer (dichloro-[[[(2R,3S,4R,5R)-3,4-dihydroxy-5-[6-(2-methyl sulfanylethylamino)-2-(3,3,3-trifluoropropylsulfanyl)purin-9-yl]oxolan-2-yl]methoxy-hydroxyphosphoryl]oxy-hydroxy phosphoryl]methyl]phosphonic acid) was a kind gift of Medicines Company (Parsippany, NJ, USA) and agonist Asinex 1 (2-[[5-(2-methoxyphenyl)-4-(4-methoxyphenyl)-4H-1,2,4-triazol-3-yl]thio]-N-phenyl-propanamide; CAS 483283-39-2,

previously published as ASN 02563583), was purchased from Ambinter (c/o Greenpharma, Orlèans, France) as racemic mixture. The detergents were from Anatrace, the anti-$His_6$ antibody and other laboratory reagents were from Sigma.

## Protein Engineering

The cDNA sequence of wild type human GPR17 receptor (short isoform, Uniprot id: Q13304-2) cloned into the pcDNA3.1 vector was used as template for DNA amplification. A modified cysteine-free version of T4 lysozyme (T4L) was inserted in the third intracellular loop (IC3), replacing residues 224–229, by short overlap extension (SOE) PCR. Briefly, three overlapping fragments encoding residues 1–223 of GPR17, 2–160 of T4L and 230–339 of GPR17, respectively were amplified by PCR and used as templates for a final round of amplification. The primers were designed to generate the full length (GPR17-T4 1-339) and a shorter variant lacking the first 15 amino acids (GPR17-T4 16-339) of the T4L chimeric receptor fused with a TEV cleavage site and a 10XHis-tag at the C-terminus. The two constructs were further modified by introducing the $D293^{7.49}N$ mutation using the QuikChange II Site-Directed Mutagenesis Kit (Stratagene). The resulting sequences were cloned into the pFastBac vector (Invitrogen).

## Expression and Purification of GPT17 Variants From Insect Cells

High titer recombinant baculovirus stocks ($>10^8$ pfu/mL) of the two variants were obtained with the Bac-toBac TOPO Expression system (Invitrogen) in SF9 insect cells. For protein expression, suspension cultures of SF9 or High Five cells at density of $2 \times 10^6$ cells/mL in suitable serum-free medium were infected with the virus at a multiplicity of infection (m.o.i.) of 3. After 48 h, cells were collected by centrifugation and resuspended in a hypotonic Lysis Buffer (LB) composed of 10 mM HEPES, pH 7.5, 10 mM $MgCl_2$, 20 mM KCl added with a protease inhibitor cocktail (Roche). The cells were disrupted by Dounce homogenization in a glass potter, the membrane fraction collected by high speed (45,000 rpm) centrifugation for 45 min and washed twice with the same buffer. After an additional high salt wash (LB with 1 M NaCl), the membranes were resuspended in LB containing 20% glycerol at total protein concentration of 3 mg/mL, flash-frozen in liquid nitrogen and stored at −80°C until use. Purified membranes were thawed on ice in presence of 1 mg/mL iodoacetamide, 50 μM Cangrelor and protease inhibitors, mixed with an equivalent volume of 2× Solubilization Buffer (SB, 100 mM HEPES pH 7.5, 0.6 M NaCl, 2% DDM/0.4% CHS) and stirred at 4°C for 2 h. The insoluble material was removed by centrifugation and the supernatant, added with 20 mM imidazole, was incubated overnight at 4°C with TALON IMAC resin (Clontech) (0.5 mL of resin for 300 mL of initial cell culture). The resin was extensively washed with 15–20 column volumes of Wash Buffer (50 mM HEPES pH 7.5, 0.3 M NaCl, 0.05% DDM/0.01%CHS, 10 μM Cangrelor, 50 mM imidazole) and the bound proteins eluted with 2 column volumes of Elution Buffer (50 mM Hepes pH 7.5, 0.3 M NaCl, 0.05% DDM/0.01% CHS, 10 μM Cangrelor, 300 mM imidazole). The purity of the final preparations was checked by SDS-PAGE and Western Blot with an anti-$His_6$ monoclonal antibody (Sigma). The apo proteins were purified with the same protocol in the absence of Cangrelor. The presence of glycosylation was assessed by PNGase F digestion on denatured samples (laboratory-made reagents). The monodispersity of GPR17 samples in absence or in presence of 10 μM Cangrelor was evaluated by size exclusion chromatography on a 10/30 G200 column equilibrated in 20 mM HEPES pH 7.5, 0.15 M NaCl, 0.05% DDM/0.01% CHS.

## Antibody Immobilization

An antibody specific for $His_6$-tagged proteins was immobilized on the Chip surface using amine coupling chemistry (Jonsson and Malmqvist, 1992; Lundquist et al., 2010). Briefly, flow cells were activated for 4 min by injecting 40 μL of 1:1 ratio of 100 mM N-hydroxysuccinimide (NHS)/400 mM ethyl-3(3-dymethylamino) propyl carbodiimide (EDC). The antibody solution (50 μL of 100 μg/mL antibody and 300 μL of Na Acetate, pH 4.5) was then injected for 10 min at 10 μL/min, followed by a 70 μL injection of ethanolamine 1 M, pH 8.0, to block any remaining activated groups on the surface. Approximately 18,000 RUs of antibody were immobilized on the three channels of the sensor chip. The immobilization step was performed in HBS buffer (Hepes 20 mM, pH 7.4, NaCl 150 mM, Tween 20 0.005%).

## Capturing the Solubilized Receptor

Engineered 10xHis-tag GPR17 receptor, expressed from two different constructs (1–339 and 16–339) in two different cell lines (H5 and SF9), was captured on the antibody for the SPR experiments. The C-terminal 10xHis-tag, situated in the intracellular region of the receptor, can be captured by the antibody allowing the extracellular N-terminal part, involved in ligand recognition, to be free to interact with the ligand.

Briefly, a frozen aliquot of crude membrane extract (0.1 mL) was mixed with 5 μL of Protease Inhibitor Cocktail 100× (Sigma) and incubated on ice for 30 min. An equal volume of solubilization buffer 2× (100 mM Hepes, pH 7.5, 0.6 M NaCl, 2% DDM/CHS 10:2) was then added to the membrane extract and incubated 2.5 h at 4°C, under gentle rotation. The membrane preparation was then centrifuged for 30 min at 14,000 rpm and the supernatant collected. Crude cell supernatant (diluted 1/3 in MES 50 mM, pH 6.0, 1% DDM/CHS 5:1) was injected (flux 5 μL/min) across the PCH sensor (channels 1 and 3) where the anti-$His_6$ antibody was previously immobilized. The chip surface was washed for several hours with running buffer (flux 150 μL/min) to remove non-specifically bound supernatant debris. Alternatively, few short injections (15 s, flux 50 μL/min) of NaCl 0.5 M in DDM/CHS 1% can be effective to quickly remove the debris. After the cleaning procedure, ∼500 RU of solubilized receptor were captured on channels 1 and 3 (channel 2 was used as reference).

The stability of the protein-antibody surface was demonstrated by the flat baseline achieved at the beginning of each sensogram. Once immobilized on the chip surface, GPR17 was found to maintain its activity over at least 24 h. Afterwards, the receptor was easily removed by few injections of regeneration solution (50 mM NaOH injected for 30 s at 50

μL/min). After the regeneration step, the chip surface was ready for capturing freshly solubilized receptor for new experiments.

## Kinetic Analysis of Cangrelor and Asinex 1

The GPR17 antagonist Cangrelor and the agonist Asinex 1, dissolved in running buffer, were tested in serial dilutions for binding to GPR17, from 1 μM to 3.125 nM for Asinex 1 and from 2 μM to 7.81 nM for Cangrelor (see **Supplementary Figures S1–S4**). Analytes were injected at a flow rate of 25 μL/min for 1 min over the three channels. Several buffer blanks were injected for double referencing. The regeneration of the surfaces between binding cycles was not necessary because the analytes completely dissociate in the 240 s dissociation phase. A DMSO calibration was performed for Asinex 1 [0.5–1.5% (vol/vol) DMSO] to correct for bulk refractive index shifts (Frostell-Karlsson et al., 2000). All the experiments were carried out in duplicate. All sensorgrams were processed by using double referencing (Myszka and Morton, 1998). Formation of the complex between GPR17 and ligands was indicated by the increase in resonance units (RUs) relative to baseline upon injection of each compound at each concentration (**Supplementary Figures S1–S4**). To obtain the kinetic and affinity constants the corrected response data were fed to the program QDAT. A kinetic analysis of each ligand/analyte interaction was obtained by fitting the response data to a 1:1 bimolecular interaction mode (**Figures 3A–D**). Constants reported in the table of **Figure 3** represent the average of two independent analyses of each GPR17/analyte interaction.

## *In silico* Molecular Modeling and Ligand Docking

All the computational procedures, except for the molecular dynamics (MD) simulations, were carried out with the Molecular Operating Environment software (MOE2019.0101 Chemical Computing Group, Montreal, Canada), using the Amber12:EHT force field with the reaction field electrostatics treatment. The MD simulation of the GPR17-T4 1-339 variant and the procedures required for the preparation of the system were performed using the Schrödinger suite (Schrödinger, New York, NY, 2018).

### Homology Modeling

The homology modeling procedure was performed using the MOE "Homology Model" program, starting from a multiple sequence alignment of the primary structures of a subgroup of structurally related class-A GPCRs, as previously described (Sensi et al., 2014; Parravicini et al., 2016). The multiple sequence alignment was performed using the TM-Coffee algorithm, a module of the T-Coffee package optimized for transmembrane proteins (Chang et al., 2012).

The tridimensional structure (3D) of the human GPR17 receptor in its wild-type form was built by comparative modeling, using as template the 2.7 Å resolution X-ray structure of the human P2Y1 receptor deposited in RCSB Protein Data Bank [PDB, code: 4XNW (Zhang et al., 2015)]. The GPR17-T4 1-339 variant was generated by a chimeric approach according to the above alignment, based on its engineered primary structure, using the structure of P2Y1 for modeling residues from Thr19-Leu223 and Lys230-Gal290, the structure of the C-X-C chemokine receptor type 4 (CXCR4) construct for modeling the T4 lysozyme (T4L) fusion, and the structure of the apelin receptor for modeling C-terminal domain (residues from Ala29 to Lys315) after structural alignment of the templates. The specific setting "C-terminal and N-terminal outgap modeling" was selected to model the N- and C-terminal regions from the full-length GPR17 sequence.

### Low Mode Molecular Dynamics Search

N-terminal conformational search was performed using the MOE "LowMode MD" search method, by associating different conformational freedom to different regions of the protein, to speed-up calculations. In detail, residues from 1 to 19, 20 to 24, 25 to 40/80 to 115/157 to 202/248 to 286 (the upper TM bundle) and 41–79/116–156/203–247/287–319 (the upper TM bundle), were treated as a rigid body, flexible, fixed and inert. Also, the T4L was treated as inert. The Low Mode MD was carried out with standard settings, except for strain energy cutoff, which was set at 100 kcal/mol.

### Ligand Docking

Molecular docking simulations were carried out using the MOE "Dock" program of the "Simulation" module, with a multi-step procedure useful for a more accurate estimation of the ligand binding free energy, as previously described (Eberini et al., 2011; Platonova et al., 2017). The GPR17 binding site was identified through the MOE "Site Finder" module. The receptor was treated as rigid for the docking calculations, while conformational space was sampled for ligands. Briefly, for each ligand 20,000 conformations were generated by sampling their rotatable bonds and placed using the Triangle Matcher methodology. Duplicate complexes were removed, and the accepted poses (1,000 for each ligand), were scored according to the London dG empirical scoring function, for an estimation of their binding free energy (Naïm et al., 2007). The 100 top scoring complexes for each ligand were submitted to a more in-depth refinement step based on molecular mechanics (MM), in which the final binding free energy was evaluated using the force-field based GBVI/WSA ΔG empirical scoring function to account for solvation effect (Wojciechowski and Lesyng, 2004). Only the 10 top-scoring complexes were kept at this stage. The "LigX" procedure was finally applied to the top-scoring pose to minimize *via* molecular mechanics (MM) both the ligand and the receptor binding site for a more accurate estimation of ligand affinity. Dissociation constant (Kd) values computed through this method have accuracy in the range of one order of magnitude (Eberini et al., 2008; Galli et al., 2014).

### Molecular Dynamics

The preparation of the GPR17-T4 1-339 variant and its MD simulation were performed using the Desmond software, implemented in the Schrödinger suite, version 2019.2 (Desmond Molecular Dynamics System of the D. E. Shaw Research, New York, NY). Downstream residues belonging to the C-terminal portion of the receptor (Gly320-Leu339) were removed for MD

simulations. The GPR17-T4 1-339 model was processed with the "Protein Preparation Wizard" tool in order to assign protonation states at pH of 7.0, cap C-terminal, optimize H-bond assignment, and minimize the protein energy. Then, the model was embedded in an explicit membrane bilayer using the "System Builder" tool. In detail, the receptor was oriented into membrane according to the OPM server prediction (Lomize et al., 2012) into a membrane model of 123 1-palmitoyl-2-oleoyl-sn-glycero-3-phosphocholine (POPC) and solvated with 11,104 TIP3P water molecules, in a cubic box with dimensions of 82 × 71 × 110 Å. The system was neutralized by adding 21 chloride ions and sodium chloride was added up to 0.1 M concentration. Prior to simulation, the system was energy-minimized and equilibrated through the relaxation protocol. The OPLS3 forcefield was used for both the MD relaxation phase and the productive MD simulations. For the membrane relaxation phase, the default protocol was applied; the productive MD was carried out for a total simulation time of 500 ns, with a recording interval for each frame of 500 ps resulting in a total of 1,000 recorded frames. The MD was performed under the following conditions: 300 K and 1.01325 bar with NPT ensemble class, Langevin as thermostat and barostat method with relaxation time of 1 and 2 ps, respectively, semi-isotropic pressure coupling style, RESPA integrator with timestep for bond-, short- and long- range bond interactions of 2, 2 and 6 fs, respectively, and 9 Å as cutoff for short range Coulombic interactions.

Analyses of the trajectories were performed with both Visual Molecular Dynamics (VMD) analysis tool (Humphrey et al., 1996) and GROMACS through VMD plugins (Berendsen et al., 1995).

## *In vitro* Assays on Cell Cultures

The Università degli Studi di Milano–La Statale (Italy) is compliant with all applicable national (D.Lgs. 26/2014) and European (Directive 2010/63/EU) regulations, for using animals in scientific research. All the experiments were approved by the Animal Care Committee of the Università degli Studi di Milano–La Statale, which is legally entitled for the use of animals for scientific purposes and by the Italian Ministry of Health (Authorization #473/2015-PR, 05/06/2015).

The pharmacological profile of Asinex 1 was assessed in three different *in vitro* assays of increasing complexity in oligodendrocyte precursor cells (OPCs) natively expressing GPR17. Primary rat OPCs were cultured either alone or in the presence of mouse DRG neurons, according to a well-established protocol, previously described in Fumagalli et al. (2015). The endogenous GPR17 ligands UDP and $LTD_4$ were selected as reference ligands. For more details on culture preparation and analysis, see **Supplementary Information**.

### cAMP Assay

In order to determine the intracellular cAMP levels, primary purified OPCs were treated with Asinex 1 after 6 days in culture, when GPR17 expression reaches the maximum peak. A competitive protein binding method was used following the procedure previously described (Fumagalli et al., 2015). Briefly, culture medium was removed, and cells were incubated at 37°C for 15 min with 400 μL of Neurobasal medium in the presence of the phosphodiesterase inhibitor Ro20-1724 (20 μM). The concentration-response curve of tested ligands was assessed by measuring their ability to inhibit cAMP accumulation stimulated by 10 μM forskolin. Asinex 1 was added to cells for 15 min at graded concentration (0.1–50 nM). When required, cells were preincubated for 10 min with the antagonist Cangrelor. Reactions were terminated by medium removal and addition of 200 μL of 0.4 N HCl. After 30 min, lysates were neutralized with 50 μL of 4 N KOH, and the suspension was centrifuged at 800× g for 5 min. For determination of cAMP, cAMP-binding protein isolated from bovine adrenal glands was incubated with [$^3$H]cAMP (2 nM), 50 μL of cell lysate or cAMP standard (0–16 pmol) at 4°C for 150 min, in a total volume of 300 μL. Bound radioactivity was separated by rapid filtration through GF/C glass fiber filters and washed twice with 4 mL of 50 mM Tris-HCl, pH 7.4. Radioactivity was measured by liquid scintillation spectrometry.

### Differentiation and Myelination Assays

GPR17 ligands were tested both in primary OPCs culture and in OPC/DRG co-cultures to assess their pro-differentiation and pro-myelination effect, respectively. According to the type of culture, a specific protocol of treatment was set up. For primary OPCs, cells were seeded on 13 mm poly-D,L-ornithine-coated coverslips (2 × $10^4$ cells/well) and maintained for 2 days in Neurobasal medium supplemented with B27 and proliferative factors (PDGF-BB and bFGF). Afterwards, OPC differentiation was induced by removing proliferative factors and by adding T3 and pharmacological treatments with Asinex 1 (1 or 10 nM) and $LTD_4$ (200 nM), selected as reference compound, were performed the following day. After 48 h, cells were fixed for immunocytochemistry (ICC). For OPC/DRG co-cultures, Asinex 1 (10 nM) and UDP (100 μM) were added to cultures at day 4. The pharmacological treatment was repeated every 2 days up to day 15, when cells were fixed for ICC analysis. For more details, see **Supplementary Information**.

# RESULTS

## Expression and Characterization of Engineered GPR17 Variants

In order to identify one or more GPR17 variants suitable for structural studies, we prepared and tested different engineered constructs of the receptor. A major bottleneck in structure determination of GPCRs by X-ray crystallography is obtaining of large amounts (>1–2 mg) of highly pure, homogeneous protein samples that are stable in detergent solutions when extracted from the lipid environment of the membranes. In the last decade, a number of protein engineering approaches have been used to overcome the problem of the intrinsic instability and conformational heterogeneity of GPCRs. These include truncations, site-directed mutagenesis, stabilization of the receptor with specific protein-binding partners (FABs and nanobodies) and the creation of chimeric constructs in which flexible loops are replaced with small soluble proteins that can favor the crystallogenesis process (Piscitelli et al., 2015). Inserting T4 lysozyme (T4L) in the third intracellular loop (ICL3)

allowed to obtain the first high resolution crystal structure of β2-adrenergic receptor (Cherezov et al., 2007; Rosenbaum et al., 2007); the same strategy was subsequently used for other types of class A GPCRs (Wu et al., 2010; Granier et al., 2012; Zhang et al., 2012). More recently, the use of other fusion partners, such as thermostabilized BRIL or rubredoxin have proven effective in obtaining diffraction quality crystals of purinergic receptor $P2Y_{12}$ (Zhang et al., 2014) and $P2Y_1$ (Zhang et al., 2015).

We initially prepared a number of modified variants of GPR17. The modifications included a combination of truncations in different positions near the N- and C- termini and the fusion of the T4L moiety either at the N-terminal or in ICL3. All these constructs were used to generate recombinant baculoviruses for the expression of the receptor in insect cells. Insect cells are the most common expression system for eukaryotic membrane proteins and have been used for the production of most of the mammalian GPCRs crystallized so far (Schneider and Seifert, 2010; Milić and Veprintsev, 2015). Small scale expression trials identified two constructs that could be produced with a good yield in SF9 cells: the full-length receptor with T4L inserted in ICL3 (GPR17-T4 1-339) and a shorter version lacking the first 15 amino acids (GPR17-T4 16-339). The expression levels were further increased by mutating the conserved $Asp^{7.49}$ (D293) into Asn, as described for other homologous P2Y receptors (Zhang et al., 2014, 2015). The modifications introduced in these two engineered variants are highlighted in the snake-plot displayed in **Figure 1A**. After optimization of the expression conditions, the two variants reached a maximum expression level of about 1–2 mg of receptor per liter of culture in both SF9 and High Five cells, with a slightly higher yield in the latter cell line (**Figure 1B**).

The two variants can be effectively extracted from the isolated membranes with a detergent mix composed of DDM and CHS and can then be purified by immobilized metal affinity chromatography (IMAC) exploiting the C-terminal His-tag as described in the Material and Methods (**Figure 1C**). A potential N-glycosylation site (Asn14) is present in the full-length construct and in fact the protein migrates as a double band in SDS-PAGE. The higher band disappeared upon treatment with PNGase F, indicating that a fraction of the receptor is actually glycosylated. Conversely, the shorter version 16–339 displays only a single well-defined band.

It is well-known that the binding of a high affinity agonist or antagonist stabilizes the GPCR in a specific signaling conformation, and increases the stability and enhances the size monodispersity of the receptor in detergent solution (Bertheleme et al., 2013; Grisshammer, 2017). We therefore assessed the effect of the antagonist Cangrelor on the two purified variants by size exclusion chromatography (SEC). **Figures 1D,E** summarize the results for GPR17-T4 1-339 and GPR17-T4 16-339, respectively. In both cases, the presence of Cangrelor increased the fraction of monodisperse receptor (the peak indicated by the blue arrow in the panels) and reduced the amount of aggregates that elute in the void volume, suggesting that these two variants retain the ability to bind the antagonist with comparable affinity. Although the use of a stabilizing ligand will be necessary to maximize the yield in large scale purifications, the presence, albeit in smaller quantities, of monodisperse apo protein in detergent solution makes these two constructs suitable for binding experiments and fragment screening by SPR.

## Molecular Modeling and Ligand Docking

In line with the increasing availability of class-A GPCR templates, thanks to homology approaches on GPR17, our previous studies have characterized the interactions of GPR17 with its known endogenous ligands (Parravicini et al., 2008, 2010, 2016; Sensi et al., 2014). We also identified a first set of entirely new and highly diverse GPR17 ligands, including the Asinex 1 compound which was identified within the Asinex Platinum Collection database (Calleri et al., 2010; Eberini et al., 2011).

To evaluate whether the engineered GPR17 constructs are thermodynamically stable and still able to recognize ligands, a chimeric model of the full length GPR17-T4 1-339 variant was generated by replacing, during the homology modeling procedure, the ICL3 with the coordinates of the T4 lysozyme (T4L) fusion of CXCR4 structure (Wu et al., 2010). The structure of this construct is shown in **Figure 2A**. For validating the homology modeling procedure, besides the engineered GPR17 variant, an entirely new GPR17 model was built (**Figure 2B**), based on the recently solved X-ray structure of the $P2Y_1$ receptor (Zhang et al., 2015). In this model, only the three-dimensional structure (3D) of residues between Thr19 and Leu311 was predicted, whereas the highly flexible N and C termini were not generated, since they are not included in the template. This GPR17 model resulted much more accurate than the previous ones, due to the closest sequence identity of GPR17 with respect to $P2Y_1$, compared to that shared with all the other available crystallographic templates among related class-A GPCRs (26.4%). A pairwise alignment identity matrix between GPR17 and the primary structures of other related class-A GPCR, whose structure has been solved (Gacasan et al., 2017), is reported in **Supplementary Figure S5**.

Structural alignment of the helical bundle of the two homology models resulted in a low value of root-mean-square deviation (RMSD), corresponding to 1.4 Å (**Supplementary Figure S6**), suggesting that the use of the T4L as fusion partner does not impair the general architecture of the receptor as also found for other crystallized GPCRs (Wu et al., 2010).

As loop modeling for such flexible regions is known to be rather inaccurate, putative conformations of the N-terminal region were computed through an efficient conformational sampling approach based on the Low Mode MD. Low Mode MD generated only 20 conformations out of the 10,000 allowed for the N-terminal region, some representative of either the "open" or the "closed" state of the receptor (**Figure 2C**), confirming the ability to efficiently explore the conformational space of the test region. As shown in **Table 1**, all the 20 conformations are associated with negative values of potential energy (E), ranging from −299.53 to −205.17 kcal/mol; values of ΔE between the lowest- and the highest-energy conformations lower than 100 kcal/mol suggest that all conformations are stable and biologically relevant.

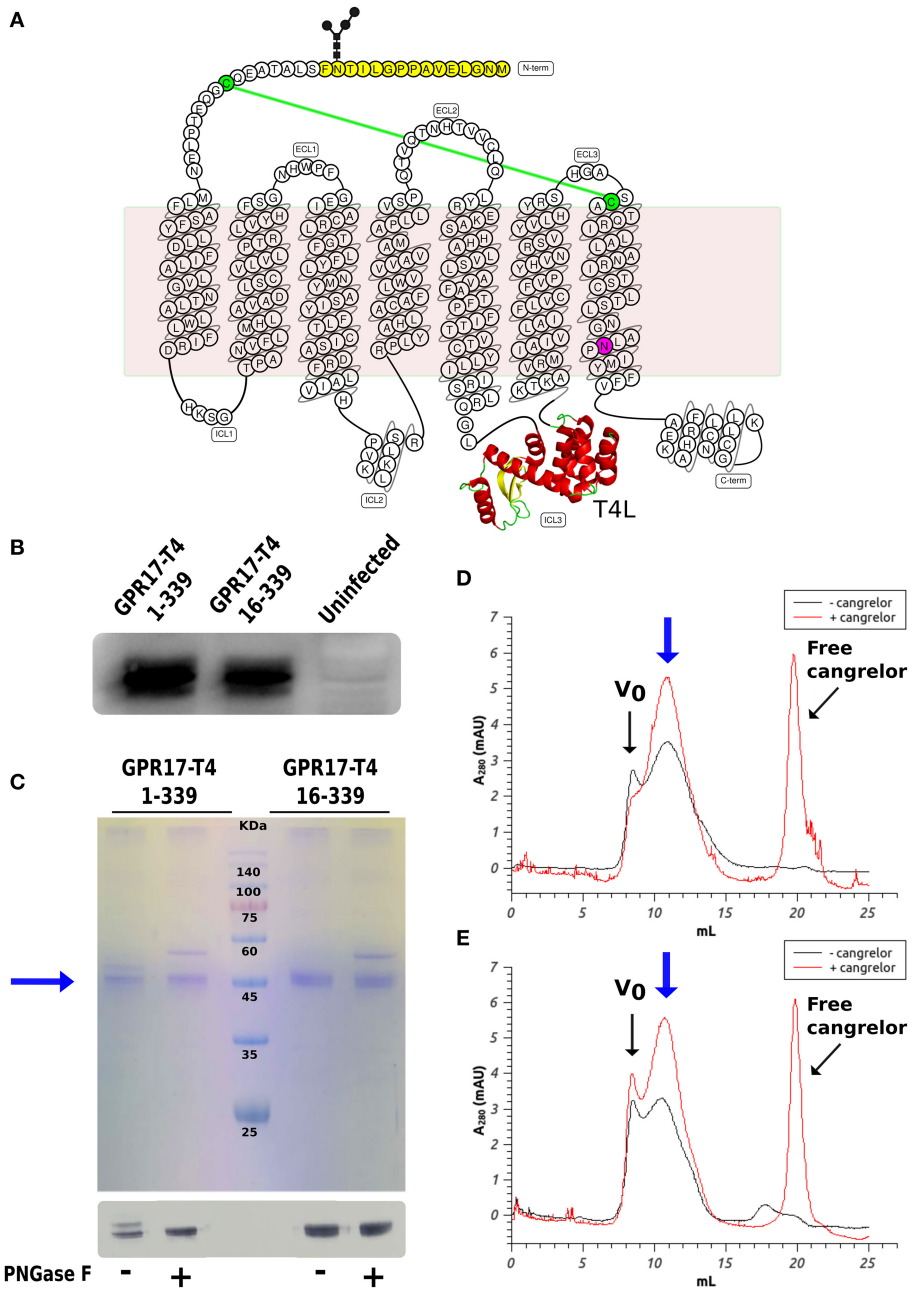


**FIGURE 1 |** Expression and characterization of GPR17 engineered variants. **(A)** Snake-plot of modified GPR17. The first 15 amino acids (with N-glycosylation on Asn14) removed in the shorter construct are highlighted in yellow and the D293N mutation in purple. The T4 lysozyme inserted in ICL3 is represented in ribbon model. The two cysteines linked by disulfide bridge are colored in green. **(B)** Western blot analysis of GPR17 variants expression in High Five cells. Same amounts of whole cell extracts were probed with anti-$His_6$-HRP conjugated antibody. **(C)** SDS-PAGE (top) and western blot (bottom) of purified GPR17-T4 1-339 and GPR17-T4 16-339 before and after treatment with PNGase F. **(D,E)** SEC profiles of purified GPR17-T4 1-339 **(D)** and GPR17-T4 16-339 **(E)** in absence or in presence of a saturating concentration of Cangrelor. The void volume is indicated with Vo.

The Low Mode MD conformation associated with the highest (32.3 Å) and lowest (31.3 Å) gyration radius were selected for further investigation as representative of the N-terminal open and closed form, respectively (**Table 1**).

The closed conformation was then submitted to a classic MD simulation performed in a heterogeneous water/membrane native-like environment, allowing unrestrained conformational sampling for the whole protein and assessing its stability over the simulation time. Overall, the analysis of the evolution of

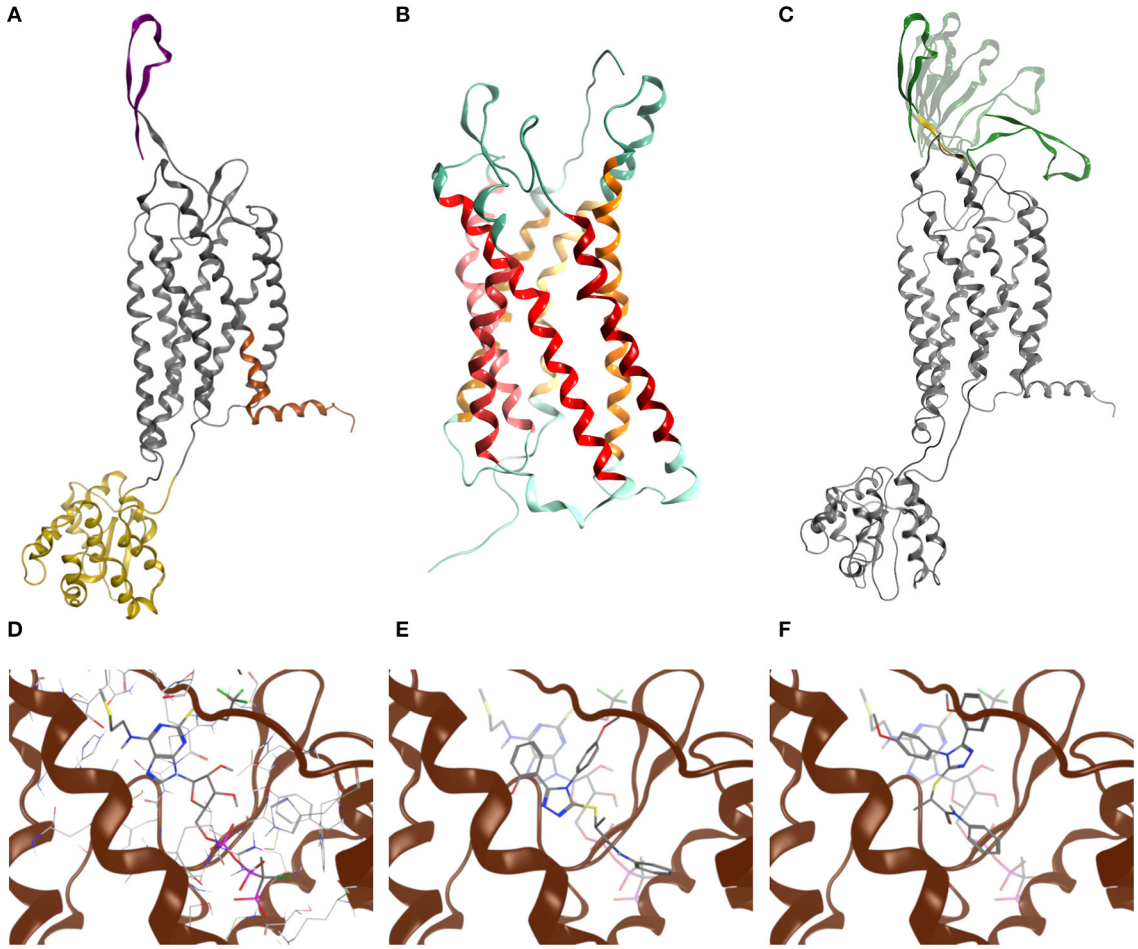


**FIGURE 2 |** Molecular modeling of GPR17. **(A)** Chimeric model of GPR17-T4 1–339 (D293N) variant. Topological domains modeled with reference to different templates, namely $P2Y_1$, CXCR4, and APJ receptor, are represented as gray, yellow, orange ribbons, respectively. The N-terminal region is purple. **(B)** Homology model of GPR17 based on $P2Y_1$ receptor as template. Ribbons are colored according to MOE GPCR annotation. **(C)** Most representative N-terminal conformations after Low Mode MD sampling. During the Low Mode MD, green ribbons are treated as rigid bodies, yellow ribbons as free to move and gray ribbons as fixed or inert. **(D)** Cangrelor binding mode. **(E)** Asinex 1 binding mode (R enantiomer). **(F)** Asinex 1 binding mode (S enantiomer). In **(E,F)**, Asinex 1 and Cangrelor docking poses are superposed to hint to the basis of their competitive antagonism.

both geometrical and energetic parameters over 500 ns of MD simulation suggests that the GPR17-T4 1–339 variant is thermodynamically stable and confirms that the presence of intracellular T4L does not affect extracellular architecture of the receptor. However, as expected due its intrinsic flexibility, the N-terminal region is subject to large conformational changes during MD simulations (**Supplementary Figure S7**).

To assess the ability of the GPR17 construct to recognize ligands, the two synthetic compounds Asinex 1 and Cangrelor were docked into the binding site of both GPR17 "open" and "closed" form. For Asinex 1, both the R and S enantiomers were analyzed, since no information on the enantiomeric ratio is available from the vendor.

In line with previously published data (Eberini et al., 2011), both ligands were able to bind to the orthosteric binding site of GPR17 with high affinity (**Table 2**), supporting the evidence of a competition between the agonist Asinex 1 and the antagonist Cangrelor for the same site. Differences in binding free energy values were found between the docking complexes obtained with the open and closed conformations of GPR17. Indeed, all the ligands showed an increased affinity for the closed receptor conformation (**Table 2**). To account for solvent contribution, the Generalized Born implicit solvent model was applied for computing accurate ligand affinity after relaxation of each complex binding site. Since both ligands are characterized by highly hydrophobic moieties, it can be hypothesized that, in the open conformation, the exposure of these groups to the extracellular aqueous solvent negatively contributes to the binding free energy of the complexes, resulting in a loss in affinity in comparison with the closed form. A 2D plot depicting all the interactions engaged by the ligands as well as the ligand/receptor groups exposed to solvent is shown in **Supplementary Figure S8**. **Figures 2D–F** report superposition of the top-scoring poses obtained for Cangrelor and Asinex 1, respectively.

**TABLE 1 |** Low mode MD conformations of the GPR17-T4 1-339 variant.

| *E* (kcal/mol) | Δ*E* (kcal/mol) | Gyration radius (Å) |
|---|---|---|
| −220.96 | 78.58 | 31.28 |
| −225.73 | 73.80 | 31.29 |
| −222.81 | 76.72 | 31.44 |
| −208.99 | 90.55 | 31.56 |
| −246.92 | 52.61 | 31.58 |
| −217.04 | 82.50 | 31.62 |
| −205.17 | 94.36 | 31.66 |
| −211.98 | 87.56 | 31.68 |
| −218.97 | 80.56 | 31.71 |
| −235.83 | 63.70 | 31.78 |
| −238.30 | 61.24 | 31.85 |
| −212.94 | 86.59 | 31.87 |
| −248.32 | 51.21 | 31.92 |
| −258.03 | 41.50 | 32.05 |
| −220.62 | 78.91 | 32.11 |
| −252.47 | 47.06 | 32.12 |
| −219.77 | 79.76 | 32.19 |
| −282.52 | 17.02 | 32.25 |
| −228.87 | 70.67 | 32.28 |
| −299.53 | 0.00 | 32.33 |

**TABLE 2 |** Binding free energy values computed through molecular docking for GPR17-T41-339.

| | Docking score (kcal/mol) | LigX (kcal/mol) | Kd [M] | pKd |
|---|---|---|---|---|
| **OPEN CONFORMATION** | | | | |
| Cangrelor | −10.23 | −13.84 | 6.5295E-11 | 10.19 |
| Asinex 1 (R) | −8.81 | −9.64 | 8.049E-08 | 7.09 |
| Asinex 1 (S) | −8.71 | −9.24 | 1.5853E-07 | 6.80 |
| **CLOSED CONFORMATION** | | | | |
| Cangrelor | −10.76 | −14.50 | 2.1339E-11 | 10.67 |
| Asinex 1 (R) | −9.06 | −10.07 | 3.8842E-08 | 7.41 |
| Asinex 1 (S) | −8.91 | −9.44 | 1.1296E-07 | 6.95 |

## SPR Experiments

GPCRs are typically highly unstable when extracted from the cell membranes, making them particularly difficult to study for ligand screening with biophysical methods. Here, we used an effective protocol which allowed us to extract from crude membranes two engineered variants of GPR17 that are relatively stable in the ligand-free state, and to immobilize them on the surface of a sensor chip for SPR analysis. The SPR results obtained with the high affinity antagonist Cangrelor and the agonist Asinex 1 demonstrated that the immobilized GPR17-T4 variants retained their ability to specifically bind the analytes. Full kinetic analysis of the agonist Asinex 1 and the antagonist Cangrelor, when binding to GPR17-T4 (constructs 1–339 and 16–339) is shown in **Figure 3**, with calculated binding parameters listed in the table.

Although the ratio between Cangrelor and Asinex 1 affinities measured by SPR is similar to that reported in the literature (Abbracchio et al., 2006; Ciana et al., 2006; Eberini et al., 2011) (9.35 vs. 7), the absolute Kd values are 20–30 times higher in the SPR experiments. This discrepancy might be ascribed to some residual non-specific binding to GPR17-T4, due to the injection of crude membrane preparation, which could affect the calculated Kd values. In addition, a perfect correspondence should not be expected because SPR technique provides direct binding data, whereas the literature data refer to a functional assay that evaluates the ability of the agonist (Asinex 1) to increase the binding of [$^{35}$S]GTPγS to the activated receptor or the ability of the antagonist (Cangrelor) to counteract the effect induced by either Asinex 1 (Eberini et al., 2011) and a reference agonist (Ciana et al., 2006).

Interestingly, the affinity of both ligands toward the full-length GPR17-T4 1–339 is higher (ca. 50 times) with respect to that of the N-terminal truncated form (construct 16–339), suggesting a possible role of the N-terminal region in the binding with the receptor.

## *In vitro* Assays on Primary OPCs

### Asinex 1 Inhibits Forskolin-Stimulated Adenylyl Cyclase Activity in Primary OPCs

Tests in the previous paragraphs have demonstrated proportionality between the affinity data evaluated, by docking chemical compounds to the binding site of a GPR17 structure shaped by homology modeling, and binding data measured *in vitro*, with such an instrumental approach as SPR in which only the target protein is involved. The further development was to demonstrate proportionality between the above findings and the biological response. The first step involved an *in vitro* test performed on cells and measuring an early effect of the downstream signaling pathway activation. The effects of Asinex 1 on adenylyl cyclase activity was evaluated in primary purified OPC cultures. In line with previous data obtained for GPR17 endogenous agonists, also the synthetic compound Asinex 1 concentration-dependently inhibited forskolin-stimulated cAMP formation with an EC50 value of 6.5 ± 0.8 nM (**Figure 4A**). Moreover, this effect was competitively antagonized by Cangrelor (IC50 10.2 ± 0.8 nM), suggesting a specific involvement of GPR17 (**Figure 4B**). These results are consistent with data reported by our group in cells transfected with GPR17 (Eberini et al., 2011) and further confirm that Asinex 1 interacts with the same GPR17 nucleotide binding site recognized by the endogenous ligands UDP and UDP-glucose (Ciana et al., 2006).

### Effects of GPR17 Activation by Asinex 1 on OPC Maturation and Myelination

The second step was again an *in vitro* test in culture but involved cells of two different lineages and targeted a more complex and more delayed outcome of GPCR stimulation. Thus, we evaluated whether Asinex 1 can promote myelination *in vitro*, based on previous data showing that GPR17 activation by endogenous ligands accelerates OPC differentiation toward a mature phenotype (Fumagalli et al., 2011). In order to verify whether also the synthetic GPR17 ligand Asinex 1 has

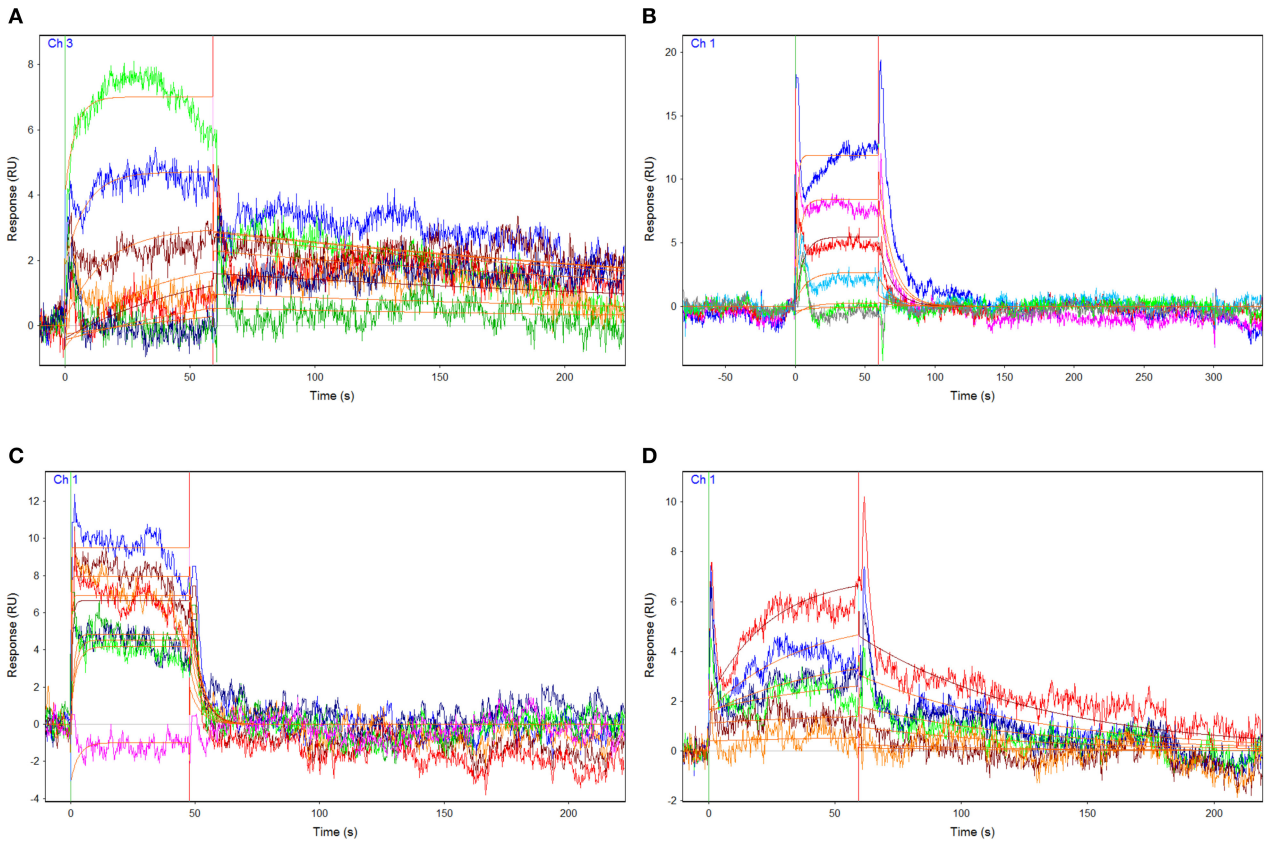


| GPR17 ligands | $k_a$ ($M^{-1}s^{-1}$) | $k_d$ ($s^{-1}$) | $K_d$ (nM) | res SD |
|---|---|---|---|---|
| **Asinex (1-339)** | **1.20±0.02e6** | **2.95±0.09e-3** | **2.46±0.08** | **0.72** |
| **Cangrelor (1-339)** | **1.05±0.07e7** | **0.237±0.007** | **23±2** | **1.02** |
| **Asinex (16-339)** | **6.5±0.2e5** | **0.103±0.002** | **159±4** | **1.06** |
| **Cangrelor (16-339)** | **1.38±0.07e4** | **0.0141±0.0002** | **1020±60** | **0.70** |

**FIGURE 3 |** SPR analyses of ligand binding. Full kinetic analysis of the agonist Asinex 1 **(A,B)** and the antagonist Cangrelor **(C,D)** binding to GPR17-T4 1–339 and GPR17-T4 16–339, with the determined binding parameters listed in the table.

myelinating properties, we tested this compound in purified OPCs, cultured alone and in the presence of DRG neurons. The endogenous ligands UDP and $LTD_4$ were selected as reference compounds. As shown in **Figure 4**, Asinex 1, tested at nanomolar concentrations, strongly increased the percentage of mature myelin basic protein ($MBP^+$)-cells in primary OPCs (CTRL: 100 ± 5.53%; $LTD_4$ 200 nM: 171.0 ± 21.70%; ASN1 1 nM: 166.5 ± 16.21%; ASN1 10 nM: 158.3 ± 15.77%) (**Figure 4C**), and promoted the formation of myelinated axons, as shown by increased "Myelination Index" in OPC-DRG co-cultures (**Figure 4D**) (CTRL: 100 ± 12.10%; UDP: 193.9 ± 32.31%; ASN1 10 nM: 240.3 ± 64.43%), compared to vehicle-treated control. Overall, these data indicate that, by acting on GPR17 receptor, Asinex 1 is able to foster OPC maturation, as also confirmed by appearance of a myelinating phenotype in culture (**Figures 4E,F**).

## DISCUSSION

SPR is a versatile and powerful technique for measuring the direct binding between an immobilized protein and its ligands. It is emerging in the last years as one of the most popular approaches in fragment-based drug discovery, due to the possibility to perform rapid and cost-effective high throughput screenings of fragment libraries. Among others, a great advantage of this method is the need for extremely low amounts of both target proteins and ligands, which makes it very useful in case of proteins, such as membrane protein, that are difficult to produce and purify. Several strategies have been developed to immobilize membrane proteins onto the sensor chip, including trapping the protein on a hydrophobic surface mimicking a membrane-like environment (e.g., lipid bilayers or nanodiscs) (Karlsson and Löfås, 2002; Glück et al., 2011). Alternatively, the tagged receptor

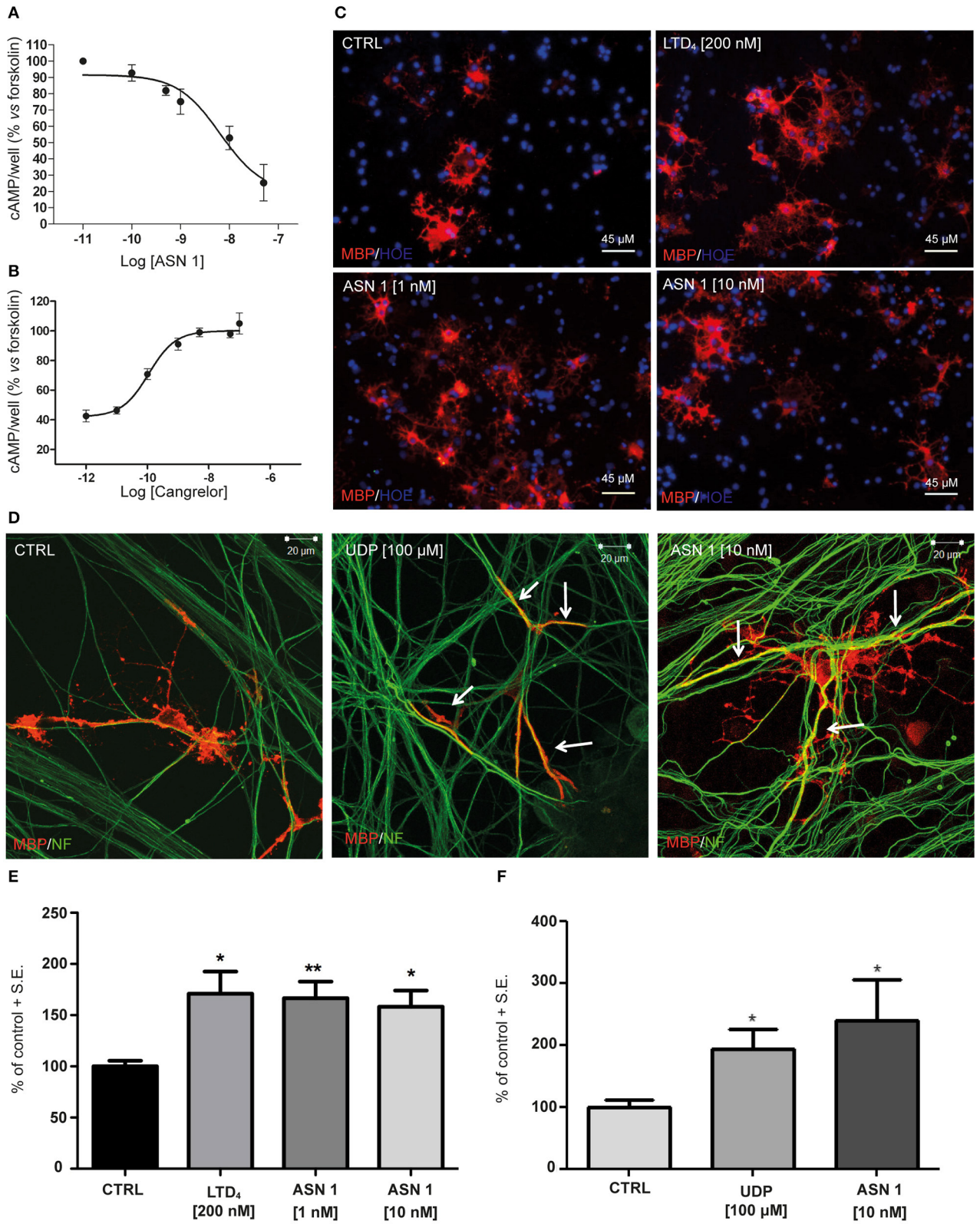


**FIGURE 4 |** Functional validation of and SPR data on primary OPCs. **(A)** Inhibition of forskolin-stimulated adenylyl cyclase activity in primary OPCs by graded concentrations (0.1–50 nM) of the GPR17 agonist Asinex 1 (ASN 1). **(B)** The GPR17 antagonist Cangrelor concentration-dependently counteracts ASN 1-mediated

*(Continued)*

**FIGURE 4 |** inhibition of forskolin-stimulated adenylyl cyclase activity in primary OPCs. Cangrelor was used in the presence of a constant ASN 1 concentrations of 10 nM. Results are expressed with reference to forskolin-stimulated cAMP levels, set to 100%. Data represent the mean ± S.E. (error bars) of three separate experiments, each performed in duplicate. **(C)** Representative images of CTRL, $LTD_4$-, ASN 1- (1 and 10 nM) treated OPCs, showing cell labeling with anti-MBP antibody (in red). Nuclei were labeled with Hoechst 33258 dye (HOE, in blue). Scale bars: 45 μm. **(D)** Representative images of control (CTRL), UDP- and ASN1-treated OPC-DRG co-cultures showing double immunostaining for anti-MBP antibody (red) and anti-neurofilament antibody (NF, green). Yellow color shows co-staining. Scale bars: 20 μm. **(E)** Histograms show quantification of the percentage of MBP+ cells in control and treated cells (with vehicle-treated control cells set to 100%) for OPC cultures. The number of positive cells was counted in 20 optical fields under a 20× magnification. Data are the mean ± S.E. of three independent experiments. $^*p < 0.05$; $^{**}p < 0.01$ compared to control; non-parametric Mann Whitney test. **(F)** Histograms show the quantification of the myelin segments, calculated as the ratio between the white pixels area and the green pixels' area (Myelination Index), for OPC-DRG co-cultures. Data are the mean ± S.E. of the index obtained from the analysis of six random fields of three coverslips for each experimental condition from three independent experiments. $^*p < 0.05$, Student's *t*-test.

can be captured by a specific antibody immobilized on the chip surface or via Ni-mediated affinity capturing (Chu et al., 2015).

A major issue in SPR analyses of membrane protein is the retention of the native conformation and binding properties of the immobilized target, and this is particularly true for GPCRs. Here we have successfully immobilized two engineered variants of the GPR17 receptor designed for crystallographic studies, GPR17-T4 1–339 and GPR17-T4 16–339, and have analyzed their binding with two high affinity ligands: the antagonist Cangrelor and the agonist Asinex 1. The two GPR17 constructs can be effectively extracted and solubilized in detergent solution, and retain good monodispersity and activity even in the ligand-free form, a mandatory prerequisite for SPR analysis. We set up a protocol for single-step immobilization of the receptor on the sensor chip through a covalently-bound anti-$His_6$-antibody. The protein was captured directly from the detergent solubilized membrane extracts, avoiding the costly and time-consuming purification of the receptor. The receptor retained its ligand binding activity for over 24 h when immobilized on the chip, thus allowing the design of fast screening experiments with fragment libraries (i.e., with a single injection for each compound) for the identification of new potential ligands. Furthermore, the use of a covalently immobilized antibody makes possible, after a mild regeneration step to remove the bound receptor, to reuse many times the same chip just re-capturing a new batch of freshly solubilized protein.

The affinity constants of the engineered full length receptor (GPR17-T4 1–339) that we have determined by SPR are in good agreement with that previously estimated for both ligands with an indirect binding assay ($[^{35}S]GTP\gamma S$) on in mammalian cells transfected with wild-type GPR17. It is worth noting that the affinity of GPR17-T4 16–339, lacking the first 15 residues, is substantially lower (about 50 times) compared to that of the full-length variant, hinting to a functional role of some N-terminal residues in ligand binding. The involvement of few residues of this region (Leu4 and Val6) in ligand recognition was already proposed in a previous computational study aimed at identifying new ligands for GPR17 (Eberini et al., 2011). Overall, our new docking/MD simulations, together with the SPR experimental results, strengthen this hypothesis and allow us to speculate on the importance of the N-terminal on GPR17 signaling. Of note, the relative ranking of the affinities of the two ligands obtained through the different assays, is inverted. This might be due to the different sensitivity of the various assays in which the affinity is measured, i.e., computational simulations in a 3D model or SPR experiments in a non-physiological system. Moreover, as already reported, the use of empirical scoring functions for estimating dissociation constant values has accuracy in the range of one order of magnitude (Eberini et al., 2008; Galli et al., 2014).

To confirm the validity of our approach for the identification of new GPR17 ligands to be exploited *in vivo* in demyelinating disorders, we performed a series of functional assays on a cell system natively expressing GPR17, e.g., primary rat OPCs grown in culture alone or in co-culture with neurons (Fumagalli et al., 2011, 2015). Our data confirm that Asinex 1 is indeed a full agonist at GPR17 acting on the nucleotide binding site of the receptor (Eberini et al., 2011), as shown by the inhibition of cAMP formation, the antagonism by Cangrelor, and the ability to promote OPC maturation and differentiation.

Taken together, the results presented in this work demonstrate that our protocol provides an effective and reliable way to measure the direct binding of GPR17 even in the sub-nanomolar range, and will be implemented for the systematic identification of new active compounds on this important pharmacological target. More generally, our findings confirm the potential of this technique, in combination with complex *in silico* analyses and functional assays on native systems, for evaluating the activity of agonist and antagonist ligands on GPRCs, a family of crucial targets in pharmacological research.

## DATA AVAILABILITY STATEMENT

The datasets generated for this study are available on request to the corresponding author.

## ETHICS STATEMENT

The animal study was approved by the Animal Care Committee of the Università degli Studi di Milano–La Statale, which is legally entitled for the use of animals for scientific purposes, and by the Italian Ministry of Health (Authorization #473/2015-PR, 05/06/2015).

## AUTHOR CONTRIBUTIONS

DC and RM performed the SPR experiments. GP designed the SPR experiments and analyzed the data. CP performed all the molecular dynamics analyses and contributed to the set-up of protocols for cell lysis. SS helped with the molecular dynamics analyses and contributed to the set-up of protocols for cell lysis. IE contributed to the molecular dynamics analyses and discussed the results. MF and EB performed the *in vitro* experiments and immunocytochemistry on OPC and OPC-neuron co-cultures and analyzed the results. SD and MT performed the cAMP assays

on OPC cultures and analyzed the results. MA discussed the experimental plan and results. SCe contributed to the set-up of protocols for cell lysis, discussed *in vitro* results. MR and CT critically reviewed the work. SCa designed and performed the expression of the recombinant engineered receptor. EC provided substantial contribution to the design of the work. SCa wrote the paper with inputs from the other authors. All authors contributed in reviewing the manuscript.

## FUNDING

This work was supported by FISM–Fondazione Italiana Sclerosi Multipla (grant nos. 2017/R/1 and 2018/R/21), Università degli Studi di Milano-Piano di Sostegno alla Ricerca 2018 Linea 2 (MF) and Prin-Progetti di Ricerca di Interesse Nazionale 2017 (grant no. 2017NSXP8J to MA). IE and SCe were supported by MIUR Finanziamento Annuale Individuale delle Attività di Base di Ricerca 2017. Members of the Department of Pharmacological and Biomolecular Sciences are supported by the Department of Excellence grant program from the Italian Ministry of Research (MIUR).

## SUPPLEMENTARY MATERIAL

The Supplementary Material for this article can be found online at: https://www.frontiersin.org/articles/10.3389/fchem.2019.00910/full#supplementary-material

## REFERENCES

Abbracchio, M. P., Burnstock, G., Boeynaems, J.-M., Barnard, E. A., Boyer, J. L., Kennedy, C., et al. (2006). International Union of Pharmacology LVIII: update on the P2Y G protein-coupled nucleotide receptors: from molecular mechanisms and pathophysiology to therapy. *Pharmacol. Rev.* 58, 281–341. doi: 10.1124/pr.58.3.3

Adamson, R. J., and Watts, A. (2014). Kinetics of the early events of GPCR signalling. *FEBS Lett.* 588, 4701–4707. doi: 10.1016/j.febslet.2014.10.043

Alavi, M. S., Karimi, G., and Roohbakhsh, A. (2019). The role of orphan G protein-coupled receptors in the pathophysiology of multiple sclerosis: a review. *Life Sci.* 224, 33–40. doi: 10.1016/j.lfs.2019.03.045

Aristotelous, T., Hopkins, A. L., and Navratilova, I. (2015). Surface plasmon resonance analysis of seven-transmembrane receptors. *Methods Enzymol.* 556, 499–525. doi: 10.1016/bs.mie.2015.01.016

Berendsen, H. J. C., van der Spoel, D., and van Drunen, R. (1995). GROMACS: a message-passing parallel molecular dynamics implementation. *Comput. Phys. Commun.* 91, 43–56. doi: 10.1016/0010-4655(95)00042-E

Bertheleme, N., Chae, P. S., Singh, S., Mossakowska, D., Hann, M. M., Smith, K. J., et al. (2013). Unlocking the secrets of the gatekeeper: methods for stabilizing and crystallizing GPCRs. *Biochim. Biophys. Acta.* 1828, 2583–2591. doi: 10.1016/j.bbamem.2013.07.013

Bocquet, N., Kohler, J., Hug, M. N., Kusznir, E. A., Rufer, A. C., Dawson, R. J., et al. (2015). Real-time monitoring of binding events on a thermostabilized human A2A receptor embedded in a lipid bilayer by surface plasmon resonance. *Biochim. Biophys. Acta.* 1848, 1224–1233. doi: 10.1016/j.bbamem.2015.02.014

Bonfanti, E., Gelosa, P., Fumagalli, M., Dimou, L., Viganò, F., Tremoli, E., et al. (2017). The role of oligodendrocyte precursor cells expressing the GPR17 receptor in brain remodeling after stroke. *Cell Death Dis.* 8:e2871. doi: 10.1038/cddis.2017.256

Calleri, E., Ceruti, S., Cristalli, G., Martini, C., Temporini, C., Parravicini, C., et al. (2010). Frontal affinity chromatography-mass spectrometry useful for characterization of new ligands for GPR17 receptor. *J. Med. Chem.* 53, 3489–3501. doi: 10.1021/jm901691y

Chang, J.-M., Di Tommaso, P., Taly, J.-F., and Notredame, C. (2012). Accurate multiple sequence alignment of transmembrane proteins with PSI-Coffee. *BMC Bioinformatics* 13:S1. doi: 10.1186/1471-2105-13-S4-S1

Cherezov, V., Rosenbaum, D. M., Hanson, M. A., Rasmussen, S. G. F., Thian, F. S., Kobilka, T. S., et al. (2007). High-resolution crystal structure of an engineered human beta2-adrenergic G protein-coupled receptor. *Science* 318, 1258–1265. doi: 10.1126/science.1150577

Chu, R., Reczek, D., and Brondyk, W. (2015). Capture-stabilize approach for membrane protein SPR assays. *Sci. Rep.* 4:7360. doi: 10.1038/srep07360

Ciana, P., Fumagalli, M., Trincavelli, M. L., Verderio, C., Rosa, P., Lecca, D., et al. (2006). The orphan receptor GPR17 identified as a new dual uracil nucleotides/cysteinyl-leukotrienes receptor. *EMBO J.* 25, 4615–4627. doi: 10.1038/sj.emboj.7601341

Congreve, M., Rich, R. L., Myszka, D. G., Figaroa, F., Siegal, G., and Marshall, F. H. (2011). Fragment screening of stabilized G-protein-coupled receptors using biophysical methods. *Methods Enzymol.* 493, 115–136. doi: 10.1016/B978-0-12-381274-2.00005-4

Eberini, I., Daniele, S., Parravicini, C., Sensi, C., Trincavelli, M. L., Martini, C., et al. (2011). *In silico* identification of new ligands for GPR17: a promising therapeutic target for neurodegenerative diseases. *J. Comput. Aided Mol. Des.* 25, 743–752. doi: 10.1007/s10822-011-9455-8

Eberini, I., Rocco, A. G., Mantegazza, M., Gianazza, E., Baroni, A., Vilardo, M. C., et al. (2008). Computational and experimental approaches assess the interactions between bovine beta-lactoglobulin and synthetic compounds of pharmacological interest. *J. Mol. Graph. Model.* 26, 1004–1013. doi: 10.1016/j.jmgm.2007.08.006

Frostell-Karlsson, A., Remaeus, A., Roos, H., Andersson, K., Borg, P., Hämäläinen, M., et al. (2000). Biosensor analysis of the interaction between immobilized human serum albumin and drug compounds for prediction of human serum albumin binding levels. *J. Med. Chem.* 43, 1986–1992. doi: 10.1021/jm991174y

Fumagalli, M., Bonfanti, E., Daniele, S., Zappelli, E., Lecca, D., Martini, C., et al. (2015). The ubiquitin ligase Mdm2 controls oligodendrocyte maturation by intertwining mTOR with G protein-coupled receptor kinase 2 in the regulation of GPR17 receptor desensitization. *Glia* 63, 2327–2339. doi: 10.1002/glia.22896

Fumagalli, M., Daniele, S., Lecca, D., Lee, P. R., Parravicini, C., Fields, R. D., et al. (2011). Phenotypic changes, signaling pathway, and functional correlates of GPR17-expressing neural precursor cells during oligodendrocyte differentiation. *J. Biol. Chem.* 286, 10593–10604. doi: 10.1074/jbc.M110.162867

Fumagalli, M., Lecca, D., and Abbracchio, M. P. (2016). CNS remyelination as a novel reparative approach to neurodegenerative diseases: the roles of purinergic signaling and the P2Y-like receptor GPR17. *Neuropharmacology* 104, 82–93. doi: 10.1016/j.neuropharm.2015.10.005

Gacasan, S. B., Baker, D. L., and Parrill, A. L. (2017). G protein-coupled receptors: the evolution of structural insight. *AIMS Biophys.* 4, 491–527. doi: 10.3934/biophy.2017.3.491

Galli, C. L., Sensi, C., Fumagalli, A., Parravicini, C., Marinovich, M., and Eberini, I. (2014). A computational approach to evaluate the androgenic affinity of iprodione, procymidone, vinclozolin and their metabolites. *PLoS ONE* 9:e104822. doi: 10.1371/journal.pone.0104822

Glück, J. M., Koenig, B. W., and Willbold, D. (2011). Nanodiscs allow the use of integral membrane proteins as analytes in surface plasmon resonance studies. *Anal. Biochem.* 408, 46–52. doi: 10.1016/j.ab.2010.08.028

Granier, S., Manglik, A., Kruse, A. C., Kobilka, T. S., Thian, F. S., Weis, W. I., et al. (2012). Structure of the δ-opioid receptor bound to naltrindole. *Nature* 485, 400–404. doi: 10.1038/nature11111

Grisshammer, R. (2017). New approaches towards the understanding of integral membrane proteins: a structural perspective on G protein-coupled receptors. *Protein Sci.* 26, 1493–1504. doi: 10.1002/pro.3200

Harrison, C., and Traynor, J. R. (2003). The [35S]GTPgammaS binding assay: approaches and applications in pharmacology. *Life Sci.* 74, 489–508. doi: 10.1016/j.lfs.2003.07.005

Hauser, A. S., Attwood, M. M., Rask-Andersen, M., Schiöth, H. B., and Gloriam, D. E. (2017). Trends in GPCR drug discovery: new agents, targets and indications. *Nat. Rev. Drug Discov.* 16, 829–842. doi: 10.1038/nrd.2017.178

Humphrey, W., Dalke, A., and Schulten, K. (1996). VMD: visual molecular dynamics. *J. Mol. Graph.* 14, 33–38, 27–28. doi: 10.1016/0263-7855(96)00018-5

Jonsson, U., and Malmqvist, M. (1992). Real time biospecific interaction analysis. The integration of surface plasmon resonance detection, general biospecific interface chemistry and microfluidics into one analytical system. *Adv. Biosens.* 2, 291–336. doi: 10.1016/B978-1-85617-161-8.50079-3

Karlsson, O. P., and Löfås, S. (2002). Flow-mediated on-surface reconstitution of G-protein coupled receptors for applications in surface plasmon resonance biosensors. *Anal. Biochem.* 300, 132–138. doi: 10.1006/abio.2001.5428

Lomize, M. A., Pogozheva, I. D., Joo, H., Mosberg, H. I., and Lomize, A. L. (2012). OPM database and PPM web server: resources for positioning of proteins in membranes. *Nucleic Acids Res.* 40, D370–D376. doi: 10.1093/nar/gkr703

Lundquist, A., Hansen, S. B., Nordström, H., Danielson, U. H., and Edwards, K. (2010). Biotinylated lipid bilayer disks as model membranes for biosensor analyses. *Anal. Biochem.* 405, 153–159. doi: 10.1016/j.ab.2010.06.030

Maynard, J. A., Lindquist, N. C., Sutherland, J. N., Lesuffleur, A., Warrington, A. E., Rodriguez, M., et al. (2009). Surface plasmon resonance for high-throughput ligand screening of membrane-bound proteins. *Biotechnol. J.* 4, 1542–1558. doi: 10.1002/biot.200900195

Milić, D., and Veprintsev, D. B. (2015). Large-scale production and protein engineering of G protein-coupled receptors for structural studies. *Front. Pharmacol.* 6:66. doi: 10.3389/fphar.2015.00066

Myszka, D. G., and Morton, T. A. (1998). CLAMP: a biosensor kinetic data analysis program. *Trends Biochem. Sci.* 23, 149–150. doi: 10.1016/S0968-0004(98)01183-9

Naïm, M., Bhat, S., Rankin, K. N., Dennis, S., Chowdhury, S. F., Siddiqi, I., et al. (2007). Solvated interaction energy (SIE) for scoring protein-ligand binding affinities. 1. exploring the parameter space. *J. Chem. Inf. Model.* 47, 122–133. doi: 10.1021/ci600406v

Olaru, A., Bala, C., Jaffrezic-Renault, N., and Aboul-Enein, H. Y. (2015). Surface plasmon resonance (SPR) biosensors in pharmaceutical analysis. *Crit. Rev. Anal. Chem.* 45, 97–105. doi: 10.1080/10408347.2014.881250

Parravicini, C., Abbracchio, M. P., Fantucci, P., and Ranghino, G. (2010). Forced unbinding of GPR17 ligands from wild type and R255I mutant receptor models through a computational approach. *BMC Struct. Biol.* 10:8. doi: 10.1186/1472-6807-10-8

Parravicini, C., Daniele, S., Palazzolo, L., Trincavelli, M. L., Martini, C., Zaratin, P., et al. (2016). A promiscuous recognition mechanism between GPR17 and SDF-1: molecular insights. *Cell. Signal.* 28, 631–642. doi: 10.1016/j.cellsig.2016.03.001

Parravicini, C., Ranghino, G., Abbracchio, M. P., and Fantucci, P. (2008). GPR17: molecular modeling and dynamics studies of the 3-D structure and purinergic ligand binding features in comparison with P2Y receptors. *BMC Bioinformatics* 9:263. doi: 10.1186/1471-2105-9-263

Patching, S. G. (2014). Surface plasmon resonance spectroscopy for characterisation of membrane protein-ligand interactions and its potential for drug discovery. *Biochim. Biophys. Acta* 1838, 43–55. doi: 10.1016/j.bbamem.2013.04.028

Piscitelli, C. L., Kean, J., de Graaf, C., and Deupi, X. (2015). A Molecular pharmacologist's guide to G protein–coupled receptor crystallography. *Mol. Pharmacol.* 88, 536–551. doi: 10.1124/mol.115.099663

Platonova, N., Parravicini, C., Sensi, C., Paoli, A., Colombo, M., Neri, A., et al. (2017). Identification of small molecules uncoupling the Notch::Jagged interaction through an integrated high-throughput screening. *PLoS ONE* 12:e0182640. doi: 10.1371/journal.pone.0182640

Ribeiro-Oliveira, R., Vojtek, M., Gonçalves-Monteiro, S., Vieira-Rocha, M. S., Sousa, J. B., Gonçalves, J., et al. (2019). Nuclear G-protein-coupled receptors as putative novel pharmacological targets. *Drug Discov. Today* 24, 2192–2201. doi: 10.1016/j.drudis.2019.09.003

Rich, R. L., Errey, J., Marshall, F., and Myszka, D. G. (2011). Biacore analysis with stabilized G-protein-coupled receptors. *Anal. Biochem.* 409, 267–272. doi: 10.1016/j.ab.2010.10.008

Rosenbaum, D. M., Cherezov, V., Hanson, M. A., Rasmussen, S. G. F., Thian, F. S., Kobilka, T. S., et al. (2007). GPCR engineering yields high-resolution structural insights into 2-adrenergic receptor function. *Science* 318, 1266–1273. doi: 10.1126/science.1150609

Schneider, E. H., and Seifert, R. (2010). Sf9 cells: a versatile model system to investigate the pharmacological properties of G protein-coupled receptors. *Pharmacol. Ther.* 128, 387–418. doi: 10.1016/j.pharmthera.2010.07.005

Sensi, C., Daniele, S., Parravicini, C., Zappelli, E., Russo, V., Trincavelli, M. L., et al. (2014). Oxysterols act as promiscuous ligands of class-A GPCRs: *in silico* molecular modeling and *in vitro* validation. *Cell. Signal.* 26, 2614–2620. doi: 10.1016/j.cellsig.2014.08.003

Seyedsadr, M. S., and Ineichen, B. V. (2017). Gpr17, a player in lysolecithin-induced demyelination, oligodendrocyte survival, and differentiation. *J. Neurosci.* 37, 2273–2275. doi: 10.1523/JNEUROSCI.3778-16.2017

Wojciechowski, M., and Lesyng, B. (2004). Generalized born model: analysis, refinement, and applications to proteins. *J. Phys. Chem. B* 108, 18368–18376. doi: 10.1021/jp046748b

Wu, B., Chien, E. Y. T., Mol, C. D., Fenalti, G., Liu, W., Katritch, V., et al. (2010). Structures of the CXCR4 chemokine GPCR with small-molecule and cyclic peptide antagonists. *Science* 330, 1066–1071. doi: 10.1126/science.1194396

Zhang, C., Srinivasan, Y., Arlow, D. H., Fung, J. J., Palmer, D., Zheng, Y., et al. (2012). High-resolution crystal structure of human protease-activated receptor 1. *Nature* 492, 387–392. doi: 10.1038/nature11701

Zhang, D., Gao, Z.-G., Zhang, K., Kiselev, E., Crane, S., Wang, J., et al. (2015). Two disparate ligand-binding sites in the human P2Y1 receptor. *Nature* 520, 317–321. doi: 10.1038/nature14287

Zhang, J., Zhang, K., Gao, Z.-G., Paoletta, S., Zhang, D., Han, G. W., et al. (2014). Agonist-bound structure of the human P2Y12 receptor. *Nature* 509, 119–122. doi: 10.1038/nature13288

**Conflict of Interest:** The authors declare that the research was conducted in the absence of any commercial or financial relationships that could be construed as a potential conflict of interest.

frontiers in Chemistry

ORIGINAL RESEARCH
published: 03 March 2020
doi: 10.3389/fchem.2020.00110

# Targeting the Oncogenic TBX2 Transcription Factor With Chromomycins

*Bianca Del B. Sahm[1], Jade Peres[2], Paula Rezende-Teixeira[1], Evelyne A. Santos[3], Paola C. Branco[1], Anelize Bauermeister[1,4], Serah Kimani[2], Eduarda A. Moreira[4], Renata Bisi-Alves[3], Claire Bellis[2], Mihlali Mlaza[2], Paula C. Jimenez[5], Norberto P. Lopes[4], Glaucia M. Machado-Santelli[3], Sharon Prince[1,2] and Leticia V. Costa-Lotufo[1]**

[1] Department of Pharmacology, Institute of Biomedical Sciences, University of São Paulo, São Paulo, Brazil, [2] Division of Cell Biology, Department of Human Biology, University of Cape Town, Cape Town, South Africa, [3] Department of Cell and Developmental Biology, Institute of Biomedical Sciences, University of São Paulo, São Paulo, Brazil, [4] Department of Physics and Chemistry, School of Pharmaceutical Sciences, University of São Paulo, Ribeirao Preto, Brazil, [5] Department of Sea Sciences, Federal University of São Paulo, Santos, Brazil

OPEN ACCESS

**Edited by:**
*Enrica Calleri,*
*University of Pavia, Italy*

**Reviewed by:**
*Lingxin Chen,*
*Yantai Institute of Coastal Zone Research (CAS), China*
*Benjamin L. Oyler,*
*United States Food and Drug Administration, United States*

***Correspondence:**
*Leticia V. Costa-Lotufo*
*costalotufo@usp.br*

**Specialty section:**
*This article was submitted to Analytical Chemistry, a section of the journal Frontiers in Chemistry*

**Received:** *22 September 2019*
**Accepted:** *05 February 2020*
**Published:** *03 March 2020*

**Citation:**
*Sahm BDB, Peres J, Rezende-Teixeira P, Santos EA, Branco PC, Bauermeister A, Kimani S, Moreira EA, Bisi-Alves R, Bellis C, Mlaza M, Jimenez PC, Lopes NP, Machado-Santelli GM, Prince S and Costa-Lotufo LV (2020) Targeting the Oncogenic TBX2 Transcription Factor With Chromomycins. Front. Chem. 8:110. doi: 10.3389/fchem.2020.00110*

The TBX2 transcription factor plays critical roles during embryonic development and it is overexpressed in several cancers, where it contributes to key oncogenic processes including the promotion of proliferation and bypass of senescence. Importantly, based on compelling biological evidences, TBX2 has been considered as a potential target for new anticancer therapies. There has therefore been a substantial interest to identify molecules with TBX2-modulatory activity, but no such substance has been found to date. Here, we adopt a targeted approach based on a reverse-affinity procedure to identify the ability of chromomycins $A_5$ ($CA_5$) and $A_6$ ($CA_6$) to interact with TBX2. Briefly, a TBX2-DNA-binding domain recombinant protein was N-terminally linked to a resin, which in turn, was incubated with either $CA_5$ or $CA_6$. After elution, bound material was analyzed by UPLC-MS and $CA_5$ was recovered from TBX2-loaded resins. To confirm and quantify the affinity ($K_D$) between the compounds and TBX2, microscale thermophoresis analysis was performed. $CA_5$ and $CA_6$ modified the thermophoretic behavior of TBX2, with a $K_D$ in micromolar range. To begin to understand whether these compounds exerted their anti-cancer activity through binding TBX2, we next analyzed their cytotoxicity in TBX2 expressing breast carcinoma, melanoma and rhabdomyosarcoma cells. The results show that $CA_5$ was consistently more potent than $CA_6$ in all tested cell lines with $IC_{50}$ values in the nM range. Of the cancer cell types tested, the melanoma cells were most sensitive. The knockdown of TBX2 in 501mel melanoma cells increased their sensitivity to $CA_5$ by up to 5 times. Furthermore, inducible expression of TBX2 in 501mel cells genetically engineered to express TBX2 in the presence of doxycycline, were less sensitive to $CA_5$ than the control cells. Together, the data presented in this study suggest that, in addition to its already recognized DNA-binding properties, $CA_5$ may be binding the transcription factor TBX2, and it can contribute to its cytotoxic activity.

**Keywords: DNA-binding agents, T-box factors, reverse affinity, microscale thermophoresis, melanoma, chromomycins**

## INTRODUCTION

Traditionally, drug discovery and development (D&D) programs have made use of phenotypic approaches, which are characterized by observable changes in a disease model (animal or cellular). Advances in molecular biology and biochemistry, as well as the sequencing of the human genome, has enabled a more reductionist and rational approach to D&D. It has made possible the principle of targeting molecular drivers of diseases as well as increasing and improving approaches to targeting these molecules (Strausberg and Schreiber, 2003; Overington et al., 2006; Swinney and Anthony, 2011). In this context, designing targeted-based drug screening protocols with integrated strategies, is an attractive point to start drug discovery programs.

Affinity-based methods have gained attraction as innovative approaches to targeted oriented drug discovery. These involve the use of a molecular probe that is specifically designed to identify one or more target proteins from many others present in a complex cell lysate mixture. The identification and quantification of the isolated targets are ascertained by liquid-chromatography coupled to tandem mass spectrometry (LC-MS) (Rylova et al., 2015). Using the reverse of this approach, Lau et al. (2015) screened natural crude extracts for compounds with affinity for a specific biological protein that had previously been characterized and, hence, proposed as an important therapeutic target. Briefly, in this approach, the target protein was attached to an affinity resin, exposed to complex natural extracts and compounds that were bound to the protein were then detected by LC-MS.

The establishment of new targets in cancer therapy is a key step in the development of new effective therapies. In this realm, the transcription factor TBX2 overexpression has been directly linked to several cancers, including rhabdomyosarcoma (Zhu et al., 2016), breast (Jacobs et al., 2000; Redmond et al., 2010), melanoma (Vance et al., 2005; Peres et al., 2010), nasopharyngeal (Lv et al., 2017), and prostate cancers (Du et al., 2017). Indeed, TBX2 functions as a potent growth-promoting factor, in part due to its ability to bypass senescence and to repress key negative cell cycle regulators such as p14ARF, p21, and NDRG (Jacobs et al., 2000; Prince et al., 2004; Redmond et al., 2010). Furthermore, there is strong *in vitro* and *in vivo* biological evidence that TBX2 may be a novel target for anti-cancer drugs that can be administered on their own or in combination with other chemotherapies. Indeed, knocking down TBX2 in melanomas or in several metastatic breast cancer cell lines resulted, respectively, in induction of senescence or in a profound inhibition of proliferation, regardless of their receptor status (Peres et al., 2010; Wansleben et al., 2014). TBX2 also confers resistance to the widely used chemotherapeutic drug cisplatin by promoting p53 activity via Chk2, further leading to an S-phase arrest and DNA repair. Importantly, depleting TBX2 sensitizes cisplatin-resistant breast cancer and metastatic melanoma cells to this drug. These results suggest that TBX2 stimulates proliferation and inappropriate survival of cells with damaged DNA (Wansleben et al., 2013). Any drug that therefore impacts TBX2 expression or activity is likely to have a major impact on cancer progression and recurrence.

Natural products have provided an important source of bioactive molecules for clinical use. They are extensively used in the pharmaceutical industry as either drugs or in influencing the synthesis and semisynthesis of therapeutic molecules. Of particular importance, ∼60% of anti-cancer agents currently in the clinic are derived from natural products (Newman and Cragg, 2016). DNA-binding agents are the most common class of anticancer drugs. They function by interacting with DNA of dividing cells, resulting in DNA-damage and, thus, blocking transcription and replication that, ultimately, halts the cell cycle and/or activates cell death pathways. They can also inhibit enzymes that are important for the maintenance of DNA integrity such as topoisomerases. Chromomycins are tricyclic glycosylated polyketides belonging to the aureolic acid family, with promising anticancer activity and antiproliferative properties (Guimarães et al., 2014; Pettit et al., 2015; Pinto et al., 2019). These molecules bind to the DNA minor groove, causing DNA damage of treated cells, enhancing the expression of apoptosis related genes (Boer et al., 2009; Zihlif et al., 2010).

In this context, the present study employed a reverse affinity approach using the DNA-binding domain of the anticancer target TBX2 as bait to access the potential affinity of the marine chromomycins $CA_5$ and $CA_6$. Microscale thermophoresis was applied to quantify the binding affinities of the natural compounds, $CA_5$ and $CA_6$, to TBX2. Cytotoxicity of these compounds were determined in TBX2-driven breast carcinoma, melanoma, and rhabdomyosarcoma cell lines.

## MATERIALS AND METHODS

### Reagents

The isolation and characterization of chromomycins $A_5$ ($CA_5$) and $A_6$ ($CA_6$) was previously described by Pinto et al. (2019). The substances were resuspended in dimethyl sulfoxide (DMSO, Sigma Aldrich, USA). **Figure 1A** shows the chemical structure of $CA_5$ and $CA_6$.

### Cell Culture

The human melanoma cells lines 501mel, MM200, and WM293a (kindly donated by Professor Dorothy Bennet, St George's University of London) were cultured in Roswell Park Memorial Institute Medium (RPMI)-1640 (Sigma Aldrich, USA). The human breast adenocarcinoma cell lines MCF-7 (ATCC® HTB-22) and T47D (ATCC® HTB-133) were cultured in Dulbecco's Modified Eagle medium:nutrient mixture F-12 (Ham) (DMEM/F-12) (Gibco by Thermo Fisher Scientific, USA). The human embryonal rhabdomyosarcoma cell line RD (ATCC® CCL-136) and the human alveolar rhabdomyosarcoma cell line RH30 (kindly provided by Professor Judith Davie, Southern Illinois University) were cultured in DMEM (Sigma Aldrich, USA). All culture medium was supplemented with 10% heat-inactivated fetal bovine serum (FBS), 100 U/mL penicillin and 100 μg/mL streptomycin. Cells were maintained at 37∘C in a 5% $CO_2$ humidified incubator and medium was replaced every 2–3 days.

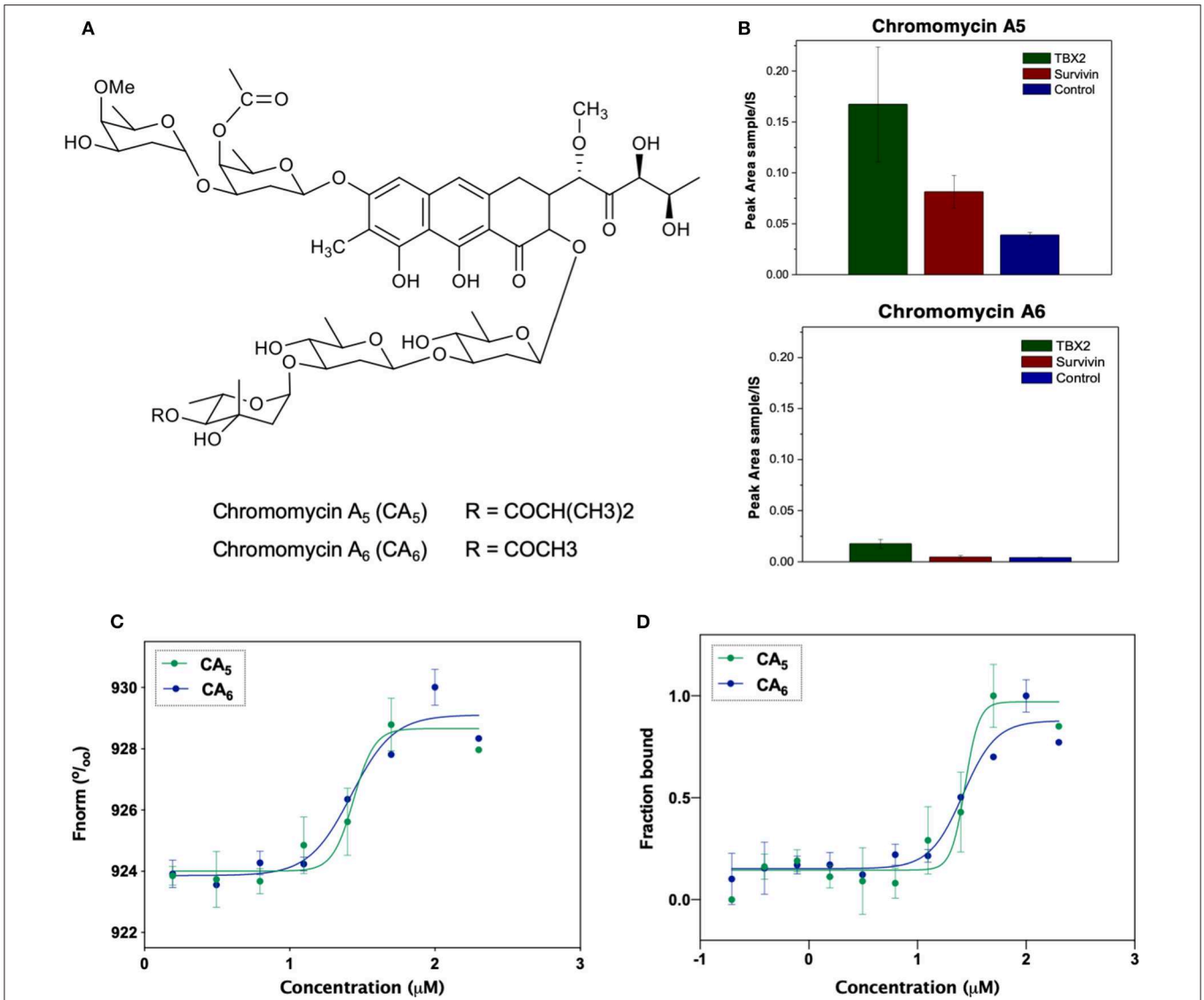


**FIGURE 1 | (A)** Chemical structures of the compounds used in the present study: chromomycin $A_5$ and chromomycin $A_6$. **(B)** Relative quantification of compounds chromomycin $A_5$ and chromomycin $A_6$ recovered from the bioaffinity chromatography technique using resins functionalized with TBX2 (green) or Survivin (red), or non-functionalized (control, blue) resin. The value of peak areas (triplicate) was used to construct the graphic. **(C)** Binding affinities of test compounds to TBX2 assessed through microscale thermophoresis. Normalized fluorescence of labeled TBX2 in the presence of serial concentrations of each of the test molecules. Data correspond to the mean values from two independent experiments. **(D)** Bound fraction of fluorescently labeled TBX2 with serial concentrations of each of the two chromomycins $CA_5$ and $CA_6$.

## TBX2 Protein Expression and Purification

The coding region of the human TBX2 DNA binding domain (residues 94–287) was amplified by PCR and cloned into a pET28b vector between Nde1 and Xho1 restriction sites to generate an N-terminal His6-tagged sequence containing a thrombin cleavage site. The construct was verified by DNA sequencing. The pET28b-TBX294-287 plasmid was transformed into *Escherichia coli* strain BL21(DE3) and expression carried out at 37∘C for 4 h, resulting in a 215-amino acid protein with a molecular weight of 24 kDa. The protein was purified by immobilized nickel affinity chromatography (GE Healthcare Life Sciences, USA); using HisTrap HP nickel affinity column (GE Healthcare Life Sciences, USA), with binding in a buffer containing 20 mM sodium phosphate buffer (pH 7.5), 500 mM NaCl and 50 mM imidazole and elution in the same buffer with a 50–300 mM imidazole gradient. The protein was further purified by size exclusion chromatography on a Superdex 200 column (GE Healthcare Life Sciences, USA) in a Reverse Affinity (RA) buffer containing 20 mM HEPES pH 7.4, 150 mM KCl, 1 mM $MgCl_2$, 2 mM β-mercaptoethanol (BME). Purity of the protein was verified by SDS-PAGE and protein concentration was determined using NANODROP 2000 system (Thermo Fisher Scientific, USA).

Survivin protein was included in the reverse-affinity chromatography assay as negative protein control. The survivin plasmid was obtained from Professor Eli Chapman (Department of Pharmacology and Toxicology, University of Arizona, USA), containing the full-length protein with an extra kanamycin-resistant histidine tail (His-tag). The plasmid was transformed into the *E. coli* strain BL21(DE3) and expression carried out at 16○C overnight. The survivin protein was purified as described for the TBX2 DNA binding domain. After removing the non-specific binders with wash buffer (lysis buffer + 2 mM BME) and complete astringent washing (50 mM Hepes pH 7.4, 1 M KCl, 5 mM $MgCl_2$, 2.5% glycerol in $ddH_2O$ + 2 mM BME), elution buffer (50 mM Hepes pH 7.4, 150 mM KCl, 5 mM $MgCl_2$, 5% glycerol, 250 mM Imidazole in $ddH_2O$) was added. The protein was further purified overnight by dialysis using Spectra/Por dialysis membrane of 3.5 kD (Spectrum Labs Inc., USA) and dialysis buffer (20 mM Hepes pH 7.4, 150 mM KCl, 1 mM $MgCl_2$ in $ddH_2O$), then concentrated in Amicon Ultra-15 10 K (Merck-Millipore, USA) centrifuge filters at 4,000 rpm at 4○C. Purity of the protein was verified as described for TBX2 DNA binding domain.

## Reverse Affinity Procedure

The samples obtained from the bioaffinity chromatography (triplicate) were solubilized with 0.5 mL of methanol containing 0.2 mg/mL of chlorogenic acid (3-caffeoylquinic acid) used as internal standard (IS). Samples were filtered in a small column (made in house on the tip of a Pasteur pipette) containing Sephadex LH-20 in order to remove the salt scraps from buffer. Filtered samples were analyzed by UPLC-MS/MS method on an Acquity TQD (WatersR Corporation, USA) instrument equipped with an ultra-performance liquid chromatography (UPLC) system coupled to a mass spectrometer fitted with an electrospray ionization source and a triple-quadrupole MS detector. Twenty microliter were injected into a Kinetex—Core-Shell Technology C18 column (100 A, 50 × 2.1 mm, 1.7 μm; Phenomenex, USA) kept at 40°C. The mobile phase consisted of deionized water (phase A) and methanol (phase B), both containing 0.2% of formic acid. The chromatographic condition applied was as follows: 5% phase B at 0 min, 100% phase B at 6 min, 100% phase B at 8 min, and 5% phase B at 10 min. The flow rate used was 0.2 mL/min. The ionization source conditions were as follows: 3.0 kV capillary voltage; 20 V cone voltage; 150°C source temperature; 300°C desolvation temperature; 500 L/h desolvation gas flow; 50 L/h cone gas flow. Data was acquired in positive ionization mode employing selected ion recording (SIR) mode. The peak area obtained for the compounds in each sample was normalized by the peak area of the IS in the same run, which allows the quantitative comparison between different sample (obtained from different proteins) for the same compound.

## Microscale Thermophoresis

Binding affinities between target proteins and ligands were measured using microscale thermophoresis (MST) according to the NanoTemper technologies protocol in a Monolith NT.115 (Nanotemper Technologies, Germany) (Duhr and Braun, 2006). Proteins were fluorescently labeled using the Monolith Protein Labeling Kit RED-NHS 2nd Generation (Amine Reactive) (Nanotemper Technologies, Germany) according to the manufacturer's' instructions. The experiments were performed in three independent replicates using Monolith NT.115 Premium glass capillaries (Nanotemper Technologies, Germany) and driven in RA buffer with final concentration of 2% DMSO and 0.05% Tween 20. PCR microtubes were prepared with ligands and the target protein solutions. Ligand concentrations ranged from 10 nM to 400 μM while protein concentrations remained constant. After 5 min at room temperature, the samples were loaded into Premium glass capillaries and the experiments were performed using 20 and 40% MST power and between 20 and 80% LED power at 24°C. MST traces were recorded using the standard parameters: 5 s MST power off, 30 s MST power on and 5 s MST power off. The binding affinities of the compounds to the protein were determined according to with dissociation values (Kd) and the generated data were processed using MO. Control software (Nanotemper Technologies, Germany).

## Western Blot Analyses

Rhabdomyosarcoma cells were lysed in whole cell lysis buffer (0.125 M Tris-HCl pH 6.8, 4% SDS, 0.2% glycerol, 0.1% BME, and a pinch of bromophenol blue) and boiled for 10 min and the remaining cell lines were lysed in RIPA buffer [50 mM Tris–HCl (pH 7.5), 150 mM NaCl, 0.1% NP-40, 0.5% sodium deoxycholate, 1 mM EDTA, and 2 mM EGTA] containing 1 mM sodium orthovanadate, 1 mM phenylmethylsulfonyl fluoride, 10 mg/ml leupeptin and 10 mg/ml aprotinin. Equal amounts of proteins were resolved by SDS-PAGE (12% gels) and transferred to Hybond ECL (Amersham Biosciences, UK) or nitrocellulose (Bio Rad Laboratories, USA) membranes. The membranes were incubated with goat polyclonal antibody to TBX2 (sc-17880) from Santa Cruz Biotechnology (USA) for rhabdomyosarcoma cells, or with rabbit polyclonal antibody to TBX2 (16930-1-AP) from Proteintech (USA) for melanoma and breast carcinoma cells. Mouse monoclonal antibody antiFlag M2 (F1804) from Sigma-Aldrich (USA) was used in the genetically engineered 501mel cells experiments. To control for loading, the rabbit polyclonal antibody to p38 MAPK (#9212) from Sigma-Aldrich (USA), or α-tubulin rabbit polyclonal antibody (#2144) or β-actin rabbit monoclonal antibody to (#4970) from Cell Signaling Technology (USA) were used. After incubation with primary antibodies, membranes were washed then incubated with HRP-conjugated secondary antibodies (#7074 Cell Signaling Technology, USA). Antibody reactive proteins were visualized by enhanced chemiluminescence using SuperSignal West Pico Chemiluminescent Substrate Kit (Thermo Fisher Scientific, USA) or WesternBright ECL HRP Substrate Kit (Advansta Company Inc., USA). Densitometry readings were obtained using UN-SCAN-IT gel 6.1 software (Silk Scientific, USA) and protein expression levels were represented as ratio signals for TBX2/respective loading control. All blots are representative of at least two independent repeats.

## Cell Viability Assays

Cells were seeded in 96-well-plates and, in the following day, they were treated with a range of $CA_5$ and $CA_6$

concentrations or vehicle (1.0 μL DMSO) for 48 or 72 h. Cell viability was measured using the 3-(4,5-dimethylthiazol-2-yl)-2,5-diphenyl-trazolium bromide (MTT) assay (Invitrogen by Thermo Fisher Scientific, USA) (Mosmann, 1983). Mean cell viability was calculated as a percentage of the mean vehicle control. Three independent experiments were performed from which the half maximal inhibitory concentration ($IC_{50}$) and their respective 95% CI (confidence interval) were obtained by non-linear regression using GraphPad Prism version 8.0 (GraphPad Software, USA).

## TBX2 Knockdown (shTBX2) 501mel Cells

To generate stably transfected cell lines in which TBX2 mRNA levels are knocked down (shTBX2), oligonucleotides targeting 5′-ACAGCTGAAGATCGACAACAA-3′ (TBX2 siRNA) of the human coding sequences was cloned into the pSuper.neo/GFP (Oligoengine) shRNA expression vector. The non-specific siRNA oligonucleotide (shControl) was directed against a 5′-ATTTCTCCGAACGTGTCACGT-3′ target sequence. 501mel cells were transfected with the pSuper.neo/GFP expression vector containing sequences targeted to TBX2 or the non-specific control using Transfectin® (BioRad, Hercules, CA). Four hundred microgram per milliliter of G418 disulfate salt (Sigma Aldrich, A1720) were used to maintain and select transfected cells (Webster and Dickson, 1983). Prior to experiments, cells were probed for TBX2 by Western blot to confirm protein knockdown relative to parental- and shControl-cell levels. Cytotoxicity of $CA_5$ was compared in these different 501mel cell models using the MTT assay following 72 h incubation. Therefore, three independent experiments were performed in duplicates from which the $IC_{50}$ was obtained by non-linear regression using GraphPad Prism version 8.0 (GraphPad Software, USA).

## FLAG-Tagged TBX2 (iTBX2) 501mel Cells—Rescue Experiments

501mel cells were genetically engineered to allow for inducible expression of 3XFLAG-tagged TBX2 (iTBX2) using a tetracycline-on (Tet-On) system (kindly provided by Professor Colin Goding, Ludwig Institute of Cancer, Oxford University, UK). TBX2 was induced using 60 ng/mL (135 nM) of doxycycline (Das et al., 2016). TBX2 was induced using 60 ng/mL (135 nM) of doxycycline either 12 h before, or 12 h following, drug treatments with $CA_5$. An iTBX2-empty cell line was used as an experimental control. Cells were exposed to serial concentrations of either drug, and the end point for both conditions was at 48 h after drug exposure. $IC_{50}$ for cell models subjected to both experimental conditions and drug treatments were obtained using the MTT assay and calculated from three independent experiments performed in duplicates by non-linear regression using GraphPad Prism version 8.0 (GraphPad Software, USA).

# RESULTS AND DISCUSSION

## Chromomycins Directly Interact With the TBX2 DNA Binding Domain

Our group has been focused on screening and developing natural products with anticancer potential. In order to optimize and test new strategies in this field, we are currently applying the reverse affinity procedure as a tool to screen and guide the isolation of target-specific anticancer substances within crude bacterial

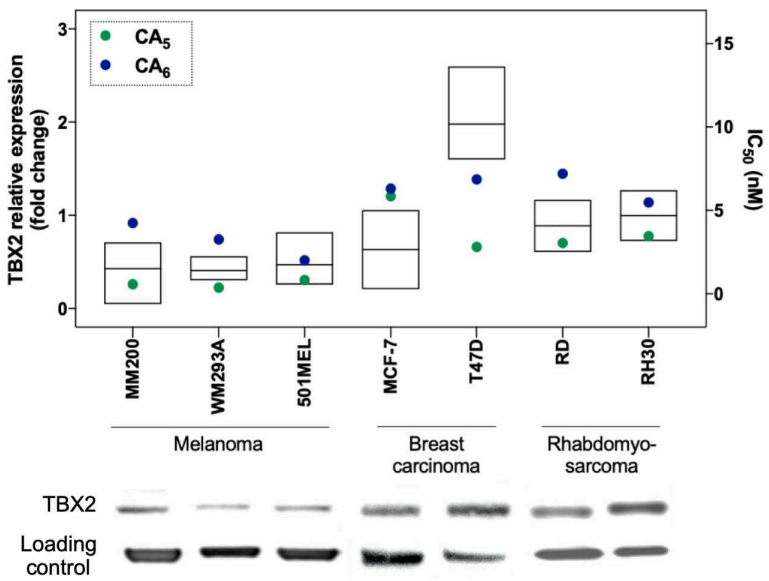


**FIGURE 2 |** Relative protein expression of TBX2 and cytotoxicity ($IC_{50}$) data in melanoma, breast cancer, and rhabdomyosarcoma cell lines. Protein expression levels are plotted in the left y axis as ratio signals for TBX2/respective loading control obtained from the densitometry readings using UN-SCAN-IT gel 6.1 software. Loading controls were obtained using α-tubulin for melanoma and breast carcinoma cells, and P-38 for sarcoma cells. $IC_{50}$ values are represented in the right y axis and were obtained by the MTT assay cytotoxicity readings after 72 h exposure of drugs to the respective cell line and analyzed by non-linear regression using GraphPad Prism version 8.0 (GraphPad Software, USA) from three independent experiments performed in duplicate.

extracts. In this context, the oncogenic TBX2 transcription factor appears as an intriguing target due to its important pro-tumor roles and the fact that no known modulator was discovery so far. In fact, the DNA binding agent trabectedin (Yondelis®) was the first compound able to displace an oncogenic transcription factor from its target promoters with high specificity (D'Incalci et al., 2014). Moreover, a comparable cytotoxicity profile of trabectedin and chromomycin $A_3$, as assessed in the COMPARE analysis using data from NCI 60 cell line panel, point to a similar mechanism of action (Marco and Gago, 2005). Therefore, pondering on these evidences, we first attempted to verify whether the chromomycins $A_5$ and $A_6$–previously isolated by our group from a marine bacteria *Streptomyces* sp. BRA384—showed affinity to the TBX2 DNA binding domain.

The analyses of samples recovered from the reverse affinity procedure (**Figure 1B**) shows that both compounds displayed a residual binding to the resin itself and to either of the protein-loaded resins, however the recovery of $CA_5$ was increased by the presence of TBX2 linked to the resin. Although this technique has been described as a cost-effective procedure to identify binding compounds based on their affinity properties to a target protein (Lau et al., 2015), further analyses are necessary to validate the observed interactions. Actually, multiple unspecific interactions could be expected due to the ability of natural products to interact with proteins (Clardy and Walsh, 2004) and, moreover, binding to the target does not necessarily turn out in any biological modulation. Herein, we describe, for the first time, that this procedure can also be applied to screen modulators of transcription factors, such as the TBX2 DNA-binding domain as target.

In order to characterize the binding affinity between TBX2 and chromomycins, we used microscale thermophoresis (MST). This technique characterizes a ligand-binder interaction based on the movement of a given protein along a temperature gradient (thermophoresis), which, in turn, depends on its molecular size, charge and hydration shell. Once a ligand is bound to the protein, a distinct thermophoretic movement is expected due to a change in at least one of the above-mentioned parameters, and the information is compared between unbound and bound states (Wienken et al., 2010; Mueller et al., 2017). **Figure 1C** shows that $CA_5$ and $CA_6$ were able to change the thermophoretic movement of TBX2. The dissociation constants ($K_D$) for interactions were calculated for each chromomycin by measuring changes in the fluorescently labeled TBX2 by thermophoresis upon compound binding then normalizing and plotting this as a function of the ligand concentration (**Figure 1D**). The results suggest that $CA_5$ and $CA_6$ exhibit similar binding affinities to the TBX2 DNA-binding domain, with $K_D$ of 31.3 ± 23.3 and 24.4 ± 13.6 μM, respectively.

Most of the available reports on this class of molecules regard the biological properties of $CA_3$ and, to a less extent, of $CA_2$. These chromomycins are, in turn, stereoisomers of $CA_6$ and $CA_5$, respectively, as demonstrated by Pinto et al. (2019) and Pettit et al. (2015). $CA_3$ binds to the minor groove of the DNA complex as a dimer in a process dependent on $Mg^{+2}$, in which a portion of the chromophore along with the D, E and F sugar moieties interact with residues of the minor groove, while the A and B sugar moieties and another portion of the chromophore interact with the phosphate backbone (Gao and Patel, 1989; Boer et al., 2009). Moreover, studies on the

**TABLE 1 |** Cytotoxic activity of chromomycins $A_5$ ($CA_5$) and $A_6$ ($CA_6$) against different tumor cells.

| Cell line | Compound $IC_{50}$ (nM) 72 h (95% confidence interval) | |
|---|---|---|
| | $CA_5$ | $CA_6$ |
| **MELANOMA** | | |
| 501-mel | 0.8 (0.6–1.0) | 2.0 (1.6–2.4) |
| WM293A | 0.3 (0.2–0.5) | 3.2 (2.4–4.3) |
| MM200 | 0.5 (0.3–1.0) | 4.2 (2.2–8.0) |
| **BREAST CARCINOMA** | | |
| MCF-7 | 2.1 (1.8–2.5) | 6.5 (5.0–8.4) |
| T47D | 6.5 (5.1–8.9) | 6.8 (2.8–16.3) |
| **RHABDOMYOSARCOMA** | | |
| RD (Embryonal) | 3.0 (2.8–3.3) | 7.2 (5.6–8.8) |
| RH30 (Alveolar) | 3.5 (3.3–3.6) | 5.5 (3.6–7.3) |

*The compounds were incubated during 72 h, and cell viability was measured through the MTT assay. $IC_{50}$ and the 95% confidence interval were obtained through non-linear regression using GraphPad Prism version 8.0.*

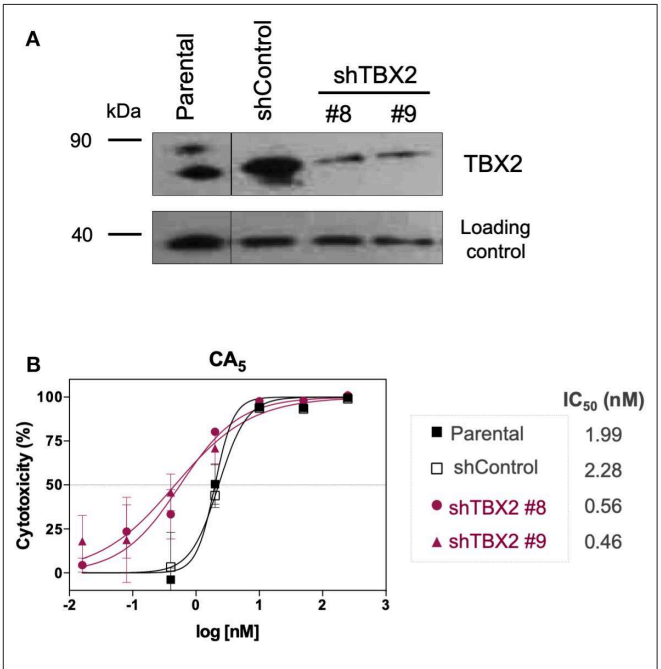


**FIGURE 3 |** Cytotoxicity of $CA_5$ on stably TBX2-knockdown cells (shTBX2). **(A)** TBX2 protein expression in parental, shControl and shTBX2 clones #8 and #9 501mel cell models, achieved by Western blot. **(B)** Cytotoxicity profiles of 501mel cell models exposed to $CA_5$. $IC_{50}$ (nM) values for $CA_5$ in the 501mel cell models. Cytotoxicity curves and respective IC50 values were obtained by MTT assay, after cells were exposed to the respective drugs during 72 h and calculated by non-linear regression on GraphPad Prism 8.0 (GraphPad Software, USA) from three independent experiments performed in quadruplicate.

interaction of $CA_3$ and DNA revealed an apparent affinity constant in the micromolar range (Behr et al., 1969; Aich et al., 1992). To the best of our knowledge, there is no data on the interaction of $CA_5$ and $CA_6$ with DNA. Nonetheless, the structural similarities among this class of compounds suggest that DNA-binding properties should be expected. Further studies are necessary to verify whether these molecules are directly binding to DNA and, furthermore, whether the interaction of TBX2 with DNA could be altered in the presence of chromomycins.

## $CA_5$ Displays Potent Cytotoxicity Against Different TBX2-Driven Cancer Cell Lines

In order to characterize the anticancer activity of $CA_5$ and $CA_6$ in TBX2-driven cancers, we first assessed their cytotoxicity in melanoma, breast carcinoma and rhabdomyosarcoma cell lines. These cell lines were selected based on previous data showing that TBX2 plays an important role in their proliferation and survival (Peres et al., 2010; Wansleben et al., 2013; Zhu et al., 2016). Briefly, the cells were treated with a range of concentrations of $CA_5$ and $CA_6$, for 72 h followed by MTT assay. Regardless of the origin of the cancer, the $IC_{50}$ values obtained for both compounds were in the nanomolar range but the $IC_{50}$ values obtained for $CA_5$ were lower (**Figure 2** and **Table 1**). These results suggest that both chromomycins are highly cytotoxic and that $CA_5$ was more potent than $CA_6$ in this cell panel (**Table 1**). It is worth noting that, among the cell lines tested, those derived from melanomas were the most sensitive to both chromomycins. Indeed, the $IC_{50}$ values obtained for the melanoma cell lines ranged from 0.3 to 0.8 nM for $CA_5$ and from 2.0 to 4.2 nM for $CA_6$. **Figure 2** shows data where the relative levels of basal TBX2 in all cell lines tested were plotted against $IC_{50}$ values for $CA_5$ and $CA_6$. The results show that the T47D cells showed slightly higher levels of TBX2 and there is no significant correlation between $IC_{50}$ values and TBX2 levels.

Other chromomycins were previously reported for their anticancer activities with similar potencies as those described here. Indeed, Toume et al. (2014) reported that $CA_2$ (a stereoisomer of $CA_5$) and $CA_3$ (a stereoisomer of $CA_6$) are cytotoxic against a human gastric adenocarcinoma cell line, with $IC_{50}$ values ranging from 1.7 to 22.1 nM. Pettit et al. (2015) also assessed the cytotoxicity of $CA_5$ against a mini-panel of human cancer cell lines and found $IC_{50}$ values ranging from 0.6 (MCF-7) to 3.4 nM (KM20L2, colon cancer cell). An earlier investigation from our group also evaluated the cytotoxicity of $CA_2$ against a panel of tumor cells from different origins, including colon, prostate, leukemia and melanoma. Consistent with the current study, we showed that the melanoma cells were among the most sensitive to $CA_2$. However, $CA_2$ had an $IC_{50}$ of 18.8 nM in the metastatic melanoma cell line Malme-3M and was thus less cytotoxic than the $CA_5$ and $CA_6$ chromomycins tested in this study against melanoma cells (Guimarães et al., 2014). Furthermore, a recent study from our group compared the cytotoxicity of 4 different chromomycins in a 5 human tumor cell line panel and showed that $CA_5$ was the most potent, especially against the MM200 ($IC_{50}$ of 0.2 nM) and 501Mel ($IC_{50}$ of 0.8 nM) melanoma cells (Pinto et al., 2019).

To investigate whether $CA_5$ exerts its cytotoxicity, in part, through binding TBX2, we firstly tested the effect of knocking down TBX2 on the sensitivity of 501mel cells to the

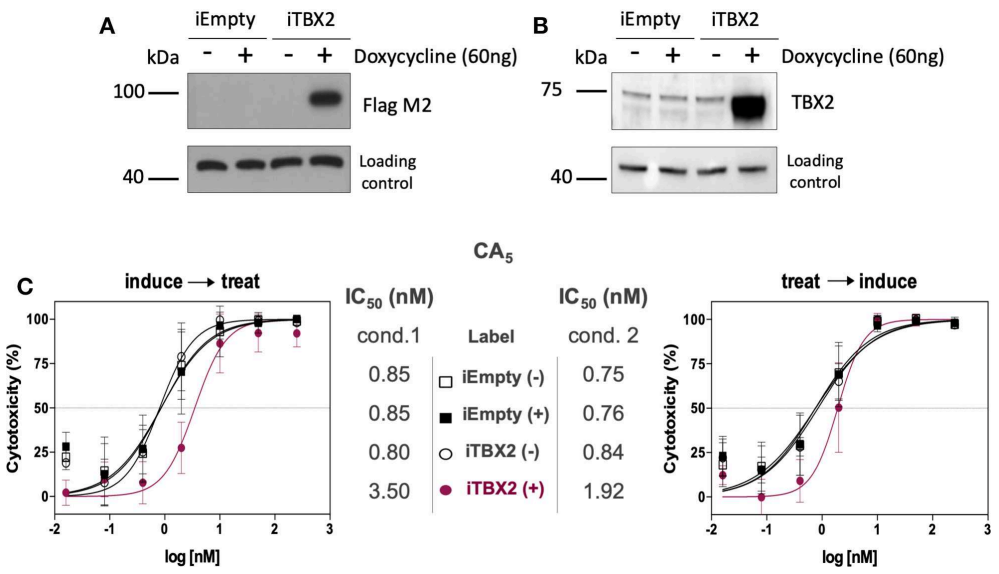


**FIGURE 4 |** Cell viability assay (MTT) of $CA_5$ in 501mel cells with induced and non-induced TBX2-overexpression. **(A,B)** Western blot membranes of samples from iEmpty and iTBX2 cells, without (–) and with (+) 60 ng/mL doxycycline, showing that only iTBX2 (+) is inducing TBX2 overexpression; A—probed for anti-Flag M2; B—probed for anti-TBX2. **(C)** $CA_5$ cytotoxicity profiles and respective $IC_{50}$ (nM) values accessed under cond.1 and cond.2 after 48 h drug exposure. $IC_{50}$ values were obtained by non-linear regression using GraphPad Prism version 8.0 (GraphPad Software, USA) from three independent experiments performed in duplicate. Cond.1, experiment setup where induction of TBX2 expression was done before drug treatment; Cond.2, experiment setup where drug treatment was done prior to TBX2 induction.

chromomycin. Results from MTT assays show that depleting TBX2 reduced the $IC_{50}$ of $CA_5$, by at least 4 times in 501mel cells (**Figure 3**).

Furthermore, when TBX2 expression was induced (iTBX2) in 501mel cells genetically engineered to express TBX2 in the presence of doxycycline for 12 h prior to $CA_5$ treatment for 48 h, the cells were more resistant to the drug (**Figure 4A**). When the same experiment was carried out but TBX2 was induced for the last 12 h of $CA_5$ treatment, the cells were also more resistant to $CA_5$ when compared to their iTBX2-empty counterparts (**Figure 4B**). Indeed, the $IC_{50}$ values increased by 7 times (from 0.6 to 4.2 nM) when TBX2 was induced prior to $CA_5$ treatment and by 1.8 times (from 0.8 to 1.4 nM) when TBX2 was induced post $CA_5$ treatment (**Figure 4C**). The induction of TBX2 prior to exposure to $CA_5$ thus produced a greater resistance response in TBX2-expressing cells.

Taking together, the evidences herein suggest that TBX2 is indeed conferring resistance to these drugs, as observed to cisplatin (Davis et al., 2008; Wansleben et al., 2013). Although these findings point to a direct association between TBX2 levels and $CA_5$ cytotoxicity, the previously observed relation between TBX2 and DNA repair pathways (Wansleben et al., 2013) should also be taken in account to explain the increased toxicity observed in TBX2-knockdown cells.

In summary, $CA_5$ and $CA_6$ displayed high levels of cytotoxicity at relatively low concentrations against all TBX2-driven cancer cell lines tested. Taken together, the evidences generated in the present study through reverse affinity chromatography, and MST assays, then pondered with data from the literature, suggest that, beyond the already established DNA-damaging effects, chromomycins, and especially $CA_5$, bind TBX2 and its modulation may contribute to the observed cytotoxic properties of this group of molecules.

## DATA AVAILABILITY STATEMENT

The datasets generated for this study are available on request to the corresponding author.

## AUTHOR CONTRIBUTIONS

All authors listed have made a substantial, direct and intellectual contribution to the work, and approved it for publication.

## FUNDING

This work was funded by Fundação de Amparo à Pesquisa do Estado de São Paulo (FAPESP) process # 2015/17177-6; 2018/08400-1; 2019/02008-5; 2018/24865-4; and 2017/09022-8; Conselho Nacional de Desenvolvimento Científico e Tecnológico (CNPq, LC-L and GM-S are CNPq researcher fellows); Coordenação de Aperfeiçoamento de Pessoal de Nível Superior (CAPES) and ArboControl Brasil Project (FNS/UnB TED74/2016 and TED42/2017). This work was supported by the Cancer Association of South Africa (CANSA), the South Africa National Research Foundation (NRF), the South Africa Medical Research Council (SA MRC) and the University of Cape Town.

## ACKNOWLEDGMENTS

We are grateful to Dr. Otilia Pessoa for the supply of chromomycins $A_5$ and $A_6$ and, also, to Helori Vanny Domingos and Simone Aparecida Teixeira for technical assistance. We further thank the National Laboratory of Biosciences (LNBIO-CNPEM, Campinas, São Paulo) for making available their facilities, and finally, Dr. Daniel Maturana for valuable discussions.

## REFERENCES

Aich, P., Sen, R., and Dasgupta, D. (1992). Role of magnesium ion in the interaction between chromomycin A3 and DNA: binding of chromomycin A3-Mg2+ complexes with DNA. *Biochemistry* 31, 2988–2997. doi: 10.1021/bi00126a021

Behr, W., Honikel, K., and Hartmann, G. (1969). Interaction of the RNA polymerase inhibitor chromomycin with DNA. *Eur. J. Biochem.* 9, 82–92. doi: 10.1111/j.1432-1033.1969.tb00579.x

Boer, D. R., Canals, A., and Coll, M. (2009). DNA-binding drugs caught in action: the latest 3D pictures of drug-DNA complexes. *Dalton. Trans.* 3, 399–414. doi: 10.1039/B809873P

Clardy, J., and Walsh, C. (2004). Lessons from natural molecules. *Nature* 432, 829–837. doi: 10.1038/nature03194

Das, A. T., Tenenbaum, L., and Berkhout, B. (2016). Tet-On Systems for doxycycline-inducible gene expression. *Curr. Gene. Ther.* 16, 156–167. doi: 10.2174/1566523216666160524144041

Davis, E., Teng, E., Bilican, B., Parker, M. I., Liu, B., Carriera, S., et al. (2008). Ectopic Tbx2 expression results in polyploidy and cisplatin resistance. *Oncogene* 27, 976–984. doi: 10.1038/sj.onc.1210701

D'Incalci, M., Badri, N., Galmarini, C. M., and Allavena, P. (2014). Trabectedin, a drug acting on both cancer cells and the tumor microenvironment. *Br. J. Cancer.* 111, 646–650. doi: 10.1038/bjc.2014.149

Du, W. L., Fang, Q., Chen, Y., Teng, J. W., Xiao, Y. S., Xie, P., et al. (2017). Effect of silencing the T Box transcription factor TBX2 in prostate cancer PC3 and LNCaP cells. *Mol. Med. Rep.* 16, 6050–6058. doi: 10.3892/mmr.2017.7361

Duhr, S., and Braun, D. (2006). Why molecules move along a temperature gradient. *Proc. Natl. Acad. Sci. U.S.A.* 103, 19678–19682. doi: 10.1073/pnas.0603873103

Gao, X., and Patel, D. J. (1989). Solution structure of the Chromomycin-DNA complex. *Biochemistry* 28, 751–762. doi: 10.1021/bi00428a051

Guimarães, L. A., Jimenez, P. C., Sousa, T. D. S., Freitas, H. P. S., Rocha, D. D., Wilke, D. V., et al. (2014). Chromomycin A2 induces autophagy in melanoma cells. *Mar. Drugs* 12, 5839–5855. doi: 10.3390/md12125839

Jacobs, J. J. L., Keblusek, P., Robanus-Maandag, E., Kristel, P., Lingbeek, M., Nederlof, P. M., et al. (2000). Senescence by-pass screen identifies TBX2, which represses Cdkn2a (p19ARF) and is amplified in a subset of human breast cancers. *Nat. Genet.* 26, 291–299. doi: 10.1038/81583

Lau, E. C., Mason, D. J., Eichhorst, N., Engelder, P., Mesa, C., Kithsiri-Wijeratne, E. M., et al. (2015). Functional chromatographic technique for natural product isolation. *Org. Biomol. Chem.* 13, 2255–2259. doi: 10.1039/c4ob02292k

Lv, Y., Si, M., Chen, N., Li, Y., Ma, X., Yang, H., et al. (2017). TBX2 over-expression promotes nasopharyngeal cancer cell proliferation and invasion. *Oncotarget* 8, 52699–52707. doi: 10.18632/oncotarget.17084

Marco, E., and Gago, F. (2005). DNA structural similarity in the 2:1 complexes of the antitumor drugs trabectedin (yondelis) and chromomycin A3 with an oligonucleotide sequence containing two adjacent TGG binding sites on opposing strands. *Mol. Pharm.* 68, 1559–1567. doi: 10.1124/mol.105.015685

Mosmann, T. (1983) Rapid colorimetric assay for cellular growth and survival: application to proliferation and cytotoxicity assays. *J. Immunol. Methods* 65, 55–63. doi: 10.1016/0022-1759(83)90303-4

Mueller, A. M., Breitsprecher, D., Stefan, D., Philipp, B., Schubert, T., and Längst, G. (2017). "Chapter 10 – MicroScale thermophoresis: a rapid and precise method to quantify protein-nucleic acid interactions in solution," in *Functional Genomics: Methos and Protocols, Methods in Molecular Biology*, Vol. 1654, eds M. Kaufmann, C. Klinger, and A. Savelsbergh (Springer Science+Business Media, LLC), 151–164. doi: 10.1007/978-1-49397231-9_10

Newman, D. J., and Cragg, G. M. (2016). Natural products as sources of new drugs from 1981 to 2014. *J. Nat. Prod.* 79, 629–661. doi: 10.1021/acs.jnatprod.5b01055

Overington, J. P., Al-Lazikani, B., and Hopkins, A. L. (2006). How many drug targets are there? *Nat. Rev. Drug Discov.* 5, 993–996. doi: 10.1038/nrd2199

Peres, J., Davis, E., Mowla, S., Bennett, D. C., Li, J. A., Wansleben, S., et al. (2010). The highly homologous T-Box transcription factors, TBX2 and TBX3, have distinct roles in the oncogenic process. *Genes Cancer* 1, 272–282. doi: 10.1177/1947601910365160

Pettit, G. R., Tan, R., Pettit, R. K., Doubek, D. L., Chapuisa, J. C., and Webera, C. A. (2015). Antineoplastic agents 596. isolation and structure of chromomycin A5 from a Beaufort Sea microorganism. *RSC Adv* 5, 9116–9122. doi: 10.1039/C4RA16517A

Pinto, F. C. L., Silveira, E. R., Vasconcelos, A. C. L., Florêncio, K. G. D., Oliveira, F. A. S., Sahm, B. D. B., et al. (2019). Dextrorotatory chromomycins from the marine *Streptomyces* sp. associated to *Palythoa caribaeorum. J. Braz. Chem. Soc.* 31, 1–10. doi: 10.21577/0103-5053.20190144

Prince, S., Carreira, S., Vance, K. W., Abrahams, A., and Goding, C. R. (2004). Tbx2 directly represses the expression of the p21(WAF1) cyclin-dependent kinase inhibitor. *Cancer Res.* 64, 1669–1674. doi: 10.1158/0008-5472.can-03-3286

Redmond, K. L., Crawford, N. T., Farmer, H., D'Costa, Z. C., O'Brien, G. J., Buckley, N. E., et al. (2010). T-box 2 represses NDRG1 through an EGR1-dependent mechanism to drive the proliferation of breast cancer cells. *Oncogene* 29, 3252–3262. doi: 10.1038/onc.2010.84

Rylova, G., Ozdian, T., Varanasi, L., Soural, M., Hlavac, J., Holub, D., et al. (2015). Affinity-based methods in drug-target discovery. *Curr. Drug Targets.* 16, 60–76. doi: 10.2174/1389450115666141120110323

Strausberg, R. L., and Schreiber, S. L. (2003). From knowing to controlling: a path from genomics to drugs using small molecule prodes. *Science* 300, 294–295. doi: 10.1126/science.1083395

Swinney, D. C., and Anthony, J. (2011). How were new medicines discovered? *Nat. Rev. Drug Discov.* 10, 507–519. doi: 10.1038/nrd3480

Toume, K., Tsukahara, K., Ito, H., Arai, M. A., and Ishibashi, M. (2014). Chromomycins A2 and A3 from marine actinomycetes with TRAIL resistance-overcoming and Wnt signal inhibitory activities. *Mar. Drugs* 12, 3466–3476. doi: 10.3390/md12063466

Vance, K. W., Carreira, S., Brosch, G., and Goding, C. R. (2005). Tbx2 is overexpressed and plays an important role in maintaining proliferation and suppression of senescence in melanomas. *Cancer Res.* 65, 2260–2268. doi: 10.1158/0008-5472.CAN-04-3045

Wansleben, S., Davis, E., Peres, J., and Prince, S. (2013). A novel role for the anti-senescence factor TBX2 in DNA repair and cisplatin resistance. *Cell Death. Dis.* 4:e846. doi: 10.1038/cddis.2013.365

Wansleben, S., Peres, J., Hare, S., Goding, C. R., and Prince, S. (2014). T-box transcription factors in cancer biology. *Biochim. Biophys. Acta.* 1846, 380–391. doi: 10.1016/j.bbcan.2014.08.004

Webster, T. D., and Dickson, R. C. (1983). Direct selection of saccharomyces cerevisiae resistant to antibiotic G418 following transformation with a DNA vector carrying the kanamycin-resistance gene of Tn903. *Gene*. 26, 243–252. doi: 10.1016/0378-1119(83)90194-4

Wienken, C. J., Baaske, P., Rothbauer, U., Braun, D., and Duhr, S. (2010). Protein-binding assays in biological liquids using microscale thermophoresis. *Nat. Commun.* 1:100. doi: 10.1038/ncomms1093

Zhu, B., Zhang, M., Williams, E. M., Keller, C., Mansoor, A., and Davie, J. K. (2016). TBX2 represses PTEN in rhabdomyosarcoma and skeletal muscle. *Oncogene* 35, 4212–4224. doi: 10.1038/onc.2015.486

Zihlif, M., Catchpoole, D. R., Stewart, B. W., and Wakelin, L. P. G. (2010). Effects of DNA minor groove binding agents on global gene expression. *Cancer Genomics Proteomics* 7, 323–330.

**Conflict of Interest:** The authors declare that the research was conducted in the absence of any commercial or financial relationships that could be construed as a potential conflict of interest.

# Advantages of publishing in Frontiers

**OPEN ACCESS**
Articles are free to read for greatest visibility and readership

**FAST PUBLICATION**
Around 90 days from submission to decision

**HIGH QUALITY PEER-REVIEW**
Rigorous, collaborative, and constructive peer-review

**TRANSPARENT PEER-REVIEW**
Editors and reviewers acknowledged by name on published articles

**Frontiers**
Avenue du Tribunal-Fédéral 34
1005 Lausanne | Switzerland

**Visit us:** www.frontiersin.org
**Contact us:** info@frontiersin.org | +41 21 510 17 00

**REPRODUCIBILITY OF RESEARCH**
Support open data and methods to enhance research reproducibility

**DIGITAL PUBLISHING**
Articles designed for optimal readership across devices

**FOLLOW US**
@frontiersin

**IMPACT METRICS**
Advanced article metrics track visibility across digital media

**EXTENSIVE PROMOTION**
Marketing and promotion of impactful research

**LOOP RESEARCH NETWORK**
Our network increases your article's readership